The Dissertation Committee for Ranjiv Gupta certifies that this is the approved version of the following dissertation:

A Study of Geosynthetic Reinforced Flexible Pavement System

Committee:

Jorge G. Zornberg, Supervisor

Kenneth H. Stokoe

Robert B. Gilbert

Jorge A. Prozzi

Eric B. Becker

A Study of Geosynthetic Reinforced Flexible Pavement System

by

Ranjiv Gupta, B.E.; M.Tech.

Dissertation

Presented to the Faculty of the Graduate School of

The University of Texas at Austin

in Partial Fulfillment

of the Requirements

for the Degree of

Doctor of Philosophy

The University of Texas at Austin

December 2009

Dedication

To My Parents

Acknowledgements

This research is the product of investments others have made in me and my research. The contributions have varied from intangible assets like intellectual stimulation and emotional support to more tangible items, such as project materials. I would be remiss if I did not strive to thank all of the persons who made this research a reality.

I would like to begin my acknowledgements by thanking my supervisor, Dr. Jorge Zornberg, for his guidance and support through my years as a PhD student. He has been an important mentor who helped me develop research, teaching and presentation skills. He has been a great friend and resource for the past five years of my work at UT.

I would also like to thank Dr. Ken Stokoe for sharing his enthusiasm and ideas while I was designing the testing component of my research. I would like to thank Dr. Jorge Prozzi for sharing his invaluable experience regarding pavements during our long drives for the field trips. I would also like to thank Dr. Bob Gilbert for sharing his wealth of knowledge, particularly through his coursework at UT. I have tremendous respect for Dr. Gilbert's ability to inspire students to learn. I would also like to express my sincerest gratitude to Dr. Eric Becker for his interest in this research and for his willingness to serve on my dissertation committee. I appreciate the time that all of my committee members have invested in this research; over the course of my doctoral research, our discussions challenged my abilities as a graduate student and strengthened my research.

This research was funded by the Texas Department of Transportation. I appreciate the support I received from TxDOT staff at different stages of this research. In particular, I would like to thank Darlene Goehl for investing her time and energy in coordinating the project and arranging field visits. I value the opportunity to work on a project that has deepened my understanding of geosynthetic reinforcement and will hopefully serve as a solid base for future work in this field.

I would also like to convey my thanks to Sam Allen and John Allen at TRI, Austin for allowing me to conduct initial testing at their laboratory. I am grateful to Rob Swan for helping me in the design of the new pullout box system. His accessibility, patience and knowledge made him an invaluable resource. The help from the geosynthetic manufacturers, Tensar and Mirafi, in supplying the material for my research is also acknowledged.

Sincere gratitude is also expressed to the administrative staff at the Civil Engineering Department, specifically to Teresa Tice-Boggs and Chris Trevino from Geotechnical Engineering Center and Kathy Ross from Graduate Studies Office. Their support, quick wit and skill made my life as a graduate student easier.

I would like to thank my undergraduate advisor Dr. S.C. Dhawan from PEC, Chandigarh for motivating me to pursue graduate studies. Also, I would like to thank professors Dr. K.G. Sharma, Dr. Manoj Datta and Dr. G.V. Rao from my masters program for guiding me during my stay at IIT, Delhi. Special thanks to Dr. A. Varadarajan, Dr. G.V. Ramana, Dr. Kalra, Dr. Khitoliya and Dr. Devgun for helping me with my decision to study abroad.

I would like to thank my friends and colleagues who I came to know during my stay in Austin. In particular, I would like to thank John for being my mentor during my initial years of PhD; Julio, Jeff and Emily for diligently reviewing my dissertation and for giving me insights into how to improve my work; Jongwan and Danny for helping with the pullout test; Albert for critiquing my research and posing the tough questions, pushing me to learn; William and Aviral for being amazing roommates; Christine, Nate and Brian for discussing strategies to combat stress during these times. Special thanks to friends (Mary, Tony, Lou, Jennie, Kimberly, Ayman, Kwangsoo, Choi, Min Jae, Pooyan, Rami, Shalini, Himanshu, Vishal, Amit, Summet, Sashank, Prachi, Sid, Rutu, Karan, Michael, Dennis and Martin). It was great to have you people around during these years of my life; I thoroughly enjoyed your company.

I would also like to acknowledge the support of my friends from undergraduate degree years (Goel, Bubber, Bansal, Garg, Mansa, Aggarwal, Jindal, Kathuria, Rathi, Rastogi, Monu and Sunil). Also, special thanks to Bansal bhaiya and Ashima didi. Thanks to all of you, for bearing with me.

Most importantly, my eternal gratitude goes to my grandparents (Nanaji, Nanima, Mataji and Baiji). Thanks to my family (my father, my mother and my sister) for their support. All of you have kept me in good spirits with your love and humor over all these years. It is because of all of you that I have been able to pursue and achieve my goals.

A Study of Geosynthetic Reinforced Flexible Pavement System

Publication No._____

Ranjiv Gupta, Ph.D.

The University of Texas at Austin, 2009

Supervisor: Jorge G. Zornberg

The use of geosynthetics as reinforcement for the base layer of flexible pavement systems has grown steadily over the past thirty years. In spite of the evidence that geosynthetic reinforcements can lead to improved pavement performance, the specific conditions or mechanisms that enable and govern the reinforcement are unclear, largely remaining unidentified and unmeasured. The appropriate selection of design parameters for geosynthetics is complicated by the difficulty in associating their relevant properties to the improved pavement performance. In addition, pavement structures deteriorate under the combined effects of traffic loading and environmental conditions, such as moisture changes. However, these factors have not been studied together in the evaluation of the overall performance of pavement systems. Consequently, this research focused on the assessment of the effect of geosynthetics on the pavement structural section's ability to support traffic loads and to resist environmental changes. Accordingly, the primary objectives of this research were: (i) to determine the governing mechanisms and relevant properties of geosynthetics that contribute to the enhanced performance of pavement systems; (ii) to develop appropriate analytical, laboratory and field methods that are capable of quantifying the above properties for geosynthetics; and (iii) to enable the prediction of pavement performance depending on the various types of geosynthetics

used. To fulfill these three objectives, an evaluative, laboratory and field study was performed. The improved performance of pavements due to addition of geosynthetics was attributed to the ability of geosynthetics to laterally restrain the base course material, thereby providing a confinement effect to the pavement. A parameter to quantify the soil-geosynthetic interaction at low displacement magnitudes based on the solution of an analytical model for geosynthetics confined in pullout box was proposed. The pullout tests were then conducted on various geosynthetics to obtain the proposed parameter for various geosynthetics. The quantitative magnitude of the parameter value from the laboratory tests was compared with the qualitative performance observed in the field test sections. Overall, a good agreement was obtained between the laboratory and field results, thereby providing confidence in the ability of the proposed analytical model to predict the governing mechanism for geosynthetic reinforced pavements.

Table of Contents

Table of Contents x

List of Tables xix

List of Figures xxii

Chapter 1: Introduction 1

1.1 Research motivation 1

1.2 Benefits of using geosynthetics in flexible pavements 2

1.3 Methods to investigate geosynthetic behavior in flexible pavements 3

1.4 Research objectives 4

1.5 Dissertation outline 5

Chapter 2: Geosynthetic Reinforced Pavements – An Evaluative Study 6

2.1 Introduction 6

2.2 Philosophy of geosynthetic reinforced flexible pavements 7

2.2.1 Flexible pavements 7

2.2.1.1 Critical points in pavement design 8

2.2.1.2 Type of pavement distress 9

2.2.2 Geosynthetics 10

2.2.2.1 Geogrids 11

2.2.2.2 Geotextiles 12

2.2.3 Reinforcement function 13

2.2.3.1 Lateral Restraint 16

2.2.3.2 Increased bearing capacity 16
2.2.3.3 Tensioned membrane effect 17
2.2.4 Discussion 17
2.3 Design methodologies for geosynthetic reinforced flexible pavements 18
2.3.1 AASHTO Guide (1993) 19
2.3.1.1 Traffic Benefit Ratio 20
2.3.1.2 Base Course Reduction 21
2.3.1.3 Limitations 22
2.3.2 NCHRP Mechanistic-Empirical Guide (2004) 23
2.3.2.1 Applicability to geosynthetic reinforced pavement design 26
2.3.2.2 Limitations 26
2.3.3 Discussion 27
2.4 Performance data for geosynthetic reinforced flexible pavements 28
2.4.1 Field tests 29
2.4.1.1 Types of test tracks 29
2.4.1.2 Types of distress measurement techniques 30
2.4.1.3 Discussion 32
2.4.2 Laboratory tests 33
2.4.2.1 Unconfined tests 34
2.4.2.2 Confined tests 38
2.4.2.3 Discussion 47
2.4.3 Numerical methods 50

2.4.3.1 Finite element method.....50
2.4.3.2 Discrete element method.....52
2.4.3.3 Discussion.....53
2.5 Conclusions of the literature review.....54
Chapter 3: Geosynthetic Reinforced Pavements – An Analytical Study.....56
3.1 Introduction.....56
3.2 Pullout testing of geosynthetics.....58
3.2.1 Mechanisms involved.....58
3.2.2 Effect of boundary conditions.....60
3.2.3 Limit equilibrium methods.....64
3.3 Materials used.....66
3.3.1 Properties of soils used.....66
3.3.1.1 Subgrade soil.....66
3.3.1.2 Base course.....70
3.3.2 Characteristics of geosynthetics used.....72
3.3.2.1 Percent open area.....73
3.3.2.2 Rib thickness.....73
3.3.2.3 Single rib tensile test.....73
3.3.2.4 In-isolation junction strength test.....76
3.3.2.5 Wide width tensile testing.....79
3.3.3 Discussion.....81
3.4 Coefficient of interaction.....81

3.4.1 Test Matrix 81
3.4.2 Test Apparatus 82
3.4.3 Test Preparation 84
3.4.4 Testing Procedure 85
3.4.5 Results 86
3.4.6 Limitations 88
3.5 Analytical model for pullout test 89
3.5.1 Governing differential equation 90
3.5.1.1 Shear stress-confined force relationship 91
3.5.1.2 Confined force-strain relationship 91
3.5.1.3 Strain-displacement relationship 92
3.5.2 Assumptions involved 93
3.5.2.1 Geosynthetic load-strain relationship 93
3.5.2.2 Absolute movement of soil surrounding the geosynthetic 95
3.5.2.3 Shear stress- relative displacement relationship at the interface 96
3.5.3 Displacement distribution along geosynthetic length 97
3.5.4 Boundary conditions 99
3.5.4.1 Constant strain distribution 100
3.5.4.2 Linear strain distribution 102
3.5.5 Discussion 103
3.6 Soil-geosynthetic interaction model 103
3.6.1 Proposed solution 104

3.6.2 Parameter for geosynthetic reinforced pavement 107
3.6.3 Parameter estimation using pullout tests.....110
3.6.4 Repeatability of the estimated parameter.....117
3.6.5 Discussion.....120
3.7 Conclusions.....121
Chapter 4: Geosynthetic Reinforced Pavements - A Laboratory Study 122
4.1 Introduction.....122
4.2 Pullout test equipment.....123
4.2.1 Rate of testing 124
4.2.2 Normal pressure system.....125
4.2.3 Clamping system.....127
4.2.4 Displacement measurement system 128
4.2.5 Data acquisition system 129
4.2.6 Discussion.....130
4.3 Description of pullout testing program 133
4.3.1 Testing Matrix.....133
4.3.2 Soil.....137
4.3.3 Test setup 140
4.4 Tests on geosynthetics using pullout equipment 142
4.4.1 Series I: Tests conducted to calibrate the model.....142
4.4.1.1 Baseline test 143
4.4.1.2 Repeatability 151

4.4.1.3 Effect of specimen length 154
4.4.1.4 Effect of specimen width 158
4.4.1.5 Effect of normal pressure 162
4.4.1.6 Effect of orientation 165
4.4.1.7 Discussion 167
4.4.2 Series II: Comparison between two geogrids of same material 169
4.4.2.1 Materials used 169
4.4.2.2 Scope of testing program 170
4.4.2.3 Pullout Test results 171
4.4.2.4 Discussion 176
4.4.3 Series III: Test on geogrid made of different material 176
4.4.3.1 Material used 176
4.4.3.2 Scope of testing program 177
4.4.3.3 Test results 178
4.4.3.4 Discussion 180
4.5 Discussion of results from pullout tests on geosynthetics 181
4.5.1 Machine direction 181
4.5.2 Cross-Machine direction 184
4.5.3 Unconfined and Confined stiffness 186
4.5.4 Discussion 187
4.6 Conclusions 188
Chapter 5: Geosynthetic Reinforced Pavements - A Field Study 190

5.1 Introduction....190
5.2 Types of distress in flexible pavements....191
5.2.1 Mechanism of longitudinal crack development....192
5.2.2 Remedial measures adopted....193
5.2.3 Discussion....195
5.3 Case studies....196
5.3.1 Case History 1....199
5.3.2 Case History 2....201
5.3.3 Case History 3....203
5.3.4 Discussion....206
5.4 Field test section....208
5.4.1 Site Details....209
5.4.2 Average Annual Daily Traffic....210
5.4.3 Weather Conditions....210
5.4.4 Pre-construction field evaluation....211
5.4.5 Reconstruction of FM-2 site....214
5.4.6 Layout of Test Sections....216
5.4.7 Post-construction field evaluation....218
5.4.8 Discussion....223
5.5 Evaluation of moisture sensor information....224
5.5.1 Moisture sensor details....225
5.5.2 Moisture sensor calibration....226

5.5.3 Moisture sensor installation 227
5.5.3.1 Horizontal moisture sensor installation 229
5.5.3.2 Vertical moisture sensor installation.....231
5.5.4 Moisture sensor results 232
5.5.4.1 Horizontal Moisture Profile Results from Sensors 233
5.5.4.2 Vertical Moisture Profile Results from Sensors 235
5.5.5 Discussion.....239
5.6 Field monitoring using condition survey 239
5.6.1 Field surveying details 239
5.6.2 Performance of test sections 241
5.6.2.1 Control test section 242
5.6.2.2 Lime treated unreinforced test sections 244
5.6.2.3 Reinforced non lime-stabilized test sections.....247
5.6.2.4 Reinforced lime-stabilized test sections.....250
5.6.2.5 Comparison of test sections performance 251
5.6.3 Discussion.....253
5.7 Field monitoring using falling weight deflectometer.....254
5.7.1 FWD testing details.....254
5.7.2 Performance of test sections 256
5.7.3 Comparison of test sections 258
5.7.3.1 Effect of lime stabilization.....258
5.7.3.2 Effect of geosynthetic reinforcement.....259

5.7.3.3 Effect of geosynthetic reinforcement and lime stabilization ...260
5.7.4 Discussion 261
5.8 Conclusions 262
Chapter 6: Summary and Conclusions 264
6.1 Summary of research components 264
6.2 Conclusions from evaluative study 266
6.3 Conclusions from analytical study 267
6.4 Conclusions from laboratory study 267
6.5 Conclusions from field study 268
6.6 Recommendations for future research 268
References 270
Vita 281

List of Tables

Table 2.1 Features of confined tests 47

Table 2.2 FEM studies for geosynthetic reinforced flexible pavement design.....50

Table 3.1 Main features of pullout boxes developed in various pullout studies....62

Table 3.3 Properties of base course material 71

Table 3.4 Manufacturer's specification for the geogrids 72

Table 3.5 Single rib tensile testing results for the geogrids 76

Table 3.6 Junction efficiency results for the geogrids 78

Table 3.7 Wide width tensile tests results for the geogrids 81

Table 3.8 Testing matrix for pullout test to determine coefficient of interaction..82

Table 3.9 Coefficient of interaction obtained from the pullout tests 88

Table 4.1 Testing matrix for large scale pullout testing 136

Table 4.2 Soil properties of Monterey No. 30 sand.....138

Table 4.3 Mechanical properties of Monterey No. 30 sand (Li, 2005) 138

Table 4.4 Wide width tensile tests results for the geotextile 143

Table 4.5 Computation for yield shear stress.....146

Table 4.6 Regression analysis to obtain K_{SGI} 150

Table 4.7 Repeatability of test results.....153

Table 4.8 Effect of specimen length on K_{SGI}.....158

Table 4.9 Effect of specimen width on K_{SGI}.....161

Table 4.10 Effect of normal pressure on K_{SGI} 164

Table 4.11 Effect of specimen direction on K_{SGI}.....165

Table 4.12 Properties of geogrids G1 and G4 (Tensar, 2002) 170

Table 4.13 Effect of geogrid type on K_{SGI}.....174

Table 4.14 Effect of geogrid testing orientation on K_{SGI}.....174

Table 4.15 Results for geosynthetic G2 testing 179

Table 4.16 Comparison of K_{SGI} for geosynthetics in machine direction 183

Table 4.17 Comparison of K_{SGI} for geosynthetics in cross-machine direction....184

Table 4.18 Comparison of unconfined and confined stiffness of geosynthetics .186

Table 5.1 Summary of survey response of TxDOT districts 197

Table 5.2 Comparison of Geogrid (type 1 and 2) properties with project specifications given by TxDOT.....202

Table 5.3 Details of test section at FM 1915 205

Table 5.4 Mean values for pavement modulus obtained using Modulus 6.0, for various pavement layers of the three test sections at FM 1915 205

Table 5.5 Navasota 30 Year Climate Averages and Records 210

Table 5.6 Profiles used in field monitoring study at FM-2.....215

Table 5.7 Numbering system adopted to identify individual test section.....216

List of Figures

Figure 1.1 Conceptual life-cycle cost illustration for reinforced and unreinforced pavements (adapted from Perkins et. al, 2005).....2

Figure 2.1 Typical examples of soil reinforcement application (Palmeira, 1987)...6

Figure 2.2 Cross-section of flexible pavement system (Muench, 2006) 7

Figure 2.3 Stress distributions with depth in a flexible pavement (a) high stress area directly under wheel load; (b) reduced load at subgrade level 8

Figure 2.4 Geosynthetics used as reinforcement (a) woven geotextile (b) non-woven geotextile (c) geogrid (d) geocells (adapted from Bathurst, 2007)...10

Figure 2.5 Geogrid reinforcements (adapted from Zornberg et.al, 2008) 11

Figure 2.6 Geotextiles (a) woven and non-woven (b) nomenclature (adapted from Zornberg et.al, 2008).....12

Figure 2.7 Relative load magnitudes at subgrade layer level for: (a) unreinforced flexible pavement and (b) geosynthetic-reinforced flexible pavement14

Figure 2.8 Reinforcement mechanisms induced by geosynthetics (Holtz et. al, 1998): (a) Lateral restraint; (b) Increased bearing capacity; and (c) Membrane-type support.....15

Figure 2.9 Evolution of pavement design methods (adapted from Reck, 2009) ...18

Figure 2.10 Typical TBR values for an unreinforced and reinforced pavement to reach a given rut depth (Shukla, 2002) 21

Figure 2.11 Flowchart for M-E Design (NCHRP, 2004).....24

Figure 2.12 Comparison of Resilient Modulus, M_R, and Modulus of Elasticity, E. (adapted from Abusaid, 2006) 25

Figure 2.13 Interrelationship between different facets of pavement design (adapted from Hugo et. al, 1991).....28

Figure 2.14 APT test facilities (a) ATLAS at the Illinois Center for Transportation, USA; (b) a pavement fatigue carousel at LCPC, France 29

Figure 2.15 Non-destructive testing methods used in the current research study include: (a) a Falling Weight Deflectometer, and (b) a Rolling Dynamic Deflectometer.....31

Figure 2.16 Additional forces due to soil-geosynthetic interaction when a lateral restraint mechanism occurs in a pavement (adapted from Perkins, 1999) 33

Figure 2.17 Wide-width tensile frame with roller grips at the University of Texas at Austin.....35

Figure 2.18 Geogrid specimens for biaxial testing (McGown et al., 2005).....36

Figure 2.19 Torsional rigidity tests (Kinney and Yuan, 1995).....37

Figure 2.20 Cyclic plate load test (Perkins, 1999).....39

Figure 2.21 Cyclic triaxial test (a) Test equipment (Perkins et al., 2004); (b) Schematic of test setup (Tutumluer, 2004).....40

Figure 2.22 Cyclic pullout test (a) Plan view (b) Side view (c) Loading protocol (adapted from Cuelho and Perkins, 2005) 42

Figure 2.23 Bending stiffness test (a) Actual test apparatus (b) Schematic of the test (c) Deviator stress and recoverable deformation plots for a typical test (adapted from Abusaid, 2006) 44

Figure 2.24 Modified pavement analyzer test (a) schematic of the test (b) APA testing machine (c) modified box (d) geosynthetic placed in the middle of the box (e) base course layer over the geosynthetic (f) test with loaded wheels (g) rut observed at the end of test (h) rut measurement using dial gauge (adapted from Han et al., 2008).....46

Figure 2.25 Soil-geosynthetic interface test (a) Modified direct shear test (b) Pullout test (adapted from Palmeria, 2008).....49

Figure 2.26 Flexible pavement (a) Finite element model (b) Horizontal stress vs. strain profile for various cases (adapted from Perkins and Edens, 2002) 51

Figure 2.27 Discrete element model (a) pullout test with cubic clumps (b) pullout test with embedded geogrid (c) aperture of geogrid (d) detailed view at node (adapted from McDowell et al., 2006).....52

Figure 3.1 Geosynthetic reinforced pavement (a) Mechanism of lateral restraint in field under traffic loads (b) Replicating field behavior with laboratory plane- strain test using pullout device.....56

Figure 3.2 Soil reinforcement interaction mechanisms when geosynthetic is subjected to pullout force (a) cross- section of geotextile specimen (b) forces on geotextile (c) cross-section of geogrid specimen (d) forces on geogrid (adapted from Elias et al., 2001).....59

Figure 3.3 Grain size distribution for subgrade soil 67

Figure 3.4 Plasticity chart for subgrade soil 67

Figure 3.5 Standard Proctor compaction test for subgrade soil.....68

Figure 3.6 Effective vertical stress-strain curve for subgrade soil.....68

Figure 3.7 Hydraulic conductivity of subgrade soil.....69

Table 3.2 Properties of subgrade soil.....69

Figure 3.8 Grain size distribution curve for base course material 70

Figure 3.9 Standard Proctor Compaction curve for base course material 71

Figure 3.10 Geosynthetics used in pullout test (a) G1 (b) G2 72

Figure 3.11 Percent open area of geogrid (Source: TxDOT Laboratory, Austin) .73

Figure 3.12 Single rib tensile test results for geogrids: (a) G1-machine, (b) G1-cross machine, (c) G2-machine, (d) G2-cross machine direction.....74

Figure 3.13 Single rib tensile testing of geogrids: (a) Specimen clamped at the grips (b) Specimen after the test (Source: TxDOT Laboratory, Austin) ...76

Figure 3.14 Junction strength test results for geogrids: (a) G1-machine (b) G1-cross machine (c) G2-machine (d) G2-cross machine direction.....77

Figure 3.15 Wide width tensile test setup for (a) Geogrid G1 (b) Geogrid G2 79

Figure 3.16 Wide width tensile test results for geosynthetics: (a) G1-machine (b) G1-cross machine (c) G2-machine (d) G2-cross machine direction.....80

Figure 3.17 Pullout test setup.....82

Figure 3.18 Pullout test apparatus: (a) Air flow pump; (b) Rubber membrane; (c) Wide-plate compaction rod; (d) Vibratory hammer; (e) LVDT's 83

Figure 3.19 Pullout test preparation: (a) Compaction of bottom half of box; (b) Attaching the geosynthetic specimen to the grips; (c) Attaching tell tale wires to the specimen; (d) Compacting top half of the box; (e) Assembling normal pressure system.....84

Figure 3.20 Tensile mode of failure due to: (a) slippage at the clamping grips; (b) rupture of the specimen at the end of the test 85

Figure 3.21 Typical pullout test load-displacement curve for a given geogrid 86

Figure 3.22 Variation of maximum pullout force with confining pressure and soil type for geogrids: (a) G1 -MD (b) G1-XD (c) G2-MD (d) G2-XD 87

Figure 3.23 Axial load-strain relationship for various reinforcements with soil (adapted from McGown et al., 1978).....90

Figure 3.24 Free body diagram for geosynthetic element of length ∂x in pullout test 91

Figure 3.25 Response of geosynthetic: (a) Unconfined force (b) Confined force (c) Longitudinal ribs mobilized under unconfined loads (d) Both longitudinal and transverse ribs mobilized under confined loading conditions.....94

Figure 3.26 Difference between confined and unconfined stiffness of a geosynthetic 95

Figure 3.27 Shear stress distribution as a function of displacement at a given point97

Figure 3.28 Predictions based on constant strain distribution: (a) Schematic of displacement profile for given pullout force (b) actual vs. predicted strain distribution (c) actual vs. predicted displacement.....101

Figure 3.29 Pullout test model for hypothetical point xi: (a) Location inside the pullout box (b) Assumed frontal force vs. displacement profile at any given time t 111

Figure 3.30 Distribution for hypothetical point xi based on the proposed model: of (a) Frontal force Fp, (b) Displacement, w(x), (c) Confined force F(x), at any given time t.....112

Figure 3.31 Based on proposed model, for hypothetical point xi: (a) F (xi) vs. w (xi), (b) KSGI, at any given time t.....114

Figure 3.32 Pullout test on a geosynthetic: (a) Instrumented points at distance x_1, x_2 and x_3 (b) Frontal pullout force vs. displacement profile for three points 117

Figure 3.33 Based on analysis of pullout test data, profiles at three points for any given time t: (a) Displacement with length (b) Force with length..118

Figure 3.34 Confined force vs. measured displacement profile at point: (a) x_1 (b) x_2 (c) x_3.....119

Figure 3.35 Plot for given soil-geosynthetic system at known confining pressure for all LVDT's used during a test: (a) Confined force vs. displacement (b) K_{SGI} 120

Figure 4.1 Hydraulic system for controlling rate of pullout testing 124

Figure 4.2 Normal pressure system (a) Air cylinders on top of compressed plywood (b) Top plates acting as the reaction system 126

Figure 4.3 Automated hoist system used to assemble the reaction frame 126

Figure 4.4 Clamping system (a) Original design consisting of plastic sheets (b) Modified design with roller grips 127

Figure 4.5 Displacement measurement system: (a) spring loaded LVDT (b) support system for attaching LVDT to the pullout box 129

Figure 4.6 Data acquisition system (a) USB-device (b) Frontal unit with a chassis130

Figure 4.7 Large scale pullout testing equipment: (a) Side view; (b) Top view .131

Figure 4.8 Large scale pullout box testing equipment.....132

Figure 4.9 Monterey No. 30 sand bags.....137

Figure 4.10 Gradation curve of Monterey No. 30 sand (Li, 2005).....137

Figure 4.11 Results of triaxial compression test on Monterey No.30 sand: (a) deviatoric stress and axial strain; (b) volumetric and axial strain; and (c) compression and volumetric strain, (Yang, 2009).....139

Figure 4.12 Pullout test setup (a)First layer of soil (b) Compaction to slit level (c) Placement of the geosynthetic (d) Attaching the LVDT's (e) Compacting the soil on top of specimen (f) Placing the plywood boards (g) Installing air cylinders (h) Assembling reaction frame.....141

Figure 4.13 Geosynthetic used for baseline tests (a) Geotextile (G3); (b) specimen used in wide-width tensile test.....142

Figure 4.14 Wide width tensile test results for geotextile at different strain rates (a) Machine direction (b) Cross-Machine direction.....143

Figure 4.15 Location of LVDT's on geosynthetic specimen for test I-1 with dimensions of 0.6m confined length and 0.45m width (All dimensions in millimeters).....144

Figure 4.16 Frontal pullout force vs. displacement curve for each LVDT.....144

Figure 4.17 Computation of yield shear stress parameter graphically (a) Frontal pullout force and displacement as function of time from start of test; (b) Frontal pullout force vs. active length of the reinforcement.....145

Figure 4.18 Confined force vs. displacement curve for baseline test.....147

Figure 4.19 Estimating K_{SGI} graphically.....148

Figure 4.20 Comparison of measured and predicted data for frontal pullout force vs. displacement for the baseline test 150

Figure 4.21 Test conducted for repeatability: (a) Frontal pullout force vs. displacement for LVDT 1 in Test I-1 and Test I-2 (b) Yield shear stress for test I-2.....151

Figure 4.22 Comparison of confined force vs. displacement profile for test I-1 and test I-2: (a) LVDT 1 (b) LVDT 2.....152

Figure 4.23 Comparison of K_{SGI} values obtained for test I-1 and I-2 graphically153

Figure 4.24 LVDT location for test I-3 and test I-4 of specimen width of 0.45 m and confined length: (a) 0.9 m; (b) 0.3 m (All dimensions in millimeters)154

Figure 4.25 Frontal pullout force vs. displacement for test I-1, I-2, I-3 and I-4 at location: (a) LVDT 1 (b) LVDT 2 155

Figure 4.26 Yield shear stress for (a) test I-3, (b) test I-4.....156

Figure 4.27 Confined force vs. displacement for test I-1, I-2, I-3 and I-4 at point x_2 157

Figure 4.28 Comparison of K_{SGI} value obtained for test I-1, I-2, I-3 and I-4 157

Figure 4.30 Comparison of frontal pullout force vs. displacement response for test I-4 and I-5 159

Figure 4.31 Dilation mechanisms for narrow and wide specimens in pullout test (adapted from Ghionna et al., 2001) 160

Figure 4.32 Yield shear stress calculation for test I-5 160

Figure 4.33 Comparison of K_{SGI} values for test I-4 and test I-5 161

Figure 4.34 Frontal pullout force vs. displacement for test I-1, I-6 and I-7 for LVDT 2 162

Figure 4.35 Yield shear stress for (a) Test I-6 at 7 kPa (b) Test I-7 at 35 kPa normal pressure 163

Figure 4.36 Confined force vs. displacement for Test I-1, I-6 and I-7 (a) LVDT 1 (b) LVDT 2 163

Figure 4.37 Comparison of K_{SGI} for test I-1, I-6 and I-7 to quantify effect of normal pressure 164

Figure 4.38 Comparison of tests (I-1 and I-8) conducted to evaluate effect of specimen direction on parameters: (a) Maximum pullout force (b) Yield shear stress (c) K_{SGI} 166

Figure 4.39 Geogrids: (a) Tensar BX-1100 (G1); (b) Tensar BX 1200 (G4) (adapted from Finnefrock, 2008) 169

Figure 4.40 Frontal pullout force vs. displacement for G1 and G4: (a) 7kPa; (b) 21kPa; (c) 35 kPa 171

Figure 4.41 Yield shear stress for G1 and G4: (a) 7kPa; (b) 21kPa; (c) 35 kPa..172

Figure 4.42 K_{SGI} for G1 and G4: (a) 7kPa; (b) 21kPa; (c) 35 kPa.....173

Figure 4.43 Comparison of tests conducted to evaluate effect of specimen orientation on parameters for geogrid G1 and G4: (a) Maximum pullout force (b) Yield shear stress (c) K_{SGI} 175

Figure 4.44 Geogrid G2 with machine and cross-machine direction 177

Figure 4.45 Tests conducted to evaluate effect of confining pressure on parameters for geogrid G2 in cross machine direction: (a) Maximum pullout force (b) Yield shear stress (c) K_{SGI} 178

Figure 4.46 Comparison of tests conducted to evaluate effect of specimen direction on parameters for geogrid G2: (a) Maximum pullout force (b) Yield shear stress (c) K_{SGI}.....180

Figure 4.47 Comparison of tests conducted in machine direction for geosynthetics G1, G2, G3 and G4: (a) Maximum pullout force (b) Yield shear stress (c) K_{SGI}.....182

Figure 4.48 Comparison of tests conducted in cross-machine direction for geosynthetics G1, G2, G3 and G4: (a) Maximum pullout force (b) Yield shear stress (c) K_{SGI}.....185

Figure 5.1 Mechanisms of pavement deflection over expansive clay subgrades: (a) settlements during dry season, (b) heave during wet season. 192

Figure 5.2 Typical longitudinal crack developed on pavements over expansive clays 193

Figure 5.3 Typical pavement cross-section of a low-volume road in Central Texas using reinforcement for mitigation of cracks induced by expansive subgrades.....194

Figure 5.4 Map showing usage of geosynthetics in Texas based on districts which responded to the survey 197

Figure 5.5 Map showing location of the three site a) FM 542 b) FM 1744 c) FM 1915 199

Figure 5.6 Typical cross-section of pavement at FM 542 199

Figure 5.7 Longitudinal cracks in the unreinforced section of FM 542 pavement200

Figure 5.8 A typical geogrid reinforced pavement section at FM 1774 201

Figure 5.9 (a) Longitudinal crack on the pavement reinforced with geogrid type 2 (b) Slippage between longitudinal and transverse ribs at junction of geogrid type 2.....202

Figure 5.10 Project details and cross section of test sections at FM 1915 site....204

Figure 5.11 (a) Location of FM 2 relative to Houston and Austin; (b) Layout of FM 2 209

Figure 5.12 Wet and dry season at the site based on 30 year average climate data211

Figure 5.13 GPS marking for FM 2 road close to FM-362 end.....212

Figure 5.14 Preliminary results of non-destructive testing at FM 2 212

Figure 5.15 Cross section of the FM 2 pavement before reconstruction 213

Figure 5.16 Cross section of the FM-2 pavement during scarification.....214

Figure 5.17 Pavement test sections at FM- 2: (a) Unreinforced without lime stabilization; (b) Unreinforced with lime stabilization; (c) Reinforced without lime stabilization; (d) Reinforced with lime stabilization .215

Figure 5.18 Schematic layout of the test section as per station number on FM 2 site 217

Figure 5.19 Distance of weather station from the site 218

Figure 5.20 Data collected from Hempstead weather station for (a) Precipitation (b) Relative humidity and temperature.....219

Figure 5.21 Details of borehole sampling operation (a) Rig placed at marked location (b) Auger and split spoon being assembled (c) Auger driven into the soil (d) Sampler retrieved from the borehole (e) 0-5 feet of sample obtained (f) 5-10 feet of sample obtained consisting of black clay followed by sand clay.....220

Figure 5.22 Gravimetric water content profiles from the boreholes for January and August 2006 at: (a) Station 184; (b) Station 199 221

Figure 5.23 Shrinkage limit of the soil based on drying of cores 222

Figure 5.24 Profile at FM-2 for (a) subgrade cross-section based on borehole survey (b) pavement cross-section based on elevation survey 222

Figure 5.25 Instruments used in field study (a) Moisture sensor (b) Data logger225

Figure 5.26 Devices used for calibration of moisture sensors (a) Rectangular mould (b) Piston compactor 226

Figure 5.27 Moisture sensor calibration for subgrade soil 227

Figure 5.28 Moisture migration below pavement (a) Sources of water entry (b) Flow boundary conditions.....228

Figure 5.29 Horizontal array of moisture sensors.....229

Figure 5.30 Horizontal Moisture sensor installation procedure: (a) Trenching; (b) Separation of base and subgrade layer; (c) Leveling of installation site; (d) Tools for insertion of sensor; (e) Pre-insertion slit into the subgrade; (f) Installed sensor; (g) Compaction near sensor head; (h) Data logger; (i) Protective tube and casing for data logger 230

Figure 5.31 Vertical array of moisture sensors.....231

Figure 5.32 Vertical Moisture sensor installation procedure: (a) Trenching; (b) Placing sensors in protective tubing; (c) Pre-insertion slit into the soil; (d) Placing the protective tube in the trench; (e) Data logger; (f) Backfilling the trench.....232

Figure 5.33 Time series of moisture data for each sensor at Station 84 233

Figure 5.34 Comparison of data obtained from weather station and edge moisture sensor 234

Figure 5.35 Isochrones of moisture data for each sensor at Station 84 234

Figure 5.36 Time series of gravimetric water content data for Station 184 235

Figure 5.37 Time series of gravimetric water content data for Station 199 236

Figure 5.38 Isochrones for vertical moisture sensor array at stations (a) 184 (b) 199 237

Figure 5.39 Comparison of top moisture sensors located at station 84 and 199 .237

Figure 5.40 Change in water content of the surface sensor (152 mm): (a) Station 184; (b) Station 199.....238

Figure 5.41 Tools used during field visual inspection of the FM-2 pavement: (a) Measurement devices, (b) Surveying datasheet.....240

Figure 5.42 Development of crack at a location over time (a) November 2006; (b) November 2007; (c) August 2008; (d) August 2009 241

Figure 5.43 Continuous cracks through three section due to steep slope on east side of the pavement; (a) 6Ea (b) 7Ea, (c) 8Ea.....242

Figure 5.44 Location of control section on FM-2 road.....243

Figure 5.45 Longitudinal crack in different stages in sections (a) 1Ea, (b) 1Eb, (c) 1Wa, and (d) 1Wb.....243

Figure 5.46 Type of distress observed in the control section (a) Bleeding; (b) Potholes; (c) Lane to shoulder drop off; (d) Raveling and weathering244

Figure 5.47 Location of lime treated no-reinforcement sections on FM-2 road..245

Figure 5.48 Longitudinal crack in section 5Ea (a) No cracking till May 2009 (b) Appearance of cracks in August 2009 246

Figure 5.49 Distress cracking in test section 5Eb.....246

Figure 5.50 Location of no-lime treated geosynthetic reinforced sections on FM-2 road 247

Figure 5.51 Performance of geosynthetic reinforced non-lime treated test sections (a) G1 (b) G2 (c) G3.....248

Figure 5.52 Checking integrity of geosynthetic reinforced non-lime treated test sections (a) G1; (b) G2; (c) G3 249

Figure 5.53 Location of lime treated geosynthetic reinforced sections on FM-2 road 250

Figure 5.54 Soil profiles at two lime treated geosynthetic reinforced sections based on the borehole survey (a) Station 84 (b) Station 199 251

Figure 5.55 Stages in crack propagation (a) Unreinforced section (b) Reinforced section 252

Figure 5.56 Analysis procedure adopted for FWD data analysis of a given field trip (a) Four load levels used at a section (b) Average deflection value for a series of test sections used to compare their relative performance.255

Figure 5.57 Test sections used in FWD analysis 256

Figure 5.58 Deflection profile in February 2006 and 2009 (a) Control (b) Geosynthetic reinforced non lime stabilized (c) Lime stabilized unreinforced (d) Lime stabilized geosynthetic reinforced test sections257

Figure 5.59 Deflection profile for control and lime stabilized unreinforced section for (a) February 2006 (b) February 2009.....258

Figure 5.60 Deflection profile for three geosynthetic reinforced and non- lime stabilized sections for (a) February 2006 (b) February 2009.....259

Figure 5.61 Deflection profile for three geosynthetic reinforced and lime stabilized sections for (a) February 2006 (b) February 2009 260

Chapter 1: Introduction

"If you think education is expensive, try ignorance!"
Derek Bok

1.1 RESEARCH MOTIVATION

The objective of this research is to provide a better understanding of the mechanisms governing the performance of geosynthetic reinforced pavements. During the course of this research, a literature review revealed that numerous studies have been conducted to quantify the effectiveness of geosynthetics in pavements (Al-Qadi 1997; Berg et al. 2000; Fanin 1996; Perkins and Ismeik 1997). Through empirical observations these studies concluded that geosynthetic reinforced base course and subgrade layers enhanced pavement performance. However, the actual mechanisms governing the contribution of geosynthetics to pavement stability have not been clearly identified.

While geosynthetics have been used in pavements for the past thirty years, there is still a lack of test methods to quantify the benefits of geosynthetics and the variables governing their design. Furthermore, the proliferation of geosynthetic products and the aggressive marketing by the manufacturers have made it difficult for designers to identify the appropriate geosynthetic to be used in a specific project. Also, in projects that have used different geosynthetics in the field, results from the post-construction evaluation of the performance of these systems are controversial, thus making it difficult to determine design guidelines for future projects.

This research includes a reevaluation of existing design methodologies, a process that involved obtaining data to quantify the performance response of geosynthetic reinforced pavement sections. The overall goal of this research is to identify the mechanism governing geosynthetic reinforced flexible pavement and then to develop the appropriate tools to measure it with a laboratory tests. The results obtained from the laboratory setup were then verified against the performance of geosynthetic reinforced test sections constructed in the field environment, thereby combining these approaches in a unified framework.

1.2 BENEFITS OF USING GEOSYNTHETICS IN FLEXIBLE PAVEMENTS

There are two main benefits of using geosynthetics in the form of geogrids and geotextiles in the base course layer of flexible pavements. For a given cross-section of the pavement, addition of geosynthetic leads to an increase in serviceability life and reduction in the maintenance cost of the pavement as shown in Figure 1.1a and 1.1b respectively. This alternative is feasible when the maintenance and replacement costs during the service life of the pavement are offset by the high initial cost of using the geosynthetic for a given project (Perkins and Ismeik, 1997). Also, if the pavement is designed for same serviceability life as an unreinforced pavement, addition of geosynthetic may results in the reduction in the thickness of the base course layer. This alternative is feasible if the cost of the geosynthetic is less than the combined cost of the replaced base course material and any construction related costs associated with a reduced base thickness (Perkins and Ismeik, 1997). Both of the above alternatives are desirable, as part of the design process involves minimizing the total cost of the pavement structure, including initial costs plus maintenance costs. The savings of 10-20% of total project cost have been estimated by combining these benefits (Berg et al., 2000).

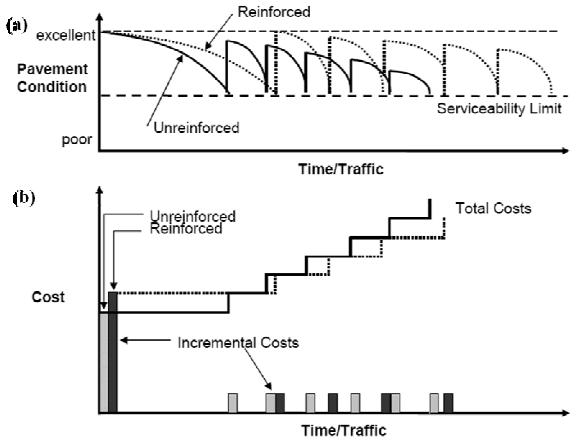

Figure 1.1 Conceptual life-cycle cost illustration for reinforced and unreinforced pavements (adapted from Perkins et. al, 2005)

The aforementioned benefits are primarily related with the ability of geosynthetic reinforcement to resist traffic loads. However, the pavement structures deteriorate as a result of the combined effects of traffic and environment-related damage. An additional use of geosynthetics in flexible pavement to resist environmental loads has been proposed recently (Zornberg and Gupta, 2009). The benefits involve the mitigation of longitudinal cracks when pavements are constructed over expansive subgrades. The construction of roadways over these subgrades (which are common in central and eastern Texas) have lead to significant volume changes during subsequent cycles of seasonal wetting and drying due to moisture fluctuations. These volume changes induce vertical movements, accelerate the degradation of pavement materials, and ultimately shorten the service life of the roadway. The specific problem addressed in this research included the occurrence of longitudinal cracks that develop due to above environmental loading on pavements constructed over such expansive subgrades.

In summary, the current research focuses on evaluating the benefits of using geosynthetics in improving pavement performance under traffic loads and preventing longitudinal cracks over expansive subgrades due to environmental loads.

1.3 METHODS TO INVESTIGATE GEOSYNTHETIC BEHAVIOR IN FLEXIBLE PAVEMENTS

According to Zornberg (1994), "In the geosynthetic reinforced structures, practice often leads theory, so the optimum design methods incorporating performance prediction criteria which help in fully understanding the behavior of structure may not exist." Also, the study of geosynthetic reinforced pavement involves a complex interaction between its various components which cannot be fully characterized using a single method. Therefore, numerical modeling, laboratory testing and instrumentation of field structures are generally used together to understand the principles of soil reinforcement interaction and the mechanism that characterize their behavior. The research needs for this study were addressed using all the above methods to understand the behavior of geosynthetic reinforced pavements.

The research included an analytical treatment of the governing mechanisms responsible for pavement performance when geosynthetics were used as reinforcements. Then, laboratory testing in the form of pullout tests was conducted to quantify the mechanisms at low displacements, taking into account the interaction of the geosynthetic with surrounding soil under applied confinement at low displacement magnitudes. To fully understand the effectiveness of geosynthetics in flexible pavement, full scale pavement test sections with different geosynthetics were constructed and monitored. Finally, the laboratory pullout test results based on analytical model were validated against the performance of field test sections reinforced with various geosynthetics thereby combining all the research components in a unified framework.

1.4 RESEARCH OBJECTIVES

The specific objectives of this study are the following:

- Identify the governing mechanism involved in geosynthetic reinforced pavement design to resist environmental and traffic loads;
- Identify the soil-geosynthetic interaction parameters governing these mechanisms;
- Develop an analytical model to quantify these soil-geosynthetic interaction parameters realistically;
- Develop laboratory testing procedures based on analytical model for quantification of soil-geosynthetic interaction under confinement at low displacements magnitudes;
- Establish a unified framework for providing a consistent basis of comparison for predicting the performance of various geosynthetics (geotextiles and geogrids) using laboratory tests; and
- Validate the findings of the laboratory tests against the performance of field sections for these geosynthetics.

1.5 DISSERTATION OUTLINE

This dissertation is organized into six chapters. After this introductory chapter, the background information on the use of geosynthetics as reinforcement in flexible pavements is provided in Chapter 2. It summarizes the existing pavement design methodologies for incorporating the use of geosynthetics as reinforcement. This chapter also includes a review of the literature on the field, laboratory and numerical methods being used to quantify the performance of the geosynthetic reinforced pavement system.

Based on the review of the literature presented in Chapter 2, the laboratory test method to quantify the governing mechanism for geosynthetic reinforced pavement is established. The pullout test method and its application to reinforced pavement design are discussed in Chapter 3. This discussion is followed by the development of an analytical model to quantify the soil-geosynthetic interaction behavior under pullout test conditions. The model assumptions and its applicability for predicting the performance of various geosynthetics is then discussed.

The validation of model using laboratory pullout tests is described in Chapter 4. This involves the development of new laboratory equipment for conducting tests on geosynthetics to evaluate the model assumptions. This is followed by a series of pullout tests on various types of geosynthetics and obtaining the model parameter to compare their performance under confined conditions to represent the field conditions realistically.

A field investigation study to evaluate the performance of geosynthetic reinforced test sections for environmental and traffic loads is presented in Chapter 5. The details of the field study involving thirty two test sections with post construction monitoring in the form of moisture monitoring using sensors, FWD testing and visual inspection is provided. The results of field performance of geosynthetic reinforced sections are then compared with parameter obtained from laboratory tests.

A summary of the conclusions drawn from each research component conducted as part of this dissertation is finally presented in Chapter 6.

Chapter 2: Geosynthetic Reinforced Pavements – An Evaluative Study

"Common sense in an uncommon degree is what the world calls wisdom."
Samuel Taylor Coleridge

2.1 INTRODUCTION

Soil reinforcement involves the placement of a material in a given soil layer where the presence of the material causes a redistribution of stresses and strains in the soil favorable to the purpose at hand (Palmeira, 1987). Currently, soil reinforcement is most commonly performed with geosynthetics, leading to an increase in the strength and a decrease in the compressibility of the composite material. In other words, the addition of geosynthetic reinforcement in regions of tensile strain helps to inhibit the stresses in the soil, thereby increasing the shearing characteristics of the composite material (Jewell, 1981). The common usage for soil-geosynthetic reinforcement includes the construction of roads, retaining walls, foundations and embankments, as shown in Figure 2.1. The current research focused on the application of geosynthetic reinforcement in the base-course layer of flexible pavements. The review of work completed is described in this chapter.

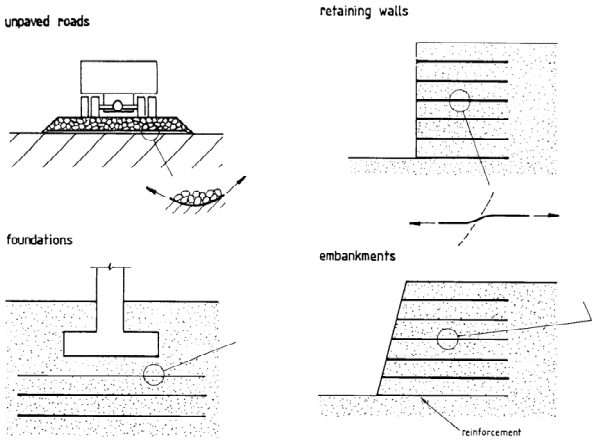

Figure 2.1 Typical examples of soil reinforcement application (Palmeira, 1987)

2.2 PHILOSOPHY OF GEOSYNTHETIC REINFORCED FLEXIBLE PAVEMENTS

To highlight the significance of the current research, a literature review centered on flexible pavements, geosynthetics, and the function of geosynthetics in these pavements is provided below.

2.2.1 Flexible pavements

According to Huang (1993), "Flexible pavements are layered systems with better material on top where intensity of stress is high and inferior materials on the bottom where the intensity is low. Adherence to this design principle makes possible the use of local materials and usually results in a most economical design. This is particularly true in regions where high quality materials are expensive but local materials of inferior quality are readily available."

A typical flexible pavement system is composed of four distinct layers: asphalt concrete, base course, subbase, and subgrade as shown in Figure 2.2. The surface layer is typically asphalt concrete which is composed of a bituminous hot-mix aggregate (HMA) obtained from distillation of crude petroleum. The asphalt concrete is underlain by a layer of base course, typically consisting of 6 to 12 inches of unbound coarse aggregate. An optional subbase layer generally composed of lower quality crushed aggregate can be placed down before the base course to achieve cost savings or reduce capillary action of moisture under the pavement. The constructed layers are placed directly onto a prepared subgrade which is generally graded and compacted natural in-situ soil.

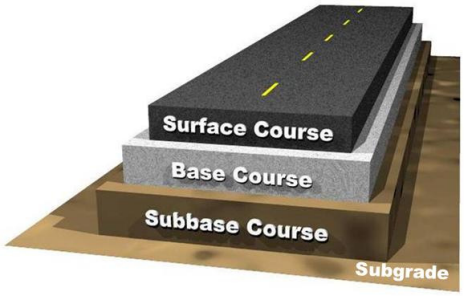

Figure 2.2 Cross-section of flexible pavement system (Muench, 2006)

2.2.1.1 Critical points in pavement design

Flexible pavements are constructed so that traffic loads are distributed from the contact surface to the underlying layers. The pavement flexes under the load, resulting in a conical stress distribution that spreads the load over a greater area than that of the actual tire footprint. Consequently, stresses imparted by the wheel load are effectively dissipated with depth as shown in Figure 2.3. The flexible pavement design is checked for two critical strain points. The horizontal tensile strain at the bottom of asphalt layer is used as a design parameter to prevent fatigue cracking which occurs due to repeated traffic loading. On the other hand, the vertical stress on the top of subgrade is an important factor in the design in order to prevent permanent deformations, which occur due to the accumulation of stress during the service life of the pavement.

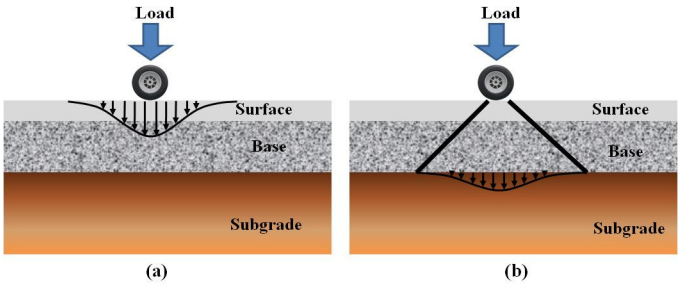

Figure 2.3 Stress distributions with depth in a flexible pavement (a) high stress area directly under wheel load; (b) reduced load at subgrade level

A pavement's function is to reduce the vertical stress on the subgrade so that detrimental pavement deformations do not occur. The allowable vertical stress on a given subgrade depends on the shear strength of the subgrade. The effect of stress and strength is combined together in a form of allowable vertical compressive strain, which is used as design criteria. Therefore, according to Yoder and Witczak (1975), “the basic concept of granular base flexible pavements is to provide a base thickness such that the vertical compressive subgrade stress is reduced to some limit value less than the allowable distress level developed from the relevant criteria.”

2.2.1.2 Type of pavement distress

During its lifetime, a flexible pavement can experience two different types of failure modes. Structural failure leads to the collapse of the pavement, thereby making it incapable of sustaining the loads imposed upon its surface. Functional failure, on the other hand, renders the pavement incapable of carrying out its intended function, causing discomfort to the passenger. Subsequently, structural failure requires a complete rebuilding of the pavement whereas functional failure can be remedied by the regular maintenance of the pavement.

The above distress conditions may develop due to two main reasons: traffic loads and environmental conditions. Traffic loads result from the high repetition of loads and from high tire pressure, which can cause either structural or functional failure. Secondly, climatic conditions, such as extreme variations in temperature and moisture values at the site, as well as environmental loading, cause surface irregularities and structural weaknesses in the pavement. The wetting and drying, or the freezing and thawing of the pavement causes base course materials to breakdown generating fines in the subgrade which lead to the development of cracks. Furthermore, construction practices also affect pavement distress conditions. For example, the use of unclean aggregates and inadequate inspection lead to rapid pavement deterioration. Finally, according to Yoder and Witczak (1975), “pavement distress is also a function of maintenance or more correctly, lack of maintenance.” Therefore, sealing cracks and joints at proper intervals and maintaining the shoulders help improve pavement performance.

Based on the above discussion, it can be seen that pavement distress is a combination of different factors. Therefore, when designing a pavement, it is not only necessary to build into the design the pavement's resistance against structural failure, it is also imperative to ensure that the pavement will carry out its intended function. Ultimately, a pavement's intended longevity represents a calculated decision on the part of the engineer who balanced increased initial construction costs against increased maintenance costs during the design process.

2.2.2 Geosynthetics

Geosynthetics can be defined as planar products manufactured from polymeric material, which are used with soil, rock or other geotechnical engineering related material as an integral part of a man-made project, structure or system (ASTM, 1995). Geosynthetics are manufactured in factory-controlled environments and widely used in many geotechnical and transportation applications. Geosynthetics have numerous material properties which are important during their manufacturing, quality control process and use in design. The material properties related to the manufacture and quality control of geosynthetics are generally referred to as index properties while those that are related to the design are known as performance properties.

Considering their different properties, several geosynthetic products can perform different functions and, consequently, they should be designed in order to satisfy the minimum criteria needed to adequately perform these functions. The main functions of geosynthetics used in soil reinforcement are: separation, reinforcement, filtration, drainage, infiltration barrier, and protection. The geosynthetics typically used for reinforcement are as shown in Figure 2.4. Among these products, geotextiles and geogrids have been used in pavement applications for reinforcement purposes and are the focus of this study.

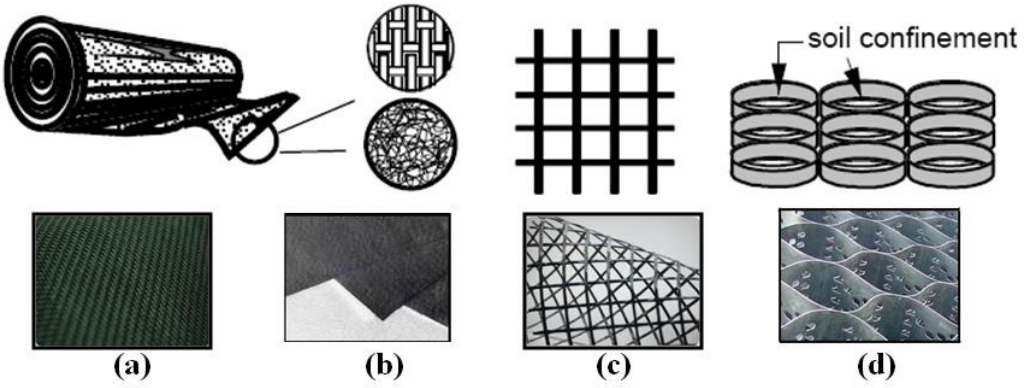

Figure 2.4 Geosynthetics used as reinforcement (a) woven geotextile (b) non-woven geotextile (c) geogrid (d) geocells (adapted from Bathurst, 2007)

2.2.2.1 Geogrids

Geogrids constitute a category of geosynthetics that are designed primarily to fulfill a reinforcement function. They have found numerous applications in transportation projects (Zornberg and Christopher, 2000; Zornberg et al., 2001). Geogrids have a uniformly distributed array of apertures between their longitudinal and transverse elements. The openings allow direct contact between soil particles on either side of the installed sheet, which increases the interaction between the geogrid and the backfill soil.

Geogrids are composed of polypropylene, polyethylene, polyester, or coated polyester. The polyester geogrids and coated polyester geogrids are flexible, and their junctions are typically woven, knitted or laser bonded. Coating is generally performed using PVC or acrylics to protect the filaments from construction damage. The polypropylene and polyethylene geogrids are rigid, and either extruded or punched sheet drawn. These geogrids have in- plane ribs with integral junctions. Geogrids are classified by whether they can provide resistance to in-plane loads in one direction (uniaxial) or any direction (biaxial) as shown in Figure 2.5. Uniaxial geogrids are often appropriate for walls and slopes, but biaxial geogrids are preferred for base reinforcement in pavements.

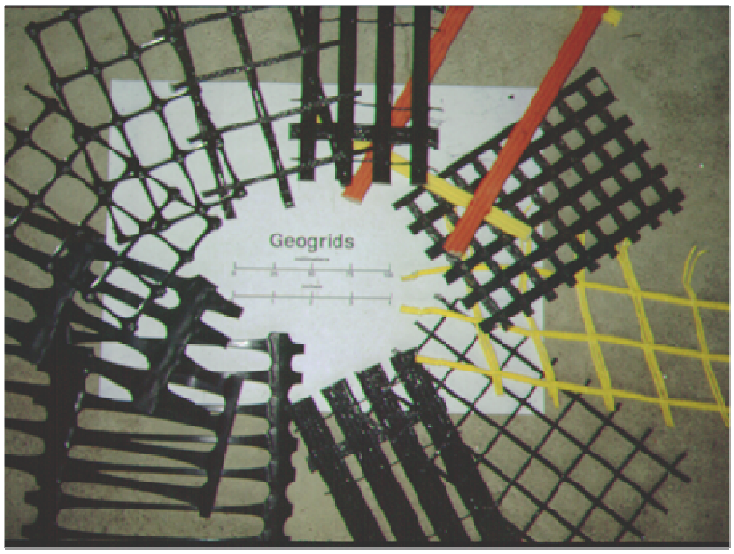

Figure 2.5 Geogrid reinforcements (adapted from Zornberg et.al, 2008)

2.2.2.2 Geotextiles

Geotextiles are defined as a permeable geosynthetic made of textile materials. Among the different geosynthetic products, geotextiles are the ones that present the widest range of properties (Zornberg and Christopher, 2006) and can be used to fulfill variety of functions for many different geotechnical, and transportation applications.

The polymers used in the manufacture of geotextile fibers include the following: polypropylene (≈85%), polyester (≈12%), polyethylene (≈2%), and polyamide (≈1%). The most common types of filaments used in the manufacture of geotextiles include monofilament, multifilament, staple filament and slit-film. Figure 2.6a shows a number of typical geotextiles. Woven geotextiles are manufactured using traditional weaving methods and a variety of weave types: plain weave, basket weave, twill weave and satin weave. Non-woven geotextiles are manufactured by placing and orienting the filaments or fibers onto a conveyor belt, which are subsequently bonded by needle punching or by melt bonding. Common terminology associated with geotextiles includes machine direction, cross machine direction, and selvage as shown in Figure 2.6b. Machine direction refers to the direction in the plane of the fabric in line with the direction of manufacture. Conversely, cross machine direction refers to the direction in the plane of fabric perpendicular to the direction of manufacture. The selvage is the finished area on the sides of the geotextile width that prevents the yarns from unraveling.

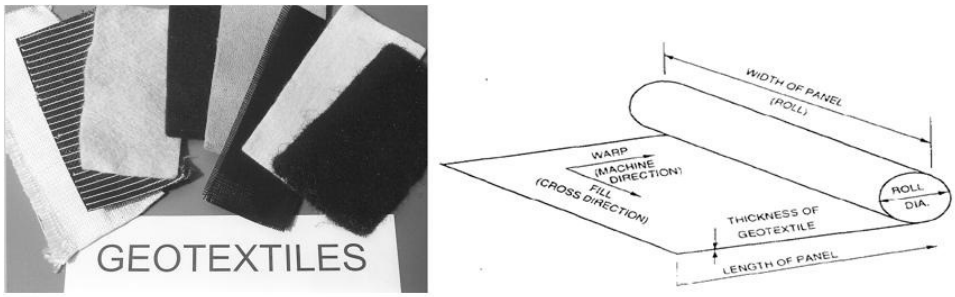

(a) **(b)**

Figure 2.6 Geotextiles (a) woven and non-woven (b) nomenclature (adapted from Zornberg et.al, 2008)

2.2.3 Reinforcement function

The typical functions of geosynthetics used in the construction of roadways include reinforcement, separation, filtration, lateral drainage and sealing (Koerner, 2005). The purpose of using a geosynthetic in its reinforcement capacity is to increase the structural or load-carrying capacity of a pavement system by transferring the load to the geosynthetic material. When performing its separation function, a geosynthetic prevents the subgrade soil from intruding into the aggregate base or sub-base. The potential for the mixing of soil layers is greatest when the base course is compacted over the subgrade during construction and secondarily, during the operation of traffic. Additionally, a geosynthetic performs a filtration function by restricting the movement of soil particles while allowing water to move from the filtered soil to the coarser soil adjacent to it over the lifespan of the structure's performance. The need for filtration is strongly dependent on the fines content of the base course and subgrade soils and on the plasticity limit of the subgrades. Finally, the lateral drainage function, i.e. the transmissivity function of a geosynthetic, allows the lateral movement of water within the plane of the geosynthetic. Besides these four functions, geosynthetics can perform secondary functions like the mitigation of crack propagation by sealing the asphalt layer when used in the overlay of the pavement.

Certain geosynthetic products can perform different functions while, similarly, the same function can often be performed by different types of geosynthetics. Geogrids, however, are generally used for only one primary function (reinforcement) in pavement design. Geotextiles, however, can also perform one or more secondary functions, which must also be considered when selecting the geotextile material for optimum performance. For example, a geotextile can provide for the separation of two dissimilar soils (for example, the separation of gravel from clay in a road), but it may also provide a secondary function of filtration by minimizing the buildup of excess pore water pressure in the soil beneath the separator.

This research effort focused on quantifying the reinforcement function of geosynthetics in flexible pavements. Reinforcement is the synergistic improvement of the pavement created by the introduction of a geosynthetic into a pavement layer. While the function of reinforcement has often been fulfilled by geogrids, geotextiles have been used extensively as reinforcement inclusions in transportation applications (Bueno et al. 2005, Benjamin et al. 2007). The stress distribution at the level of subgrade layer for an unreinforced flexible pavement is generally higher than that for a geosynthetic reinforced pavement as shown in Figures 2.7a and 2.7b respectively. The addition of geosynthetic for reinforcement purposes generally involves placing it at the interface between the base and sub-base layers or the interface between the sub-base and subgrade layers. This leads to stress redistribution at the subgrade layer, causing reduced vertical deformations and improved performance of the pavement.

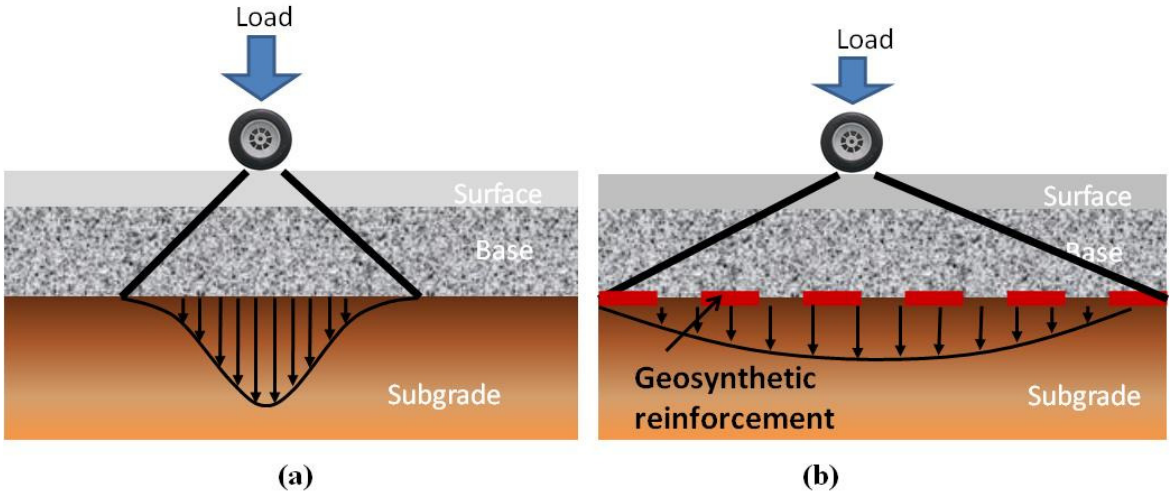

Figure 2.7 Relative load magnitudes at subgrade layer level for: (a) unreinforced flexible pavement and (b) geosynthetic-reinforced flexible pavement

The improved performance of the pavement due to geosynthetic reinforcement has been attributed to three main mechanisms (Giroud and Noiray, 1981; Giroud et al., 1984; Perkins and Ismeik, 1997; Holtz et al., 1998). Specifically, the reinforcement

function performed by a geosynthetic is thought to be achieved primarily through: (1) lateral restraint; (2) increased bearing capacity; and (3) the tensioned membrane effect produced by the geosynthetic when it is placed within the base course or subgrade layers or when it is placed as the interface between these two layers as shown in Figure 2.8. The theory behind these three phenomena or mechanisms was originally based on observations and analyses done for unpaved roads. The relevance of these mechanisms for paved roads (flexible pavements) is discussed.

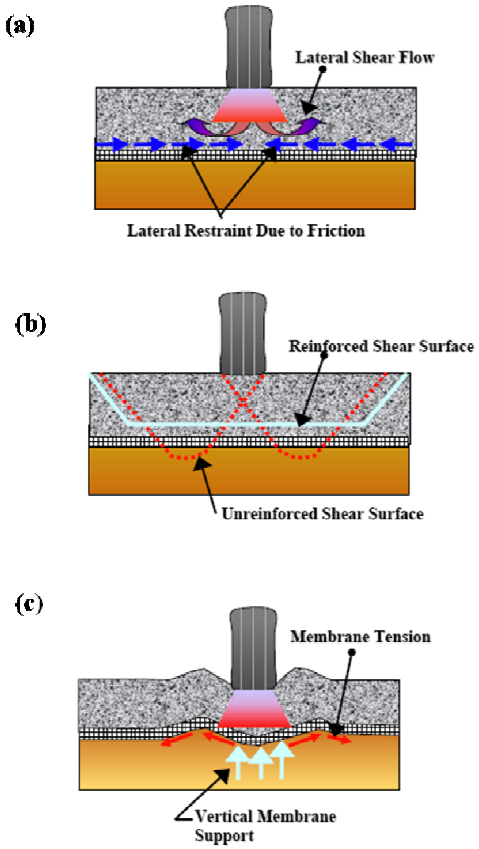

Figure 2.8 Reinforcement mechanisms induced by geosynthetics (Holtz et. al, 1998): (a) Lateral restraint; (b) Increased bearing capacity; and (c) Membrane-type support

2.2.3.1 Lateral Restraint

The primary mechanism associated with the reinforcement function is lateral restraint or confinement (Bender and Barenberg, 1978) for paved flexible pavements as shown in Figure 2.8a. The name is misleading as lateral restraint is developed through interfacial friction between the geosynthetic and the aggregate, thus the mechanism is one of a shear-resisting interface (Perkins, 1999). When an aggregate layer is subjected to traffic loading, the aggregate tends to move laterally unless it is restrained by the subgrade or geosynthetic reinforcement. Interaction between the base aggregate layer and the geosynthetic transfers shear load from the base layer to a tensile load in the geosynthetic. The geosynthetic has high tensile stiffness and limits the extensional lateral strains in the base layer. Furthermore, a geosynthetic layer confines the base course layer thereby increasing its mean stress and leading to an increase in its shear strength. Both frictional and interlocking characteristics between the soil and the geosynthetic are necessary to realize this mechanism. For a geogrid, this implies that the geogrid apertures and base soil particles must be sized properly. A geotextile with good frictional capabilities can also provide tensile resistance to lateral aggregate movement.

2.2.3.2 Increased bearing capacity

As shown in Figure 2.8b, the increased bearing capacity mechanism leads to soil reinforcement when the presence of a geosynthetic causes the potential bearing surface failure plane to develop at an alternate, higher shear strength surface. This forced initiation of the potential failure surface along an alternate plane, with modified configuration, provides a higher total resistance. The geosynthetic reinforcement can decrease the shear stresses transferred to the subgrade and provide vertical confinement outside the loaded area. The bearing failure mode of the subgrade is expected to change from punching failure without reinforcement to general failure with ideal reinforcement.

2.2.3.3 Tensioned membrane effect

The theory of tensioned membrane type of support of the wheel loads as shown in Figure 2.8c. In this case, the reinforcement provides a vertical component of reaction to the applied wheel load. This tensioned membrane effect develops as a result of vertical deformations creating a concave shape in the geosynthetic. This tensioned membrane effect develops as a result of vertical deformations creating a concave shape in the geosynthetic. The tension developed in the geosynthetic helps support the wheel load and reduce the vertical stress on the subgrade, but significant rut depths are necessary to realize this effect. Generally, higher deformation is required for the mobilization of tensile membrane resistance as the stiffness of the geosynthetic decreases. In order for this type of reinforcement mode to be significant, there is a consensus that the subgrade CBR should be less than 3 (Barksdale et al., 1989).

2.2.4 Discussion

The three mechanisms require different magnitudes of deformation in the pavement system to occur in the field. Since the early study of geosynthetic reinforcement of base course layers focused on unpaved roads where rut depths in excess of 25 mm were tolerable, the increased bearing capacity and tensioned membrane support mechanisms were included for paved roads, too. However they exceed the serviceability requirements of paved roads (flexible pavements). Thus, when the flexible pavement is loaded, lateral restraint is generated due to the development of interface shear stresses and the interlocking between geosynthetics and aggregate, leading to the transfer of the load from the aggregate to the geosynthetics, thereby governing its performance.

The current research focused on quantifying the primary mechanism of lateral restraint provided by geosynthetics in flexible pavements for reinforcement purposes which is developed at very low displacement magnitudes. Section 2.3 discusses the various design methodologies currently adopted for design of geosynthetic reinforced flexible pavements.

2.3 DESIGN METHODOLOGIES FOR GEOSYNTHETIC REINFORCED FLEXIBLE PAVEMENTS

The basic philosophy of flexible pavement systems was originally envisioned by the Romans and it continues to form the basis of flexible pavement design today. This approach involves providing a protected layer over the subgrade, thereby ensuring the serviceability of the pavement under given traffic and environmental loading. Figure 2.9 shows the evolution of road design methods from the 1930s until today.

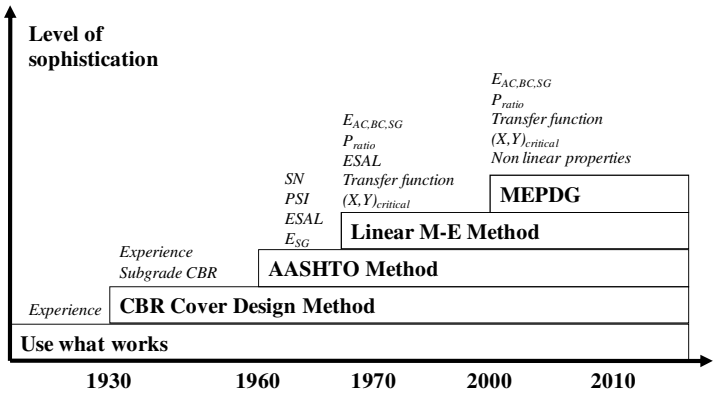

Figure 2.9 Evolution of pavement design methods (adapted from Reck, 2009)

After the great depression in the 1930s, the Cover Based Design Method was developed. It required a single input in terms of the California Bearing Ratio (CBR), but it still involved a significant amount of engineering judgment. Following the American Association of State Highway Officials (AASHO) Road Test, which was popularized in the 1960s, a series of design methods were proposed that were more sophisticated than the Cover Based Method and that required greater number of design inputs. For example, in the 1970's, the linear mechanistic-empirical (M-E) design method was proposed by researchers from South Africa. Since the early 1990s, the focus has shifted to mechanistic-empirical design methods that incorporate features from purely empirical methods to sophisticated finite element non-linear mechanized methods. Attempts have been made to incorporate the geosynthetic reinforcement into AASHO and M-E design methods. The advantages and limitations of these approaches for designing geosynthetic reinforced flexible pavements are discussed.

2.3.1 AASHTO Guide (1993)

Published in 1993, the American Association of State Highway and Transportation Officials' (AASHTO) guide for design of pavement structures is one of the most widely used methods for flexible pavement design in North America. The AASHTO guide uses empirical equations developed from the AASHO road tests, which were conducted in the late 1950s. The method considers the pavement to be a multi-layer elastic system with an overall structural number (SN) that reflects the total pavement thickness and its resiliency to repeated traffic loading. The required SN is selected such that the pavement will support anticipated traffic loads and experience a loss in serviceability no greater than that allowed based on the requirements for the pavement. The SN is determined using a nomograph that solves the following equation:

$$\log W_{18} = Z_R \times S_O + 9.36 \times \log(SN+1) - 0.2 + \frac{\log\frac{\Delta PSI}{2.7}}{0.4 + \frac{1094}{(SN+1)^{5.19}}} + 2.32 \log M_R - 8.07 \qquad (2.1)$$

where W_{18} is the anticipated cumulative 18-kip Equivalent Single-Axle Loads (ESALs) over the design life of the pavements, Z_R is the standard normal deviate for reliability level, S_O is the overall standard deviation, Δ_{PSI} is the allowable loss in serviceability, and M_R is the resilient modulus (stiffness) of the underlying subgrade. Once the required overall SN has been determined, the individual layers can be designed according to Equation 2.2 through a series of iterations:

$$SN = (a \times d)_{hma} + (a \times d \times m)_{base} + (a \times d \times m)_{subbase} \qquad (2.2)$$

where,

a = coefficient of relative strength,

d = thickness in inches of each layer,

m= modifier accounting for moisture characteristics of the pavement

The purpose of geosynthetic reinforcement in flexible pavements is to extend a pavement's lifespan or to enable the construction of a pavement with a reduced quantity of base course material without sacrificing pavement performance. The early design of reinforced flexible pavements focused at modifying Equations 2.1 and 2.2 to reflect the benefit achieved by the addition of geosynthetics to its structure. These improvements to the pavement system provided by geosynthetic reinforcement have been measured in terms of ratios and expressed in design equations as shown below.

2.3.1.1 Traffic Benefit Ratio

Traffic Benefit Ratio (TBR), as per Berg et al. (2000), is defined as the ratio of the number of load cycles on a reinforced section (N_R) to reach a defined failure state (a given rut depth) to the number of load cycles on an unreinforced section (N_U), with the same geometry and material constituents, to reach the same defined failure state.

$$TBR = \frac{N_R}{N_U} \tag{2.3}$$

While designing a pavement using TBR, the extended life of pavement is estimated as follows:

$$W_{18}\,(reinforced) = TBR * W_{18}\,(unreinforced) \tag{2.4}$$

TBR is sometimes referred to as the traffic improvement factor (TIF). The TBR is commonly used to relate the long-term performance of reinforced and unreinforced pavements. As shown in Figure 2.10, it is also used to calculate the number of traffic passes that a reinforced pavement can withstand as compared to unreinforced pavement for the same rut depth. For most geotextiles, the range in TBR value lies between 1.5 and 10, and for geogrids between 1.5 and 70, as reported by Shukla (2002).

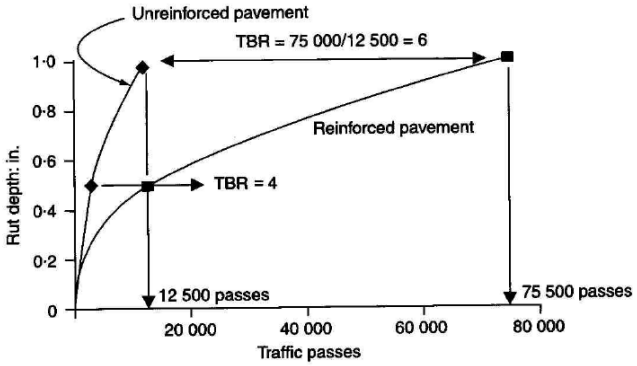

Figure 2.10 Typical TBR values for an unreinforced and reinforced pavement to reach a given rut depth (Shukla, 2002)

2.3.1.2 Base Course Reduction

Base course reduction (BCR) is defined as the percent reduction in the base-course or sub-base thickness layer due to an addition of geosynthetic reinforcement (T_R) when compared with the unreinforced thickness (T_U) of the flexible pavement with the same material constituents, to reach the same defined failure state.

$$BCR = \frac{T_R}{T_U} \tag{2.5}$$

BCR is sometimes referred to as the layer coefficient ratio (LCR). A modifier is applied to the SN of the pavement, as shown in Equation 2.6.

$$SN = (a \times d)_{hma} + BCR.(a \times d \times m)_{base} + (a \times d \times m)_{subbase} \tag{2.6}$$

While designing a pavement using BCR, the reduced depth of the base course can be estimated as follows:

$$d_{base,(R)} = \frac{SN_u - (a \times d)_{hma} - (a \times d \times m)_{subbase}}{BCR.(a \times m)_{base}} \quad (2.7)$$

where $d_{base,(R)}$ is the reduced base course thickness due to reinforcement and SN_u is the structural number corresponding to the equivalent W_{18} for the unreinforced pavement.

BCR has been determined from the laboratory and field tests. Anderson and Killeavy (1989) constructed test sections with different base course thicknesses within an access road and truck staging area. The study showed that geotextile reinforced section with 350 mm base layer performed similar to unreinforced section with 450 mm thick base layer. Miura et al. (1990) constructed field test sections of road that contained 50 mm less of base course than the unreinforced section and were observed to perform better than the control sections for all the rut depths. Furthermore, for a subgrade with CBR of 8, Webster (1993) showed that a section containing a geogrid with 150 mm thick base had equivalent performance to an unreinforced section with 250 mm thick base. Thus, base course reductions in the range of 20% to 40% have been reported in the literature with greater percentage reduction for the stronger subgrade materials.

2.3.1.3 Limitations

The AASHTO design method is empirical in nature and does not directly consider the mechanics of the pavement structure, climatic effects, or changes in traffic loading and material properties over the design-life of the pavement. The correlation to CBR and the Texas Triaxial Test are used to determine appropriate layer coefficients which provide the strength of material at failure whereas the stiffness at low displacement is key for pavement design. Moreover, when this design methodology is extended to geosynthetic reinforced pavements they are limited in their application to the specific product, material, geometry, failure criteria and load used in the tests to quantify their values. Thus, they lack a generic approach and cannot be easily transferred from one site to another.

Moreover, the method above is not capable of providing a consistent base for performance comparison between various geosynthetics. In addition to this drawback, it is difficult to incorporate these ratios into the design for a particular project if the goal of geosynthetic reinforcement is to provide both functions, i.e. to increase the pavement's performance life and to reduce the base course thickness. Therefore, every time a design has to be done using geosynthetics, one needs to assess the applicability of these proposed ratios to project-specific criteria. Although research conducted to date has supported some of the suggested procedures, long-term performance information of projects designed based on this method is not available at this time such that confidence limits can be established.

2.3.2 NCHRP Mechanistic-Empirical Guide (2004)

The National Cooperative Highway Research Program (NCHRP) developed a guide for mechanistic-empirical design of new and rehabilitated pavement structures in 2004. The method uses mechanistic principles and detailed data input to minimize design reliance on empirical observations and correlations which may or may not be applicable for a specific application. The mechanistic-empirical (M-E) method is an attempt to improve design reliability, reduce life-cycle costs, better characterize the effects of drainage and seasonal moisture variations, and to help predict susceptible failure modes to prevent premature failures (Olidis and Hein, 2004).

The M-E Design Method is a road performance prediction method that has two key components, which are mechanistic and empirical, and interdependent. The calculation models require input parameters in terms of pavement layers, traffic conditions, climatic conditions and materials used. The output generated is then measured against the original design hypothesis and if it fails, the design is modified using an iterative process and then re-evaluated. The flowchart of the various components in the design method is as shown in Figure 2.11.

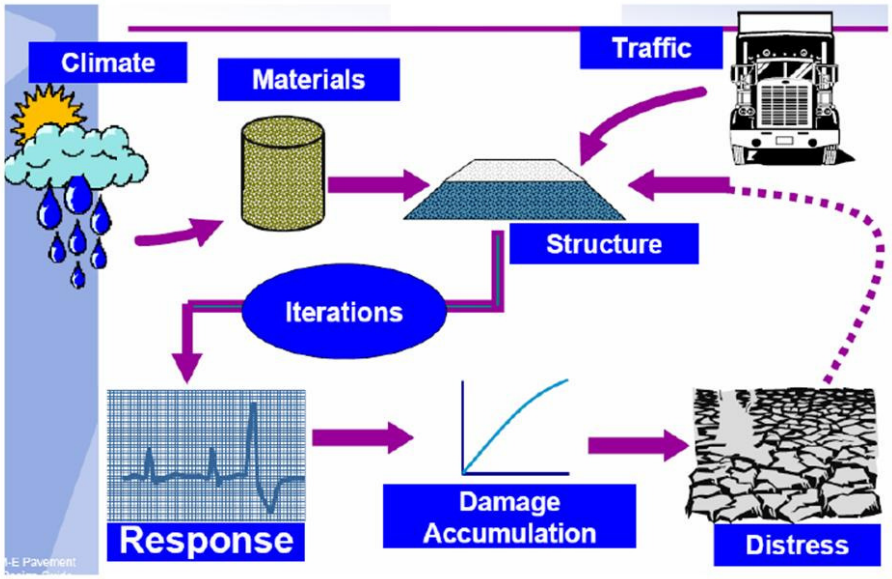

Figure 2.11 Flowchart for M-E Design (NCHRP, 2004)

According to Finnefrock (2008), "The primary parameters used in M-E method are the mechanistic properties of each pavement layer, which include poisson's ratio (□) and resilient modulus (M_R). Poisson's ratio is the ratio of lateral strain to axial strain exhibited in response to axial loading and typically ranges from 0.15-0.5 for materials used in pavement design. The M_R is a representation of the Modulus of Elasticity (E) after cyclic loading," and is given by:

$$M_R = \frac{\sigma_d}{\varepsilon_r} \tag{2.8}$$

where σ_d is the cyclic deviator stress (or cyclic principal stress difference) and ε_r is the recoverable (elastic) strain. Thus, M_R and E represent the strain response of the material to applied stress, but are not considered the same due to different load application rates as shown in Figure 2.12. Furthermore, the value of E refers to the initial deformation (with some permanent component) of the material, whereas M_R refers to the elastic deformation of the material after cyclic loading.

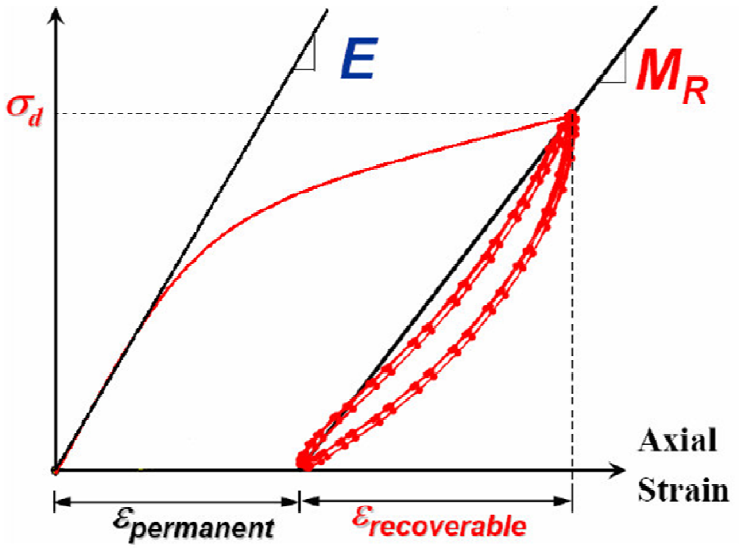

Figure 2.12 Comparison of Resilient Modulus, M_R, and Modulus of Elasticity, E. (adapted from Abusaid, 2006)

The M-E method uses a hierarchical approach to design, based on the importance of the project and available information. Level 1 is the highest confidence level, typically reserved for research or very high volume roads. Level 2 is moderate confidence level, intended for routine pavement design. Level 3 is the lowest confidence level, typically reserved for low-volume roads. Based on the design level selected, the material properties are determined using the specific materials to be used in the field, or are estimated from the correlations using routine tests or by using default values from the database.

The mechanistic properties of pavement materials are used to estimate stresses and displacements under loading. These estimates are in turn converted into pavement surface distresses using regression models of the Long Term Pavement Performance (LTPP) program database, which contains comprehensive data from field-scale road test sections. Surface distresses are broadly classified into three groups: fracture, deformation, and degradation. These surface distresses can be used to evaluate performance, estimate life cycle and anticipate failure modes of the pavement.

2.3.2.1 Applicability to geosynthetic reinforced pavement design

Designing pavement using the M-E approach involves measuring the traffic load cycles to achieve a limited level of surface distress. This check can be applied to geosynthetic reinforced pavement and its response against damage contribution can be measured. The M-E design approach is better suited to include geosynthetic benefits as it requires inputs from the user to define the local materials, thus helping to provide a consistent basis for evaluation of geosynthetic properties.

In the mechanistic model, the contribution of a thin geosynthetic material has been defined in terms of equivalent resilient modulus and Poissons' ratio. Furthermore, in the empirical design, calibrating the equivalent damage model in terms of subgrade rutting has not provided similar results for thin and thick asphalt geosynthetic reinforced flexible pavements. In thin asphalt pavement the geosynthetic contribution has been included in base course layer, whereas in thick asphalt pavement it has been simulated as equivalent delay in the onset of fatigue cracking when compared to an unreinforced pavement section. Thus, the performance benefits of geosynthetics cannot be easily defined in M-E design.

2.3.2.2 Limitations

The mechanistic-empirical design approach is a more appropriate method for estimating field behavior of flexible pavements than the multi-layered elastic analysis because it provides a more rigorous and adaptable design method (Al-Qadi, 2006). However, the practicality of the method is limited in that a significant amount of information and test data are required to characterize the pavement and its anticipated performance (Finnefrock, 2008). Few test agencies are capable of performing the complex tests required to determine properties such as M_R, and even when they are, the associated costs could be too high to justify a materials testing program on a typical road project. Finally, when used in practice, the M-E approach often relies heavily on correlations to material properties (like the AASHTO 1993 method).

2.3.3 Discussion

The prediction of the behavior of flexible pavements is complicated as it depends on a number of factors. Pavement is composed of multiple layers with different construction materials and the overall performance being controlled by numerous factors, including load magnitude, subgrade strength, layer thickness, interlayer mixing, material degradation, cracking and rutting, and seasonal and climactic fluctuations (WsDOT, 2007; Dougan, 2007; and Al-Qadi, 2006). Geosynthetic reinforcement further complicates the understanding by introducing a whole new set of variables, including reinforcement mechanism, geosynthetic type and stiffness, tensile strength, aperture size and optimal placement location. Therefore, due to uncertainty in quantifying the mechanisms of geosynthetic reinforcement, neither the AASHTO (1993) nor the MEPDG (2004) design approaches allow the direct consideration of the effects of specific geosynthetic properties on pavement performance.

The design of geosynthetic reinforced pavements is still heavily based on empirical results which have been calibrated for unpaved roads. However, the flexible pavements are restricted to smaller rutting depths, and are subjected to high-volume low-intensity traffic loading rather than low-volume high-intensity loading typical of unpaved roads. Giroud and Han (2004) developed a procedure for the design of geogrid reinforced unpaved roads, which considers stress distribution at depth, base course resilient modulus, and degradation of material stiffness with repeated loading. Unfortunately, there is little or no published literature investigating the applicability of this approach for flexible pavements.

There is a lack of theoretical design procedure available for considering the effect of geosynthetic reinforcement in flexible pavements. Consequently, there has been numerous research studies performed to better understand the geosynthetic reinforced pavement behavior, using field-scale testing, laboratory-scale testing and numerical simulations. The important findings of these procedures are discussed.

2.4 PERFORMANCE DATA FOR GEOSYNTHETIC REINFORCED FLEXIBLE PAVEMENTS

The methods for collecting pavement performance data are field scale testing, laboratory testing, and numerical simulations. These three methods not only differ widely, but lead to the collection of significantly different performance data as well, as shown in Figure 2.13. Ultimately, the quality of pavement performance data generated depends on the cost and the method being used for collection (Reck, 2009).

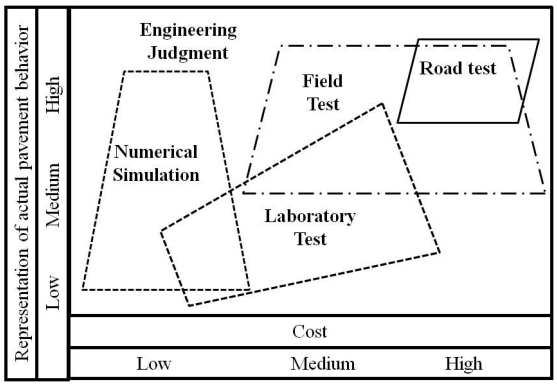

Figure 2.13 Interrelationship between different facets of pavement design (adapted from Hugo et. al, 1991)

Full-scale tests include field studies and accelerated pavement tests that simulate actual pavement behavior. In both of these cases, the cost of testing is high and fairly limited tests can be done as a consequence. Thus, the test matrix and its scope are generally expanded by undertaking smaller scale laboratory studies or numerical simulations. Laboratory tests are generally cheaper than field tests and can be performed under controlled conditions. However, it is difficult to replicate the true behavior of the system using laboratory tests, which are further limited by the instrumentation used during the given test. For this reason, numerical simulations can be useful in developing models based on field and laboratory tests to perform parametric studies. Thus, these three approaches to data collection can be combined to develop a comprehensive design methodology. The important developments pertinent to geosynthetic reinforced pavement design in each of these three areas are discussed in Section 2.4.1.2.

2.4.1 Field tests

2.4.1.1 Types of test tracks

Full-scale field tests have been performed on public roadways and in-service roads. Vehicular loading on public roadways is typically applied by random patterns of actual traffic. Constructed test sections provide a valuable opportunity to better understand the as-built properties of the pavement and the realistic quantification of mechanism controlling how the pavement system performs as a unit. However, in recent years complex design processes have been developed which require data for calibration and validation purposes (Watts and Blackman, 2009). The monitoring of the in-service roads has thus become a time consuming process. Therefore, recently useful data has been generated using accelerated pavement testing (APT).

APT consists of test tracks in a facility, which may be either indoor or outdoor, as shown in Figure 2.14. It employs the use of an automated one or two axle, single wheel load that is repeatedly run over the surface of the test track. It provides a good simulation of the performance of in-service pavements and can give a rapid indication of pavement performance under more severe conditions. The summary of research done using test tracks, i.e. roadways, and APT for geosynthetic reinforced sections and the important distress modes studied are presented in the next section.

(a) **(b)**

Figure 2.14 APT test facilities (a) ATLAS at the Illinois Center for Transportation, USA; (b) a pavement fatigue carousel at LCPC, France

2.4.1.2 Types of distress measurement techniques

There are several ways to evaluate and compare pavement performance in field-scale test sections. In flexible pavements, the two most common failure modes are surface deflection and cracking (including longitudinal, transverse and fatigue). While measuring the performance of a field test section, surface deflections are measured using instruments and cracking is documented using visual inspection and condition surveys. Surface deflections are the most common performance criterion for both reinforced and unreinforced pavements in the field. There are two ways to evaluate distress in the field. The already existing surface deflections are measured in term of the rutting depth. On the other hand, the response of the pavement for a given load is measured in terms of surface deflection to determine its structural capacity.

Rutting occurs because of permanent deformation in any of the pavement layers or the subgrade caused by the lateral movement of the material due to traffic loads. Rutting is generally measured in square meters of surface area for a given severity level, based on rut depth with a dipstick profiler at 15m (50ft) intervals. Measurements of rutting depth are easy to obtain as they are taken at the pavement surface and provide a simple method of comparing pavement performance against multiple test sections. Rutting depth is also often correlated with the traffic benefit ratio (TBR) and base course reduction (BCR) values during the design of geosynthetic reinforced pavements.

Deflection measurements are made using non-destructive testing (NDT) devices on pavement to evaluate their structural capacity and to calculate the elastic moduli of various pavement components. The most widely used device to measure pavement deflections is the Falling Weight Deflectometer (FWD) as shown in Figure 2.15a. It applies an impulse force on the pavement. The device is trailer-mounted and driven to the desired test location. A loading plate is hydraulically lowered to the pavement surface, after which an impulse force is applied to the pavement by dropping a weight from a known height onto the loading plate. The magnitude of the load is measured using the load cell while deflections are measured using the seven velocity transducers. A new tool, known as a Rolling Dynamic Deflectometer (RDD), was developed recently developed

for assessing the conditions of pavements and determining pavements' continuous deflection profiles (Bay and Stokoe, 1998). A picture of the RDD is shown in Figure 2.15b. Unlike FWD testing method, the RDD performs continuous rather than discrete deflection measurements. The ability to perform continuous measurements makes RDD testing very effective in quickly characterizing large sections of pavement while simultaneously providing a comprehensive picture of the pavement condition. It applies sinusoidal dynamic forces to the pavement through specially designed loading rollers. The resulting deflections are measured by rolling sensors designed to minimize the influence of noise caused by rough pavement surfaces. The Dynatest FWD device and RDD was used in the current research to monitor the structural performance of the pavement.

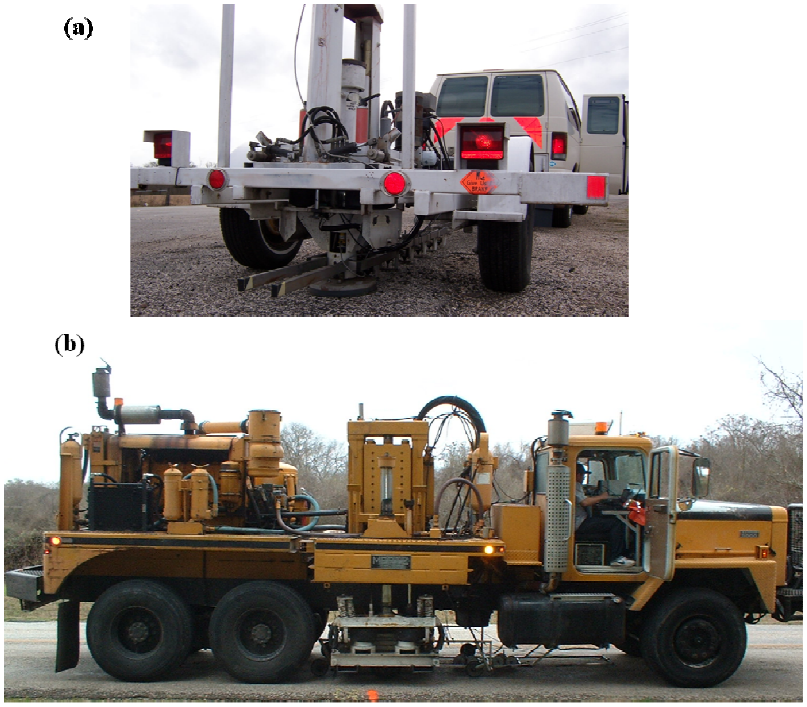

Figure 2.15 Non-destructive testing methods used in the current research study include: (a) a Falling Weight Deflectometer, and (b) a Rolling Dynamic Deflectometer

2.4.1.3 Discussion

Field tests employing full-scale road sections have been performed to evaluate the effect of geosynthetic reinforcement in flexible pavement systems. Perkins and Ismeik (1997) compared results from nine such studies, out of which four were constructed on indoor test tracks, three on outdoor test tracks, one on a public roadway and one in field truck-staging area. The indoor test tracks used a single moving wheel as load on the test sections and were constructed by Brown et al. (1982), Barksdale et al. (1989), Collin et al. (1996), Moghaddas-Nejad and Small (1996). The outdoor test tracks constructed by Barker (1987) and Webster (1993) also had a single moving wheel, whereas the track test constructed by Halliday and Potter (1984) used a two-axle, dual wheel truck to load the pavement. Anderson and Killeavy (1989) used loaded truck traffic whereas Miura et al. (1990) used daily traffic to load the pavement test sections.

Recently, Cancelli and Montanelli (1999), Perkins (2002), Perkins and Cortez (2005), Al-Qadi et Al. (2008), and Reck et al. (2009) have reported studies on geosynthetic reinforced base course test sections using APT equipment. The review of these test sections indicated rut development with given load cycles as the most common method to evaluate the pavement distress. All of the nine test sections and the four APT sections reported results from profilometer readings at the end of design loading cycles. However, FWD tests were conducted only at four field sections and at one APT section.

The method chosen to quantify the performance of a given test section determines the perceived level of improvement achieved by reinforcing a pavement with a geosynthetic. The test results indicated that the geosynthetic reinforced test sections had less rut depth than the unreinforced sections. The improved performance was attributed to the interlocking ability of the geogrid and its role in preventing lateral spreading of the base layer soil. Overall, the field results suggest that both geogrids and geotextiles significantly reduce surface deformations in flexible pavements.

2.4.2 Laboratory tests

A number of laboratory tests have been proposed to quantify the lateral restraint mechanism that governs the performance of geosynthetic reinforcement in flexible pavements. When the lateral restraint mechanism is mobilized, the geosynthetic develops additional tensile stresses under given loading thereby providing confinement to the surrounding aggregates as shown in Figure 2.16. This degree of confinement has been attributed to the effect of interface shear provided by geotextiles and dynamic interlocking provided by geogrids when used in the base course layer of the pavement.

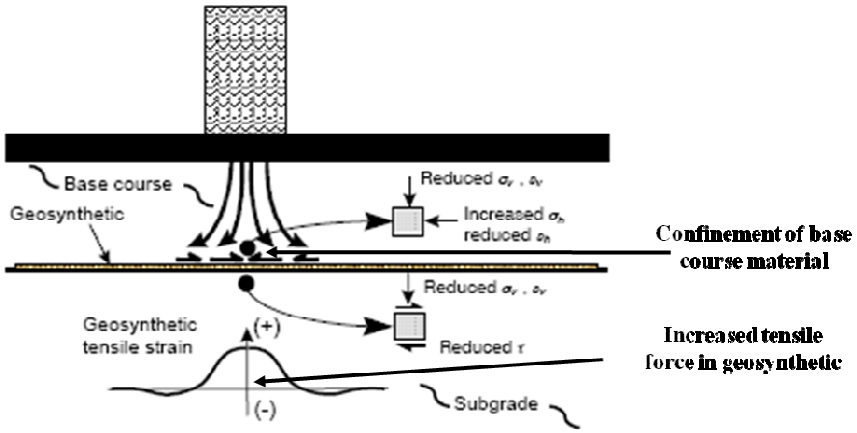

Figure 2.16 Additional forces due to soil-geosynthetic interaction when a lateral restraint mechanism occurs in a pavement (adapted from Perkins, 1999)

The primary objective of laboratory tests has been to predict these soil-geosynthetic interaction mechanisms in flexible pavement system either by measuring the index properties of geosynthetics or by replicating the field conditions. Based on the approach adopted, the tests reported in the literature have been divided into two main categories i.e., unconfined and confined tests. In unconfined tests, the geosynthetic properties are generally measured in-air, independent of the site soil. On the other hand, in the confined tests the geosynthetic is placed within the soil and confinement is applied at the interface. The advantages and limitations of the various tests in each of these two categories are presented in Section 2.4.2.1.

2.4.2.1 Unconfined tests

As the name suggests, unconfined tests are generally done on the geosynthetic specimen in isolation, i.e. without the soil used in the pavement project. The primary advantages of these tests are that they are quick, easy and cost effective. They can be run in short durations of time using simple devices, thus allowing for the test to be repeated a large number of times. The repeatability of the test helps to eliminate discrepancies between test results due to any variations in the geosynthetic properties of a given specimen roll, which may occur during the manufacturing process. However, a correlation is required to interpret the index property reported by these test results with the actual field performance of the geosynthetic. The four main tests in this category are wide-width tensile test, biaxial loading test, junction efficiency test, and torsional rigidity test. While the wide-width tensile test can be used for any geosynthetic product (both geogrid and geotextiles in this study), the other three tests are limited to only geogrids.

The tensile strength of the geosynthetic material is its single most important property as all the field projects involving reinforcement application require it for design. According to Wartman et.al (2005), "The current state of practice for measuring the tensile properties of a geosynthetic involves placing the material within a set of clamps, positioning this assembly in a mechanical testing machine, and stretching the geosynthetic in tension until failure occurs. The test is generally performed without confinement at a constant strain rate." Currently, there are two ASTM standards for these tests, which are ASTM D4632 and D4595. The grab tensile test (D4632) is used for manufacturing quality control but due to the narrow width of the specimen, the results obtained are influenced by Poisson ratio effects. Therefore, a wide-width tensile test (D4595) is currently used for most design applications. The wide-width tensile testing load frame with roller grips is as shown in Figure 2.17. The test is conducted to obtain tensile stiffness at different strain values (1%, 2%, and 5%), as well as the ultimate tensile strength of a given geosynthetic.

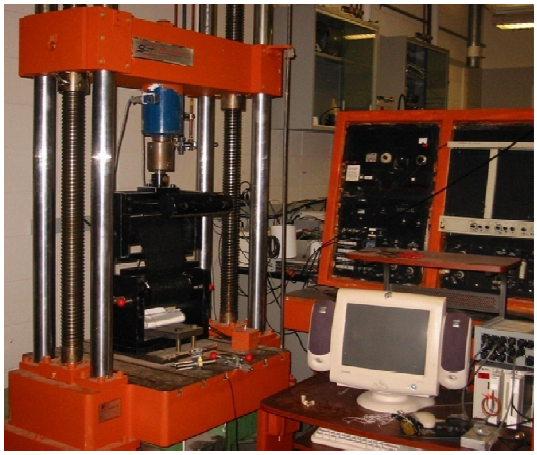

Figure 2.17 Wide-width tensile frame with roller grips at the University of Texas at Austin

The methods proposed for unpaved road design require tensile stiffness at 5% to be used as a design parameter. Based on full scale model studies for the paved roads, Berg et.al (2000) reported accumulated in-service tensile strain of 2% in the geosynthetic and thus recommended the tensile stiffness at this strain level to be used as a design value. However, the correct strain level to report tensile stiffness of geosynthetics and its correlation to the field performance has still not been established in the literature. Also, Bray and Merry (1999) showed that in reality the stress and strain conditions in these tests vary across the specimen from plane-strain, biaxial near the grips, to a uniaxial stress state near the center of the specimen. Thus, there is a misconception that the test measures geosynthetic behavior under plane strain conditions as is the case in most field applications.

To address the concerns of the tensile test, a uniaxial performance based test known as the "junction strength test" was developed. It is conducted as per the procedure recommended in GRI-GG2 specifications and involves gripping the cross member of a geogrid rib on both sides of the junction with a clamping device. Load is then applied until the junction breaks. The force required to do so is defined at the junction strength of the geogrid. Since junctions of the geogrid provide stability during the installation of the pavement and its subsequent performance under traffic load, geogrids' ability to transfer

stress at low strains is an important consideration for design. However, the junction stiffness requirements for pavement projects have not been defined. Also, this test is limited in scope as it was developed when geogrids with integral junctions were only used. Therefore, it does not incorporate the newer geogrids with entangled fibers or those with heat bonded or laser welded junctions.

The above two methods are uniaxial index based (wide-width) and performance based (junction strength) tests. According to McGown et al. (2005), "Most geogrids tested by these methods suffer severe distortion, non-uniform stressing particularly at the junctions, premature specimen rupture and problems with clamping of the specimens." Therefore, Kupec and McGown (2004) suggested a biaxial test method which was primarily focused on geogrids and allowed characterization of the combined strength of tensile ribs and junctions in a single test. The test specimen was prepared with 5 ribs in each direction and so 25 junctions within the central section of the test specimen as shown in Figure 2.18 were tested. The loads were applied to the test specimens under isotropic rate of deformation conditions of 1 mm/min. Deformations were measured at the clamps by means of linear vertical displacement transducers. The results indicated that the biaxial load-strain time behavior is markedly different from the uniaxial behavior. The increase in biaxial stiffness was related to the behavior of junctions under tensile stresses in the principal direction, due to Poisson ratio effect and re-orientation of the molecules in the junction areas.

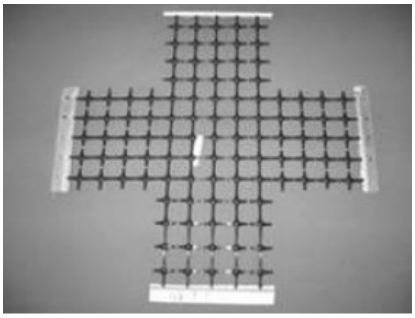

Figure 2.18 Geogrid specimens for biaxial testing (McGown et al., 2005)

The torsional rigidity test was developed by Kinney and Yuan (1995) to measure the in-plane rotational stiffness of the geogrids. It was done to correlate the performance of large scale geogrid reinforced paved road tests conducted by the US Army Corps of Engineers at the Waterways Experiment Station with the relevant laboratory property of geogrids for base reinforcement. This test was an initial attempt to quantify the interlocking capacity of the geogrid. However, the relationship between geogrid torsional rigidity and the performance of the geogrid reinforced road sections could not be established. Further, this test method also demonstrated a substantially higher torsional rigidity for stiff geogrids as compared to flexible geogrids. A study conducted by the Texas Research Institute (TRI) in 2001, reported that there was no correlation between torsional rigidity and confinement performance of the geogrids.

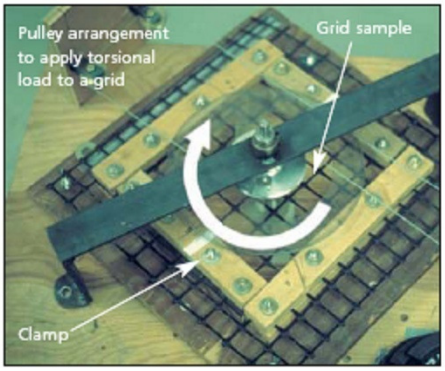

Figure 2.19 Torsional rigidity tests (Kinney and Yuan, 1995)

In general, it is difficult to replicate field conditions using the unconfined tests described above. Moreover, a geosynthetic is loaded under confinement provided by the surrounding aggregate generating a plane-strain biaxial or isotropic biaxial rather than a uniaxial state of stress in the field. In other words, the geosynthetic behavior observed in the laboratory from these tests has to be correlated with the field application, which has different loading and boundary conditions. Therefore, engineers have used these tests as an index but not for the actual design of the geosynthetic reinforced flexible pavements.

2.4.2.2 Confined tests

Geosynthetics used for base reinforcement are subjected to dynamic loading such as traffic loading and confinement by soil in the pavement layer, which cannot be simulated by unconfined test methods. According to Han et al. (2008), "Geosynthetic-soil confinement depends not only on the macro-structure and index properties of geosynthetics but also on the properties of soil and most importantly on the interaction between geosynthetics and soil particles." This interaction between soil and geosynthetic under confinement, specifically the confined stress-strain properties of the geosynthetics, has been focus of research for the past twenty five years. Based on a Federal Highway sponsored study regarding the review of the existing confined test for geosynthetics, Elias et al. (1998) concluded that the unconfined response is overly conservative and that the confined response should significantly improve the characterization of geosynthetic materials in engineering applications. Recently, a number of confined tests have been proposed, out of which five tests have specifically focused on characterizing field behavior of geosynthetic reinforced flexible pavements. This section discusses the features of these five tests, namely the cyclic plate load test, cyclic triaxial test, cyclic pullout test, bending stiffness test and the modified pavement analyzer test.

The cyclic plate load test was designed for the purpose of conducting large scale laboratory experiments on reinforced and unreinforced pavement sections (Al-Qadi et al., 1994; Cancelli et al., 1996; Has, 1988; Miura et al., 1990; and Perkins, 1999). The test setup designed by Perkins (1999) consisted of a 2m wide and 1.5m high reinforced concrete tank, as shown in Figure 2.20. The model pavement section was constructed with a geosynthetic at the interface of the base course and subgrade layers. The load was applied by a pneumatic actuator in the form of a trapezoidal wave pulse, which generated a maximum load of 40kN with an equivalent surface pressure of 550 kPa on the pavement. The corresponding force and displacement response was measured using a load cell and eight surface lvdt's.

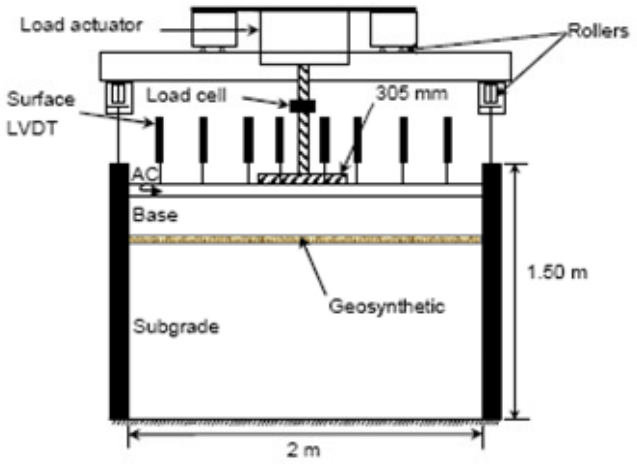

Figure 2.20 Cyclic plate load test (Perkins, 1999)

Based on the studies conducted using the cyclic plate load test, TBRs ranging from 1 to 70 and BCRs ranging from 20% to 50% were obtained for test sections consisting of geotextiles and geogrids (Hsieh and Mao, 2005). Therefore, these tests have been successfully used to evaluate geosynthetic confinement effects with soil under dynamic loading in a large box. However, facilities in which cyclic plate loading can be conducted are not readily available, thus limiting the application of this test to universities and research institutes. In addition, the cyclic plate loading test has a major drawback as the test procedure is tedious and slow and cannot simulate rolling wheel loads (Han et al., 2008).

The cyclic triaxial test, as shown in Figure 2.21, is used to measure the ability of the soil to endure the shearing stresses induced in it due to cyclic loading (ASTM D5311, 2004). The resilient modulus, M_r, of the soil aggregates computed using this test is used as an input in the mechanistic empirical design (NCHRP Project 1-28A, 2000). The above test was modified by Perkins et al. (2004), to obtain the change in resilient modulus and permanent deformation behavior due to the addition of a geosynthetic to the aggregate layer of the pavement. The results from cyclic triaxial tests indicate that the addition of reinforcement does not affect the resilient modulus of the aggregates but it has appreciable effect in reducing pavements' permanent deformation properties. Also, the

reinforcement was observed to increase the stiffness of aggregate layer in the zone above and below it which was equal to the radius of the specimen (150 mm in this case). However, relatively poor repeatability in the test results was observed such that it was difficult to make a distinction between different geogrid products. Also, the appreciable effect on permanent deformation was not observed until a mobilized friction angle of 30^0 was reached. This test has similar drawbacks as the cyclic plate load test where it is incapable of simulating wheel loads on the soil-geosynthetic system.

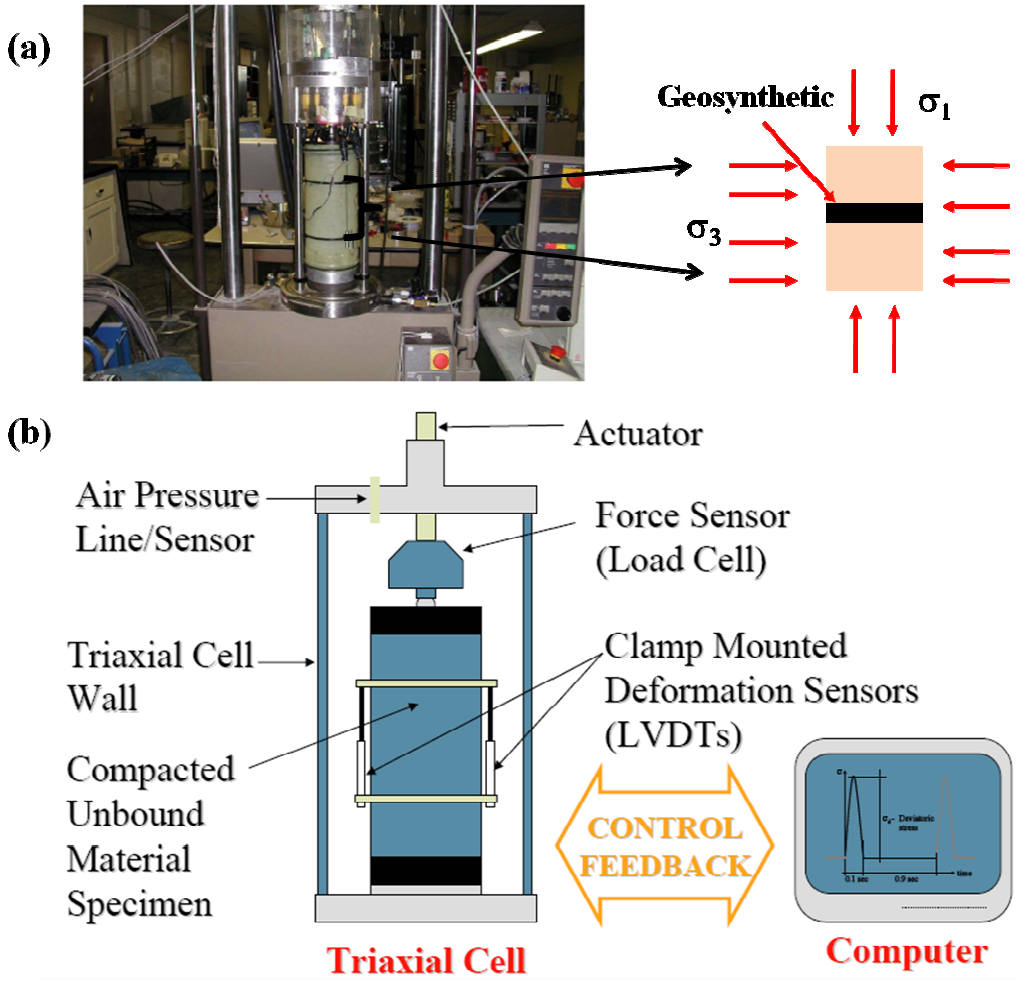

Figure 2.21 Cyclic triaxial test (a) Test equipment (Perkins et al., 2004); (b) Schematic of test setup (Tutumluer, 2004)

Cyclic pullout test were conducted by Cuelho and Perkins (2005) by modifying the standard pullout test (ASTM D6706) to resemble the loading protocol used in a cyclic triaxial test as shown in Figure 2.22. The cyclic shear load cycles (100-300 in number) were applied at each confinement level beginning with seating load of 51 kPa until pullout failure was reached. Based on test results obtained, a parameter known as geosynthetic-soil resilient interface shear stiffness (G_i) was defined to describe the reinforcement-aggregate interaction under cyclic loads and was given as:

$$G_i = \frac{\tau_i}{\Delta_i} \tag{2.9}$$

where, Δ_i is the relative displacement between the aggregate and reinforcement and τ_i is the shear stress applied to the interface. The units of G_i were kN/m^3. The parameter, G_i was assumed to closely resemble M_r as both were dependent on shear load and confinement. Therefore, three parameter log-log equations developed in NCHRP project 1-28A for M_r was modified and used to calibrate G_i for a given soil-geosynthetic interface, given as:

$$G_i = k_1 . P_a . \left(\frac{\sigma_i}{p_a} \right)^{k_2} . \left(\frac{\tau_i}{p_a} + 1 \right)^{k_3} \tag{2.10}$$

where σ_i is the normal stress on the interface, p_a is the normalized atmospheric pressure, P_a is the atmospheric pressure per unit length, k_1, k_2 and k_3 are the dimensionless material constants. The purpose of this test was to provide a parameter to be used as an input for interface shear moduli into finite element model for M-E design guide. However, the pullout tests conducted on six geosynthetics indicated that the correlations between the predicted and measured values were erratic. The results were sensitive to small changes in displacement magnitudes. Also, the shear load was cycled while normal load was kept

constant which is not representative of field conditions. Thus, additional research is still needed to improve the test equipment and to establish specific test protocol.

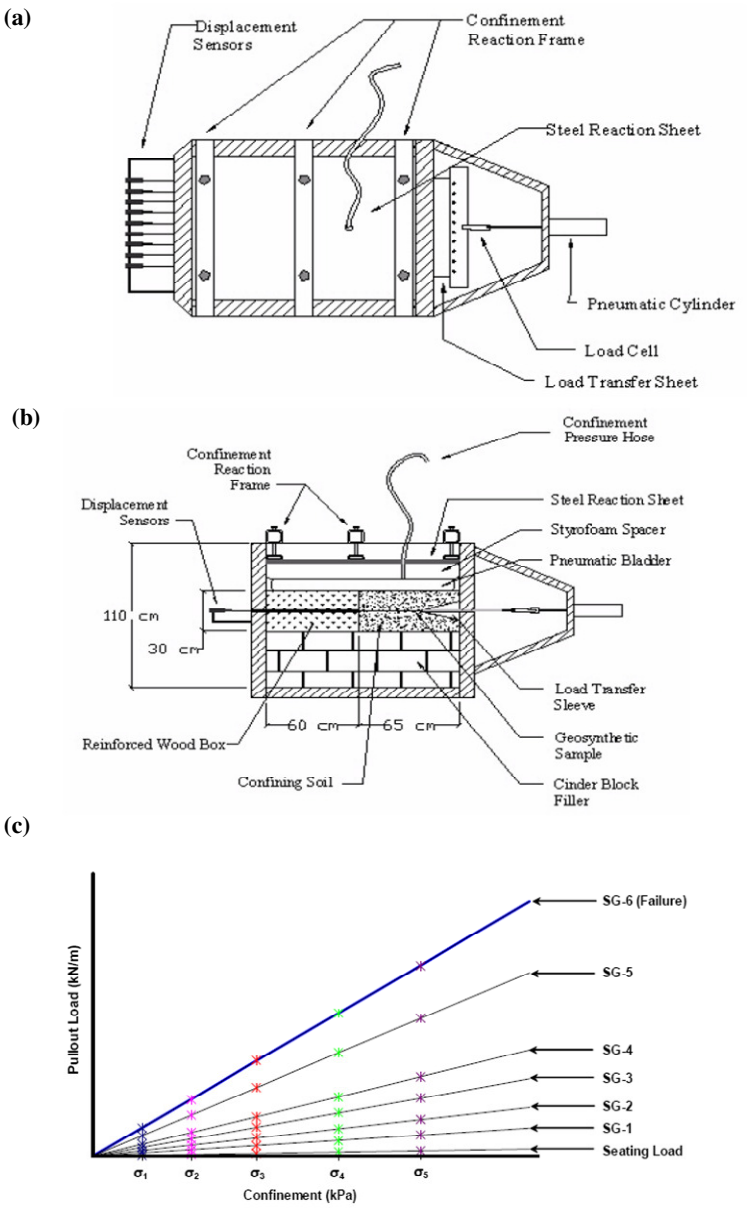

Figure 2.22 Cyclic pullout test (a) Plan view (b) Side view (c) Loading protocol (adapted from Cuelho and Perkins, 2005)

Bending stiffness test was developed by Sprague et al. (2004) as a small scale index test procedure for predicting the behavior of different geosynthetics used as reinforcing material in pavements. The test apparatus was a modified version of the multi-axial tension test for geomembrane (ASTM D 5617) as shown in Figure 2.23a and 2.23b. The details of the test procedure are provided in Abusaid (2006) and Finnefrock (2008). In brief, a uniform vacuum pressure of 100psf was applied on the soil-geosynthetic sandwich to simulate confinement under pavement conditions. Then, uniform air pressure cycles were applied to the soil-geosynthetic system and the center-point deflection was measured by a dial gauge to quantify systems response.

A property named as bending stiffness (BS) was obtained from test results and was defined as the ratio of the deviator stress (σ_d) to the recoverable deformation (Δ_r) as shown in Figure 2.23c. Specifically, bending stiffness is defined as the slope of the curve when the inflation pressure is plotted versus the resulting center-point deflection.

$$BS = \frac{\sigma_d}{\Delta_r} \tag{2.11}$$

The bending stiffness value is reported in units of pounds per square inch for one inch of deflection, similar to resilient modulus, M_r, and thus is not a measure of strength but rather of the stiffness of the system. As the test results reported by Finnefrock (2008) calculated reinforcement benefits of 20% to 25% in terms of BS ratio, the results indicate a clear distinction between the performances of geogrid reinforced and unreinforced specimens. However, the comparison between the relative performances of different geogrid products could not be obtained due to variability of test results. The theoretical analysis conducted by Yuan (2005) indicated significant influence of edge shear resistance on the test results. The tests performed on geotextile reinforced base course sections did not indicate any benefit over control sections.

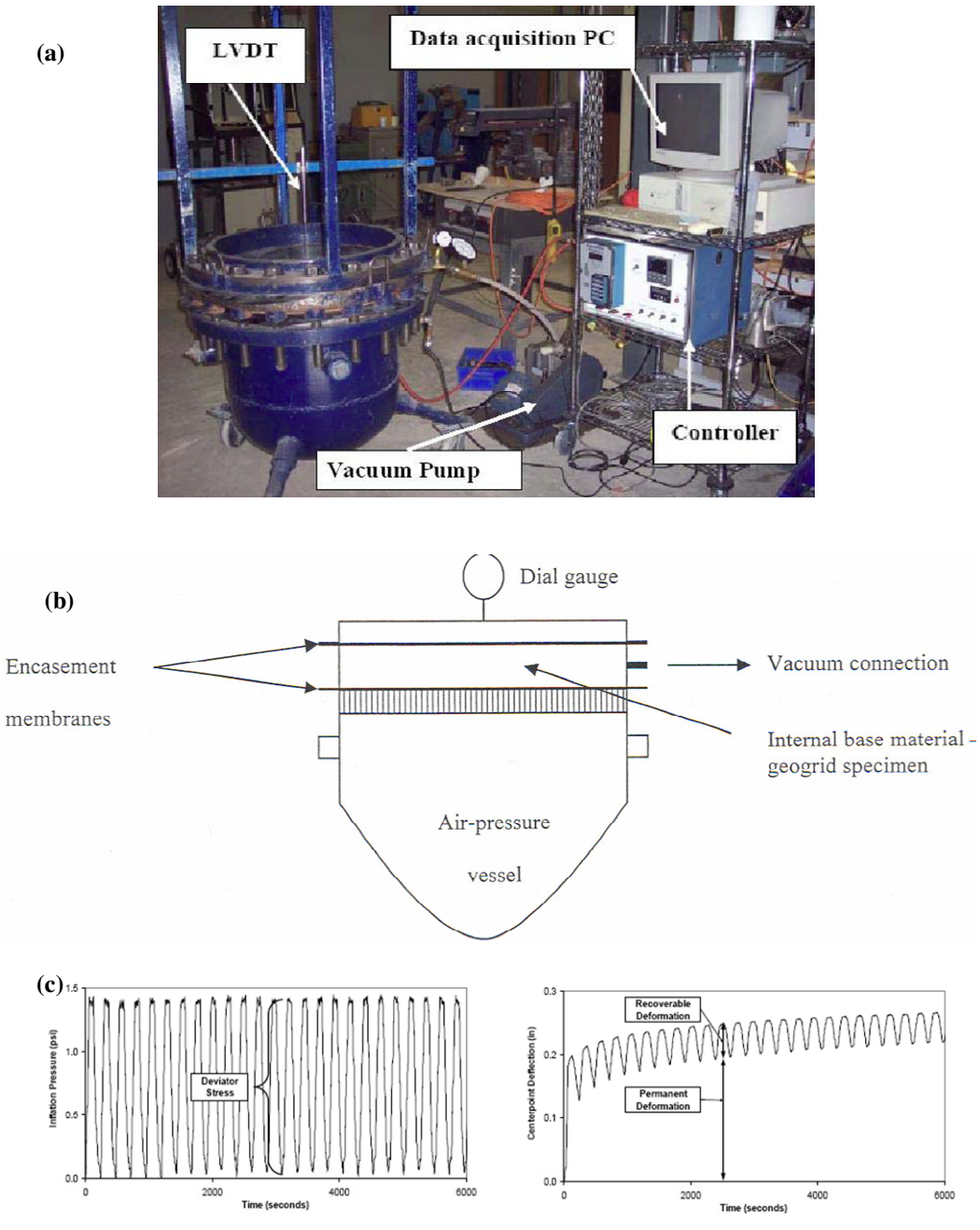

Figure 2.23 Bending stiffness test (a) Actual test apparatus (b) Schematic of the test (c) Deviator stress and recoverable deformation plots for a typical test (adapted from Abusaid, 2006)

Han et al. (2008) proposed a test method to use asphalt pavement analyzer (APA) to evaluate the benefit of geosynthetic reinforcement in the base course layer of the pavement, as shown in Figure 2.24a. APA is originally a multifunctional wheel-loaded test device used for evaluating permanent deformation, fatigue cracking, and moisture susceptibility of both hot and cold asphalt mixes, as shown in Figure 2.24b. For conducting the test on the base course, this machine is modified to include a box to hold soil with or without geosynthetics. The loaded wheel is then made to move back and forth on the surface of base course as shown in Figure 2.24c through 2.4h. A relationship is established between the measured rut depths after a certain number of passes for a given section. The values obtained can be compared for geosynthetic-reinforced layer with the unreinforced base layer to evaluate the confinement effect of geosynthetics. Besides evaluating TBR for the given sections, the authors proposed a parameter known as rut reduction ratio (RRR), which was defined as the ratio of the rut of the reinforced base to that of the unreinforced base at the same service life (8000 cycles). It was argued that geosynthetic with lower RRR value is better in terms of performance improvement.

The tests were conducted on four different geosynthetics (three geogrids and one geotextile) with two different base course materials. Based on the tests conducted on three geosynthetics, the TBR values ranging from 1 to 36 and RRR values of 0.3 to 1.2 were obtained. Furthermore, the test results indicated that geotextiles that had an unconfined tensile strength higher than the geogrids at 5% strain demonstrated lower improvement factor under confined conditions. When a surcharge was applied to the soil-geosynthetic system to simulate confinement in the field, lower rut depths were observed as compared to no confinement tests for a similar setup. Thus, based on the experimental study, it was shown that the proposed test method had repeatability of test results and could reasonably distinguish the effect of geosynthetic soil-confinement among all the geosynthetics investigated. However, the test did not provide a parameter or model to be used with proposed M-E design of geosynthetic reinforced pavements.

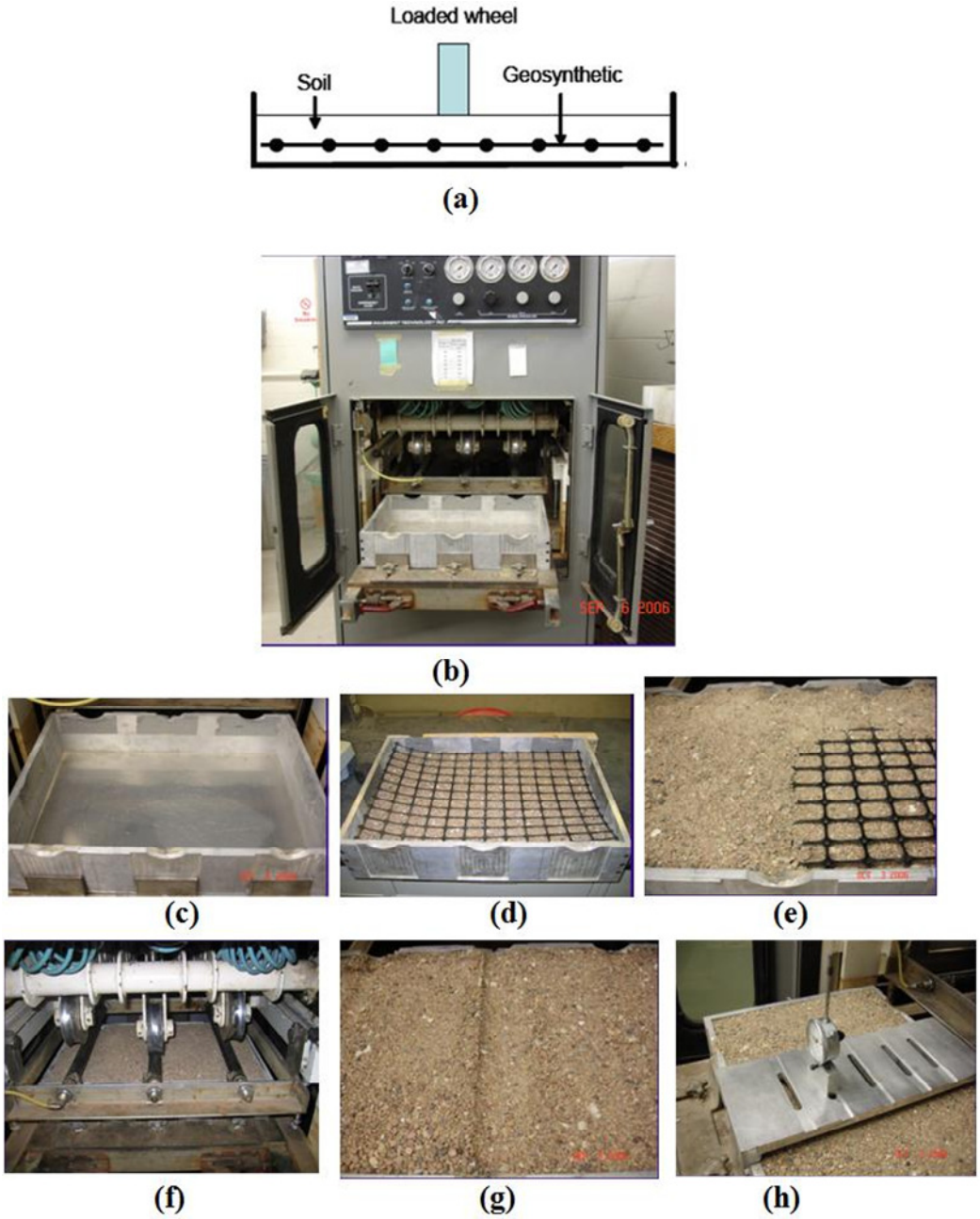

Figure 2.24 Modified pavement analyzer test (a) schematic of the test (b) APA testing machine (c) modified box (d) geosynthetic placed in the middle of the box (e) base course layer over the geosynthetic (f) test with loaded wheels (g) rut observed at the end of test (h) rut measurement using dial gauge (adapted from Han et al., 2008)

2.4.2.3 Discussion

Laboratory methods used to quantify the behavior of geosynthetics acting as reinforcement in flexible pavements were studied, and two main categories of tests were identified: unconfined and confined. The unconfined tests were found to be easy, economical and quick to execute in the laboratory but independent of the site soil. Also, these tests only provided an index for the real mechanism, which had to be then correlated with actual field performance. Moreover, in some field studies the performance trend observed was opposite to what had been predicted by the unconfined tests. Thus, based on the current assessment of literature, these tests are not recommended for performance based design of geosynthetic reinforced pavements.

The confined test methods for the design of geosynthetic reinforced pavements were also reviewed and a comparison of the important features of each test is presented in Table 2.1

Table 2.1 Features of confined tests

Features	**Cyclic plate load test**	**Cyclic triaxial test**	**Cyclic pullout test**	**Bending stiffness test**	**Modified asphalt pavement analyzer**
Loading type	Cyclic	Cyclic	Cyclic	Cyclic	Moving wheel
Design property	TBR	M_r	G_i	BS	RRR
Suitable design method	AASHTO	M-E	M-E	AASHTO	AASHTO
Ease of running test	Difficult	Difficult	Moderate	Moderate	Easy
Control section	Yes	Yes	No	Yes	Yes
Repeatability of test results	-	No	No	No	Yes
Ability to distinguish among various geosynthetics	-	No	No	No	Yes

The tests provided actual quantification of the soil-geosynthetic interaction behavior but were expensive and time consuming to run. The tests reported the performance in the form of reduced deflections (TBR, BS, and RRR) or increased interaction or confinement modulus (M_r and G_i). These performance indexes could be

used as an input in design methods discussed earlier, with ratios for AASHTO design and resilient modulus for M-E design of flexible pavements. The results obtained from above tests indicated improvement over control sections (i.e. sections without geosynthetics). However, three main drawbacks were identified with the current confined testing approach. Firstly, all of the tests required specialized equipment. Secondly, the results were found to be sensitive displacement measurements, thereby making it difficult to reproduce them for a given geosynthetic. Finally, the variability in the test results was high, such that it was difficult to distinguish between the performances of various geosynthetics. All of the above design parameters involved measurements for their computation, which were sensitive to small changes in cyclic load level. Overall, the confined testing approach was considered as a more accurate way to assess geosynthetic reinforced pavement performance than the unconfined testing method.

The current research focused on quantifying the geosynthetic performance in flexible pavements using laboratory confined tests. Based on the above discussion, it can be concluded that a reasonable test method should include the following features: (a) the ability to capture the mechanism of lateral restraint; (b) parameters for mechanistic-empirical design; (c) provides good repeatability of test results; (d) utilize a parameter that distinguishes between the performance of various geosynthetics; (e) be sensitive to low displacement magnitudes; and (f) be easy to conduct in the laboratory. Based on this conclusion, it was decided to conduct a confined test with monotonic loading in order to reduce the variability in test results and allow for the realistic measurement of the interface mechanisms.

The two common soil-geosynthetic interface tests which have above features are modified direct shear test and pullout test as shown in Figure 2.25. Both the tests involve placing a geosynthetic between the required soils and moving the assembly at constant rate of displacement. While in the direct shear box the top soil layer is moved relative to the clamped geosynthetic, on the other hand, in the pullout test the geosynthetic is moved relative to the soil. This principle difference in these two test methods mobilizes contrasting mechanisms at the soil-geosynthetic interface. In the direct shear test, the

primary mechanism is the mobilized interface friction as the goal is to characterize the interface shear strength between the soil and geosynthetic at the peak displacement. However, in pullout test due to movement of the geosynthetic relative to the soil, tensile stresses are developed in it along with interaction mechanism at the interface in terms of shear for geotextiles and interlocking for geogrids. Therefore, for application of laboratory test to reinforcement pavement design where lateral restraint between soil and geosynthetic is to be quantified, pullout tests were considered more suitable than a modified direct shear test.

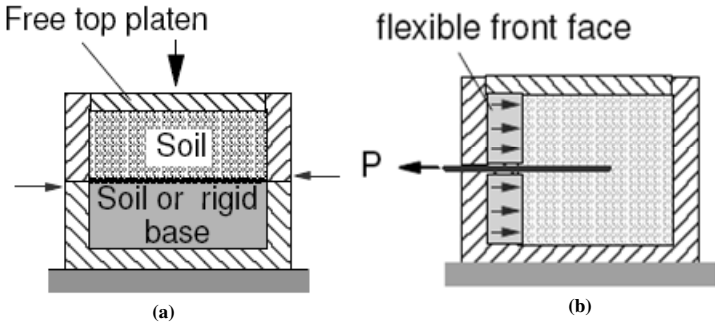

Figure 2.25 Soil-geosynthetic interface test (a) Modified direct shear test (b) Pullout test (adapted from Palmeria, 2008)

For the current research, it was decided to conduct monotonic load pullout tests with a focus on characterizing the soil-geosynthetic interaction at low displacement magnitudes. Although these pullout tests did not simulate the exact traffic load condition, they reproduced the similar interface mechanisms between the soil and geosynthetic as in real pavements. An analytical model was proposed to predict the confined load-strain characteristics of soil-geosynthetic system at these low displacement magnitudes from results obtained from pullout test. The predicted performance of geosynthetics was then compared with field test section performance constructed as part of this research. Thus, a new performance-based test method that has all the necessary features in the form of a pullout test was proposed to effectively evaluate the geosynthetic-soil confinement.

2.4.3 Numerical methods

The flexible pavement design involves understanding the behavior of and the interaction between various materials (namely, the asphalt, base course, subgrade, geosynthetic reinforcement layers). The current design methods are empirical in nature and do not provide an opportunity to predict the behavior of the flexible pavement under actual traffic loads. However, numerical methods are currently being used to provide insight into the mechanics of this system. The two most common numerical methods currently in use are finite element method (FEM) and discrete element method (DEM).

2.4.3.1 Finite element method

This section provides a review of finite element studies conducted to simulate the behavior of geosynthetics used as reinforcement in the base course layer of flexible pavements. Most of these studies were performed in addition to laboratory or field test sections so that a comparison between model predictions and experimental results could be made. The comparison of important features of these studies is shown in Table 2.2.

Table 2.2 FEM studies for geosynthetic reinforced flexible pavement design

References	Type of analysis	Geosynthetic constitutive model	Geosynthetic element type	Interface element type	Load type	Validation
Burd and Houlsby, 1986	Plane strain	Isotropic linear-elastic	Membrane	None	Monotonic	None
Barksdale et al., 1989	Axi-symmetric	Isotropic linear elastic	Membrane	Linear elastic perfectly plastic	Monotonic	Field results
Burd and Brocklehurst, 1990	Plane strain	Isotropic linear-elastic	Membrane	None	Monotonic	None
Miura et. al, 1990	Axi-symmetric	Isotropic linear elastic	Truss	Linear elastic joint element	Monotonic	Field results
Dondi, 1994	Three-dimensional	Isotropic linear-elastic	Membrane	Elasto plastic Mohr-Coulomb	Monotonic	None
Wathugala et al., 1996	Axi-symmetric	Isotropic elasto-plastic	Solid Continuum	None	Single cycle	None
Perkins, 2001	Three-dimensional	Anisotropic elasto-plastic	Membrane	Mohr-Coulomb friction	Multiple cycles	Lab and test tracks
Kwon et.al, 2005	Axi-symmetric	Isotropic linear-elastic	Membrane	Linear-elastic	Monotonic	Test tracks

The results from the studies mentioned above were generally reported in the form of surface deformation of the given system under the applied load. The comparison was then made between the magnitude of surface deformation for unreinforced and reinforced case. The finite element model for the flexible pavement developed by Perkins (2001) is shown in figure 2.26a. It indicated a reduction of lateral strain at the bottom of the base and a reduction of shear in the top of the subgrade due to the addition of the geosynthetic reinforcement, as shown in Figure 2.26b. However, further work is still required to make computationally efficient models that can simulate actual wheel loading.

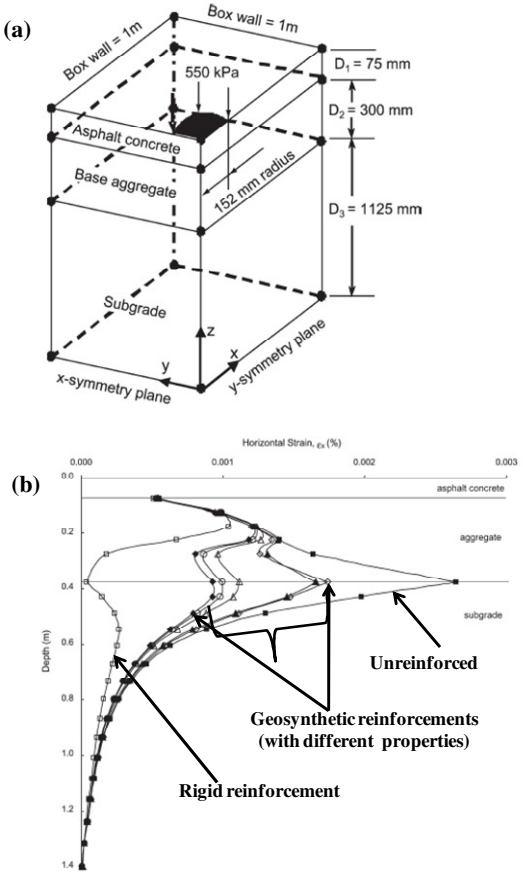

Figure 2.26 Flexible pavement (a) Finite element model (b) Horizontal stress vs. strain profile for various cases (adapted from Perkins and Edens, 2002)

2.4.3.2 Discrete element method

DEM has been recently used to model soil-geosynthetic interaction, specifically geogrid interlock with the base course material. The method has advantages over FEM as it captures the interaction between geogrid and soil more realistically in terms of load transfer mechanism and deformation behavior. The pullout test was simulated by Konietzky et.al (2004) to model interlocking effect of geogrids under static and cyclic loading whereas McDowell et.al (2006) used a biaxial geogrid to determine the effect of ratio of geogrid aperture size to soil particle size on the pullout resistance as shown in Figure 2.27. DEM model for a low volume road with geogrid reinforcement was developed by Kwon et.al (2008). The results indicated that the addition of a geogrid led to locked-in stresses during placement, compaction, and in-service loading leading to stiffer soil layer above the geogrid. However, further research is still required to establish a linkage between DEM results for pullout tests and actual field mechanisms.

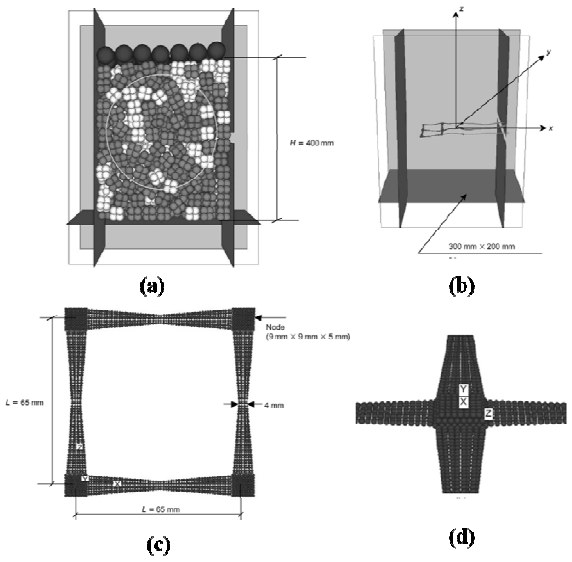

Figure 2.27 Discrete element model (a) pullout test with cubic clumps (b) pullout test with embedded geogrid (c) aperture of geogrid (d) detailed view at node (adapted from McDowell et al., 2006)

2.4.3.3 Discussion

Geosynthetic reinforced pavement design involves an interaction between various materials that can be successfully understood using numerical methods. FEM response models have recently been proposed to be used in mechanistic empirical design of such pavements. However, limited success has been achieved as the models developed use geosynthetics as a structural element directly included in the surrounding materials without consideration to the interface conditions. Also, due to computational effort required to simulate realistic traffic load, it is often applied as a single static load cycle, which does not mobilize the representative governing mechanisms in these pavements. This leads to results which underestimate the benefit of geosynthetic reinforcement when compared with the field performance (Perkins and Ismeik, 1997). To account for this discrepancy, the finite element models end up using a higher normal stiffness for the geosynthetics. These values are generally larger than an order of magnitude greater for geogrids than that obtained from the actual laboratory tests. A new method in the form of DEM has been recently suggested to better represent the interaction characteristics of soil-geosynthetic interface. The models developed under this approach account for the geosynthetic contribution in terms of locked-in stresses experienced during the service life of flexible pavement. The results have indicated that the benefit of the addition of the geosynthetic to the pavement structure is the stiffening of the base course layer.

Mechanistic response models have been proposed by Perkins and Svanø (2004) to account for compaction and trafficking stages of pavement design separately to compare with empirical damage models. According to Kwon et al. (2008), "These are rational but complex ways of showing the benefit of geogrid reinforcement and evaluating their performance in base-reinforced pavements." Attempts are still being made to improve DEM and FEM based models so they can be implemented in M-E design methods to account for the lateral confinement mechanism of geosynthetics in flexible pavements.

2.5 CONCLUSIONS OF THE LITERATURE REVIEW

Geosynthetics have been successfully used as base reinforcement for flexible pavements for the past 30 years. The results of experimental studies conducted in the form of field, laboratory and numerical tests have demonstrated the benefit of using geosynthetics to reduce the permanent deformation of the subgrade by stiffening the overlying base course layer in the flexible pavement system. Nevertheless, the appropriate selection criterion for the geosynthetic to be used in the design of reinforced pavements has been a major limitation for these projects. The purpose of this chapter was to provide a review of published material and to identify gaps in the current research related to the suitability of geosynthetics for reinforced pavement projects that need to be addressed.

According to Perkins et al. (2005), "From the body of literature as it stands today, a reasonable understanding exists in empirical sense, of how geosynthetics should be used for base reinforcement. Basic rules of thumb are available that may serve as a guide for designing flexible pavements with geosynthetic reinforcement. However, state transportation agencies have clearly indicated that geosynthetics are not used for base reinforcement because a cost-benefit analysis has not been established and because acceptable design solutions are not available." Attempts are currently being made to develop design models to be used in AASHTO and M-E design guides. The TBR and BCR ratios have been used in AASHTO design but they are limited in scope as both are specific to the product and test conditions under which they are calibrated. Thus, M-E methods due to their generic approach are more suitable for incorporating the geosynthetics in current design. However, due to the complex nature of flexible pavement involving interaction between various material layers, it has not been possible to fully calibrate geosynthetic response and damage models to be used in M-E design. Due to a lack of adequate performance data for such pavements, the current research emphasizes conducting laboratory and field tests to understand the underlying mechanisms.

There is experimental evidence that for the case of base course reinforcement, the mechanical properties of the geosynthetics are improved under the confinement provided by the soil. Based on the study of the interaction between geosynthetics and soils under confinement and traffic loads, it was found that the improved performance of geosynthetic reinforced pavements can be attributed to lateral restraint. Attempts have been made to quantify the lateral restraint in terms of the interface shear stiffness property of the soil-geosynthetic system. The field test sections constructed to evaluate this behavior showed improved performance in the reinforced sections over the unreinforced sections in terms of reduced surface deflections. However, the influence of this property on overall pavement performance has not been explicitly examined.

A number of laboratory confined tests were developed recently that focus on quantifying the interface shear stiffness of the soil-geosynthetic system. Most of these tests have applied cyclic loading to the soil-geosynthetic system in an attempt to simulate moving wheels. Since the measurements are sensitive to small changes in displacements, however, there has been great variability in the test results, thereby reducing the repeatability of the tests for given geosynthetics and making it difficult to distinguish between the performance of different geosynthetics. The current research focused on a confined test with monotonic loading to quantify the interface mechanism between the soil and geosynthetic.

Research is needed to develop and validate a transfer function wherein full-scale tests can be replicated in the laboratory setting for parametric study and then used to calibrate numerical models, which in turn provide a comprehensive design methodology for geosynthetic reinforced flexible pavement design. Finally, due to the increasing emphasis on constructing geosynthetic reinforced pavements with indigenous soils as subgrade and base course material, current needs go beyond the fundamental understanding of the problem and require the formulation of a consistent design methodology to encompass all the required factors.

Chapter 3: Geosynthetic Reinforced Pavements – An Analytical Study

"If everybody is thinking alike, somebody is not thinking."- George S. Patton

3.1 INTRODUCTION

The performance of geosynthetic reinforced pavement relies on the interaction between the soil and the reinforcement. The degree of interaction developed between the soil and the reinforcement is a function of soil type, reinforcement type and how they bond with each other. In fact, these factors are linked and the uncoupling of these factors is not straight forward. Thus, laboratory testing conditions which incorporate the various components must be chosen to realistically quantify the interaction mechanisms between the soil and the reinforcement. Although various test procedures have been developed to compute the soil-geosynthetic interaction mechanisms, the testing procedures under plane-strain monotonic-loading conditions are generally preferred, as discussed in Chapter 2. As shown in Figure 3.1, these testing procedures can be used to represent the governing mechanisms of lateral restraint for geosynthetic reinforced pavements under field working conditions.

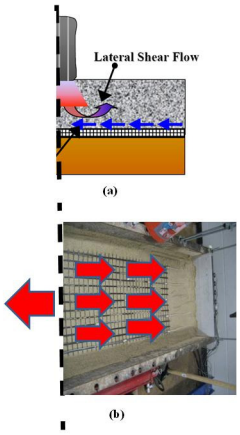

Figure 3.1 Geosynthetic reinforced pavement (a) Mechanism of lateral restraint in field under traffic loads (b) Replicating field behavior with laboratory plane-strain test using pullout device

The increasing use of geosynthetics in flexible pavements requires the evaluation of soil-geosynthetic reinforcement interface parameters. The performance of the geosynthetic reinforced pavement depends on the interaction between the soil layer and the geosynthetic inclusions. The two most common soil-reinforcement interaction testing methods currently used are direct shear and pullout tests.

The direct shear tests can be used to quantify the friction characteristics of both geogrids and geotextiles, whereas pullout tests help with the understanding of the interaction behavior of soil-geosynthetic system. The pullout tests are useful not only to study interface characteristics of geosynthetics but are especially helpful in characterizing the interlocking properties between bearing members of geogrids and surrounding soil. Furthermore, in case of pullout tests, the extensibility of reinforcement can be accounted for and boundary conditions can be chosen such that the interpretation of the test results is more realistic than in the case of direct shear tests (Palmeira, 1987). Therefore, pullout tests were conducted as part of this research to evaluate the interaction behavior of geosynthetics when used as reinforcement in the flexible pavements as explained in Chapter 2.

This chapter provides a review of the various methods proposed to conduct laboratory pullout tests and analyze the obtained data for determining the soil-geosynthetic interaction. This is followed by a discussion on the test procedure adopted for pullout tests in this research. The materials used in this testing phase consisted of two geogrids confined within base course and subgrade soil similar to one used in field test sections that will be discussed in Chapter 5. The aim for this initial phase of laboratory pullout tests was to address the underlying concepts and current method of analysis adopted to quantify soil-geosynthetic interaction. Based on the analysis of the results obtained, the limitation of this approach for applicability to geosynthetic reinforced pavements is subsequently discussed. Finally, a new analytical method is proposed to analyze pullout test data. The aim of the analytical model is to characterize the small displacement behavior of soil-geosynthetic interface using pullout tests, so they can be used for design of geosynthetic reinforced pavements.

3.2 PULLOUT TESTING OF GEOSYNTHETICS

3.2.1 Mechanisms involved

A reinforced soil mass is somewhat analogous to reinforced concrete in that the mechanical properties of the mass are improved by reinforcement inclusions placed parallel to the principal strain direction to compensate for soils' lack of tensile resistance (Elias et al., 2001). The improvement in the tensile resistance of the system results from the interaction between the reinforcement and the soil. When the reinforcements are distributed regularly throughout the soil mass, stress transfer between the soil and reinforcement takes place continuously along the reinforcement thereby improving the characteristics of the composite system. The two main mechanisms by which stress transfer between soil and reinforcement occurs is either friction or passive resistance depending on the reinforcement geometry. The friction mechanism is developed when there is a relative shear displacement corresponding to shear stresses between the soil and the reinforcement surface. On the other hand, the passive resistance mechanism is developed due to bearing type of stresses occurring on the transverse reinforcement surface which is normal to the direction of soil and reinforcement movement.

Geotextiles and geogrids are two commonly used geosynthetic types for pavement reinforcement application. Pullout tests are relevant for the study of the soil-reinforcement interaction characteristics of both these geosynthetics. Pullout resistance of geotextile reinforcement is provided mainly by friction resistance along the soil-geotextile interface as shown in Figures 3.2a and 3.2b. On the other hand, the pullout resistance of a geogrid is the result of not only its soil frictional resistance but also the coupled effect of tensile strength of longitudinal ribs and passive bearing resistance provided by its transverse members, as shown in Figures 3.2c and 3.2d. Tensile stresses are mobilized in the longitudinal reinforcing elements when they cross shear planes developed due to soil extension.

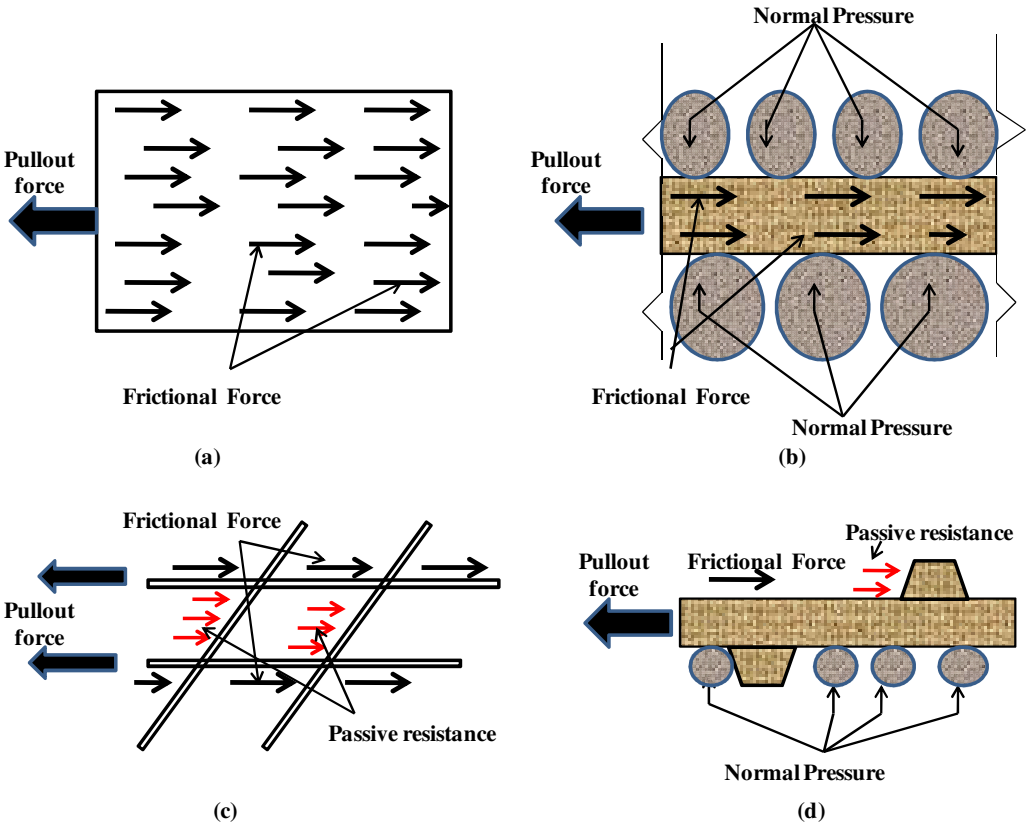

Figure 3.2 Soil reinforcement interaction mechanisms when geosynthetic is subjected to pullout force (a) cross- section of geotextile specimen (b) forces on geotextile (c) cross-section of geogrid specimen (d) forces on geogrid (adapted from Elias et al., 2001)

Pullout resistance of the reinforcement is mobilized through one or a combination of the two basic soil-reinforcement interaction mechanisms. The compositional characteristics of the geosynthetics such as its type, geometry, configuration and those of confining soil such as its grain size distribution and void ratio have significant effect on the results obtained from a pullout test. The interpretation of pullout test results is further complicated due to dilation of the soil and change in reinforcement load-strain-time characteristic during the tests due to applied confinement and displacement of the system. Therefore, it is important to quantify soil dilation behavior (generally with triaxial tests) and geosynthetics strength characteristics (wide width tensile test and creep tests) and account it in the final procedure adopted for analysis of test data.

The measured pullout resistance is influenced by the details of testing equipment and procedures. Specifically, the test results are highly influenced by the boundary conditions adopted during the pullout test for a given soil-geosynthetic system. According to Palmeira (2008), "While conducting the pullout tests one has to consider the influence of the boundary conditions on the test results, as the test is not standardized throughout the world." A thorough understanding is thus required to properly quantify the above effect while interpreting the test results obtained from a pullout test and is discussed in Section 3.2.2. This is followed by a discussion on the current limit equilibrium methods available to interpret the pullout test results.

3.2.2 Effect of boundary conditions

The interaction between the soil and the walls of the pullout box can affect test results significantly. The boundary conditions in the pullout test include the friction caused due to side walls when normal pressure is applied to the system. Also the interaction of the frontal wall with the geosynthetic needs to be accounted while conducting a pullout test.

Soil confinement during a pullout test is usually applied by means of flexible air bags to insure uniform distribution of normal stresses along a plane on the top of the specimen (Christopher et al., 1985; Palmeira and Milligan, 1989; Ingold, 1983; Farrag et al., 1993). The applied confining stress is partially carried out by the side wall friction causing a reduction in the normal pressure applied at the reinforcement level. Lubricated membranes have been used in an attempt to reduce the friction and provide a smooth boundary surface (Jewell, 1981; Farrag et al., 1993; Ferreira et al., 2008). Alternatively, for non-lubricated side wall test apparatus, the specimen-width to box-width ratio has been modified to minimize the effects of friction (Farrag et al., 1993). The theoretical and experimental studies conducted by Hayashi et al. (1996) and Ghionna et al. (2001) have shown that for geosynthetic specimens having a width smaller than the pullout box, the soil tends to dilate producing a three-dimensional confining effect. This leads to stress increases on the top of the specimen thereby causing an increase in the measured pullout

resistance. Therefore, for a non-lubricated side wall pullout box generally the specimen dimensions are adjusted such that the effect of soil dilatancy and side wall friction compensate each other thereby providing the required normal pressure at the top of the soil-geosynthetic interface. Also, the specimen length used in a pullout box affects the test results. Experiments conducted by Moraci and Recalcati (2005) indicated that longer geosynthetic specimens tend to experience extensibility effects. This leads to higher peak pullout resistance values obtained from longer specimens when compared with shorter specimens tested using the same pullout equipment.

The interaction between the reinforcement soil system and the rigid front wall can also influence the test results. As the reinforcement is pulled out of the box, the lateral earth pressure developed on the front face causes an increase in the pullout resistance (Palmeira, 1987; Palmeira and Milligan, 1989; Johnston and Romstad, 1989; Farrag et al.., 1993; Lopes and Ladeira, 1996; Raju, 1995; Sugimoto et al. 2001). Various alternatives to minimize possible influences of the box frontal face have been adopted. These include the use of sleeves around the pullout slot to transfer the point of application of the pullout load far behind the rigid front wall (Christopher et al. 1985; Wilson-Fahmy et al. 1994; Perkins and Cuelho, 1999) or using a flexible front face made of air-pressure bags (Williams and Houlihan, 1987) or a movable frontal face (Sugimoto et al., 2001).

A list of pullout boxes with various features developed by research centers is shown in Table 3.1 below. For the laboratory tests conducted in this study, the side and frontal wall clearances were adopted as per recommendations specified by the current ASTM D 6706 (2001) standard on pullout testing of geosynthetics. A side wall clearance of 150 mm (6 inches) between the specimen and the equipment boundary was maintained. Also, to minimize the effect of front wall friction, a steel sleeve 75 mm (3 inches) long with frontal aperture opening of 25mm (1 inch) was used. Both these clearances helped to minimize the influence of boundary condition on the final pullout test results.

Table 3.1 Main features of pullout boxes developed in various pullout studies

Research center	Reference	Dimensions of box L X W X H (mm)	Volume (m^3)	Frontal wall	Side wall	Clamping system
California DOT	Chang et al..,1977	1300 X 910 X 510	0.60	Removable plates	-	-
Oxford University	Palmeira and Milligan, 1989	1000X 1000 X 1000	1.00	Different roughness of front wall	Perpex Side wall	-
Kyushu University	Ochiai et al.., 1992	600 X 400 X 400	0.10	-	Lubricated inside walls	-
Louisiana State University	Farrag et al.., 1993	1520 X 900 X 760	1.04	Metal sleeves at front wall	-	Inside the box
University of British Columbia	Fanin and Raju, 1993; Raju, 1995	1300 X 640 X 600	0.50	Aluminum front and rear wall	Side wall glued with glass sheet	Outside the box
Saga University	Alfaro et al.., 1995	1600 X 600 X 500	0.48	Metal sleeves	Lubricated Rubber membrane	Inside the box
University of Porto	Lopes and Ladeira, 1996	1530 X 1000 X 800	1.2	Metal sleeves	Revetment of the internal walls	Outside the box
University of Sao Paulo, Sao Carlos	Teixeira, 1999	1500 X 700 X 500;	0.53	Metal sleeves	Silicon grease on the walls	Outside the box

Research center	Reference	Dimensions of box L X W X H (mm)	Volume (m^3)	Frontal wall	Side wall	Clamping system
Montana State University, Bozeman	Perkins and Cuelho, 1999	1250 X 900 X 1100	1.24	Two sleeves at front wall	Lubrication layer and low adhesion silicon grease	Outside the box
Asian Institute of Technology	Voottipruex et al., 2000	1270 X 762 X 508	0.50	Metal sleeves		Outside the box
Nagota University of Technology	Sugimoto et al..; 2001	680 X 300 X 625	0.12	Flexible and rigid front wall	Side walls in acrylic material	Outside the box
University of Sao Paulo, Sao Carlos	Teixeira, 2003	300 X 250 X 150	0.01	Sleeves at front wall	Silicon grease to reduce friction	Outside the box
University of Reggio, Calabria	Moraci et al., 2004	1700 X 600 X 680	0.70	Sleeves at front wall	Lubricated wall by means of adhesive and Teflon film	Outside the box
University of Texas, Austin	Zornberg and Kang, 2005	1520 X 610 X 280	0.26	Sleeves at front wall	Lubricated inside wall	Outside the box
PUC, Rio de Janeiro, Brazil	Sieira et al., 2009	1000 X 1000 X 1000	1.0	Sleeves at front wall	-	Outside the box

3.2.3 Limit equilibrium methods

The pullout resistance of geosynthetics is an important parameter for the design of reinforced structures. Currently used pullout resistance parameters were developed in early soil-reinforcement interaction studies as part of the internal stability evaluation of mechanically stabilized earth (MSE) walls (Holtz et al., 1998). In such structures, the design of soil-reinforcement system requires that the pullout capacity of the geosynthetic to be greater than the working tensile forces that develops under working stress conditions. The Federal Highway Administration (FHWA) recommends a single normalized approach for pullout evaluation of all reinforcement systems (Elias et al., 2001), which defines the pullout resistance per unit width of reinforcement, P_r as:

$$P_r = F^* \cdot \alpha \cdot \sigma'_{vo} \cdot C \cdot L_e \tag{3.1}$$

where F* is the pullout resistance factor, α is the scale effect correction factor (generally 1.0 for metallic reinforcements), σ'_{vo} is the effective vertical stress at the soil-reinforcement interface, C is the reinforcement effective unit perimeter (e.g., C=2 for metallic strips, geogrids and geotextiles), and L_e is the embedment length in the resisting zone behind the failure surface. In theory, the pullout resistance factor F* is defined as sum of pullout contributions by passive resistance and frictional resistance mechanisms in geosynthetics and is given as follows:

$$F^* = F_q.\alpha_\beta + \tan\rho \tag{3.2}$$

where F_q is the embedment bearing capacity factor, α_β is bearing factor for the passive resistance of geosynthetic and ρ is the soil-reinforcement interface friction angle. In case of geotextiles the passive resistance component is zero and pullout resistance factor is directly proportional to the frictional resistance at the interface, whereas in case of geogrids both frictional resistance and passive resistance are significant to determine the

ultimate pullout capacity of the reinforcement. However, the parameters needed to estimate the pullout resistances using the equation above are difficult to estimate in absence of site specific calibration.

Large scale pullout tests are thus conducted to estimate the extent of interaction between the soil and reinforcement to determine project specific properties. A simplified approach is followed to interpret pullout test results, which lumps all the interaction mechanisms together and is a modified form of Equation 3.1, which is given as follows;

$$P_{\max} = 2 \cdot L_e . C_i \cdot \sigma'_{vo} . \tan \phi' \tag{3.3}$$

where C_i is the coefficient of interaction based on ultimate pullout resistance, P_{max} from the pullout test and ϕ' is the effective friction angle of the confining material. The above equation can also be written as:

$$C_i = \frac{\frac{P_{\max}}{2.L_e.\sigma'_{vo}}}{\tan \phi'} = \frac{\tan \delta'}{\tan \phi'} \tag{3.4}$$

where δ' is the apparent angle of interaction between the geosynthetic and the confined material and is given as:

$$\tan \delta' = \frac{P_{\max}}{2.L_e.\sigma'_{vo}} \tag{3.5}$$

As part of the initial research effort, a series of pullout tests were conducted on the geosynthetics used in field test sections with base-course and subgrade soils at comparatively low normal pressures, which are expected under pavement working conditions. The results of 16 pullout tests (two geogrids tested in two principal directions with two different soils at two different normal pressures) were analyzed in terms of P_{max}

and C_i for these biaxial geogrids. This approach was chosen for preliminary evaluation of the soil-geosynthetic interaction and the results obtained were compared with values reported in the literature for the uniaxial geogrids used for MSE walls. This analysis helped in determining limitation of current pullout test evaluation methods developed for MSE walls to geosynthetic reinforced pavement design. Based on the lessons learnt, a new analytical model was proposed to interpret the test results, as will be discussed in Section 3.6. The properties of geosynthetics and soils used in testing are presented in Section 3.3.2.

3.3 MATERIALS USED

3.3.1 Properties of soils used

The two main soil types of interest were the base-course and subgrade soil. These were used in the field test sections to construct the pavement. On-site soil, described as black clay, was used as subgrade soil whereas the base course material was obtained from a local quarry. A suite of geotechnical tests were conducted on these two soils to characterize their properties which were used in analysis of pullout test results.

3.3.1.1 Subgrade soil

The FM2 clay which will be referred to as "Subgrade soil" was obtained from the construction site in May 2005. The soil was excavated with a backhoe from a depth of approximately 5 feet near the station 184 close to the lane K6 on FM2 road as explained in Chapter 5. The soil was then transported to the laboratory in two 55 gallon plastic drums. It was dried by placing it on metal trays in a temperature controlled room at a temperature of 49^0C for 48 hours. The dried soil was then broken down with a hammer and passed through a soil crushing machine. The soil was then sieved and particles passing No. 10 sieve were set aside for index testing. The grain size distribution curve obtained by sieve analysis conducted on subgrade soil is shown in Figure 3.3.

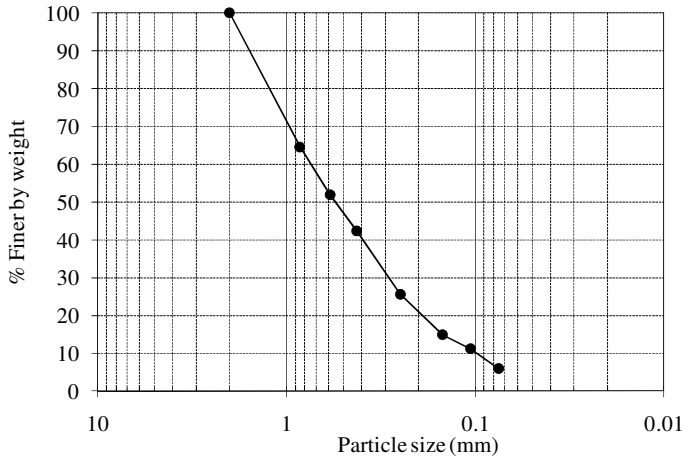

Figure 3.3 Grain size distribution for subgrade soil

According to ASTM D2488 (2001), the subgrade soil classifies as gray clay with high plasticity (CH), high dry strength, and no dilatancy. Atterberg limits in terms of liquid limit and plasticity index were determined according to ASTM D4318 (2001) for subgrade soil and the values obtained are 33 and 39 respectively (Figure 3.4). Standard proctor compaction tests were performed on the subgrade soil as per ASTM D698 (2001). The maximum dry unit weight for subgrade soil was 15.5 kN/m^3 with optimum water content at 32 % (Figure 3.5).

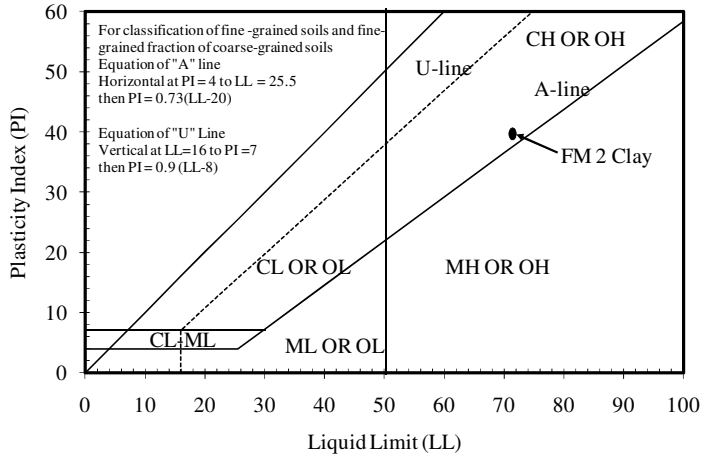

Figure 3.4 Plasticity chart for subgrade soil

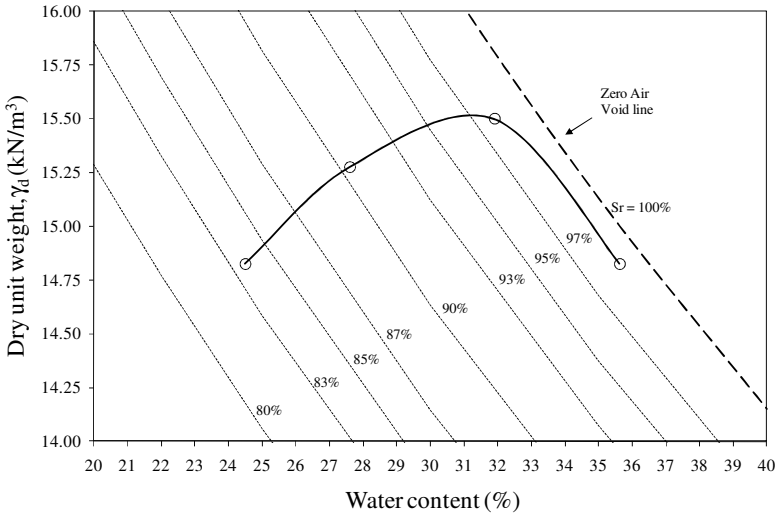

Figure 3.5 Standard Proctor compaction test for subgrade soil

A one-dimensional oedometer test was performed on a soil specimen compacted at the optimum moisture content. The vertical effective stress-strain relationship is as shown in Figure 3.6. As the specimen tested was obtained from remolded soil, a clear preconsolidation pressure value could not be obtained. Further, the sample swelled instead of shrinking until the effective vertical stress was increased beyond 500 kPa.

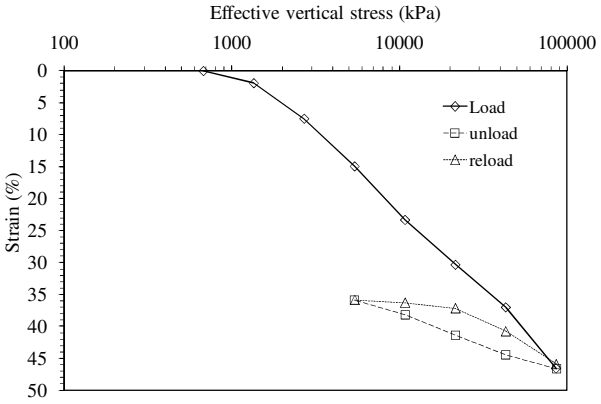

Figure 3.6 Effective vertical stress-strain curve for subgrade soil

Hydraulic conductivity test on FM 2 clay specimens prepared using standard proctor mould were conducted in a flexible wall permeameter. The saturated hydraulic conductivity values for the specimens prepared at different compaction water contents is shown in Figure 3.7. The saturated hydraulic conductivity of subgrade at optimum water content of 32% was obtained as 2 X 10^{-09} cm/s.

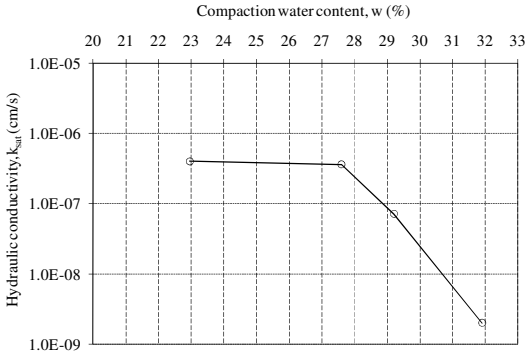

Figure 3.7 Hydraulic conductivity of subgrade soil

The geotechnical properties of subgrade soil are summarized in Table 3.2.

Table 3.2 Properties of subgrade soil

Test	Index Parameter	Value	ASTM Standard
Soil Classification		CH	D 2488
Specific Gravity	Specific Gravity, Gs	2.7	D 854
Particle size analysis	D_{10}, mm	0.1	D 422
	D_{30}, mm	0.3	D 422
	D_{60}, mm	0.7	D 422
	Uniformity coefficient, C_u	7	
	Coefficient of gradation, C_c	1.3	
Atterberg limits	Liquid limit, LL (%)	33	D 4318
	Plastic limit, PL (%)	72	D 4318
	Plasticity index, PI (%)	39	D 4318
Standard Proctor Compaction	Optimum water content, %	32	D 698
	Maximum dry unit weight, γ_d (kN/m^3)	15.5	D 698

3.3.1.2 Base course

The "Base-course" used on the FM 2 site was obtained from the contractor's yard in Navasota, Texas. The base course was transported from the contractor's yard to the geotechnical testing laboratory in two plastic drums of 55 gallon each. As per ASTM D 2488 (2001), the base course was classified as silty gravel with sand (GM). The results of sieve analysis conducted on the material are as shown in Figure 3.8.

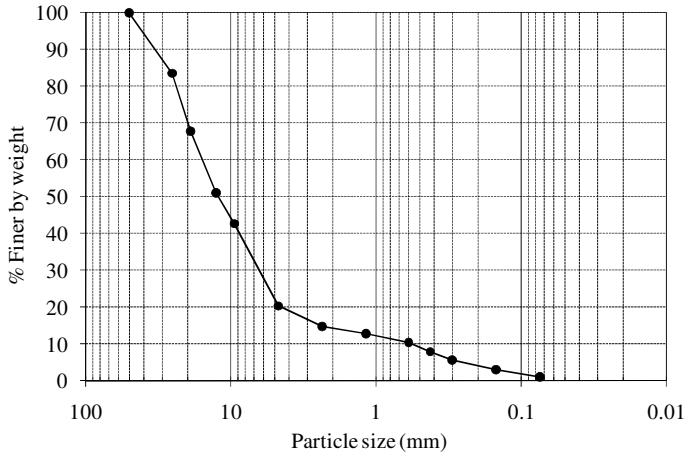

Figure 3.8 Grain size distribution curve for base course material

Standard proctor compaction tests were performed on the base course material as per ASTM D698 (2001) and the results obtained are shown in Figure 3.9. The base course had maximum dry density of 22.5 kN/m^3 and optimum water content of 8%. This was significantly lower than the optimum water content obtained for the subgrade soil. In the field conditions, generally the compaction requirements for base course require the achieved density of 95-98% of maximum density obtained from the standard proctor test for the base course material.

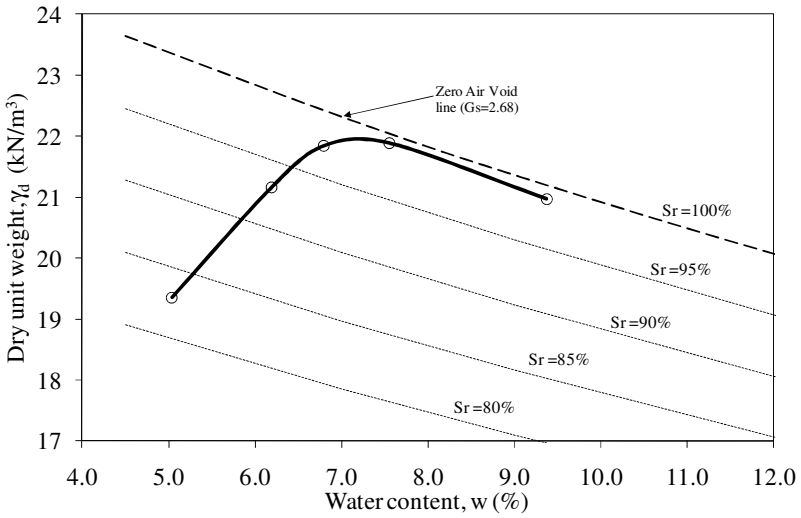

Figure 3.9 Standard Proctor Compaction curve for base course material

The relevant geotechnical properties of base course are summarized in Table 3.3.

Table 3.3 Properties of base course material

Test	Index Parameter	Value	ASTM Standard
Soil Classification		GM-ML	D 2488
Specific Gravity	Specific Gravity, Gs	2.6	D 854
Particle size analysis	D_{10} , mm	0.6	D 422
	D_{30} , mm	6.0	D 422
	D_{60} , mm	10.8	D 422
	Uniformity coefficient, C_u	18.0	
	Coefficient of gradation, C_c	5.6	
Standard Proctor Compaction	Optimum water content, %	7.5	D 698
	Maximum dry unit weight, γ_d (kN/m^3)	22.0	D 698

3.3.2 Characteristics of geosynthetics used

The geosynthetics used in this testing phase consisted of two biaxial geogrids as shown in Figure 3.10. Geogrid 1 (G1) is a biaxial polypropylene geogrid manufactured by Tensar and marketed as BX-1100 as shown in Figure 3.10a. Geogrid 2 (G2) is a biaxial polyethylene geogrid with a protective PVC coating manufactured by Mirafi and marketed as BasX-11 as shown in Figure 3.10b. The average index properties of these geosynthetics as reported by the manufacturers in both machine direction (MD) and cross-machine direction (XD) are shown in Table 3.4. A series of index test were conducted to quantify the project specific properties of these geosynthetic which included percent open area, rib thickness and single rib tensile test. Finally, junction efficiency test and wide-width tensile test were conducted as discussed in Section 2.4.2.1 for determining baseline properties of these geosynthetics to be compared with pullout tests.

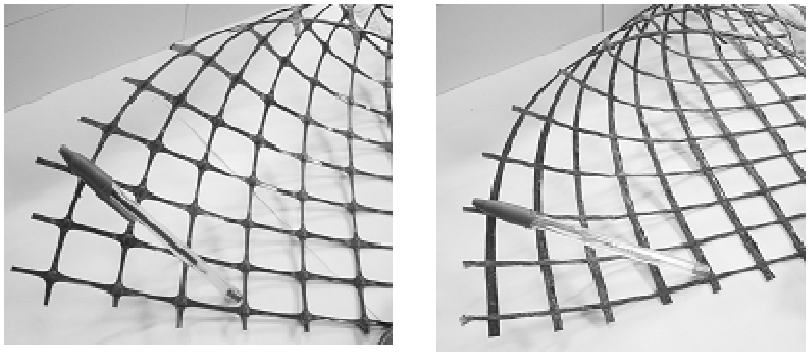

(a) **(b)**

Figure 3.10 Geosynthetics used in pullout test (a) G1 (b) G2

Table 3.4 Manufacturer's specification for the geogrids

Index properties	Units	G1		G2	
		MD	XD	MD	XD
Aperture dimensions	**mm**	25.0	33.0	25.4	25.4
Tensile strength at 2% strain	**kN/m**	4.1	6.6	7.3	7.3
Tensile strength at 5% strain	**kN/m**	8.5	13.4	13.4	13.4
Ultimate tensile strength	**kN/m**	12.4	19.0	29.2	29.2

3.3.2.1 Percent open area

The percent open area for a given geogrid is defined as the ratio of empty area to the total covered area (values reported in percentage). The value of percent open area for both geogrids was measured using digital image analysis. The geogrid specimen was placed over a scanning table and then a camera was used to take picture of the representative area as shown in Figure 3.11 below. The percent open area obtained for geogrid G1 was 75% where as that for geogrid G2 was 70%.

Figure 3.11 Percent open area of geogrid (Source: TxDOT Laboratory, Austin)

3.3.2.2 Rib thickness

The rib thickness of both the geogrids in machine and cross machine direction was measured using a vernier caliper. The average value, based on five readings for rib thickness for both geogrids are 0.76 mm for G1 and 1.0 mm for G2.

3.3.2.3 Single rib tensile test

Single rib tensile testing was conducted for two geogrids in accordance with ASTM D6337 (2009). The specimens consisted of a single rib of the geogrid with five junctions. The junctions were clamped at the ends using the serrated jaw grip to prevent slipping and crushing of the specimen. The grips were then attached to the load frame such that one rib had three junctions in the direction of concern. The tests were conducted using a constant rate of extension testing machine to pull a single rib to failure by moving at a rate of 50 mm/minute. Five tests were conducted for both geogrids in machine and cross machine direction.

The results obtained for both geogrids are as shown in Figure 3.12. In geogrid G1, the tensile properties were different in both the directions. In the machine direction, the specimen maintained an approximately constant maximum tensile strength once peak was attained as shown in Figure 3.12a, whereas in cross-machine direction the specimen had brittle failed once the peak tensile force was reached during the test as shown in Figure 3.12b. The geogrid G2 showed an S-shaped tensile curve in both machine and cross-machine direction.

The response of geogrid G2 in terms of tensile force was however different for the given strain level than that of the geogrid G1 in both the directions. It was found that for strain values less than 1%, the slope of the tensile force versus strain curve was steeper than for higher strain levels in both machine and cross machine direction for geogrid G2. The geogrid G2 had lower strength in machine direction as shown in Figure 3.12c than cross machine direction as shown in Figure 3.12d. When the ultimate tensile strength for both the geogrids was compared, it was found that the geogrid G1 had lower tensile strength as compared to geogrid G2 in both machine and cross-machine directions.

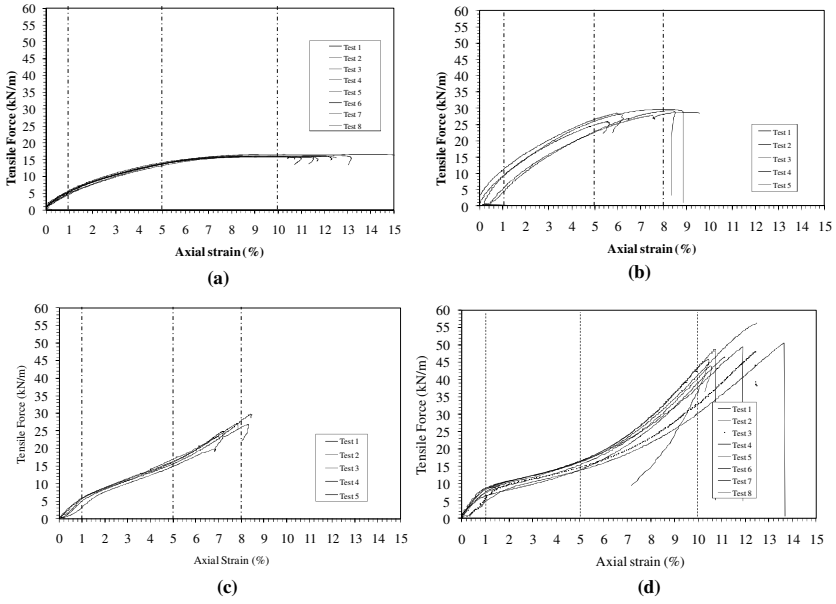

Figure 3.12 Single rib tensile test results for geogrids: (a) G1-machine, (b) G1-cross machine, (c) G2-machine, (d) G2-cross machine direction

Finally, based on the single rib tensile tests the average maximum rib tensile strength and average geogrid tensile strength for each geogrid was calculated as follows:

$$T_{rib} = \frac{\sum_{i=1}^{n} T_i}{n} \tag{3.6}$$

$$T_{grid} = T_{rib} . n_{rib} \tag{3.7}$$

where T_{rib} is the average maximum tensile strength (kN), T_i is the maximum rib tensile strength (kN) of i^{th} specimen, T_{grid} is the average geogrid tensile strength (kN/m), n is the total number of test specimens and n_{rib} is the number of ribs per meter length of the specimen. Also, the average secant modulus at 2% strain ($M_{2\%}$) was calculated based on $T_{2\%}$ which is the tensile strength of the i^{th} specimen at 2% elongation as follows:

$$M_{2\%} = \frac{\frac{n_{rib}}{n}}{0.02} \sum_{i=1}^{n} T_{2\%} \tag{3.8}$$

The average values for tensile strength and modulus of the two geogrids are reported in Table 3.5. The geogrid G1 had lower ultimate tensile strength than geogrid G2. When the secant modulus at 2% strain was compared, both the geogrids showed comparable value in cross machine direction, however G1 had twice as high value of tensile modulus in the machine direction than G2. This indicated that geogrid G1 was stiffer at low strain magnitudes, though it had lower ultimate tensile strength than geogrid G2.

Table 3.5 Single rib tensile testing results for the geogrids

Properties		Units	G1		G2	
			MD	XD	MD	XD
Number of ribs,	n_{rib}	**ribs/meter**	39	25	30	36
Ultimate tensile strength,	T_{grid}	**kN/m**	24.6	18.6	22.0	57.9
Secant modulus,	$M_{2\%}$	**kN/m**	631	439	354	590
Strain at failure		**%**	10	7.5	7.7	11.6

3.3.2.4 In-isolation junction strength test

The in-isolation junction strength was conducted on the geogrids by pulling a longitudinal rib away from its transverse ribs junction. The test is referred to as in-isolation test since there is no normal stress on the junction and thus does not represent the performance conditions of the geogrid under confined conditions (Koerner, 2005). The junction strength of both geogrids was tested using a tensile testing machine capable of moving at a constant rate of extension of 50 mm/minute. The specimens were prepared by cutting the junctions from each side of the geogrid to allow for the maximum amount of transverse ribs on each side of the junction to be tested. The specimen was mounted so that the center "T" was attached to the rib clamp and the transverse rib was attached on both sides of the junction to the junction clamp as shown in Figure 3.13.

Figure 3.13 Single rib tensile testing of geogrids: (a) Specimen clamped at the grips (b) Specimen after the test (Source: TxDOT Laboratory, Austin)

The geogrids G1 and G2 were tested in the laboratory in machine and cross-machine direction using above procedure for the junction strength. The results obtained are shown in Figure 3.14. The geogrid G1 had higher junction strength in machine direction (Figure 3.14a) as compared to cross machine direction (Figure 3.14b). Furthermore, the geogrid G1 had higher junction strength as compared to geogrid G2 in both machine (Figure 3.14c) and cross machine direction (Figure 3.14d).

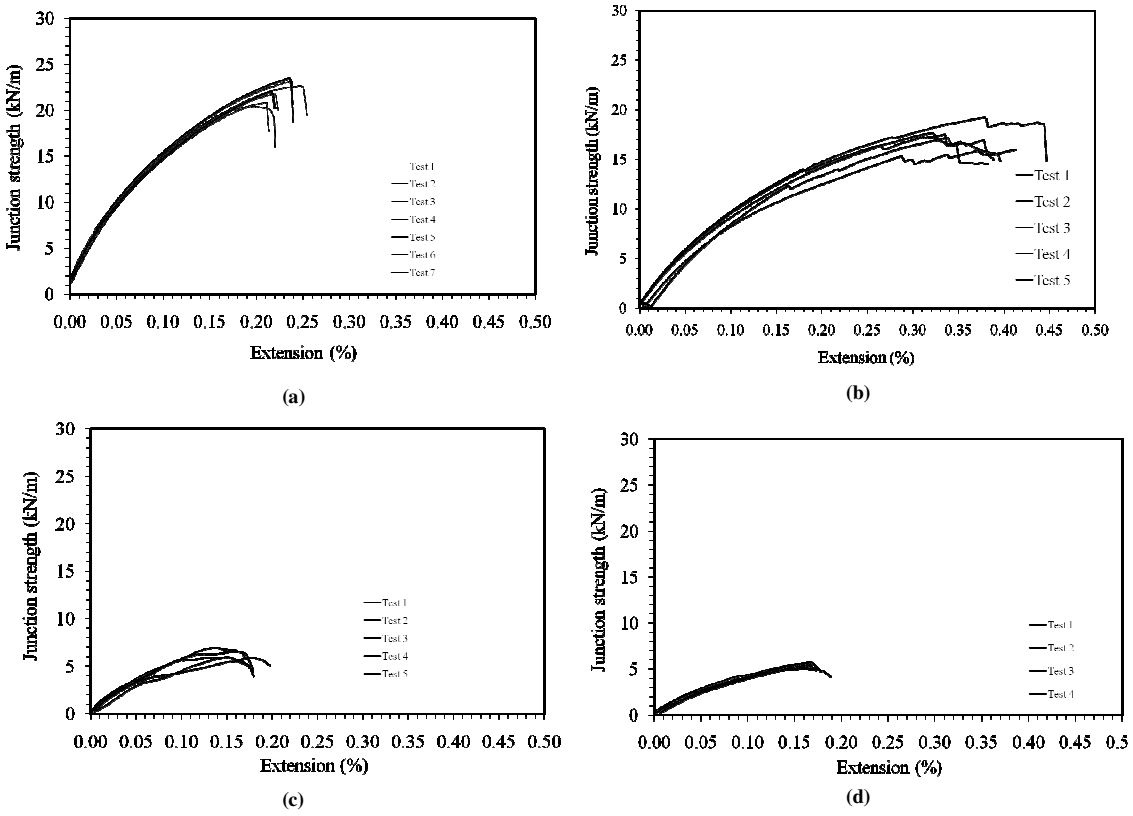

Figure 3.14 Junction strength test results for geogrids: (a) G1-machine (b) G1-cross machine (c) G2-machine (d) G2-cross machine direction

The average maximum junction tensile strength was calculated as:

$$J_{rib} = \frac{\sum_{i=1}^{n} J_i}{n} \tag{3.9}$$

$$J_{grid} = (J_{rib}).(n_{junction}) \tag{3.10}$$

where J_{rib} is the average maximum junction tensile strength (kN), J_i is the maximum junction tensile strength of ith specimen (kN), n is the total number of test specimens, J_{grid} is the average geogrid junction strength (kN/m) and $n_{junction}$ is the number of junctions per meter length of the geogrid. The above sets of data i.e. ultimate rib strength and junction strength were then used to obtain a junction strength efficiency value. The junction strength efficiency ($E_{junction}$) was calculated as:

$$E_{junction} = \frac{J_{rib}}{T_{rib}} \times 100 \tag{3.11}$$

The ultimate tensile strength and junction efficiency values obtained for both geogrids are listed in Table 3.6. The test results indicated that G1 has higher junction efficiency than G2 in both machine and cross-machine direction.

Table 3.6 Junction efficiency results for the geogrids

Properties	**Units**	**G1**		**G2**	
		MD	**XD**	**MD**	**XD**
Ultimate tensile strength	**kN/m**	24.6	18.6	22.0	57.9
Junction strength	**kN/m**	24	15.3	5.7	7.0
Junction efficiency	**%**	100	82.6	26.0	12.2

3.3.2.5 Wide width tensile testing

An important unconfined property of a geosynthetic is its tensile strength. Wide width tensile test were conducted on both geogrids in accordance with ASTM D4595 (2001), which uses a 200 mm (8 in) wide specimen which is 100 mm (4in) long. The basic idea of a tensile strength test is to place the geosynthetic within a set of clamps or jaws, and stretch the assembly in a mechanical testing machine at constant rate of extension as shown in Figure 3.15. In this study, the geosynthetics were tested in both machine and cross machine direction. Further the effect of rate of testing, on the tensile strength of these geosynthetics was evaluated by testing them at 1%, 5%, 10% and 20% strain rate per minute. A series of five tests were conducted at each of the four strain rates thereby making total of 20 tests in each direction for a given geosynthetic.

Figure 3.15 Wide width tensile test setup for (a) Geogrid G1 (b) Geogrid G2

The averages of the series of five tests conducted at each strain level for each geosynthetic direction are shown in Figure 3.16. The geogrid G1 had lower ultimate tensile strength in machine direction (Figure 3.16a) as compared to cross machine direction (Figure 3.16b). Further, the geogrid G2 also had lower ultimate tensile strength in machine direction (Figure 3.16c) as compared to cross machine direction (Figure 3.16d). The results also indicated that the tensile strength of geogrids at low strains (1%) was independent of the strain rate at which test was conducted and there was slight increase in strength at higher strain levels of 5% and 10%.

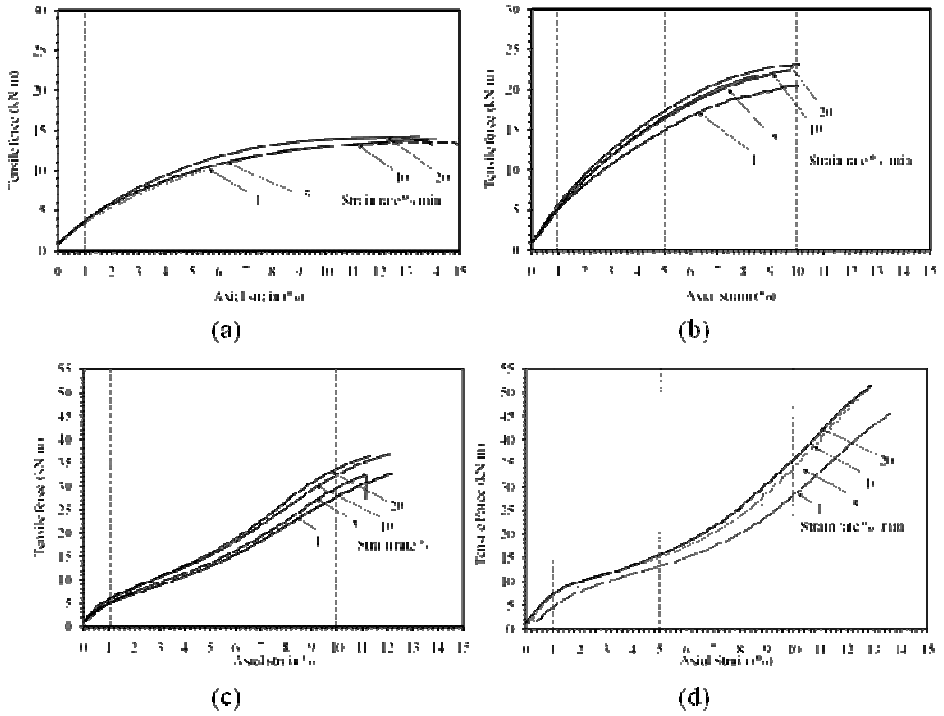

Figure 3.16 Wide width tensile test results for geosynthetics: (a) G1-machine (b) G1-cross machine (c) G2-machine (d) G2-cross machine direction

The information gained from wide width tension tests on a geosynthetic includes: the tensile strength at which the test specimen fails, the tensile elongation at which the test specimen fails i.e., its failure strain, the tensile stress at different elongations prior to specimen failure i.e., stress at 1%, 2%, 5% strain and the tensile modulus taken from the initial portion of the strength-versus-elongation curve. The average tensile stiffness obtained at rate of testing of 10 % for the two geosynthetics is shown in Table 3.7. The test results indicated that both the geogrids were stiffer in the cross-machine direction as compared to the machine direction. Furthermore, geogrid G1 had higher stiffness at 5% strain than geogrid G2, which is the criterion generally adopted for design of unpaved roads as discussed in Chapter 2. The values of tensile strength obtained using wide width tensile test showed good agreement with those obtained using the single rib tensile test as reported in Table 3.5.

Table 3.7 Wide width tensile tests results for the geogrids

Properties	Units	G1		G2	
		MD	XD	MD	XD
Stiffness at 1% strain	**kN/m**	368	531	527	579
Stiffness at 2% strain	**kN/m**	287	437	379	446
Stiffness at 5% strain	**kN/m**	199	323	278	282
Stiffness at 10% strain	**kN/m**	132	232	300	316
Stiffness at maximum load	**kN/m**	97	226	289	366
Strain at maximum load	**%**	14	10	12	13

3.3.3 Discussion

The tests discussed above helped in determining the index properties of soils and geosynthetics used in the pullout testing scheme. The unconfined tensile strength of the geosynthetic was compared with the confined stiffness of the geosynthetics obtained from pullout tests as explained in Chapter 4. The soil properties were used to understand the moisture flow pattern below the pavement as discussed in Chapter 5. Thus, these properties were useful for analysis throughout the course of this research study.

3.4 COEFFICIENT OF INTERACTION

3.4.1 Test Matrix

The laboratory pullout tests to evaluate the coefficient of interaction (C_i) for geogrids G1 and G2 when confined in base course and subgrade soils obtained from FM 2 site were conducted as part of this study. A total of 16 pullout tests were conducted which consisted of two geosynthetics (G1 and G2) in two principal directions (machine and cross-machine) at two confining pressures (7 kPa and 21 kPa) using two soils (base course and subgrade soil) as confining materials. A list of tests conducted using above combination of materials is listed in Table 3.8 below.

Table 3.8 Testing matrix for pullout test to determine coefficient of interaction

S.No	Geosynthetic type	Confining material	Test direction	Normal pressure (kPa)	Abbreviation
1	G1	Base course	MD	7	G1-BC-MD-07
2				21	G1-BC-MD-21
3			XD	7	G1-BC-XD-07
4				21	G1-BC-XD-21
5		Subgrade	MD	7	G1-SG-MD-07
6				21	G1-SG-MD-21
7			XD	7	G1-SG-XD-07
8				21	G1-SG-XD-21
9	G2	Base course	MD	7	G2-BC-MD-07
10				21	G2-BC-MD-21
11			XD	7	G2-BC-XD-07
12				21	G2-BC-XD-21
13		Subgrade	MD	7	G2-SG-MD-07
14				21	G2-SG-MD-21
15			XD	7	G2-SG-XD-07
16				21	G2-SG-XD-21

* BC-Base course SG –Subgrade MD –Machine Direction XD- Cross Direction

3.4.2 Test Apparatus

The pullout equipment used to conduct the tests (Figure 3.17) consisted of a box with internal dimensions of 1.5 m (60 inches) length, 0.6 m (24 inches) width and 0.3 m (12 inches) height. The box dimensions satisfied the criterion as specified by ASTM standard D6706 (2003) for conducting standard pullout test.

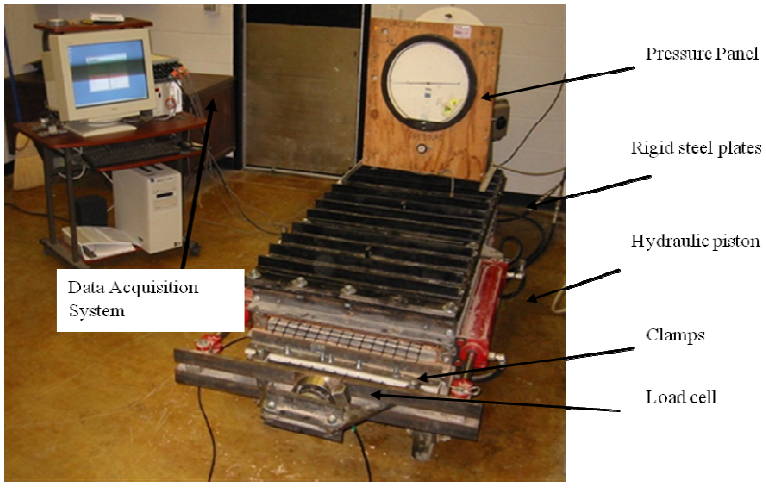

Figure 3.17 Pullout test setup

The various components of test apparatus are shown in Figure 3.18. The original equipment design consisted of a hydraulic system wherein an airflow pump system (Figure 3.18a) was used to push the oil through cylindrical pistons. This action generated the required force to pull the specimen out of the box during the test. The direction of piston movement was regulated using a three way ball valve. A flexible pneumatic device in the form of rubber membranes was used to apply and maintain a uniform normal stress over the entire pullout box area. The normal pressure was applied on the surface of the soil sample from the reaction force generated by inflating the air bags (Figure 3.18b), placed between the soil surface and the cover of the box made of the steel plates. An extension road (Figure 3.18c) was used with a vibratory hammer (Figure 3.18d) to compact the base course and subgrade soil in the pullout box. The instrumentation used during this test composed of a load cell and linear variable displacement transducers (LVDTs) as shown in Figure 3.18e.

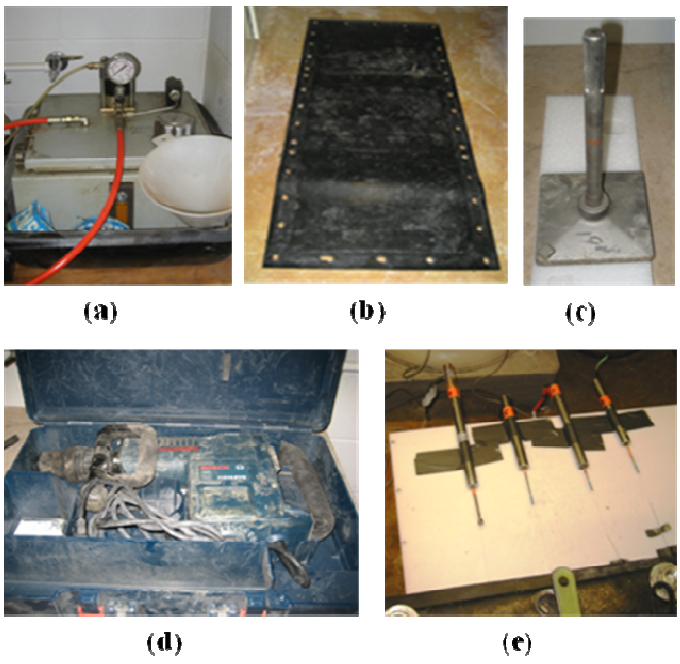

Figure 3.18 Pullout test apparatus: (a) Air flow pump; (b) Rubber membrane; (c) Wide-plate compaction rod; (d) Vibratory hammer; (e) LVDT's

3.4.3 Test Preparation

The pullout test specimen preparation consisted of cutting the geogrid specimen to the required dimensions from the roll, moisture conditioning the soil, attaching the tell tales to the geogrids, clamping the geogrid to the grips and then finally compacting the soil in the pullout box. Based on the clearance requirements, the specimen was prepared with a confined length and width of 0.6m and 0.45m, respectively. For uniform compaction of soil throughout the pullout box, it was decided to compact soil in four layers of three inch thickness each. The first two layers of soil were compacted using a vibratory hammer as shown in Figure 3.19a. Then the geogrid was placed on top of the second layer. The front end of the geogrid was attached to the grips to maintain slight tension to ensure its horizontal position on the surface of second layer as shown in Figure 3.19b. Then the tell tales were attached at the required junctions (at distance of 0.1m, 0.3m and 0.6m) from the front end of the geogrid specimen in staggered pattern as shown in Figure 3.19c. Then the top two layers of the soil were compacted using the vibratory hammer as shown in Figure 3.19d. The rubber membrane was then placed at the top of the compacted soil layer and enclosed by steel plates as shown in Figure 3.19e. Special care was taken while fastening the bolts and nuts on top of steel plates, to maintain the uniform air pressure and prevent leaks at high air pressures. Finally, the air pressure line was connected to the valve on the top of the rubber membrane to apply the required normal pressure.

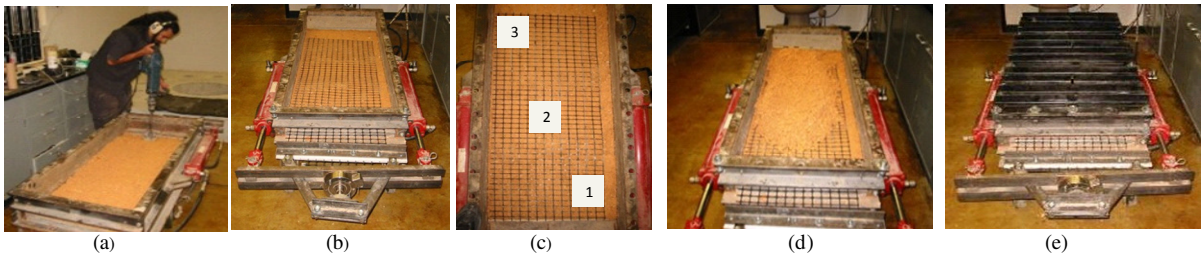

(a) (b) (c) (d) (e)

Figure 3.19 Pullout test preparation: (a) Compaction of bottom half of box; (b) Attaching the geosynthetic specimen to the grips; (c) Attaching tell tale wires to the specimen; (d) Compacting top half of the box; (e) Assembling normal pressure system

3.4.4 Testing Procedure

The pullout test was started by supplying air pressure to the rubber membrane. The air control valve was adjusted to the required pressure reading so that the top of specimen had the normal pressure value as required for the test. Once the required pressure level was reached, the system was allowed to equilibrate for thirty minutes. Then the load cell and the LVDT's were connected to the data acquisition system ports. A program was written using Labview 7.0 software developed by National Instruments (NI) and was used to acquire data from the instruments during the test. The pullout tests were conducted using a constant rate of displacement of 3mm/minute. Therefore, the flow valves on the two cylinders were adjusted to provide the constant rate of piston movement of 3 mm/minute for the entire duration of the test. The test was continued until the geogrid failed in pullout or tension mode. Pullout mode of failure was assumed to occur when displacements of all the three LVDT's became equal with no further change in frontal force or the last LVDT moved more than 25 mm (1 inch). Tensile mode of failure was assumed to occur if the geogrid slipped at the clamping end or the unconfined portion of the geogrid ruptured as shown in Figures 3.20a and 3.20b respectively. The test was stopped after failure and the top plates were removed. The soil was then stored in buckets to prevent the loss of moisture for future tests. The specimen was carefully removed and the soil layer was examined for slippage at the interface.

Figure 3.20 Tensile mode of failure due to: (a) slippage at the clamping grips; (b) rupture of the specimen at the end of the test

3.4.5 Results

The data obtained from pullout tests consisted of frontal pullout force readings from the load cell and the displacement profiles at three points from the LVDT's for a given time during the test. Typical results for a given pullout test are shown in Figure 3.21 for geogrid G2 in cross-machine direction with subgrade as the confining material at normal pressure of 7 kPa (G2-SG-XD-07). The maximum pullout force reported in this case was 11.8kN/m.

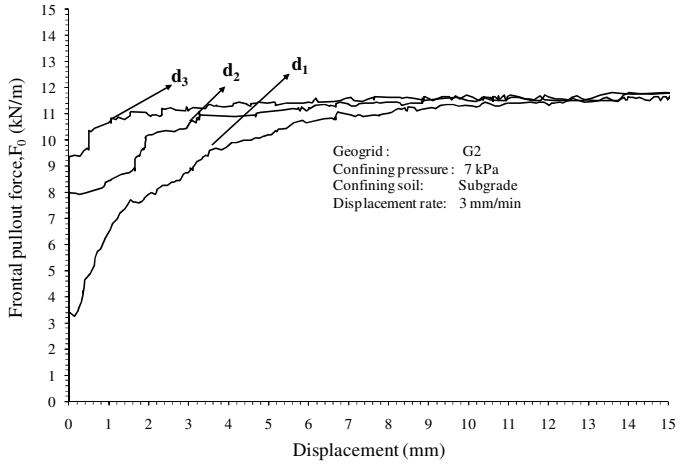

Figure 3.21 Typical pullout test load-displacement curve for a given geogrid

The maximum pullout force for all the 16 tests was then obtained as shown in Table 3.9. The variation of maximum pullout force with confining pressure for both geogrids G1 and G2 in machine and cross-machine direction for both subgrade and base course material are shown in Figures 3.22a through 3.22d. It was observed that the maximum pullout force increased with the increase in the confining pressure. The confining soil type also had an effect on the maximum pullout resistance of these geogrids. At low confining pressure of 7 kPa, both the geogrids had higher pullout resistance when confined in subgrade soil as compared to base course material. However, at higher confining pressure no such trend was observed as the pullout resistance was equal to the maximum tensile strength of the geosynthetics.

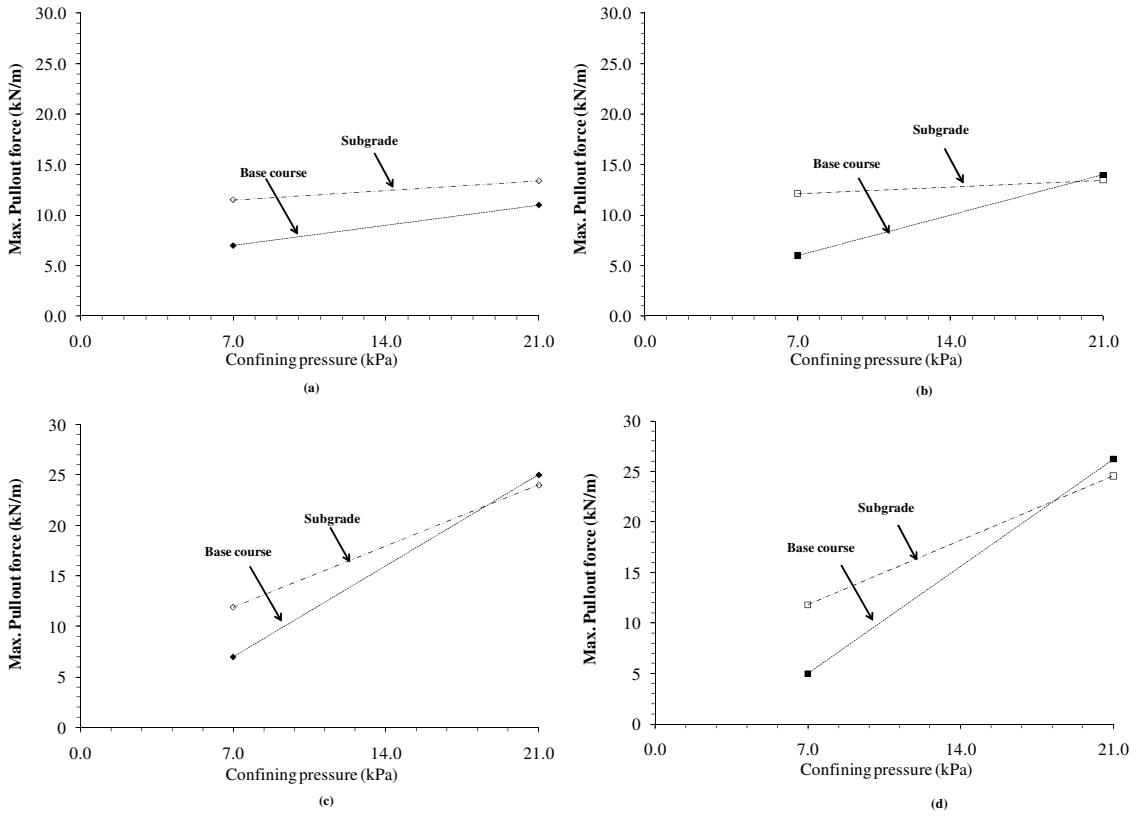

Figure 3.22 Variation of maximum pullout force with confining pressure and soil type for geogrids: (a) G1 -MD (b) G1-XD (c) G2-MD (d) G2-XD

The coefficient of interaction was computed for each test using Equation 3.4 as discussed in Section 3.2.3. For design purposes, the maximum value of coefficient of interaction is limited to 1.0, as theoretically friction angle of the interface between the soil and the geosynthetic cannot exceed the friction angle between soil-soil interfaces. The calculated values and design values of C_i for each test are listed in Table 3.9 below. The minimum value of C_i obtained was 0.7 and for most cases it was equal to the maximum value of 1.0. The value of C_i was in the range specified for most of the geogrids, which is generally between 0.65-1.0. Based on the results obtained no clear criteria for distinguishing the performance of both the geogrids could be established (either in terms of soil type or direction of testing or confining pressure). Therefore, this method was not found suitable for application to the reinforced pavement design.

Table 3.9 Coefficient of interaction obtained from the pullout tests

S.No	Test	Maximum pullout force	Maximum tensile strength	Coefficient of interaction, C_i		Failure mode
		kN/m	kN/m	Calculated	Design	
1	G1-BC-MD-07	7.0	12.4	1.24	1.0	Pullout
2	G1-BC-MD-21	11.0	12.4	0.65	0.7	Pullout
3	G1-BC-XD-07	6.0	18.9	1.06	1.0	Pullout
4	G1-BC-XD-21	14.0	18.9	0.82	0.8	Tensile
5	G1-SG-MD-07	11.5	12.4	2.4	1.0	Pullout
6	G1-SG-MD-21	13.4	12.4	0.9	0.9	Pullout
7	G1-SG-XD-07	12.2	18.9	2.5	1.0	Pullout
8	G1-SG-XD-21	13.5	18.9	0.9	0.9	Pullout
9	G2-BC-MD-07	7.0	29.1	1.24	1.0	Pullout
10	G2-BC-MD-21	25.0	29.1	1.47	1.0	Tensile
11	G2-BC-XD-07	5.0	29.1	0.88	0.9	Pullout
12	G2-BC-XD-21	26.2	29.1	1.77	1.0	Tensile
13	G2-SG-MD-07	11.9	29.1	2.5	1.0	Pullout
14	G2-SG-MD-21	24.0	29.1	1.7	1.0	Pullout
15	G2-SG-XD-07	11.8	29.1	2.4	1.0	Pullout
16	G2-SG-XD-21	24.6	29.1	1.7	1.0	Pullout

3.4.6 Limitations

The conventional pullout tests are analyzed to obtain the coefficient of interaction corresponding to the peak pullout force as explained above. This conventional analysis is based on limit equilibrium approach and focuses on ultimate loading conditions which occur under large displacements. Furthermore, this method is incapable of taking the effect of geosynthetic geometry, length, extensibility, and the amount of soil confinement into account while predicting its performance of various geosynthetics. For pavement design, the quantification of soil-geosynthetic interface stiffness at comparatively low displacements is critical. The above test is sensitive to boundary conditions and test apparatus used such that the measured soil-geosynthetic behavior at the regime of low displacement is usually not reliable. Therefore, a better analysis technique and testing equipment is required to capture the soil-geosynthetic behavior at low displacement magnitudes reliably.

An analytical model which can be obtained using pullout test data without making any unrealistic assumptions is proposed as part of this research. This model was used to predict the soil-geosynthetic interface stiffness at low displacements magnitude. This stiffness values can be used as an index to compare the performance among various geosynthetics. Furthermore, the existing pullout equipment was upgraded to meet the testing requirements of the proposed model, as discussed in Chapter 4.

3.5 ANALYTICAL MODEL FOR PULLOUT TEST

Various theoretical and empirical procedures have been developed in order to model the soil-geosynthetic interface mechanism during pullout. These procedures can be grouped into two broad categories, limit equilibrium method and analytical methods. The limit equilibrium methods neither give sufficient information on the pullout force nor displacement and strains developed in the reinforcements prior to failure (Rowe and Mylleville, 1994). On the other hand, analytical methods can be used to predict displacement, strains and force generated in the reinforcement during the deformation as well as failure (Sugimoto and Alagiyawanna 2003).

Analytical solutions to interpret and analyze data obtained by pullout test have been proposed by Juran and Chen (1988), Yuan and Chua (1991), Abramento and Whittle (1995), Sobhi and Wu (1996), Alobaidi et al. (1997), Madhav et al. (1998), Perkins and Cuelho (1999), Palmeira (2004), Teixeira et al. (2007). These models vary in their assumptions with respect to the constitutive material properties, the load transfer mechanism at the interface, and the shape of the load-strain curve during pullout (see Section 3.5.1). In general, these analytical models are used to predict the load-displacement curve of soil-geosynthetic system under confinement.

The analytical models for pullout test interpretation were developed for MSE wall design and focus on predicting the maximum pullout force magnitudes. Since, the focus of current analytical solutions is prediction of failure conditions; the displacement profile from frontal LVDT is the only displacement value used to predict the response of the geosynthetic for given load magnitude. However, the primary goal of pullout tests in the present research is the initial stiffness of the soil geosynthetic interface and it required a model which could capture small displacement behavior for application to reinforced pavement design.

This section describes the differential equation governing the behavior of soil-geosynthetic interaction in the pullout test. Then, the methods proposed by current analytical models to solve this equation are listed. Finally, the limitations of these solutions for their applicability to reinforced pavement design are discussed.

3.5.1 Governing differential equation

A pullout test is conducted by sandwiching a geosynthetic of known length L and width W between two soil layers inside the pullout box. Normal pressure is then applied on the top of the soil-geosynthetic interface to represent the field conditions under which geosynthetic is expected to perform. Finally, the geosynthetic is clamped at the loading grips and is pulled out of the box assembly at a constant rate of displacement and the required force is measured. The pullout force F measured during the pullout test is generally reported as a normalized value per unit width of the specimen and has units of force per unit width (i.e. kN/m). The same convention was used throughout this analysis.

Geosynthetics are categorized as extensible and inextensible reinforcements depending on strain magnitude required in mobilizing the maximum tensile strength. For inextensible geosynthetics the peak strain values range between 2%-5% whereas for inextensible geosynthetics they are greater than 10%. McGown et al. (1978) reported different load-deformation response for these reinforcements as shown in Figure 3.23. In this study, the initial displacement behavior of geosynthetics was analyzed and geosynthetics were assumed to be inextensible in the range of strain mobilized due to these movements.

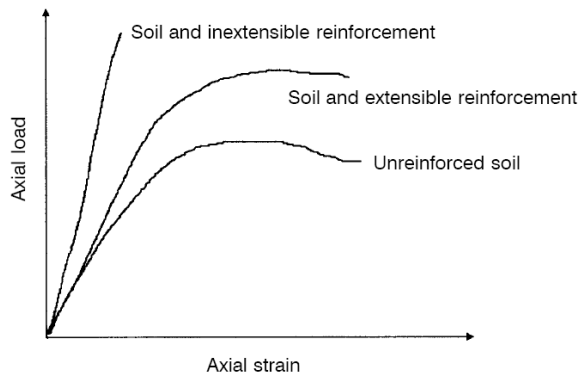

Figure 3.23 Axial load-strain relationship for various reinforcements with soil (adapted from McGown et al., 1978)

3.5.1.1 Shear stress-confined force relationship

Consider a geosynthetic element of length ∂x, confined inside the pullout box and subjected to force F in the pullout direction. Then the shear stress τ(x) is mobilized along its surface, such that the force is dissipated along its length. Assuming no extensibility of reinforcement, the free body diagram for points A and B on the either side of the element can be given as shown in Figure 3.24 below.

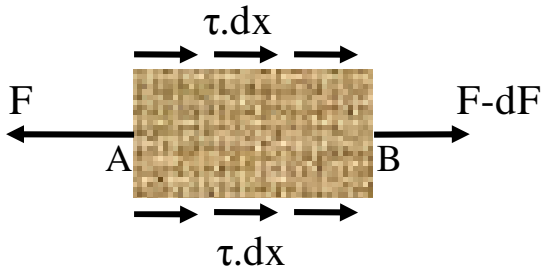

Figure 3.24 Free body diagram for geosynthetic element of length ∂x in pullout test

The force equilibrium can then be written in differential form as follows:

$$F(x) - (F(x) - dF(x)) = 2.\tau(x).dx \tag{3.12}$$

$$\tau(x) = \frac{1}{2}.\frac{dF(x)}{dx} \tag{3.13}$$

3.5.1.2 Confined force-strain relationship

Let us assume that strain ε(x) develops in the element of length dx due to the change in confined force (dF) between two points. Then, the confined force and strain are related through confined stiffness J_c of the geosynthetic and is given as,

$$F(x) = J_c.\varepsilon(x) \tag{3.14}$$

3.5.1.3 Strain-displacement relationship

The strain developed in the geosynthetic element of length dx can then be related to the displacement in the reinforcement, dw_r as:

$$\varepsilon(x) = \frac{\partial w_r(x)}{\partial x} \tag{3.15}$$

By substituting Equation 3.15 into Equation 3.14,

$$F(x) = J_c . \frac{\partial w_r(x)}{\partial x} \tag{3.16}$$

Differentiating above equation with respect to x, gives

$$\frac{\partial F(x)}{\partial x} = J_c . \frac{\partial^2 w_r(x)}{\partial x^2} \tag{3.17}$$

Substituting Equation 3.17 into Equation 3.12 gives,

$$\tau(x) = \frac{1}{2} J_c . \frac{\partial^2 w_r(x)}{\partial x^2} \tag{3.18}$$

$$\frac{\partial^2 w_r(x)}{\partial x^2} = \frac{2.\tau(x)}{J_c} \tag{3.19}$$

The above expression is a second-order differential equation governing the soil-geosynthetic interface behavior during the pullout test. The equation relates the displacement $w_r(x)$ with the shear stress $\tau(x)$ developed at the soil-geosynthetic interface in terms of confined stiffness J_c, for geosynthetic element of length ∂x in the pullout test.

3.5.2 Assumptions involved

The expression derived in Section 3.5.1 was used to predict the behavior of the soil-geosynthetic interface in a pullout test is a second-order differential equation. The solution to the governing equation requires defining three relationships. The first relation defines shape of force-strain curve for the given geosynthetic element for computing the value of confined stiffness J_c. The second relation defines the value of the relative displacement w_r of the reinforcement in relation to the soil. Finally, the distribution of shear stress $\tau(x)$ for given displacement w_r (x) for an element of length dx, needs to be defined. Perkins and Cuelho (1999) developed the solution for the governing equation of geosynthetic element in a pullout test using assumptions related to each of the above relationships. The three assumptions were related to:

a) Geosynthetic load-strain relationship
b) Absolute movement of soil surrounding the geosynthetic
c) Relationship to describe shear stress-displacement response

Based on the assumptions made, the governing equation can then be solved by incorporating appropriate boundary condition for a given pullout force measured during the test, to obtain the distribution of displacement along the length of the geosynthetic and quantify the soil-geosynthetic interface.

3.5.2.1 Geosynthetic load-strain relationship

An assumption is required for predicting the confined stiffness of the geosynthetic during the pullout test. It has been modeled as linear (Wilson-Fahmy et al., 1994), non-linear (Perkins and Cuelho, 1999) or equal to unconfined stiffness of the geosynthetic obtained from the wide-width in air tensile test (Ochiai et al. 1996, Sierra et al. 2009).

In the solution proposed in this study, the force-strain relationship for a given geosynthetic was assumed linear and proportional to the confined stiffness of the soil-geosynthetic system. It differs from the current models which assume a linear relation based on the stiffness of the geosynthetic obtained from the unconfined tensile test to predict the behavior under confinement. Due to interlocking in geogrids or impregnation

of geotextiles with the surrounding soil, the transverse ribs or fibers are mobilized leading to additional components which help in load dissipation throughout the length of the geosynthetic. This is not captured by the stiffness value of the geosynthetic obtained from isolated unconfined tensile tests in uniaxial direction. This assumption better represents the response of geosynthetics under pullout test conditions as shown in Figure 3.25. Therefore, under confinement, geogrids mobilize the junctions of longitudinal and transverse ribs which do not happen under unconfined loading conditions.

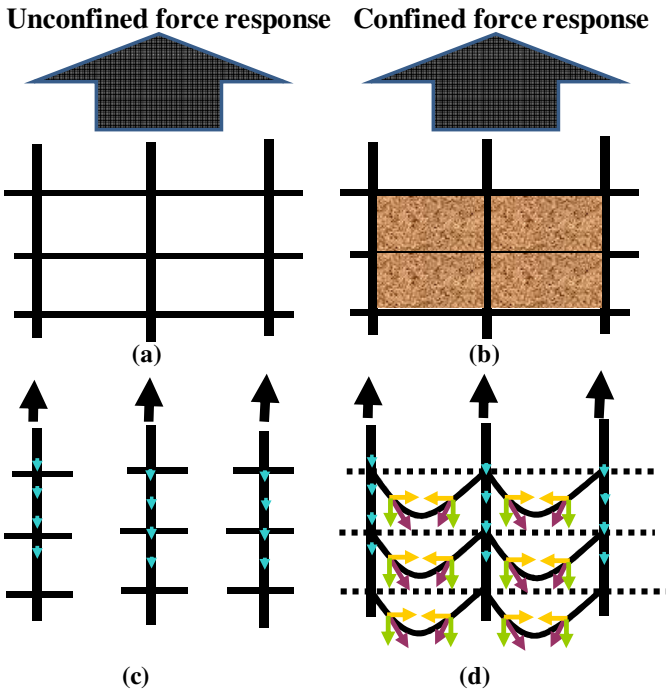

Figure 3.25 Response of geosynthetic: (a) Unconfined force (b) Confined force (c) Longitudinal ribs mobilized under unconfined loads (d) Both longitudinal and transverse ribs mobilized under confined loading conditions

The entire geosynthetic is mobilized as a response for applied force under confinement for a given soil-geosynthetic system. Accordingly, the longitudinal ribs develop less strain for the similar magnitude of force. Thus, value of confined stiffness of the geosynthetic is greater than the unconfined stiffness of the geosynthetic as shown in Figure 3.26.

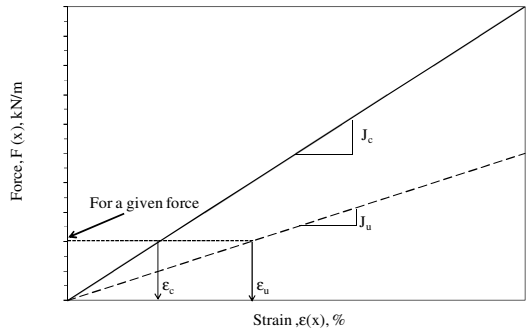

Figure 3.26 Difference between confined and unconfined stiffness of a geosynthetic

3.5.2.2 Absolute movement of soil surrounding the geosynthetic

The differential movement ∂w at a point along the reinforcement is sum of two components ∂w_s and ∂w_r. According to Sobhi and Wu (1996), "The component ∂w_s is defined as the displacement due to shear strain at the soil-geosynthetic reinforcement and ∂w_r is defined as the displacement due to tensile elongation of reinforcement." For the present analysis ∂w_s was considered to have zero magnitude and ∂w_r was considered equal to the total displacement measured during the test. In other words, the soil is assumed stationary and all the displacement measured during the test is assumed to occur in the geosynthetic reinforcement which equals the displacement at the interface. Sobhi and Wu (1996) assumed no slippage occurs at the soil-reinforcement interface and the displacement undergone by the soil and reinforcement in a bonded manner is negligible. The above assumption can be expressed in the mathematical form using the following equations:

$$\partial w(x) = \partial w_s(x) + \partial w_r(x) \tag{3.20}$$

$$\partial w_s(x) = 0 \tag{3.21}$$

$$\partial w(x) = \partial w_r(x) \tag{3.22}$$

3.5.2.3 Shear stress- relative displacement relationship at the interface

Juran and Chen (1988) indicate that modeling of the load transfer mechanism generated in a pullout test requires an appropriate interaction law to relate the shear stress mobilized at any point of the interface to the reinforcement displacement. In previous studies, the distribution of shear stress has been assumed constant (Sobhi and Wu, 1996), linear (Abdelouhab et al., 2008), bi-linear (Juran and Chen 1988, Madhav et al. 1999), non-linear (Perkins and Cuelho, 1999) or hyperbolic (Gurung and Iwao, 1998) with increasing geosynthetic displacement magnitude. Also, Sugimoto and Alagiyawanna (2003) showed that the direct evaluation of the interface properties from the ultimate state may not be appropriate to simulate the actual geosynthetic behavior in reinforced soil masses before failure in a pullout test. Sobhi and Wu (1996) defined limit shear stress for pullout test which was lower than the maximum shear stress and a function of overburden pressure applied to the soil-geosynthetic interface. They showed results from finite element analyses indicating development of uniform shear stress independent of the frontal pullout force magnitude and length of the geosynthetic.

The analyses in this study assumes a parameter called as yield shear stress (τ_y), which is assumed to be uniform over the active length of the reinforcement (explained in Section 3.5.3). The yield shear stress is a key parameter for a given soil-geosynthetic system subjected to normal pressure and is independent of the displacement at a point along the confined length of geosynthetic as shown in Figure 3.27. It is computed based on the movement of LVDT's used in the test as explained in Section 3.6.2 and has lower magnitude than that obtained from maximum pullout conditions (τ_{max}). In principal, the yield shear stress is a parameter which accounts for shear, bearing and passive mechanisms experienced by the geosynthetic in the pullout box at small displacements.

The above assumptions can be used to solve the governing differential equation for the pullout test of a geosynthetic. The solution can be used to obtain the displacement, strain and force at any point x along the length of the geosynthetic. Derivation of the governing differential equation is discussed in Section 3.5.3.

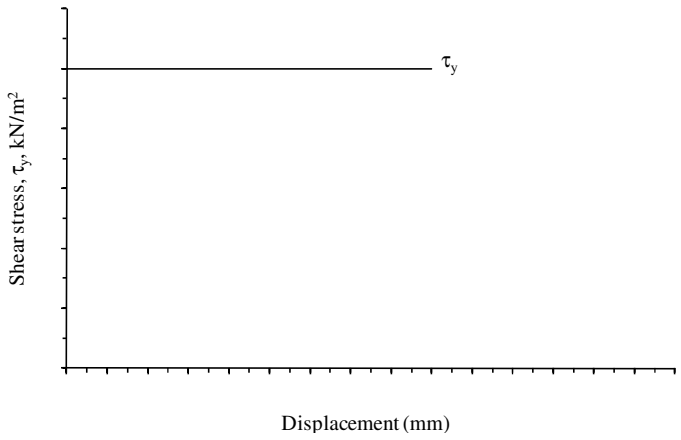

Figure 3.27 Shear stress distribution as a function of displacement at a given point

3.5.3 Displacement distribution along geosynthetic length

Assuming that the shear stress is constant and equal to the yield shear stress τ_y, and substituting ∂w for ∂w_r as derived in Equation 3.22, the governing differential Equation 3.19 at any given time t for a given frontal pullout force, can be written as,

$$\frac{\partial^2 w(x)}{\partial x^2} = \frac{2.\tau_y}{J_c} \tag{3.23}$$

The two model parameters are τ_y and J_c. Since both these parameters are assumed to have a unique value for a given pullout test, the right hand side of Equation 3.23 can be replaced by another constant β, such that Equation 3.23 can be written in simplified form as,

$$\frac{2.\tau_y}{J_c} = \beta \tag{3.24}$$

where β is a constant. Substituting Equation 3.24 into Equation 3.23,

$$\frac{\partial^2 w(x)}{\partial x^2} = \beta \tag{3.25}$$

Integrating both sides, we obtain

$$\frac{\partial w(x)}{\partial x} = \beta.x + C_1 \tag{3.26}$$

Then the strain at any confined point x can be expressed as shown in Equation 3.26 and can be written as:

$$\varepsilon(x) = \beta.x + C_1 \tag{3.27}$$

Then the force at any point x can be given by substituting the Equation 3.27 in Equation 3.14,

$$F(x) = J_c.\varepsilon(x) = J_c.(\beta.x + C_1) \tag{3.28}$$

Further integrating both sides of Equation 3.26, leads to

$$w(x) = \frac{1}{2}\beta.x^2 + C_1.x + C_2 \tag{3.29}$$

where C_1 and C_2 are constants whose values can be estimated using boundary conditions. The expressions derived in Equations 3.27, 3.28 and 3.29 above can be used to predict the strain, force and displacement profile at any point x within the pullout box in terms of model parameters τ_y and J_c provided C_1 and C_2 are known.

3.5.4 Boundary conditions

The governing differential equation for the pullout test is of the second-order form and requires values of two coefficients for complete solution. These coefficients are required to obtain the distribution of the displacement profile for a given force along the length of the geosynthetic as shown in Equation 3.29. The coefficient values are computed based on the boundary conditions adopted by a given model while proposing a solution to the governing equation. The boundary conditions involve knowing two quantities at a given instant of time. These are generally force at pullout end and displacement at other end of the specimen. Therefore, a known force value at one boundary and known displacement value at other boundary at any given instant of time can be used to solve for both the coefficients.

For the force boundary condition, the force at pullout end of the specimen is known at any given time and can be used to solve for one coefficient (C_1 in this case). Since the analytical solutions for pullout test were developed in previous studies to assess the collapse of MSE walls, the focus has to be modeling of the failure conditions. Therefore, the displacement boundary condition in these solutions was based on the mobilization of the entire length of the geosynthetic. It was assumed that when maximum pullout force was reached in a given test, the entire length of the geosynthetic is mobilized and displacement at the embedded end is zero. This condition was then used to solve for second coefficient (C_2 in this case). The magnitudes of these coefficients were finally used for predicting the displacement distribution for the entire geosynthetic length at failure.

However, the applicability of pullout tests to reinforced pavement design involves understanding of the soil-geosynthetic interface stiffness developed at low displacement magnitudes. The solution is thus required to model the entire frontal force and displacement curve for a pullout test with emphasis on capturing the initial displacement mobilized at the interface. In other words, the solution requires a displacement boundary condition such that it can be solved for increment of frontal pullout force value throughout the test and not the maximum pullout force alone. The displacement values

for a given frontal force can be obtained by integrating the strain profile over the entire length of the geosynthetic. Consequently, solutions for second coefficient have involved assuming a strain distribution and solving it to predict the subsequent displacement profile for the entire geosynthetic length.

Two methods have been proposed in the literature to solve the coefficient for second boundary condition in regards with strain distribution. The first approach involves solving the displacement boundary by assuming constant strain distribution over the entire length of the geosynthetic. The second approach involves assuming a linear distribution of strain and substituting the value for the coefficient from another test like wide width tensile test or direct shear test. This solution is then used to predict displacement profile along the length of the geosynthetic. Thus, these models proposed in the literature utilize the force boundary condition at the pullout end and assume one of the possibilities listed above to substitute for the second boundary condition. The limitations of these methods to solve for displacement boundary condition are discussed in Sections 3.5.4.1 and 3.5.4.2.

3.5.4.1 Constant strain distribution

A constant strain distribution assumes the uniform strain between two measurement points. Then the average strain between these points is calculated based on the displacement measurements made using LVDT's during the test. This approach was proposed by Ochiai et al., (1996) and the strain throughout the entire length of the geosynthetic was assumed as a step function.

The above assumption is illustrated in Figure 3.28. Consider a geosynthetic of confined length L subjected to pullout force F_p at a given time t, as shown in Figure 3.28a. Then let x_1, x_2 and x_3 be three points on the geosynthetic such that the distance between 1 and 2 is L_1 and 2 and 3 is L_2. Also, the displacements for given force are d_1, d_2 and d_3 at these three points. Then using the above assumption of constant strain, its value can be calculated. The resulting strain and displacement profile predicted based on above assumption is shown in Figure 3.28b and 3.28c respectively.

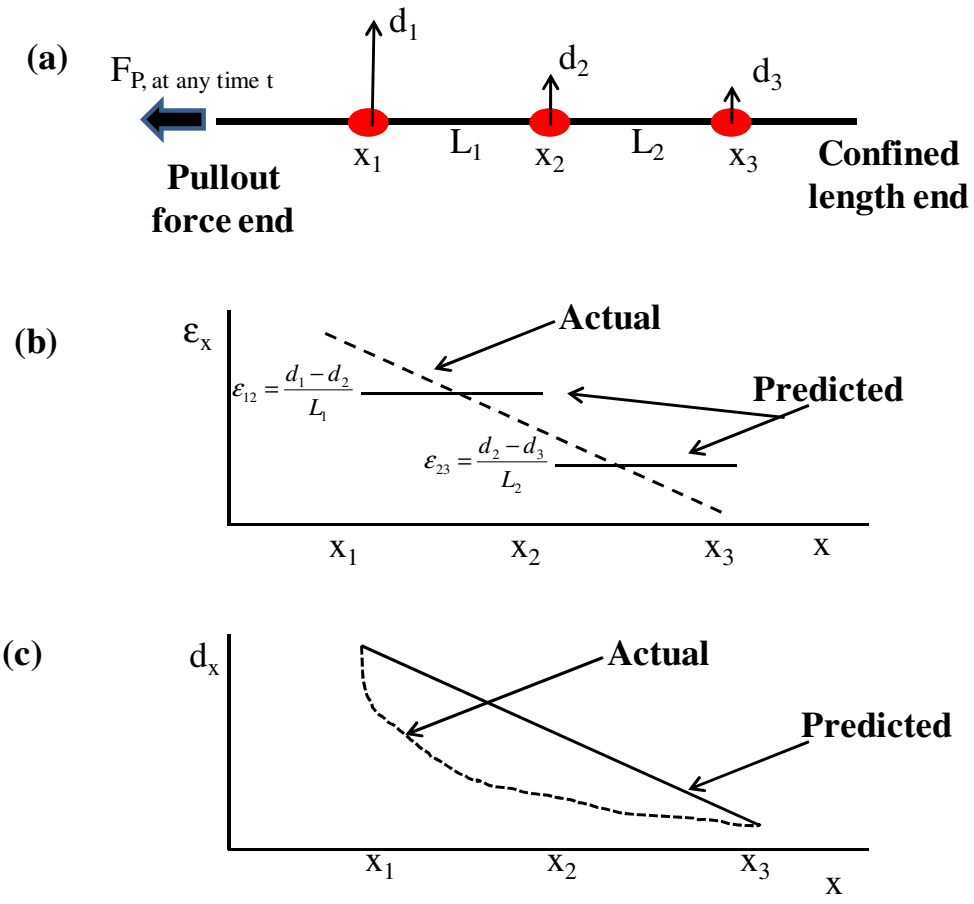

Figure 3.28 Predictions based on constant strain distribution: (a) Schematic of displacement profile for given pullout force (b) actual vs. predicted strain distribution (c) actual vs. predicted displacement

Based on model assumptions it can be seen that strain is a linear function whereas displacement is a quadratic function over the length of the geosynthetic for given frontal pullout force (as shown in Equation 3.27 and 3.29). However, the assumption of constant strain leads to linear distribution of displacement along the length of the geosynthetic. i.e., value for second coefficient is assumed zero. The equation for displacement distribution can be obtained for the given geosynthetic under pullout conditions by integration of the strain relationship. The actual strain profile is not a series of discrete

values but a continuous function along the entire length of the geosynthetic whose magnitude decreases from pullout end to the embedded end.

This approach under predicts the strain magnitude at points closer to the pullout end and over predicts the strain at point closer to the embedded end of the geosynthetic. Furthermore, based on pullout test results conducted as part of this research it was observed that the actual displacement profile along the length of the geosynthetic is parabolic in shape rather than linear as predicted by this analysis. Therefore, this assumption leads to error in displacement prediction which cannot be used to model the interface behavior at low strain magnitudes for reinforced pavement application.

3.5.4.2 Linear strain distribution

This assumption involves modeling the strain distribution as a continuous function over the mobilized length of the geosynthetic. The solutions incorporating boundary condition based on this hypothesis represent the model conditions realistically. Two approaches have been reported in the literature to model this behavior.

The first approach involves assuming the strain distribution under confined conditions in the reinforcement equals that under unconfined conditions. In other words, these models assume confined stiffness equal to the unconfined stiffness of the geosynthetic. Then knowing the frontal force, the strain magnitude is calculated as shown in Equation 3.28. Once the strain magnitude is known, the displacement value can be calculated by integrating Equation 3.27. Sierra et al. (2009) proposed a load transfer model to predict force-displacement relationship of the geogrid under pullout conditions by subdividing it into rheological units but used load–elongation curves from tensile tests on the geogrids.

The other approach involves developing the entire solution and then calibrating the second coefficient from a test other than the pullout test. Sobhi and Wu (1996) proposed a model to predict pullout force and displacement at a point under confined conditions but it required another test as proposed by Ling et al. (1992) to calibrate the model. The drawback of this approach is that the strain levels used to calibrate the

parameter are different from one observed in the pullout test. This leads to test results which are sensitive to small changes in value of the assumed parameter. Furthermore, this approach does not utilize all the displacement data obtained using various LVDT's across the length of the geosynthetic but uses only frontal LVDT to match the results.

3.5.5 Discussion

The current analytical solutions either incorporate the limited data obtained from the pullout test or use other tests to predict the model parameters. The assumptions made in the current models with regards to second boundary condition leads to errors which are critical when predicting behavior of soil-geosynthetic interface at regime of low displacements. However, the primary goal of pullout tests in the present research was its application to reinforced pavement design. To avoid any unrealistic assumptions, the proposed model in this research suggests a new approach to compute the second boundary condition. The data obtained from LVDT's at various points along the length of the geosynthetic is taken into account to model the soil-geosynthetic behavior realistically.

3.6 SOIL-GEOSYNTHETIC INTERACTION MODEL

The solution for governing differential equation of the pullout test involves two coefficients. The first coefficient can be computed by using the force boundary condition at the pullout end of the geosynthetic. The second coefficient is computed using assumption regarding strain distribution within the geosynthetic for a given force level. The limitations of this approach were discussed in the section 3.5.5. A new model called soil-geosynthetic interaction (SGI) model is proposed as part of this research which involves a different approach in terms of displacement rather than strain values to compute the second boundary condition for the pullout test.

Specifically, rather than assuming the strain distribution for a given geosynthetic, the incremental distance travelled by increase in frontal pullout force through the confined geosynthetic specimen length during the test is monitored. In other words, the

length of geosynthetic mobilized for a given frontal pullout force value is computed. This concept was proposed by Sobhi and Wu (1996) and called active length of reinforcement where the force is zero within the embedded geosynthetic for a given magnitude of frontal pullout force. The similar definition for active length (L') of the geosynthetic was adopted in the present model. However, it is different from the total length (L) of geosynthetic specimen used in the pullout test which is a fixed quantity and does not vary with frontal pullout force during the test. The active length increases with increasing frontal pullout force and becomes equal to the total length only when the entire geosynthetic is mobilized.

The SGI model uses this concept of active length to define the second boundary condition during the pullout test. The active length of the geosynthetic for a given frontal pullout force value is the point where the force front has just been reached. Since the geosynthetic is in equilibrium, the force and displacement at any location in the confined geosynthetic beyond this point beyond is zero. Thus, a boundary condition can be defined at this point where the displacement magnitude is known (zero for the given case). This boundary will move towards the embedded end of the geosynthetic from the pullout end as the frontal pullout force increases during the test.

The boundary condition is based on evaluating the equilibrium of the mobilized geosynthetic length for a given pullout force magnitude. Rather than monitoring the conditions at the far end of the geosynthetic at maximum pullout force, the conditions at this moving boundary are analyzed at every increment of frontal pullout force during the test. This additional boundary condition in terms of known displacement magnitude is then utilized to obtain the solution for the governing differential equation of the pullout test for a geosynthetic.

3.6.1 Proposed solution

As described above, the active length of reinforcement L' is a boundary condition where the displacement equals zero. Then, the frontal boundary condition where frontal pullout force F_p is known along with displacement boundary condition at point L' can be

used to solve for Equation 3.29 to obtain displacement distribution for the given geosynthetic as shown below.

Applying the boundary conditions to solve for coefficients C_1 and C_2 at a given frontal force magnitude as derived in Equation 3.29,

At x=0, F(x=0) = F_P (Measured frontal pullout force) (3.30)

At x=-L', w (x=-L') = 0 (Moving boundary condition) (3.31)

To obtain the value of C_1 Equation 3.28 can be solved by using boundary conditions as shown in Equation 3.30. Then,

$$C_1 = \frac{F_P}{J_c} \tag{3.32}$$

Furthermore, solving Equation 3.29, using boundary conditions as shown in Equation 3.31, and substituting C_1 from Equation 3.32, we get C_2 as follows;

$$C_2 = \frac{F_P}{J_c}.L' - \beta.\frac{L'^2}{2} \tag{3.33}$$

Now substituting the values of C_1, C_2 and β in the Equation 3.29 we obtain the expression for displacement w(x) at any confined point x for a given frontal pullout force F_p in terms of τ_y, J_c, and L' as,

$$w(x) = \frac{\tau_y}{J_c}.x^2 + \frac{F_P}{J_c}.x + \frac{F_P}{J_c}.L' - \frac{\tau_y}{J_c}.L'^2 \tag{3.34}$$

Rearranging,

$$w(x) = \frac{(L'+x)}{J_C}[F_P - \tau_y(L'-x)] \tag{3.35}$$

To obtain the strain distribution, the above equation can be differentiated with respect to x, the strain ε(x) at any point can be given as,

$$\varepsilon(x) = \frac{\partial w(x)}{\partial x} = \frac{1}{J_C}[F_P + 2.\tau_y x] \tag{3.36}$$

Then the force at any point x can be given by substituting the expression above in Equation 3.15,

$$F(x) = J_c.\varepsilon(x) = F_P + 2.\tau_y x \tag{3.37}$$

Furthermore, for a given pullout force F_p, the force at point L' i.e. at the end of the boundary is zero, thus substituting for x = -L' in Equation 3.37, we obtain

$$F(x = -L') = F_P - 2.\tau_y.L' = 0 \tag{3.38}$$

$$L' = \frac{F_P}{2.\tau_y} \tag{3.39}$$

Thus the point L' where the force front has just been reached for a given frontal pullout force can be calculated knowing the yield shear stress parameter. Substituting the above expression for L' in Equation 3.35, the displacement distribution can be obtained in terms of model parameters τ_y and Jc as,

$$w(x) = \frac{\tau_y}{J_c}.x^2 + \frac{F_P}{J_c}.x + \frac{F_P{}^2}{4.\tau_y.J_c} \tag{3.40}$$

Thus, using the Equations 3.35, 3.36 and 3.40, strain $\varepsilon(x)$, force $F(x)$ and the displacement $w(x)$ at a point x can be calculated for a given frontal pullout force F_p in terms of yield shear stress, τ_y and confined stiffness J_c of the geosynthetic.

3.6.2 Parameter for geosynthetic reinforced pavement

The boundary conditions used to solve the governing differential equation for the pullout test was explained in Section 3.6.1. However as discussed in Section 2.4.2.3, the focus of conducting the pullout tests was to quantify the soil-geosynthetic interaction at low displacement magnitudes and there subsequent application to geosynthetic reinforced pavement design. Therefore, a parameter was defined based on the solution of the pullout test equations developed above, which is considered representative of the stiffness of the system. This parameter was used to quantify the governing mechanism of lateral restraint for reinforced pavement design. It can also be used as an index for comparing performance of various geosynthetic under confined condition and is explained in the Chapter 4.

Conventional analysis of pullout test as discussed in Section 3.2.3 has been limited to defining the relation between frontal pullout force and LVDT displacement obtained at the points located inside the pullout box. Where this approach is suited to characterizing the failure conditions, it does not provide insight into the interactions developed between soil and geosynthetic at low displacement magnitudes. For capturing the interface behavior realistically, it is necessary to compute force values where the displacements are being measured during the pullout test. The relationship thus developed can be used to determine the response of geosynthetic for given displacement increment. This can then be translated to quantify the soil-geosynthetic response to obtain a measure for lateral restraint mechanism developed in the reinforced flexible pavements by using pullout test data. Thus, equations were solved to obtain the relation between confined force and displacement in terms of model parameters as shown below.

Replacing F_p in Equation 3.40 with Equation 3.37, we get

$$w(x) = \frac{\tau_y}{J_c}.x^2 + \frac{(F(x) - 2.\tau_y.x)}{J_c}.x + \frac{(F(x) - 2.\tau_y.x)^2}{4.\tau_y.J_c} \tag{3.41}$$

$$w(x) = \frac{F(x)^2}{4.\tau_y.J_c} \tag{3.42}$$

$$F(x)^2 = (4.\tau_y.J_c).w(x) \tag{3.43}$$

This is the governing equation for the soil-geosynthetic interaction in the pullout test at each point on the geosynthetic. It suggests that the displacement at a point is related to square of the force at that point through parabolic relation and the constant is given by Equation 3.43. The force and displacement at any given point x throughout the geosynthetic can be related by model parameters i.e., yield shear stress, τ_y and confined stiffness J_c of the soil-geosynthetic system. The solution proposed here is similar to one proposed by Bergado et al. (2008) which assumed the parabolic function between displacement w(x) and distance x.

The above model parameters can be lumped into a single constant, called coefficient of soil geosynthetic interaction (K_{SGI}) which can be directly estimated using the pullout test and is given as,

$$K_{SGI} = 4.\tau_y.J_c \tag{3.44}$$

Then Equation 3.43 can be written as:

$$F(x)^2 = K_{SGI}.w(x) \tag{3.45}$$

According to Bonaparte et al. (1987), "There are two important soil-reinforcement interaction characteristics for design: soil reinforcement interface shear behavior and the influence of soil confinement on tensile characteristics of the reinforcement." Therefore, constant K_{SGI} allows for combing both these characteristics in a unified approach and evaluating them quantitatively. The parameter K_{SGI} can be used as an index for comparison of performance for various geosynthetic in the pullout test. For a geotextile, it is typically expected that the yield shear stress would be higher whereas the confined stiffness would be lower than that obtained for a geogrid using the same soil and confining pressure in a given pullout test. Since the above constant is function of both interface shear and confined stiffness of the system, it can be used to compare the performance of both geogrids and geotextiles using the same criteria. Moreover, it can be calibrated using the data obtained only from the pullout test as explained in Section 3.6.3 thereby eliminating the need to use other tests.

The current pavement design methodologies require a modulus as an input for design. Thus, while designing a geosynthetic reinforced pavement, the effect of geosynthetic cannot be directly input using K_{SGI} value. Therefore based on above model, an equivalent confined modulus M_{SGI} at a given displacement w(x) was calculated as,

$$M_{SGI} = \sqrt{\frac{K_{SGI}}{w(x)}} \tag{3.46}$$

$$M_{SGI} = \sqrt{\frac{K_{SGI}}{w(x)}} = \sqrt{\frac{F(x)^2 \big/ w(x)}{w(x)}} = \frac{F(x)}{w(x)} \tag{3.47}$$

In other words, confined modulus M_{SGI} is defined as the ratio of the confined force F(x) to the displacement w(x) at a given point x. The units of confined modulus are that of stress (kN/m^2). According to Edil et al. (2007), inclusion of geosynthetic to a flexible pavement provides a zone of increased confinement estimated to be 150 mm (6

inches) on top and bottom of the reinforcement. When designing the pavement if the displacements magnitudes expected in the field are known, then the corresponding modulus value for geosynthetic can be computed using Equation 3.47. This value can be assigned to this zone in the flexible pavement to quantify the geosynthetic benefit. This would help in defining the zone of influence of a geosynthetic in the pavement. The analysis can then be performed for the modified pavement structure with a higher stiffness layer which incorporates the effect of geosynthetics in reinforced pavement design. However, it should currently be used as an approximate estimate as further testing would be required to correlate the obtained M_{SGI} value with actual pavement modulus.

The analysis of pullout tests to obtain coefficient of soil-geosynthetic interaction (K_{SGI}) which can be used to quantify the low displacement interface behavior of soil-geosynthetic system was described. Based on discussion it was shown that K_{SGI} is a better index for geosynthetic reinforced pavement design (quantifying the lateral restraint mechanism at low displacements) and the coefficient of interaction (C_i) is better for defining the ultimate loading conditions which can be used for designing MSE walls at large displacement magnitudes.

3.6.3 Parameter estimation using pullout tests

The SGI model involves estimating constant K_{SGI} for a given soil-geosynthetic system under confinement. K_{SGI} is a product of two parameters which are confined stiffness J_c of the reinforcement and yield shear stress τ_y of soil-geosynthetic interface. They can be estimated based on the data obtained by conducting a pullout test. This involves analyzing the equilibrium of the soil-geosynthetic system for an increment in frontal pullout force (at each time step) and solving the system of equations derived above. The steps followed to obtain the parameters are illustrated by solving a hypothetical pullout test as described below.

Consider a geosynthetic specimen of known dimensions (e.g., 0.6 m confined length and 0.45 m width as per ASTM standards) placed in a standard soil in a pullout box. The normal pressure is applied at the top of the specimen to simulate the

confinement load similar to one expected in field conditions. Furthermore, the frontal pullout force value at any given time can be measured by means of a load cell attached to the front of the box. A number of linear variable differential transducers (LVDT's) are attached along the length of the specimen at known distances from the front to the embedded end of the specimen. The test is performed by pulling out the specimen at constant rate of displacement. The data obtained consists of the force reading from the load cell and the displacement readings of the confined points obtained from various LVDT's.

For analysis of the results, let us consider a point at distance x_i from the front end of the specimen on which pullout test is performed as shown in Figure 3.29a. Then, the distribution of the frontal pullout force with displacement at x_i is given as shown in Figure 3.29b. The frontal pullout force $F_{p,t}$ increases with time as the test progresses till it reaches maximum pullout force value. This curve is similar to one shown in Figure 3.21 used for estimating coefficient of interaction C_i for the given soil-geosynthetic system. The magnitude of maximum pullout force obtained during the test is designated as F_{max}.

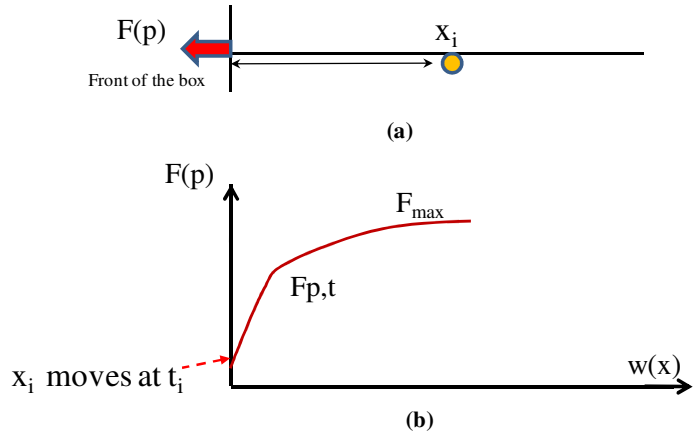

Figure 3.29 Pullout test model for hypothetical point xi: (a) Location inside the pullout box (b) Assumed frontal force vs. displacement profile at any given time t

Let us assume an LVDT is attached to point x_i such that the displacement $w(x_{i,t})$ with increase in frontal pullout force $F_{p,t}$ at any given time t can be measured. Then, the

distribution of force and displacement at point x_i for given magnitude of frontal pullout force F_p at any given time t, can be divided into three categories as shown in Figure 3.30a. The graph can then be expressed in mathematical form as follows:

For $t < t_i$, $F(x_{i,t}) = 0$ and $w(x_{i,t}) = 0$ (3.48)

At $t = t_i$, $F(x_{i,t}) = 0^+$ and $w(x_{i,t}) = 0^+$ (3.49)

For $t > t_i$, $F(x_{i,t}) > 0$ and $w(x_{i,t}) > 0$ (3.50)

Using the above equations displacement w(x) and force F(x) can be computed for point x_i. The resulting profile for force and displacement at any time t at x_i are shown in Figures 3.30b and 3.30d as,

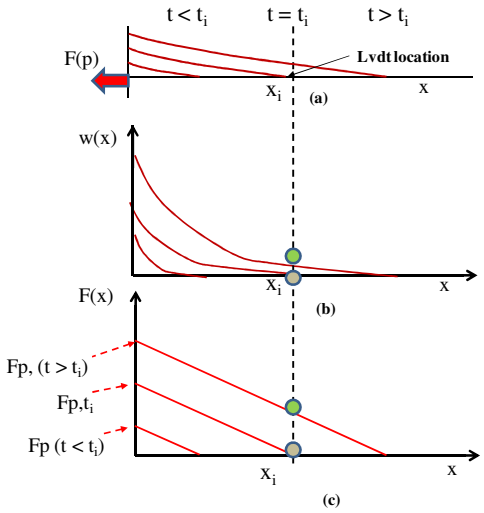

Figure 3.30 Distribution for hypothetical point xi based on the proposed model: of (a) Frontal force Fp, (b) Displacement, w(x), (c) Confined force F(x), at any given time t.

The step-wise procedure for parameter estimation based on the proposed model is as follows:

(a) Compute yield shear stress

Let the force front just reaches the point x_i at time t_i as shown in Equation 3.49 above.

$$\text{Then, } t = t_i, \quad F(x_{i,t}) = 0 \tag{3.51}$$

As shown in Equation 3.37, the force at any confined point x_i at time t, is given as

$$F(x_{i,t}) = F_{P,t} + 2.\tau_y x_i \tag{3.52}$$

Substituting Equation 3.51 in Equation 3.52 above, yield shear stress at each point can be computed as follows;

$$\tau_y = \frac{F_{p,t}}{2x_i} \tag{3.53}$$

If more than one LVDT is used during the test, then the value of τ_y can be calculated at each LVDT point and the average value can be used for the analysis. Also, as a first approximation τ_y value can be estimated knowing the maximum pullout force F_{max} and total length of confined specimen, L;

$$\tau_y = \frac{F_{\max}}{2L} \tag{3.54}$$

The value of τ_y obtained using Equation 3.54 is generally higher than one calculated based on Equation 3.53 as the pullout force increases even after the entire length of the geosynthetic has been mobilized.

(b) Calculating confined force F ($x_{i,t}$) at a point x_i

At any time t > t_i, the confined force at the point x_i is greater than zero. It can be calculated using Equation 3.52; since yield shear stress τ_y and frontal pullout force $F_{p,t}$ are known;

$$F(x_{i,t}) = F_{P,t} + 2.\tau_y x_i$$

Since an LVDT is attached to the point x_i, the displacement w ($x_{i,t}$) for a given frontal pullout force $F_{p,t}$ is known. Then the results can be combined to plot the calculated confined force F ($x_{i,t}$) vs. measured displacement w ($x_{i,t}$) as shown in Figure 3.31a.

(c) Estimating confined stiffness, J_c

Since the force and displacement at point x_i are known and also yield stress τ_y is computed, the J_c value can be directly obtained as shown in Figure 3.31b. It can be also calculated based on Equation 3.43,

$$F(x_{i,t})^2 = (4.\tau_y.J_c).w(x_{i,t}) \tag{3.55}$$

$$J_c = \frac{F(x_{i,t})^2}{4.\tau_y.w(x_{i,t})} \tag{3.56}$$

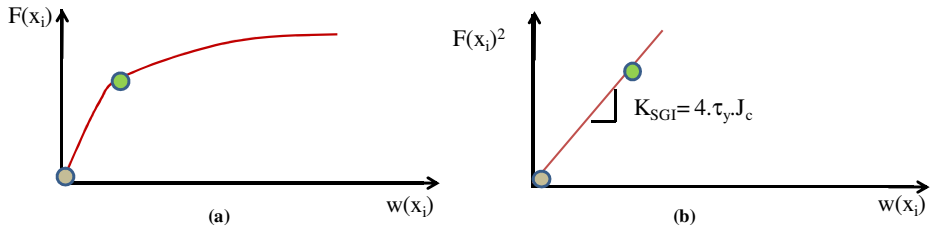

Figure 3.31 Based on proposed model, for hypothetical point xi: (a) F (xi) vs. w (xi), (b) KSGI, at any given time t

(d) Computing coefficient of soil geosynthetic interaction, K_{SGI} *and equivalent confined modulus at a given displacement,* M_{SGI}

Knowing J_c and τ_y, K_{SGI} value is calculated as follows:

$$K_{SGI}(x_i) = 4.\tau_y.J_c \tag{3.57}$$

Then for any given displacement w (x_i) (generally 1mm for simplicity) M_{SGI} can be calculated as follows:

$$M_{SGI}(x_{i,t}) = \frac{F(x_{i,t})}{w(x_{i,t})} = \sqrt{\frac{4.\tau_y.J_c}{w(x_{i,t})}} = \sqrt{\frac{K_{SGI}}{w(x_{i,t})}} \tag{3.58}$$

The above procedure can be repeated for any instrumented point to obtain the coefficient of soil geosynthetic interaction from a pullout test.

(e) Check the estimated parameters

Let us assume another point x_j inside the pullout box such that an LVDT is attached to it. Then the value of w (x_j) for a given $F_{p,t}$ is known throughout the test. As τ_y and J_c were estimated from point x_i, they can be used to predict the displacement profile at point x_j using the Equation below.

$$w(x_{j,t}) = \frac{\tau_y}{J_c}.x_j^{\,2} + \frac{F_{P,t}}{J_c}.x_j + \frac{F_{P,t}^{\,2}}{4.\tau_y.J_c} \tag{3.59}$$

Then the measured and predicted value of w (x_j) can be compared to check the accuracy of estimated parameters; τ_y and J_c.

(f) Using regression analysis

The data obtained from the pullout test can be used in a linear regression model to estimate the value of K_{SGI}. The regression model can be setup by applying transformation to Equation 3.59 for all the LVDT's as follows:

$$Y(X) = \beta_1.X_1 + \beta_2.X_2 + \beta_3.X_3 \tag{3.59}$$

In the above model, Y(X) is the independent variable, X_1, X_2, X_3 are the dependent variables and β_1, β_2, β_3 are the coefficients such that,

$$Y(X) = w(x_{j,t}) \tag{3.60}$$

$$X_1 = x^2 \tag{3.61}$$

$$X_2 = F_{P,t}.x_j \tag{3.62}$$

$$X_3 = F_{P,t}{}^2 \tag{3.63}$$

$$\beta_1 = \frac{\tau_y}{J_c} \tag{3.64}$$

$$\beta_2 = \frac{1}{J_c} \tag{3.65}$$

$$\beta_3 = \frac{1}{4.\tau_y.J_c} \tag{3.66}$$

The analytical model assumptions allow for regression analyses on data obtained during the test until maximum pullout force is reached. The inverse of coefficient β_3 then gives the value of K_{SGI}. This analysis helps to estimate bounds and confidence intervals on estimated value of K_{SGI}. Furthermore, it can be compared with the value of K_{SGI} obtained based on analytical solution proposed above.

3.6.4 Repeatability of the estimated parameter

Section 3.6.3 detailed the procedure to estimate the model parameters τ_y and J_c based on pullout test data. Specifically, it involved monitoring the frontal pullout force and displacement at a confined point inside the pullout box. The above analysis can be extended to any point inside the pullout box and the two model parameters can be obtained to compute the value of K_{SGI}. This section discusses the repeatability of model parameters and K_{SGI} for a given soil-geosynthetic system tested at given confining pressure in the pullout test. In other words, the value of K_{SGI} is independent of the location of LVDT where displacement measurements are made during the pullout test.

Let us assume three instrumented points x_1, x_2 and x_3 on a geosynthetic confined inside the pullout box as shown in Figure 3.32a. Then, $F_{p,t}$ is the pullout force at any given time t and the maximum pullout force at the end of the test is F_{max}. The variation of frontal pullout force with displacement at each instrumented point is as shown in Figure 3.32b. Based on the location of three points, the force front reaches them at different times. The point x_1 being the closest to the pullout force end, experiences force and displacement earlier than x_2 which is followed by x_3. As the force front reaches the points x_1, x_2 and x_3, they begin moving at times t_1, t_2 and t_3 respectively. After the entire length of the geosynthetic is mobilized the peak pullout force magnitude F_{max} is reached and there is no further change in the frontal pullout force with increase in the displacement of the points x_1, x_2 and x_3.

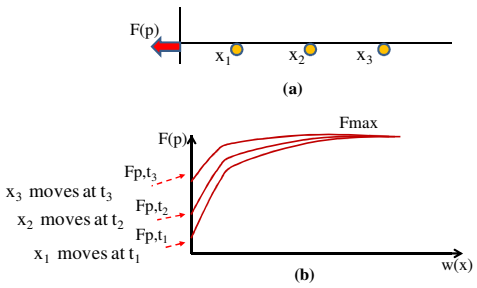

Figure 3.32 Pullout test on a geosynthetic: (a) Instrumented points at distance x_1, x_2 and x_3 (b) Frontal pullout force vs. displacement profile for three points

Then the data obtained from the pullout test can be analyzed based on the proposed model to obtain the displacement and force profile at any given time t for the entire length of the geosynthetic as shown in Figures 3.33a and 3.33b respectively.

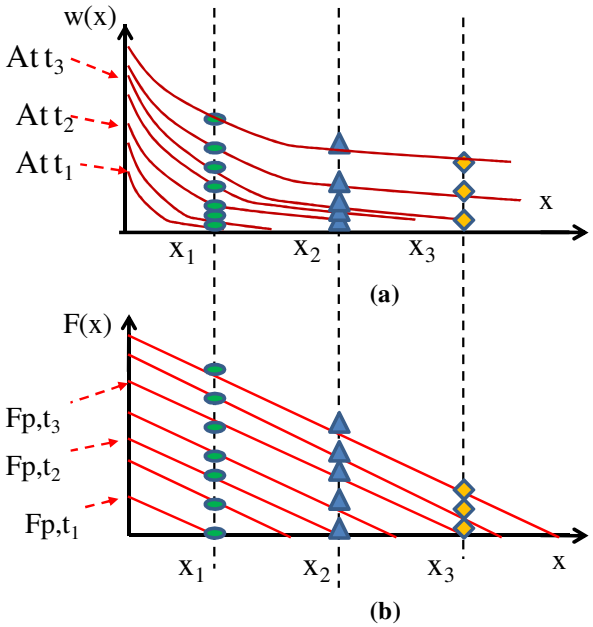

Figure 3.33 Based on analysis of pullout test data, profiles at three points for any given time t: (a) Displacement with length (b) Force with length

Then the information obtained above can be combined to plot the individual confined force vs. displacement profile at points x_1, x_2 and x_3 as shown in Figure 3.34.

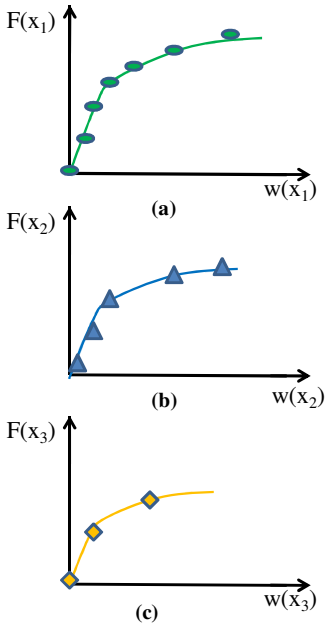

Figure 3.34 Confined force vs. measured displacement profile at point: (a) x_1 (b) x_2 (c) x_3

Furthermore, by solving the equations developed for the proposed model, the values of both the parameters τ_y and J_c can be calculated at each of the three points x_1, x_2 and x_3. Then the curves can be combined to get confined force vs. displacement relationship for the soil-geosynthetic system as shown in Figure 3.35a. Finally, as shown in Figure 3.35b, the value of soil-geosynthetic interaction coefficient for the entire test can be obtained. This value of K_{SGI} appears to be unique for a given soil-geosynthetic system at a given confining pressure. Test results that show evidence of this behavior are discussed in Chapter 4. Hence, it can be used as a parameter for predicting the performance of geosynthetics under confinement at low displacements as in the case of geosynthetic- reinforced pavements.

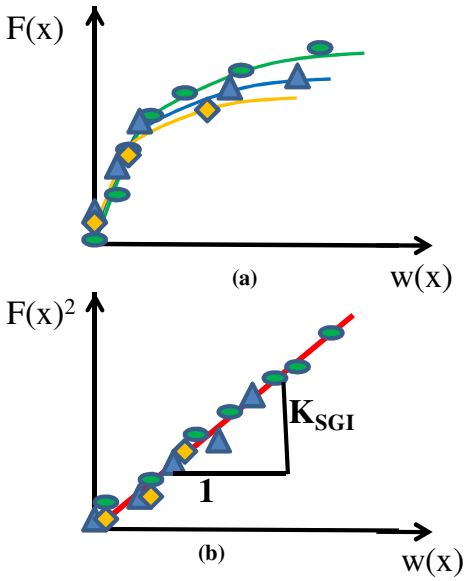

Figure 3.35 Plot for given soil-geosynthetic system at known confining pressure for all LVDT's used during a test: (a) Confined force vs. displacement (b) K_{SGI}

3.6.5 Discussion

The interpretation of the pullout test results based on an analytical model requires an accurate evaluation of the displacement and force distribution throughout the geosynthetic specimen at any time during the test. Section 3.6.4 listed the features of proposed analytical model to characterize the soil-geosynthetic interface properties at low displacements under confined conditions. Based on the analysis of the pullout test data a unique parameter K_{SGI} can be calculated to quantify this behavior.

The proposed approach has advantages over available models as it uses only the pullout test data and makes realistic assumptions in solving the governing differential equation. Further it allows for calculating a single value which can be used as the basis for comparing performance of two different types of geosynthetics i.e., geogrids and geotextiles or similar products placed under same working conditions in the field. It can be applied to reinforced pavement design as it better characterizes the low displacement interaction behavior of soil-geosynthetic interface.

3.7 CONCLUSIONS

The performance of the geosynthetic reinforced pavement depends on the interaction between the soil matrix and the geosynthetic inclusions. The currently available analytical models were developed for MSE walls and focused on maximum pullout force conditions. Therefore, the soil-geosynthetic interface model (SGI) was proposed to quantify the low displacement interaction behavior of the soil-geosynthetic system. The model is based on two parameters: yield shear stress (τ_y) and confined stiffness (J_c) of the system.

Based on the model, the equilibrium of geosynthetic specimen was analyzed at each time step for known frontal pullout force. The concept of active length of reinforcement during pullout testing was introduced which helped in establishing the displacement boundary condition. The governing differential equation was then solved thereby providing a continuous function to predict displacement, strain and force at each point along the length of the geosynthetic. Unlike analytical models proposed in the literature, there were no additional tests involved while back calculating the magnitudes of these parameters. They were estimated exclusively from the data obtained by conducting the pullout test. Further, an alternate approach based on the regression analysis was proposed to obtain the parameters. The advantage of this method was its ability to incorporate the data obtained from all LVDT's to be used in parameter calculation. Furthermore, when the results from all the LVDT locations were combined based on the proposed model, a unique confined force-displacement relationship for a given soil-geosynthetic system could be predicted for the applied normal pressure on the interface.

The coefficient of soil-geosynthetic interaction (K_{SGI}) was then computed which combined both the parameters in a single framework. Finally, this constant was used as an index for comparing the performance of various geosynthetics. The suitability of the proposed SGI model for the analysis of the geosynthetic reinforced pavements was evaluated by conducting pullout tests and is discussed in the Chapter 4.

Chapter 4: Geosynthetic Reinforced Pavements - A Laboratory Study

"Give a man a fish and you feed him for a day. Teach him how to fish and you feed him for a lifetime."- Lao Tzu

4.1 INTRODUCTION

Pullout tests for geosynthetics were developed to support the design of MSE walls to calculate maximum force required for internal stability calculation. In this case, the stability of the system at ultimate or limit state was of concern. The pullout tests described in Chapter 3 were conducted on geogrids and results were reported in terms of coefficient of interaction (C_i). However, the present research focused on application of pullout tests for quantifying soil-geosynthetic interaction in reinforced pavement design. For this function, the performance of geosynthetics at low displacement magnitudes is important.

An analytical model was proposed to assess the performance of soil-geosynthetic interaction. Based on the model, a new parameter to quantify soil-geosynthetic interaction (K_{SGI}) was defined. This parameter is a function of yield shear stress and confined stiffness of the geosynthetic which can be obtained from pullout test. The quantification of this new parameter required test equipment which would be able to define the low displacement behavior of interfaces. The available pullout box described in Chapter 3 is capable of predicting the ultimate pullout force but requires long testing times, lack of adequate instrumentation and slippage at grips. Thus it could not to be used for computing the new parameter directly. Therefore, the original pullout box was modified to allow testing geosynthetics for reinforced pavement application.

This chapter describes the development of new pullout test equipment. Also, a testing program of geosynthetics conducted to calibrate the proposed parameter based on analytical model for reinforced pavement design. Finally, comparison is made of the new parameter value for various geosynthetics tested using the new equipment.

4.2 PULLOUT TEST EQUIPMENT

Pullout tests were originally conducted on the geosynthetics to calculate the coefficient of interaction (C_i). The present research involved computation of the new parameter, i.e., coefficient of soil-geosynthetic interaction (K_{SGI}) based on the proposed model. This required certain modifications of the original design of the pullout equipment as the focus was low-displacement rather than limit-displacement behavior of geosynthetics in the pullout test.

The pullout test equipment consisted of a steel box with internal dimensions of 1.5 m (length) X 0.6 m (width) X 0.3 m (height). The front end of the box had an opening of 50 mm and had two sleeves of 75 mm length to minimize the influence of frontal box wall on pullout test results. The original pullout box was modified to adapt it to the testing needs for the present research. The pullout box, load cell, hydraulic pistons and steel plates from the original box were retained in the modified design.

Development of the new pullout system was guided by lessons learned from evaluation of preliminary pullout characterization tests. Specifically, issues such as the use of appropriate clamping system and normal pressure system were evaluated in conventional tests to better develop the pullout box. Also, emphasis was placed in design to have uniform rate of testing throughout the test. Instrumentation in the pullout box was changed to incorporate better devices for quantifying soil-geosynthetic interaction precisely. The motivation for this research component was to enable straightforward, repeatable interpretation of instrumentation results, boundary conditions, and data to determine the low displacement behavior of the soil-geosynthetic interface. Also, conducting a large scale pullout test on geosynthetics is a labor intensive and time consuming process. Therefore, the goal was to decrease the time required to setup the test as compared to the original design. The five major areas where modifications were done included normal pressure system, rate of testing, clamping system, displacement measurement system and data acquisition system.

4.2.1 Rate of testing

In the original equipment, an air flow pump was used to push the two hydraulic cylinders located on either side of the pullout box. This mechanism generated the required force to push the geosynthetic specimen out of the box for a given test. The use of air flow pump led to pressure drop at high pullout force magnitudes, resulting in reduction of the speed of piston movement during the test. In the modified system, air flow pump was replaced by an electric flow pump. Due to inbuilt self compensating system, it prevented the reduction in pressure thereby generating a constant force through the hydraulic pistons as they moved out of their core during the test. The new system helped in obtaining a constant rate of testing throughout the test. To adjust the speed of hydraulic piston movement, a flow regulating valve was connected to this electric pump system. Also, a needle valve was attached at each piston end. The needle valve was adjusted to regulate the flow of oil volume entering the piston from the pump. The flow valve and needle valves were adjusted to obtain rate of testing from 0.1mm/minute to 10 mm/minute. Finally, a three way ball valve was attached to the electric flow pump to control the direction of piston movement during the test. The hydraulic system with all components is as shown in Figure 4.1.

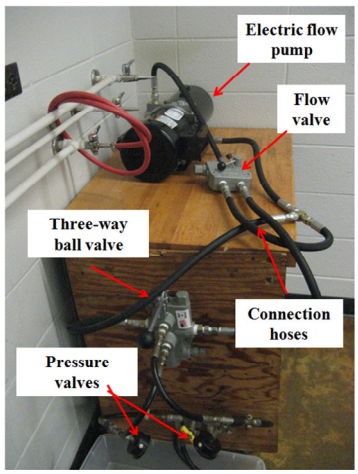

Figure 4.1 Hydraulic system for controlling rate of pullout testing

4.2.2 Normal pressure system

The normal pressure in the original pullout box was applied by inflating a rubber membrane which was sandwiched between confining soil and steel plates placed on top of the pullout box. The system had drawbacks as it was difficult to generate and maintain low confining pressures as required for the present research to simulate the geosynthetic conditions under pavement realistically. Furthermore, the assembly of this system was complicated as it required lifting the heavy steel plates manually to the top of the specimen and tightening of thirty-six bolts to maintain proper contact between the steel plates and the rubber membrane. The rubber membrane repeatedly developed leaks as it punctured while reacting against the angular soil particles. This also led to reduction in normal pressure during the test.

The new design for normal pressure system consisted of a rigid assembly as opposed to flexible assembly used in original design. The modified system consisted of three wooden plywood sheets placed on top of the confining soil. Then, six air cylinders were placed on top of the last board as shown in Figure 4.2a. The steel plates were mounted on top of the cylinders and supported using all-thread rods as shown in Figure 4.2b. These plates were lifted using an automated hoist attached to an external frame as shown in Figure 4.3. An air pressure valve was attached to the main line which was then connected to all the six cylinders. The air cylinders had pistons which reacted against the steel plates to generate the uniform normal pressure on the entire pullout box area. The cylinders were calibrated to compute the force generated by them for a given air pressure.

The system was easy to assemble and reduced the test setup time considerably. Also, the sources of leakage were minimized as compared to the original design. Normal pressure magnitudes ranging from 7 to 100 kPa (1 to 15 psi) could be applied at the top of the specimen by changing the number of cylinders and their location in the given system. This normal pressure system could also be used to conduct reduced volume test by changing the area of pullout box used for a given test.

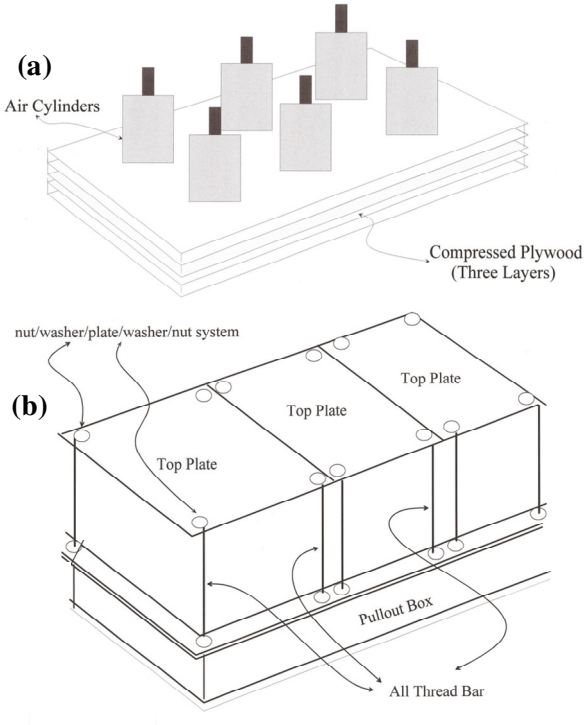

Figure 4.2 Normal pressure system (a) Air cylinders on top of compressed plywood (b) Top plates acting as the reaction system

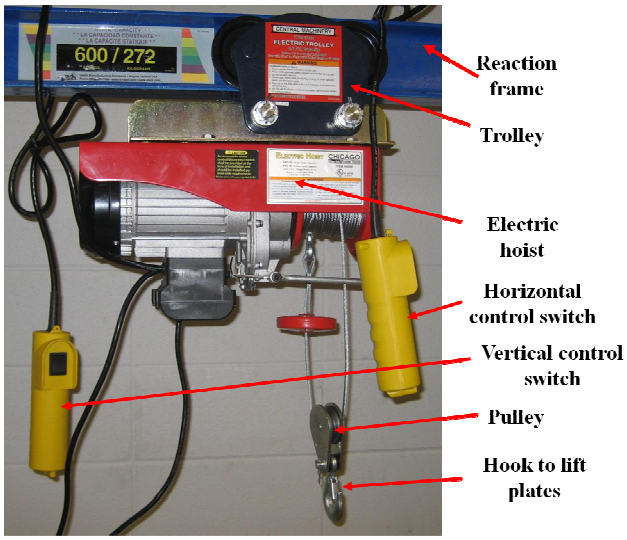

Figure 4.3 Automated hoist system used to assemble the reaction frame

4.2.3 Clamping system

The grips required to clamp the geosynthetic specimen play an important role during the test. The original clamping system for the pullout test equipment consisted of two plastic sheets which were epoxied with the specimen as shown in Figure 4.4a. The sheets and the geosynthetic specimen were then cured for 24 hours to allow for bond to develop between the materials. These were then bolted to two L-shaped angle iron plates in front of the pullout box which were finally attached to the hydraulic pistons during the test. This system had drawbacks as it delayed the test due to long curing time. Furthermore, slippage at the grips was common at high pullout force level especially when geogrids with thick junctions were used during the test.

To avoid the above problems, a roller grip mechanism was designed to clamp the geosynthetic specimen to the pullout box as shown in Figure 4.4b. It consists of a steel cylinder with a slit where the specimen could be attached and bolted using screws to main system. The grip was supported on a trolley system independent of the pullout box to prevent additional extension of the geosynthetic specimen. The roller grip design helped to prevent the stress concentration at a single plane throughout the specimen by distributing it uniformly over a wider area. This mechanism prevented the development of tensile failure in the unconfined portion of the geosynthetic specimen during testing. The new design required no curing time and the specimen could be directly attached to the grips.

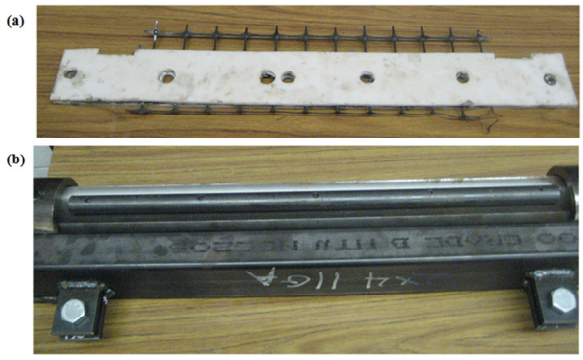

Figure 4.4 Clamping system (a) Original design consisting of plastic sheets (b) Modified design with roller grips

4.2.4 Displacement measurement system

The displacement occurring at low strain levels within the geosynthetic during the pullout test was an important input parameter for computation of K_{SGI}. The original displacement measurement system consisted of linear variable displacement transducer (LVDT) with a hollow cylindrical core. The displacement was measured as the change in voltage generated due to movement of rod inside the core. The rod was in turn attached to the geosynthetic by a thread which was passed through a thin cylindrical pipe. This design had drawbacks as the rod was not fixed inside the LVDT thereby causing slippage during the test. Also, the thread tended to lose tension and developed slack if it was not properly attached to the geosynthetic thereby providing erroneous readings at low displacement magnitudes.

In the modified design, new LVDT's (LX-PA sensors from Unimeasure) were installed which consisted of a cable and spring assembly. The spring helped in maintaining a constant pull back tension on the cable as shown in Figure 4.5a. The moving part of the sensor was attached to the cable while the spring was fixed to the main body of the LVDT. The cable movement led to pull on the spring which was attached to the potentiometer in a Wheatstone bridge circuit. The change in cable length causes changes in resistance which was used to compute the required displacement. The system minimized the development of slacks as it was pre-tensioned. Also the pull back speed of the cable was limited by the torque which could be applied to the spring, thereby preventing abrupt movements in connecting wire during the test.

The thread in the original design to connect the LVDT cable to the appropriate geosynthetic point inside the pullout box was replaced by orthodontic wires (manufactured by Lancer Corporation). These wires are 5 mm thick and essentially inextensible for pullout force magnitudes used in the present testing. The geosynthetic and wire connection was improved by sliding a metal bracket at their junction and crimping the assembly in place. This helped in preventing the slippage of the wire at the connection and minimized the errors in measurement which could occur due to slack in the system. Finally, an LVDT support system was installed using a steel angle piece and

attached to the back of the pullout box as shown in Figure 4.5b. This helped in preventing the differential movement between the pullout box and the LVDT's during the test.

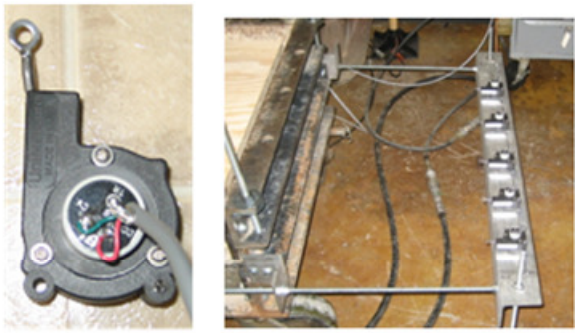

(a) (b)

Figure 4.5 Displacement measurement system: (a) spring loaded LVDT (b) support system for attaching LVDT to the pullout box

4.2.5 Data acquisition system

To validate the proposed model discussed in Section 3.6.4, the tests were conducted using seven LVDT's and a load cell. Five LVDT's were placed at the end of the box to monitor displacement measurements at various locations along the length of the geosynthetic during the test. The other two LVDT's one on each piston was attached to monitor the rate at which test was conducted. Also, a load cell was attached in the front of the box to measure the frontal pullout force during the test.

To meet the present instrumentation requirements, a new data acquisition system was added to the pullout box. The new design consisted of a National Instrument NI-USB-6211 card capable of supplying constant input voltage of ±5 Volts as shown in Figure 4.6a. The five displacement LVDT's were attached to this box which was programmed to measure the required output from these instruments. The frontal load cell had output voltage response is in range of milli-volts. Therefore, a data acquisition system consisting of a NI chassis with terminal block SCXI-1520 attached to module SCI-1314 was used as shown in Figure 4.6b. The chassis was in turn connected to the PCI-6221 card on the mother board of the computer using a connector block NI-1349 by

a 68 pin cable SHC-68-68-EPM. The system was programmed to supply a constant voltage of 10 Volts and read an input from sensor which had sensitivity range of ± 3 mV. Finally a program was written in Labview software version 8.0 developed by the National Instruments (NI) to read the input from the sensors during testing at 1 second intervals.

Figure 4.6 Data acquisition system (a) USB-device (b) Frontal unit with a chassis

4.2.6 Discussion

The schematic layout of the large-scale pullout testing equipment developed as part of this study is shown in Figure 4.7. The side view of the pullout box includes the details of the reaction frame system with wooden boards and air cylinders used for applying normal pressure on the specimen (Figure 4.7a). Further, the roller grips and its support trolley designed to avoid stress concentration at the geosynthetic reinforcement are shown. The top view of the pullout (Figure 4.7b) includes the two hydraulic pistons used to apply pullout force on the specimen. Also, the five LVDT's used in the test along with the support frame to attach them to the main pullout box are illustrated.

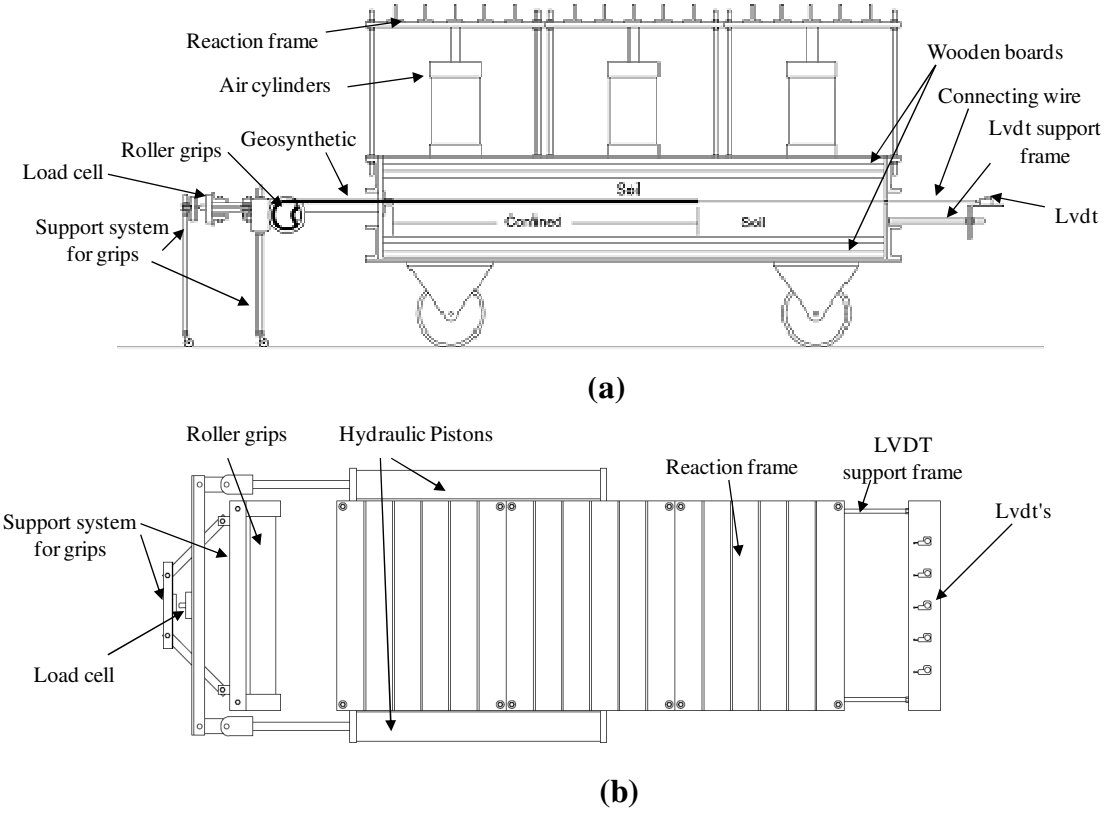

Figure 4.7 Large scale pullout testing equipment: (a) Side view; (b) Top view

The modified pullout box system with all the accessories is shown in Figure 4.8. The reaction frame system was found to reliable means of applying uniform normal pressure on top of the geosynthetic specimen. Roller grips were found to be suitable means of clamping different kinds of geosynthetics used during the test. Further, the use of new electric pump enabled better control over the rate of testing which could be independently controlled using the flow valve attached to it. Displacement transducers were attached to new system enabling faster data acquisition. The above changes led to reduction in test preparation time, better control over test procedure thereby providing repeatability among similar tests and reducing variability in test conditions for different geosynthetics. Overall, these modifications led to better equipment design capable of accurately characterizing low displacement soil-geosynthetic interface properties in the pullout box to be used for analysis using the proposed analytical model.

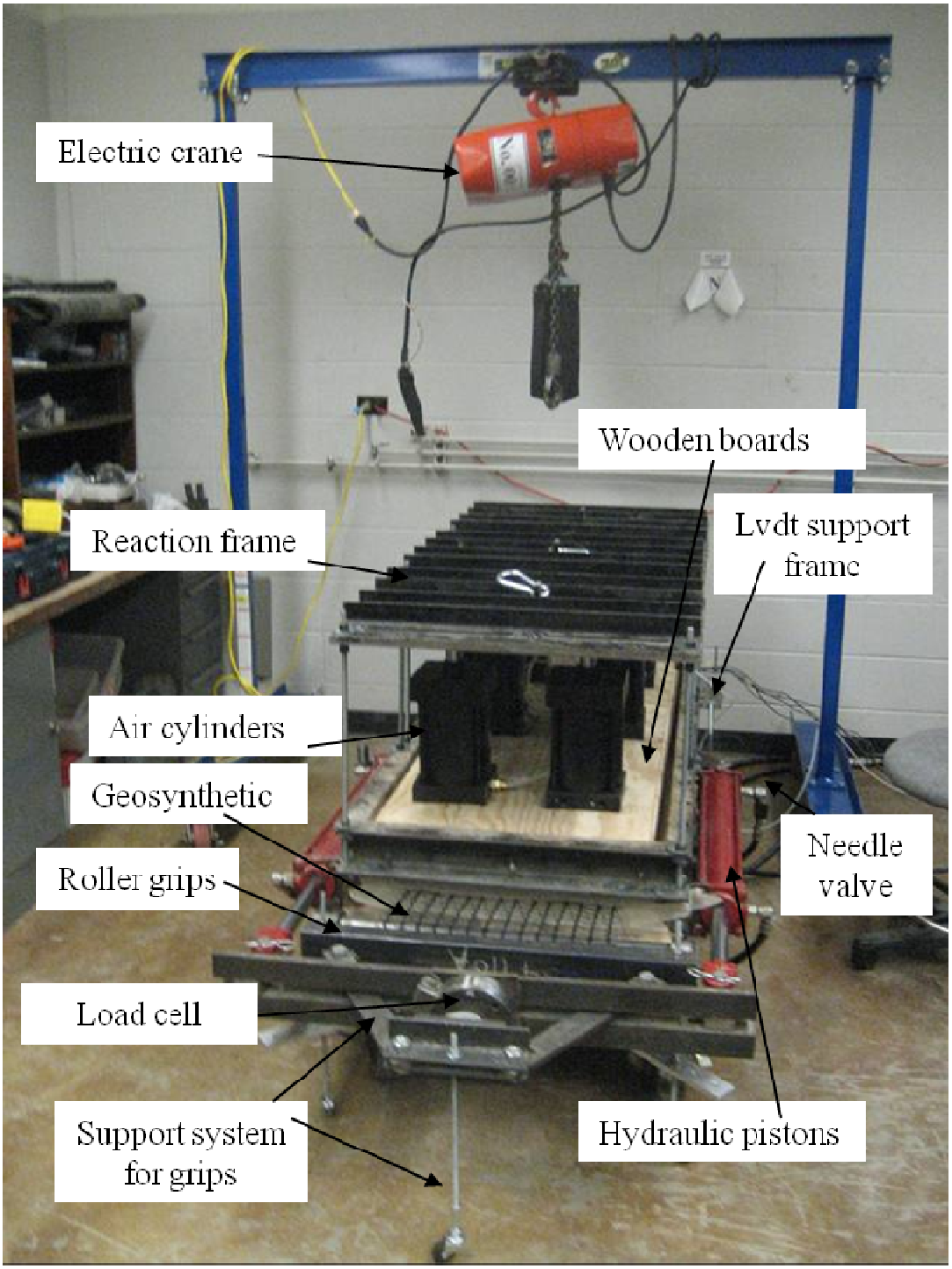

Figure 4.8 Large scale pullout box testing equipment

4.3 DESCRIPTION OF PULLOUT TESTING PROGRAM

The experimental component of this study aimed at validating the analytical approach to analyze the pullout test results and determine the coefficient of soil-geosynthetic interaction (K_{SGI}) (Chapter 3). The testing philosophy and assumptions involved in pullout testing were described in Section 3.2. Modifications were done to the original equipment used in preliminary testing phase to develop new equipment with capability of measuring low displacement soil-geosynthetic interaction.

The tests conducted on various geosynthetics along with test setup used for running a given pullout test are discussed. This is followed by explanation of the procedure followed to interpret results obtained from a given test to estimate the model parameters. The testing matrix incorporated four different geosynthetics (one geotextile and three geogrids). Two geogrids G1 and G2 from the initial testing in Chapter 3 were used along with a geotextile (G3) and another biaxial geogrid (G4) as explained in Section 4.3.1. Finally, the rationale for their selection and typical results for each one of them are described.

4.3.1 Testing Matrix

The pullout testing program was developed to establish a procedure to compute the K_{SGI} value for geosynthetics. Two major concerns were highlighted based on the review of literature as discussed in Chapter 2 for laboratory confined test procedures. First of all, it was found difficult to establish repeatability of test results for a soil-geosynthetic system subjected to a given normal pressure. Secondly, the variability in test results was found to be high enough where to distinguish between the performances of different geosynthetics. The present pullout testing scheme was planned to address these two issues. Therefore, preliminary set of tests were conducted on a geosynthetic to determine the capability of the present equipment to produce repeatable test results. Then the variability in the value of K_{SGI} for a given test was established. After this initial calibration, various geosynthetics were tested to obtain the K_{SGI} values under similar testing conditions and values obtained were compared. To incorporate these features, the

overall large pullout testing scheme was grouped into three main series. A total of twenty large-scale pullout tests were conducted using four different kinds of geosynthetics as listed in Table 4.1.

According to Palmeira (2008), "The geosynthetic reinforcements are generally modeled as linear elastic materials to match the model predictions. When simplifying assumptions are made, it is possible to make predictions fit reasonably well with the measurements for the geotextiles. However, in case of geogrids, if it is assumed as an equivalent rough planar reinforcement, predictions may deviate from measurements, depending on its geometrical characteristics and soil type." Therefore while planning the pullout tests it was decided to conduct an initial series of tests using geotextile reinforcement.

In the first series, a total of eight tests were conducted. The baseline test I-1 was conducted on geotextile specimen (G3) with sand as confining soil as explained in Section 4.4. The data analysis procedure adopted for interpreting results to compute model parameters (τ_y and J_c) and subsequently K_{SGI} value for this test were explained. The next test I-2 was conducted to establish the repeatability of test results for the same soil-geosynthetic system as used in Test I-1. The results were analyzed to establish bounds on values of K_{SGI} obtained from analysis of results for these two tests. The next three tests (I-3, I-4, and I-5) were conducted to quantify the effect of change in specimen dimensions (from that specified by ASTM standards) on the value of K_{SGI}. In testes I-3 and I-4, the length of specimen was changed whereas the width was kept same as the initial specimen. In the test I-5, the width of the specimen was decreased. These tests also helped in quantifying the effect of boundary conditions on the results. Then the effect of normal pressure on K_{SGI} was evaluated by conducting a test at lower (I-6) and higher normal pressure (I-7) than used in Test I-1. Finally, the effect of specimen dimension was evaluated by running the test in machine direction (I-8) than cross-machine direction as used in the test I-1. The first series of tests helped in understanding various components which could influence K_{SGI} value obtained from the pullout test for a given soil-geosynthetic system.

The second series of pullout tests consisted on eight tests conducted on two geogrid products (G1 and G4) manufactured using the same material. Based on the manufacturing process it was established that one product had slightly better performance properties than the other geogrid. The main objective of this phase of testing was to obtain K_{SGI} values for both the products and check if the predicted values reflected same performance order as expected based on their manufacturing quality. Three tests at normal pressure of 7 kPa, 21 kPa and 35 kPa were conducted on geogrid G1 (II-1, II-2, II-3) and geogrid G4 ((II-4, II-5, II-6) similar to the baseline test (I-6, I-1 and I-7). Then two more tests, one for each geosynthetic were conducted in machine direction (II-7 and II-8). The results obtained were used to compare the performance of products of known properties under pullout test conditions. Furthermore, these tests helped in verifying the applicability of proposed model and parameter to pullout results on geogrid reinforcements.

In the third series, four tests were conducted on a geogrid (G2) obtained from different manufacturer. Tests III-1, III-2, and III-3 were conducted at normal pressure of 7 kPa, 21 kPa and 35 kPa respectively. The test III-4 was conducted in different direction from the principal direction in test III-2. The objective of this series of testing was to compare the performance of the geosynthetics manufactured using different material from those used in series II.

Overall, the aim of the pullout testing scheme was to establish evidence for capability of proposed parameter to compare performance of various geosynthetics in the laboratory setting. The geosynthetics G1, G2 and G3 were also used in the field test sections. The performance predicted in terms of K_{SGI} value from pullout test results for these geosynthetics was compared qualitatively with field measurements and is discussed in the Chapter 5.

Table 4.1 Testing matrix for large scale pullout testing

Series	Test No.	Geosynthetic	Type	Direction	Normal pressure	Length	Width	Testing rate	Test abbreviation	Test characteristics	Comments
					kPa	m	m	mm/min			
I	1	Geotextile	G3	XD	21	0.60	0.45	1.0	G3-XD-21	Baseline	Test to calibrate the equipment and proposed model
	2	Geotextile	G3	XD	21	0.60	0.45	1.0	G3-XD-21-RP	Repeatability	
	3	Geotextile	G3	XD	21	0.90	0.45	1.0	G3-XD-21-LI	Effect of length	
	4	Geotextile	G3	XD	21	0.30	0.45	1.0	G3-XD-21-LR	Effect of length	
	5	Geotextile	G3	XD	21	0.30	0.28	1.0	G3-XD-21-WR	Effect of width	
	6	Geotextile	G3	XD	7	0.60	0.45	1.0	G3-XD-07	Normal pressure	
	7	Geotextile	G3	XD	35	0.60	0.45	1.0	G3-XD-35	Normal pressure	
	8	Geotextile	G3	MD	21	0.60	0.45	1.0	G3-MD-21	Direction	
II	1	Geogrid	G1	XD	7	0.60	0.45	1.0	G1-XD-07	Normal pressure	Test conducted to compare performance of two geogrids from same material.
	2	Geogrid	G1	XD	21	0.60	0.45	1.0	G1-XD-21	Normal pressure	
	3	Geogrid	G1	XD	35	0.60	0.45	1.0	G1-XD-35	Normal pressure	
	4	Geogrid	G4	XD	7	0.60	0.45	1.0	G4-XD-07	Normal pressure	
	5	Geogrid	G4	XD	21	0.60	0.45	1.0	G4-XD-21	Normal pressure	
	6	Geogrid	G4	XD	35	0.60	0.45	1.0	G4-XD-35	Normal pressure	
	7	Geogrid	G1	MD	21	0.60	0.45	1.0	G1-MD-21	Direction	
	8	Geogrid	G4	MD	21	0.60	0.45	1.0	G4-MD-21	Direction	
III	1	Geogrid	G2	XD	7	0.60	0.45	1.0	G2-XD-07	Normal pressure	Test conducted to predict the performance of geosynthetics made of different material.
	2	Geogrid	G2	XD	21	0.60	0.45	1.0	G2-XD-21	Normal pressure	
	3	Geogrid	G2	XD	35	0.60	0.45	1.0	G2-XD-35	Normal pressure	
	4	Geogrid	G2	MD	21	0.60	0.45	1.0	G2-MD-21	Direction	

G1-Tensar BX1100 G2-Mirafi Bas X11 G3-Mirafi HP570 G4-Tenar BX1200

XD- Cross Direction MD-Machine Direction RP-Repeat LI-Length Increase LR-Length reduced WR-Width reduced

7, 21, 35 are the normal pressure magnitudes (in kPa) applied during the test

4.3.2 Soil

Monterey No. 30 sand (Figure 4.9) was used for the initial baseline series of large scale pullout testing of geosynthetics. The reason for this selection was the commercial availability of the soil and existing geotechnical database available to characterize the given soil. Furthermore, the volume of soil required to run a full scale pullout test was large, therefore the ease of handling of Monterey No. 30 sand in sample preparation and post-processing phase of the test made it a suitable choice.

Figure 4.9 Monterey No. 30 sand bags

Monterey No. 30 sand is clean uniformly graded sand classified as SP in the unified system and gradation curve of the soil is as shown in Figure 4.10. The particles are rounded to sub rounded consisting predominantly of quartz with a smaller amount of feldspar and other minerals (Zornberg, 1994).

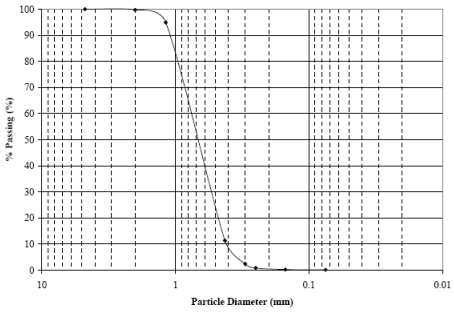

Figure 4.10 Gradation curve of Monterey No. 30 sand (Li, 2005)

The properties of Monterey No. 30 sand (Yang, 2009) are listed in Table 4.2.

Table 4.2 Soil properties of Monterey No. 30 sand

Soil Type	**Monterey No. 30 sand**
D_{50} (mm)	0.4
Uniformity coefficient, C_u	3.0
Coefficient of gradation, C_g	1.1
Specific gravity, G_s	2.65
Soil classification	SP
Max. dry unit weight, $\gamma_{d,\,max}$ (kN/m^3)	16.7
Min. dry unit weight, $\gamma_{d,\,min}$ (kN/m^3)	14.76
Maximum void ratio, e_{max}	0.76
Minimum void ratio, e_{min}	0.56

The shear strength of the soil is reported based on large scale triaxial tests performed by Li (2005). The specimens had a diameter of 152 mm (6 inches) and a height of 304 mm (12 inches). The specimens were prepared at a relative density of 48% and 65%. The test results indicated decrease in strain at peak deviatoric stress with increasing relative density of the soil. The mechanical properties for Monterey No. 30 sand are reported in Table 4.3. The stress-strain curves obtained from triaxial tests are as shown in Figure 4.11. At the relative density of 65%, peak friction angle of sand was 35^0 and residual friction angle was 31^0.

Table 4.3 Mechanical properties of Monterey No. 30 sand (Li, 2005)

Dr (%)	48	65
γ_d (kN/m^3)	15.54	15.91
ϕ' (°)	31.6	35.2
c (kPa)	0	0

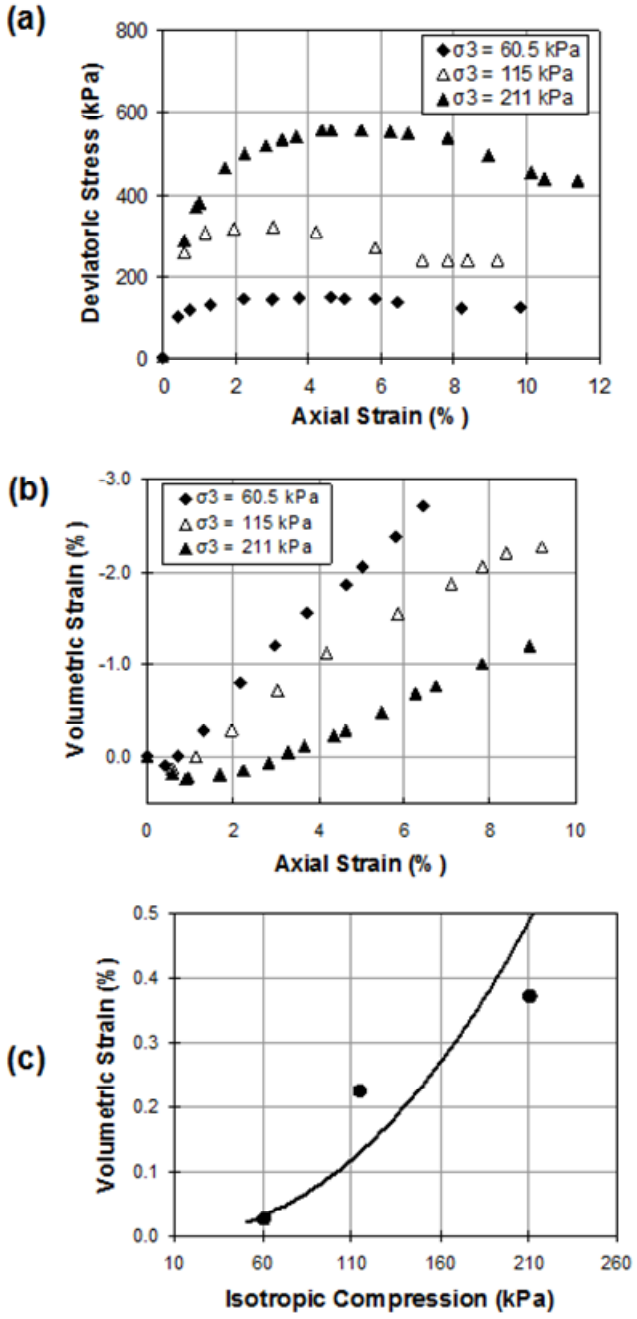

Figure 4.11 Results of triaxial compression test on Monterey No.30 sand: (a) deviatoric stress and axial strain; (b) volumetric and axial strain; and (c) compression and volumetric strain, (Yang, 2009)

4.3.3 Test setup

The basic test preparation method adopted for the pullout test was similar to the one used for evaluating maximum pullout resistance as described in Section 3.4.3. This involved cutting the geosynthetic specimen to the required dimensions from the roll, attaching the inextensible orthodontic wires to it and finally clamping it to the roller grips. The test soil was prepared for a given pullout test by moisture conditioning it to the required water content (2% in case of Monterey No. 30 sand).

The initial step for the pullout test involved compaction of the soil to required relative density in the box. For uniform compaction of soil throughout the pullout box, it was decided to compact soil in four layers of 75mm thickness each. The first layer of soil was placed at the bottom of the pullout box and was compacted using hand compactors as shown in Figure 4.12a. Then the second layer of soil was compacted such that the total thickness of 150mm was obtained and the soil layer was at the same height as the frontal opening of the pullout box as shown in Figure 4.12b. The geosynthetic specimen was then passed through the slit and attached to the roller grips as shown in Figure 4.12c. Then, the geosynthetic specimen was attached to the roller grips in the front of the box and the confined length of the specimen was adjusted to meet the test requirements. The inextensible thin steel wires were hooked at the marked distances from the front end of the geosynthetic as shown in Figure 4.12d. Then two more layers of soil were compacted on top of the geosynthetic specimen so that the total thickness of 150 mm as shown in Figure 4.12e was attained.

To apply the required normal pressure, the three layers of plywood were placed on top of the soil layer as shown in Figure 4.12f. The air cylinders were then placed on the marked location and the steel reaction frame was assembled as shown in Figure 4.12g and 4.12h respectively. The air pressure was then applied to the cylinders so that the piston stroke could react with the steel plates thereby applying force on the plywood and generating the required normal pressure on the top of the specimen.

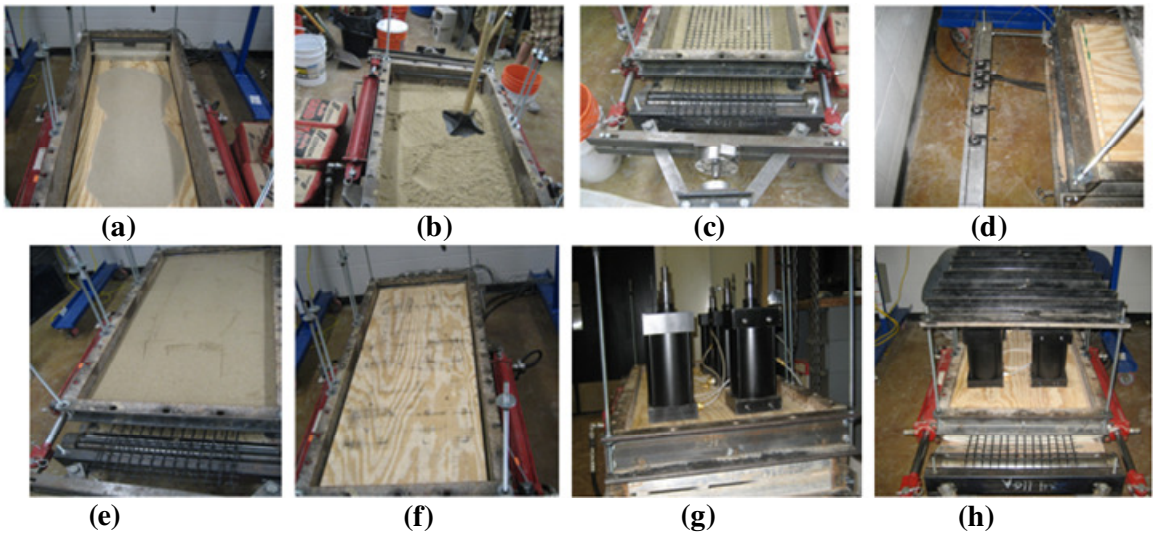

Figure 4.12 Pullout test setup (a)First layer of soil (b) Compaction to slit level (c) Placement of the geosynthetic (d) Attaching the LVDT's (e) Compacting the soil on top of specimen (f) Placing the plywood boards (g) Installing air cylinders (h) Assembling reaction frame

The instrumentation including seven LVDT's and a load cell was attached to the data acquisition system. The test was started by operating the flow pump and adjusting the needle valve such that a constant displacement rate of 1mm/min could be applied to the frontal clamp of the pullout box. The readings obtained from two LVDT's attached to the piston were observed during the test to monitor the rate at which test was being conducted. The needle valves were adjusted to prevent the differential movement of greater than 0.5mm between both the pistons at any stage during the test.

The frontal pullout force data was obtained using the load cell which reacted against the clamp system as the specimen was being pulled out of the box. The five LVDT's attached at various points along the geosynthetic length were used to monitor the displacement response for the given test. The test was terminated when all the LVDT's moved such that there was no increase in pullout force with further increase in displacement. The results obtained for various tests conducted based on above procedure are discussed in the Section 4.4.

4.4 TESTS ON GEOSYNTHETICS USING PULLOUT EQUIPMENT

4.4.1 Series I: Tests conducted to calibrate the model

The material used in the first series of pullout tests was geotextile (G3). It is a polypropylene woven geotextile manufactured by Mirafi and branded as HP-570 (Figure 4.13a). Wide width tensile test were conducted on the geotextile specimens similar to those conducted on both geogrids as explained in Section 3.3.2.5. In accordance with ASTM D4595 (2001), a 200 mm (8 in) wide and 100 mm (4in) long specimen of geotextile was prepared from the geosynthetic roll for the given test and attached to the load frame as shown in Figure 4.13b. The geotextile was tested in machine and cross machine direction at four different rates of testing (1%, 5%, 10% and 20% strain rate per minute).

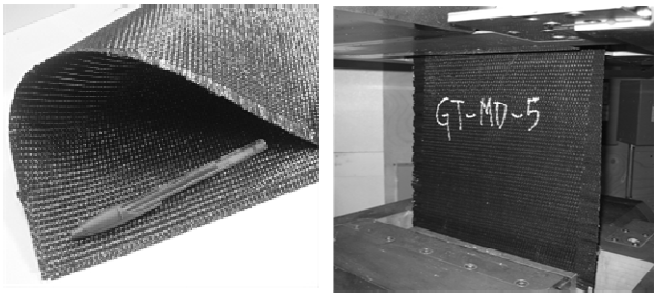

(a) (b)

Figure 4.13 Geosynthetic used for baseline tests (a) Geotextile (G3); (b) specimen used in wide-width tensile test

The average results obtained from a series of five tests conducted at each of the four strain rates are shown in Figure 4.14. The average tensile stiffness obtained at rate of testing of 1 % for the two directions of the geotextile is shown in Table 4.4. The test results indicated that the geotextile was stiffer in cross-machine direction than machine direction. Furthermore, the tensile strength of geotextile was dependent on strain rate adopted for the test. It increased with increase in strain rate used in the test. The results of pullout tests conducted using the geotextile are discussed in Section 4.4.1.1.

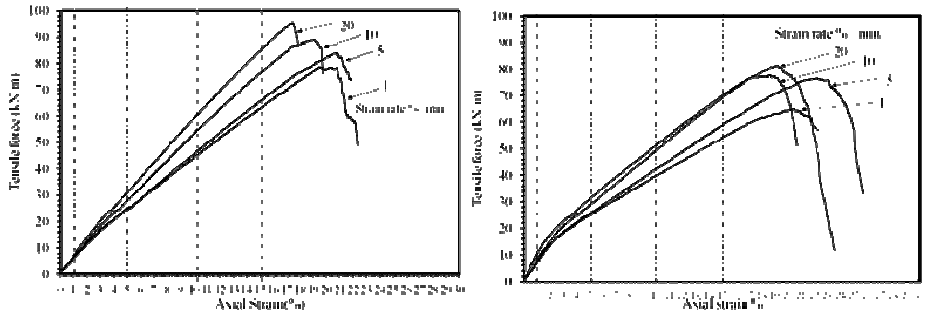

(a) (b)

Figure 4.14 Wide width tensile test results for geotextile at different strain rates (a) Machine direction (b) Cross-Machine direction

Table 4.4 Wide width tensile tests results for the geotextile

Properties	Units	1% strain per minute	
		MD	XD
Stiffness at 1% strain	**kN/m**	618	825
Stiffness at 2% strain	**kN/m**	595	697
Stiffness at 5% strain	**kN/m**	469	487
Stiffness at 10% strain	**kN/m**	426	383
Stiffness at maximum load	**kN/m**	389	307
Strain at maximum load	**%**	20	20

4.4.1.1 Baseline test

The test I-1 as shown in Table 4.1 is designated as the baseline test for calibrating the proposed analytical model. The specimen for geotextile (G3) was prepared with dimensions of 0.6m length and 0.45m width as per the guidelines described in ASTM D6706 (2003) for conducting pullout test. Five LVDT's were used at the horizontal spacing of 100 mm, 200 mm, 300 mm, 450 mm and 600 mm from the front end of the specimen as shown in Figure 4.15. The advantage of having five LVDT's was that the displacement profile throughout the length of the geosynthetic could be monitored. Furthermore, the readings from three LVDT's could be used to calibrate the model parameters and the other two LVDT's could be used to verify them. However, for the present analysis all the five LVDT's were used for parameter estimation.

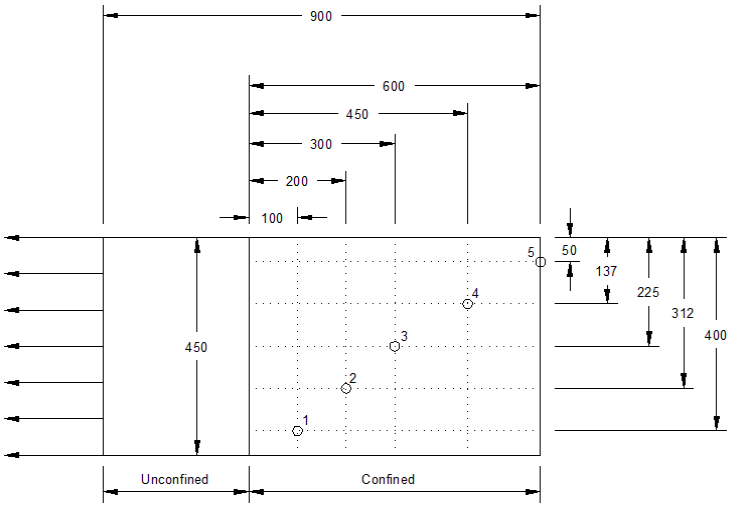

Figure 4.15 Location of LVDT's on geosynthetic specimen for test I-1 with dimensions of 0.6m confined length and 0.45m width (All dimensions in millimeters)

Monterey No. 30 sand was used as the confining soil. The normal pressure applied at the top of the specimen was 21 kPa (3psi). The displacement rate of testing was set to 1mm/min. The value of frontal pullout force (F_p) for displacement measured at location of five LVDT's was obtained from the given test as shown in Figure 4.16. The maximum pullout force value for the given test was 14.5 kN/m.

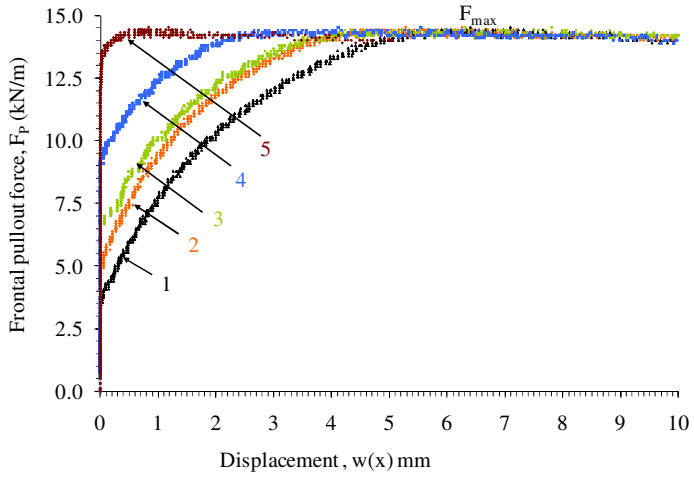

Figure 4.16 Frontal pullout force vs. displacement curve for each LVDT

After completion of the test, the data was analyzed to obtain the two parameters yield shear stress (τ_y) and confined stiffness (J_c) proposed in the analytical model. The yield shear stress (τ_y) could be obtained either graphically or using equations proposed by the model. For computation of τ_y graphically, data obtained from pullout test in terms of frontal pullout force and displacement at each LVDT were plotted as a function of time from the start of the test as shown in Figure 4.17a. This plot helped to determine the magnitude of frontal pullout force when each LVDT just started to move ($F_{p,t1}$ through $F_{p,t5}$). That is, the magnitude of frontal pullout force corresponding to the active length of reinforcement was defined. Then, these values were plotted against the location of each LVDT on the geosynthetic specimen as shown in Figure 4.17b.

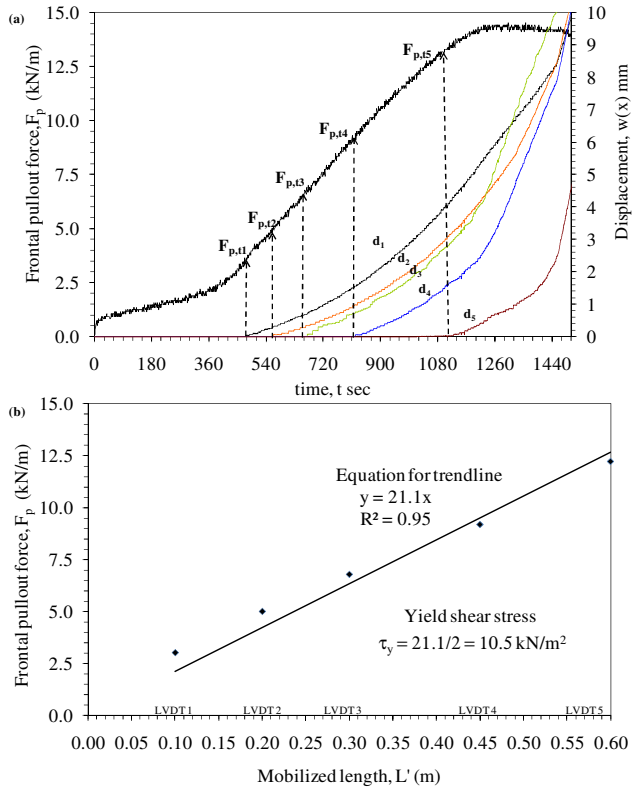

Figure 4.17 Computation of yield shear stress parameter graphically (a) Frontal pullout force and displacement as function of time from start of test; (b) Frontal pullout force vs. active length of the reinforcement

The line was then fitted through these points and its slope was determined. Since shear stress is mobilized on top and bottom of the specimen, it value was half of the value obtained from slope of the curve. The yield shear stress (τ_y) for the given soil-geosynthetic system was calculated as 10.5 kN/m^2.

Alternatively, the magnitude of frontal pullout force at which each individual LVDT starts moving can be determined from the test data. At this frontal pullout force the active length of reinforcement is known and is equal to the location where LVDT was placed before the start of test. So the value of yield shear stress can be calculated using Equation 3.53 as shown in Table 4.5.

Table 4.5 Computation for yield shear stress

LVDT Number	**Location from front end, L′**	**Time to start of displacement**	**Force F_p**	**Yield Shear $\tau_y=F_p/2L'$**
	mm	**seconds**	**kN/m**	**kN/m^2**
1	100	466	3.0	15
2	200	562	5.5	13
3	300	669	6.8	11
4	450	820	9.19	10
5	600	1014	12.22	11

The present model assumed a constant value of τ_y throughout the geosynthetic specimen for the given test. However in the above analysis, the first LVDT had higher shear stress value and last two LVDT's have lower values than those obtained from middle LVDT's. Thus, it can be seen that yield shear stress was influenced by the boundary conditions. For calculation purposes an average value of τ_y was assumed for the entire test for a given soil-geosynthetic system subjected to known normal pressure.

To compute the value of confined stiffness (J_c), it was necessary to obtain the confined force and displacement response at each LVDT. Therefore, after computing the yield shear stress τ_y, the confined force F(x) at LVDT point x_i, for a given frontal pullout force F_p was estimated as shown in Equation 3.52 as,

$$F(x_i) = F_P + 2.\tau_y x_i$$

The confined force F(x) and displacement w(x) at each of the five LVDT points is shown in Figure 4.18. The LVDT's 2 and 3 which are in the middle of the geosynthetic specimen were least influenced by the boundary conditions and had similar confined force and displacement response. This trend was as hypothesized by in the development of the analytical model, where it was suggested that the confined force and displacement response is unique for a given soil-geosynthetic system.

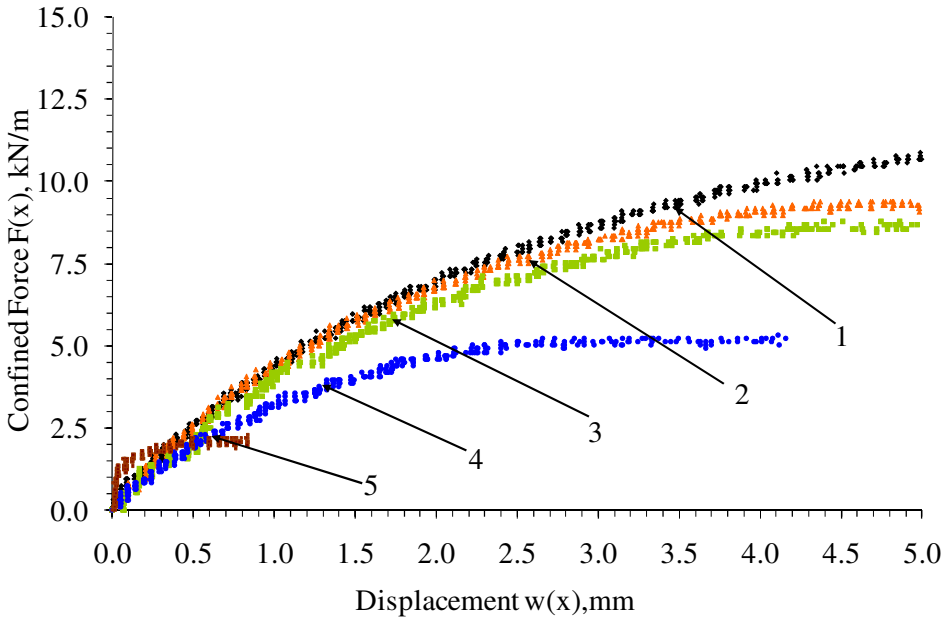

Figure 4.18 Confined force vs. displacement curve for baseline test

The next step in the analysis involved determining the magnitude of the confined stiffness (J_c) for the given system. It could be estimated graphically by plotting the square of the confined force at a point vs. displacement at that point as shown in Figure 4.19. Then, the slope of this curve directly gives the value of constant K_{SGI}, which can be used to back-calculate the value of J_c for a given average value of τ_y using Equation 5.1. This graphical method was used in the present analysis to estimate this parameter.

$$J_c = \frac{K_{SGI}}{4.\tau_y} \tag{5.1}$$

Alternatively, J_c could be computed by using Equation 3.56 shown below for a given value of confined force and displacement at a point.

$$J_c = \frac{F(x_i)^2}{4.\tau_y.w(x_i)}$$

The average value of confined stiffness based on the data obtained from LVDT 2 (at 1 mm displacement) was estimated at 590 kN/m.

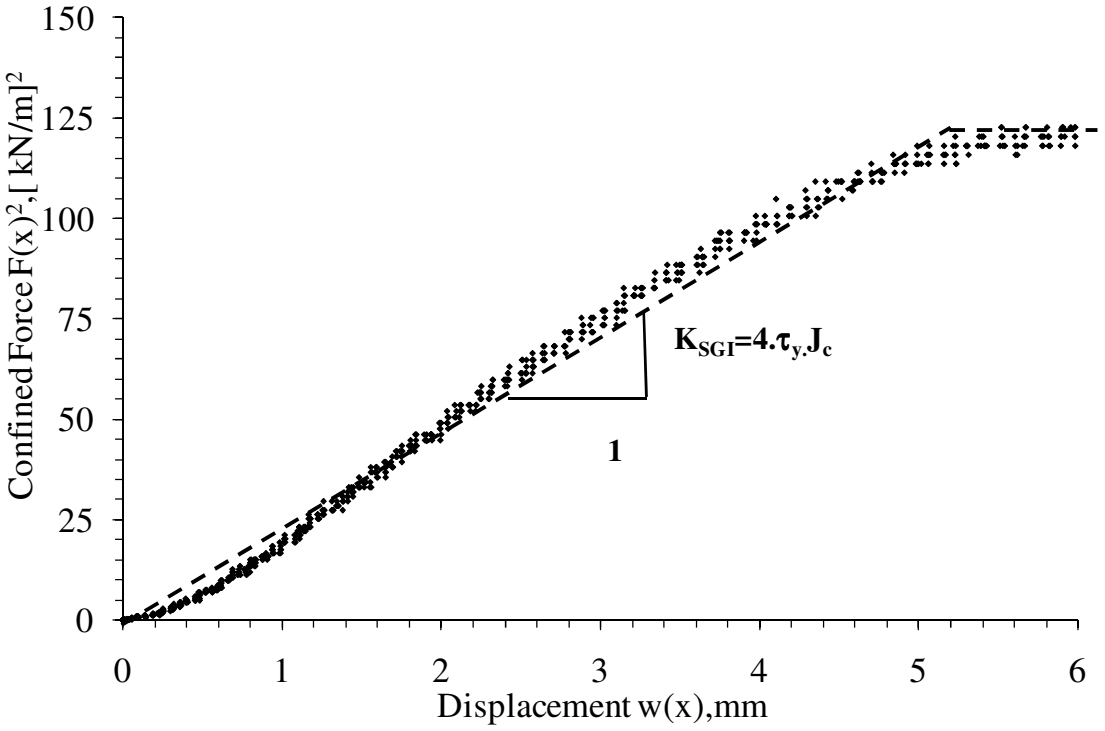

Figure 4.19 Estimating K_{SGI} graphically

Alternatively, after computing the value of two model parameters (knowing the τ_y and J_c magnitude mathematically), the value of K_{SGI} could be obtained using Equation 3.57. For the given test, K_{SGI} was estimated at 24990 kN^2/m^3 (or 24.9$(kN/m)^2$/mm). The above value of K_{SGI} can also be converted to equivalent modulus M_{SGI} at 1 mm displacement using the Equation 3.58 and was given as,

$$M_{SGI}(x_i) = \sqrt{\frac{K_{SGI}}{w(x_i)}} = \sqrt{\frac{24990}{1/1000}} \cong 5000 kN/m^2 \qquad (5.2)$$

Finally, the prediction of the pullout force and displacement based on estimated parameters τ_y and J_c were compared with that measured during the test at all the five locations using the Equation 3.59.

$$w(x_{j,t}) = \frac{\tau_y}{J_c}.x_j^{\,2} + \frac{F_{P,t}}{J_c}.x_j + \frac{F_{P,t}^{\,2}}{4.\tau_y.J_c}$$

The curve showing the predicted vs. measured displacement is shown in Figure 4.20. Good agreement was obtained between the measured and predicted values of frontal pullout force and LVDT displacements at five LVDT locations in terms of two model parameters.

The regression analysis was conducted on the data obtained from the pullout test to directly obtain the K_{SGI} value as discussed in Section 3.6.3. Furthermore, the upper and lower bounds on the estimates of K_{SGI} were established as shown in Table 4.6. Based on these results it was estimated that the variation in K_{SGI} value for a given test is within 1000 $(kN/m)^2$/m for 95% upper and lower bound interval.

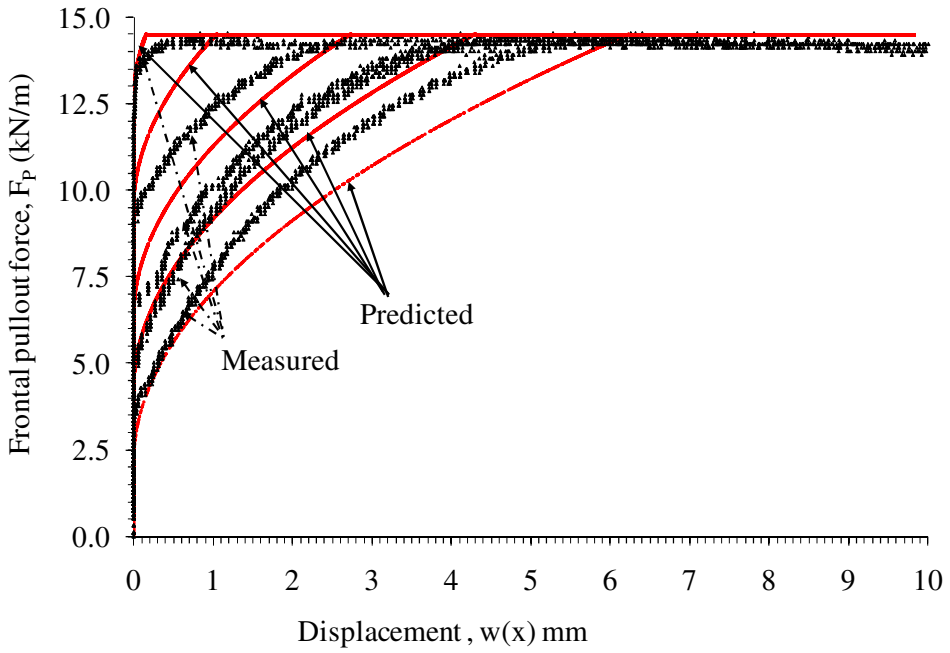

Figure 4.20 Comparison of measured and predicted data for frontal pullout force vs. displacement for the baseline test

Table 4.6 Regression analysis to obtain K_{SGI}

K_{SGI}	24663 $(kN/m)^2/m$
Upper 95%	25840 $(kN/m)^2/m$
Lower 95%	23991 $(kN/m)^2/m$
Observations	619
R Square	0.995
t Stat	55.51
P-value	6.7E-242
Standard Error	9.16E-07

The procedure detailed above was used for data analysis of tests conducted using large scale pullout system to estimate the model parameters (τ_y and J_c). These parameters were used to compute coefficient of soil-geosynthetic interaction (K_{SGI}) for given system. The results for tests listed in Table 4.1 for test series-1 are presented to calibrate the model and the average value of K_{SGI} obtained in each case is reported.

4.4.1.2 Repeatability

To check the repeatability of tests for given soil-geosynthetic system with the pullout apparatus, Test I-2 was setup under similar conditions as Test I-1. A new specimen of geotextile (G3) was tested with Monterey No.30 sand at 21 kPa normal pressure. The rate of testing during both the tests was maintained at 1 mm/minute. The frontal pullout force vs. displacement of first LVDT for both the tests is shown in Figure 4.21a. The value of maximum pullout force obtained in test I-2 was 12.1 kN/m as compared to 14.5 kN/m for Test I-1. Furthermore, the yield shear stress obtained based on analysis of test I-2 was 10.3 kN/m^2 as compared to 10.5 kN/m^2 for test I-1 as shown in Figure 4.21b.

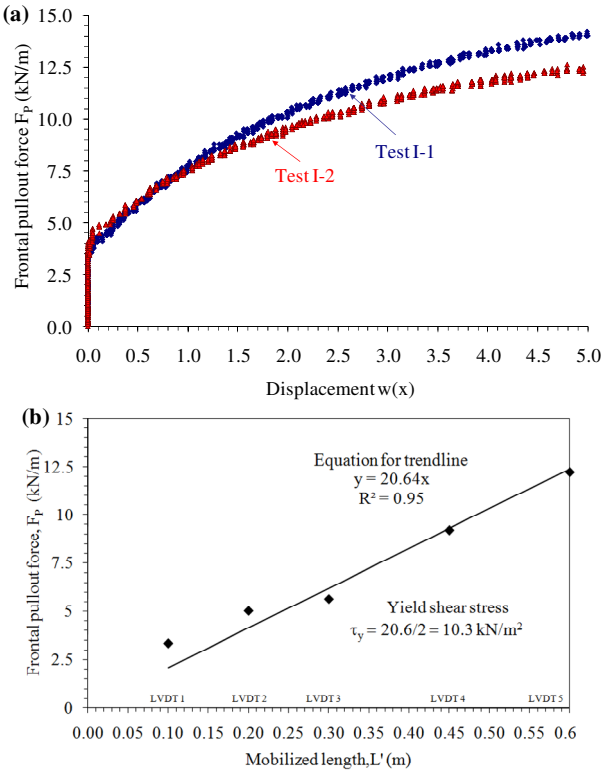

Figure 4.21 Test conducted for repeatability: (a) Frontal pullout force vs. displacement for LVDT 1 in Test I-1 and Test I-2 (b) Yield shear stress for test I-2

Based on the magnitude of τ_y, confined force values at each LVDT point were calculated to compute J_c. The values of confined force vs. displacement for LVDT's 1 and 2 for both the test are shown in Figure 4.22a and 4.22b respectively. The LVDT 2 readings for both the tests showed better match specifically at low displacement magnitudes (till 1 mm) as compared to LVDT 1 due to less effect of boundary conditions on it. Thus LVDT 2 was used in case 2 to compute the confined stiffness J_c value.

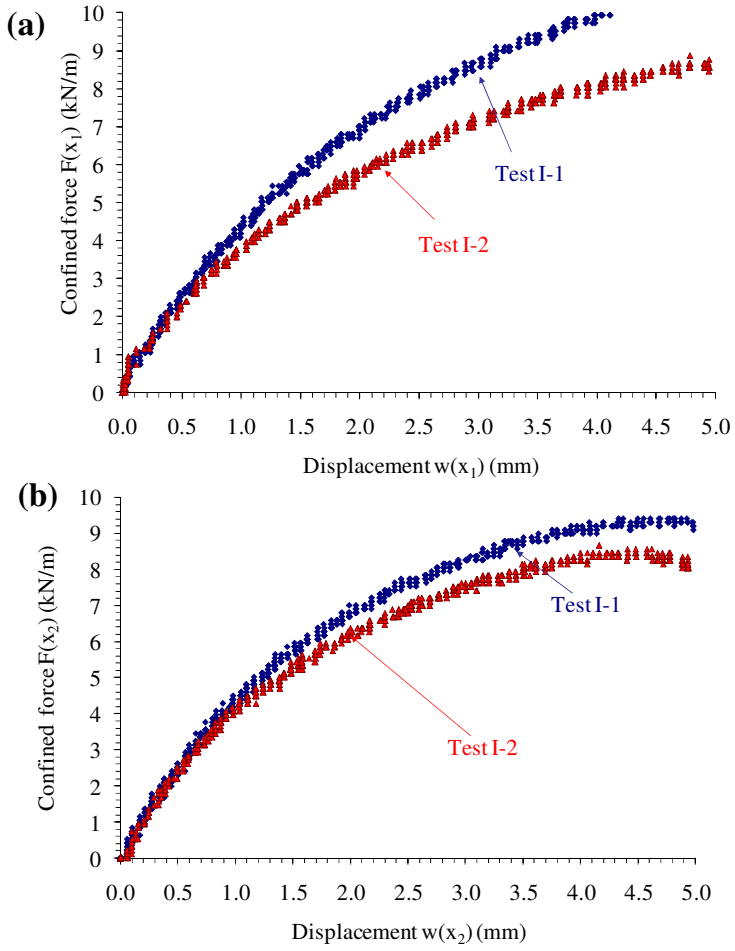

Figure 4.22 Comparison of confined force vs. displacement profile for test I-1 and test I-2: (a) LVDT 1 (b) LVDT 2

Using the above values of F(x) and w(x), K_{SGI} value was calculated for test I-2. The comparison of slope for the curve obtained by plotting square of confined force with displacement for LVDT 2 for both tests is shown in Figure 4.23. The value of K_{SGI} was slightly lower than that obtained in test I-1. However, the slope of the curve showed good agreement at the low displacement magnitudes (less than 1mm) which is the area of concern for current analysis.

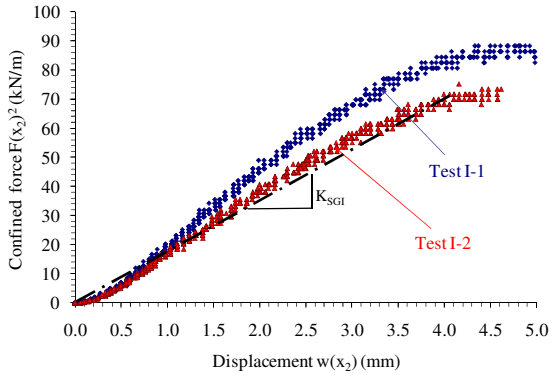

Figure 4.23 Comparison of K_{SGI} values obtained for test I-1 and I-2 graphically

The average values of each parameter for both the tests are reported in Table 4.7. The results obtained from both the tests indicated less variability in the model parameters obtained at small displacements compared to pullout test parameters obtained at large displacements for the two tests. Also the value of K_{SGI} from both tests were comparable and within the range of confidence intervals as determined in the previous case.

Table 4.7 Repeatability of test results

Test	Specimen dim.		Pullout parameters		Model parameters		Constant	
	L	W	F_{max}	τ_{max}	J_c	τ_y	K_{SGI}	$M_{SGI,1mm}$
	m	m	kN/m	kN/m^2	kN/m	kN/m^2	$(kN/m)^2/m$	kN/m^2
I-1	0.60	0.45	14.5	12.1	590	10.5	24780	4978
I-2	0.60	0.45	12.1	10.1	570	10.3	23484	4846

4.4.1.3 Effect of specimen length

The effect of change in specimen length was quantified by conducting tests at two different specimen lengths of 0.9m and 0.3m from the baseline specimen length of 0.6m. The width of specimen in all these tests was 0.45m. The LVDT's were relocated on both the specimens in test I-3 (0.9 m long) and test I-4 (0.3 m long) as shown in Figure 4.24a and 4.24b respectively. The tests were conducted by applying a normal pressure of 21 kPa on the top of soil-geosynthetic specimen.

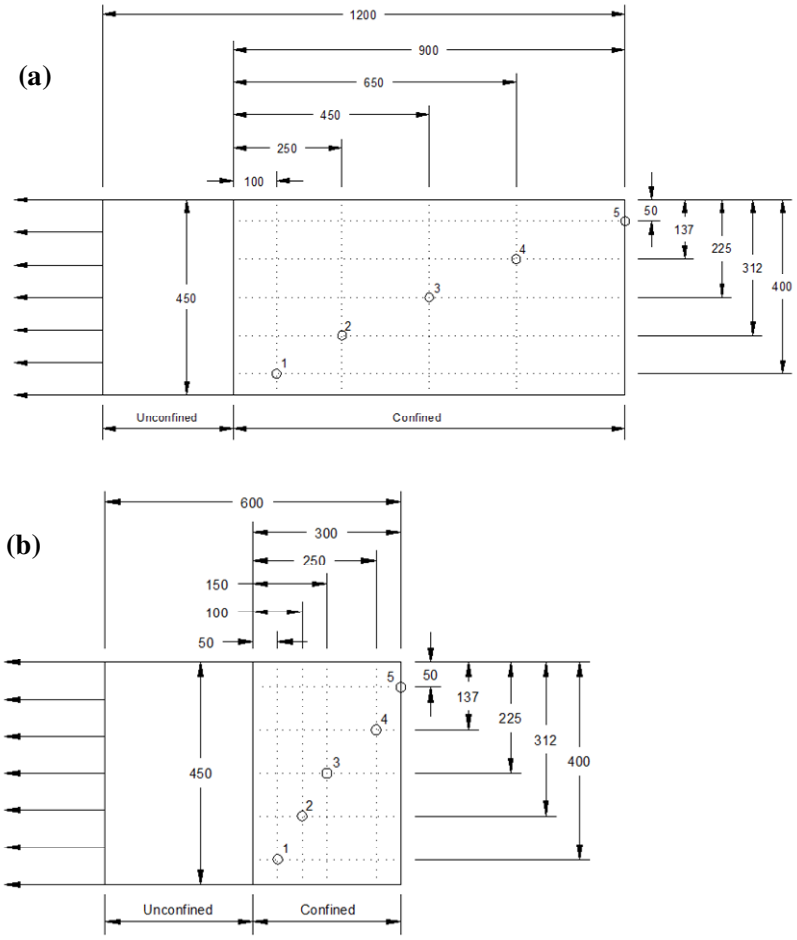

Figure 4.24 LVDT location for test I-3 and test I-4 of specimen width of 0.45 m and confined length: (a) 0.9 m; (b) 0.3 m (All dimensions in millimeters)

The frontal pullout force values corresponding to displacements for the four tests (Test I-1, I-2, I-3 and I-4) are plotted for LVDT locations 1 and 2 as shown in Figure 4.25a and 4.25b. Based on the results obtained from these tests it was observed that the maximum pullout force increased with the increase in the length of the specimen for the same width.

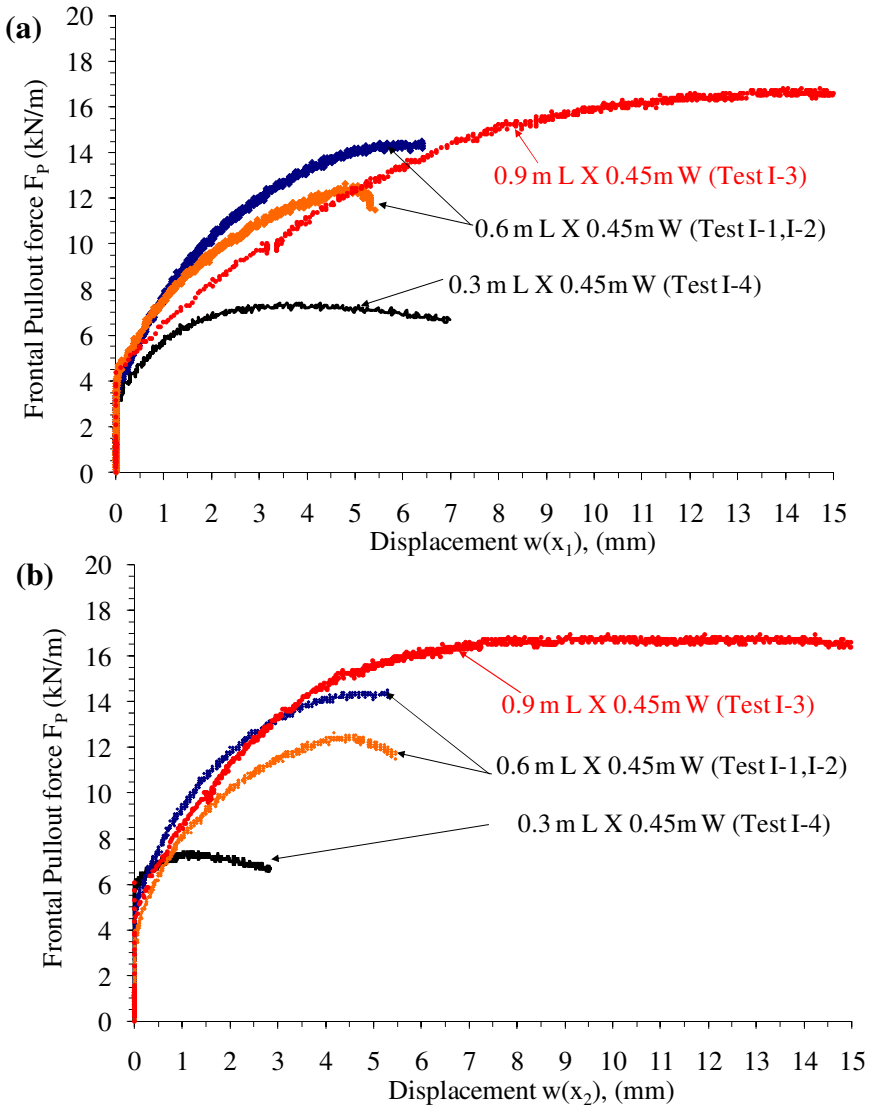

Figure 4.25 Frontal pullout force vs. displacement for test I-1, I-2, I-3 and I-4 at location: (a) LVDT 1 (b) LVDT 2

The results were used to compute the value of the yield shear stress for test I-3 and test I-4 as shown in Figure 4.26a and 4.26b respectively. In test I-3, due to increase in the length of the test specimen, the front of the specimen was stretched (extensibility) before the force reached its back end, thereby causing non-uniform yield shear stress distribution in the specimen close to maximum pullout resistance value. Thus the model assumptions were not valid in this range of pullout force. This can be seen for LVDT 5 in Test I-3 which moved at lower shear stress value that the rest of the specimen. Thus, it was not used to compute τ_y value. Further, this also indicated there is limiting value of specimen length for which model assumptions are valid at a given confining pressure.

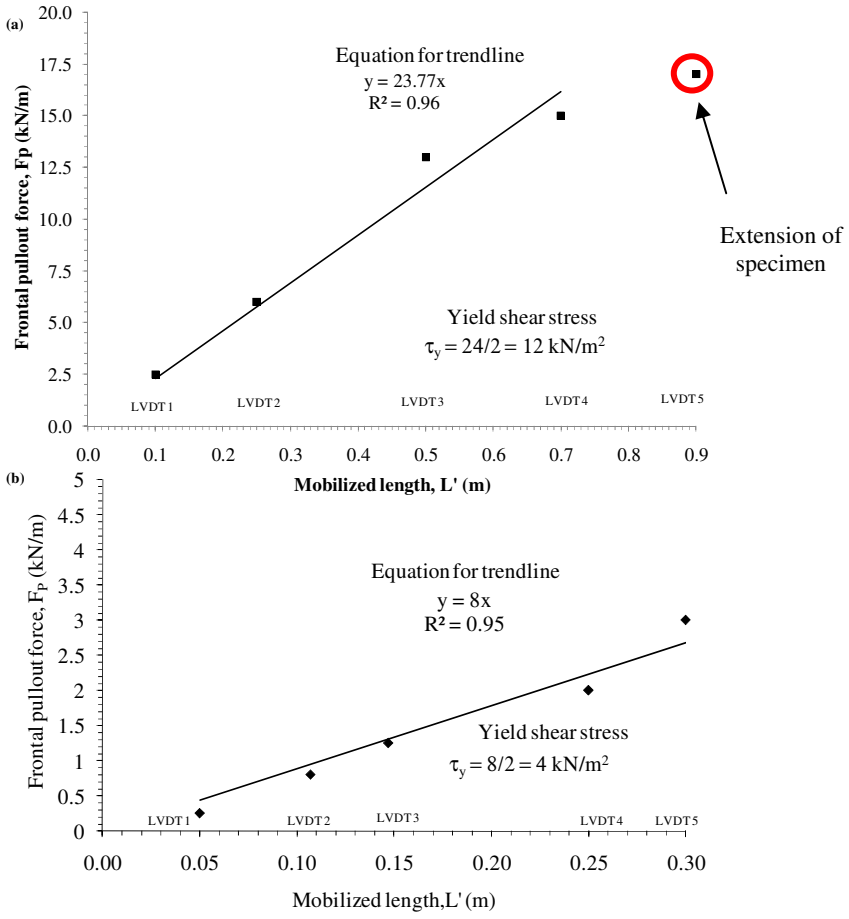

Figure 4.26 Yield shear stress for (a) test I-3, (b) test I-4

The value of yield shear stress obtained from each test was used to calculate the confined force values for each LVDT location as shown in Figure 4.27 The results were used to compute the K_{SGI} value for test I-3 and test I-4.The results of confined force and displacement at LVDT location 2 for the four tests are as shown in Figure 4.28.

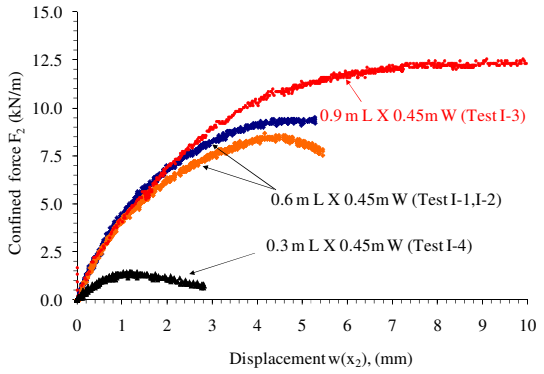

Figure 4.27 Confined force vs. displacement for test I-1, I-2, I-3 and I-4 at point x_2

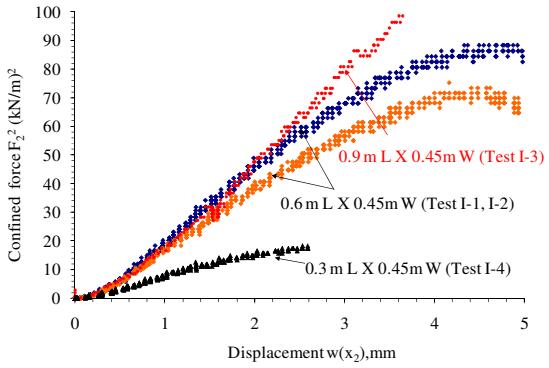

Figure 4.28 Comparison of K_{SGI} value obtained for test I-1, I-2, I-3 and I-4

The values of confined stiffness, J_c and constant K_{SGI} based on analysis of data obtained for the tests are shown in Table 4.8. Based on the results, it can be concluded that the change in the length of specimen does not affect the confined stiffness of the geosynthetic significantly (I-1, I-2, I-3 and I-4). Furthermore as the specimen length decreases, the yield shear stress decreases thereby reducing the corresponding value of K_{SGI}.

Table 4.8 Effect of specimen length on K_{SGI}

Test	Specimen dim.		Pullout parameters		Model parameters		Constant	
	L	W	F_{max}	τ_{max}	J_c	τ_y	K_{SGI}	$M_{SGI,1mm}$
	m	m	kN/m	kN/m^2	kN/m	kN/m^2	(kN/m)^2/m	kN/m^2
I-1	0.60	0.45	14.5	12.1	590	10.5	24780	4978
I-2	0.60	0.45	12.1	10.1	570	10.3	23484	4846
I-3	0.90	0.45	16.9	9.4	575	12.0	27600	5254
I-4	0.30	0.45	7.4	12.3	585	4.0	9360	3059

4.4.1.4 Effect of specimen width

The effect of specimen width on model parameters was evaluated by conducting a reduced width test on the geotextile. The test I-5 was setup under similar conditions as Test I-4 but with a specimen width of 0.28m instead of 0.45m. The new locations of LVDT's for specimen dimension of 0.3m length and 0.28 m width are as shown in Figure 4.29. The specimen was confined in Monterey No. 30 sand and normal pressure of 21 kPa was applied at the top of soil-geosynthetic interface. The rate of testing was 1mm/minute.

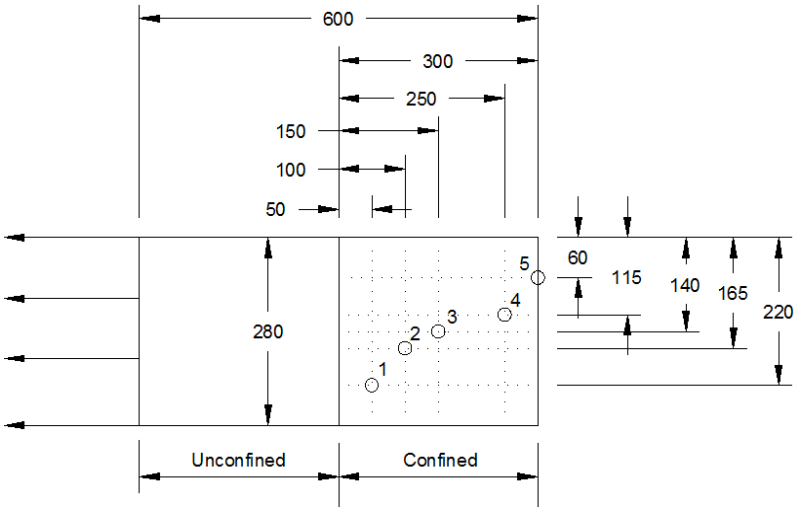

Figure 4.29 LVDT locations for test I-5 with confined length of 0.3m and width of 0.28m (All dimension in millimeters)

The comparison of results obtained for frontal pullout force from LVDT 1 for test I-4 and I-5 is shown in Figure 4.30. The maximum pullout force magnitude obtained in test I-5 had a value of 8.7 kN/m which was greater than value of 7.4 kN/m obtained for Test I-4. Thus, reducing the width of the geosynthetic specimen for similar test conditions in a pullout box lead to its stiffer response in term of pullout resistance.

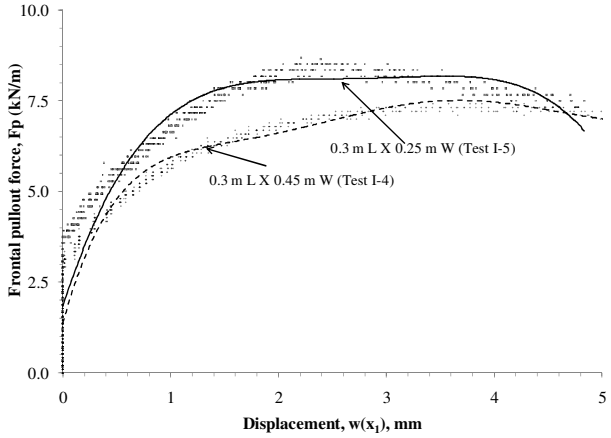

Figure 4.30 Comparison of frontal pullout force vs. displacement response for test I-4 and I-5

Similar observations were made by theoretical and experimental studies carried out by Hayashi et al. (1996) and Ghionna et al. (2001). They showed that for geosynthetic specimens having a width smaller than the pullout box, a three-dimensional soil dilatancy effect develops. The non-dilating zones in the soil surrounding narrower geosynthetic specimen (i.e., zone a in Figure 4.31a) behaves as a restraint against soil dilatancy in the dilating zone (i.e., zone b). This leads to generation of additional shear stresses at the border between the two zones thereby increasing the effective normal stress on the soil–geosynthetic interface and, consequently, an increase of pullout resistance. When a wider specimen is used, the soil dilatancy effect from the edges is reduced as shown in Figure 4.31b because the soil area that blocks the dilatancy decreases. Therefore, it is recommended to use the geosynthetic specimen with width comparable to that of the pullout box used for testing it.

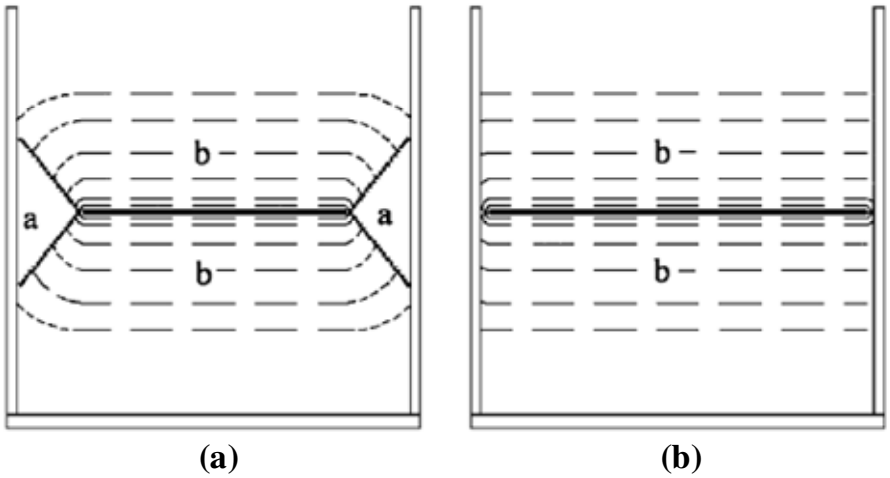

Figure 4.31 Dilation mechanisms for narrow and wide specimens in pullout test (adapted from Ghionna et al., 2001)

The yield shear stress based on the test data was calculated as shown in Figure 4.32. The value of yield shear stress in this case was 15.3 kN/m^2 which was greater than 4 kN/m^2 obtained in Test 4 and 10.5 kN/m^2 obtained in the baseline test I-1. The results confirm the above hypothesis of the influence of soil dilatancy leading to increase in the yield shear stress value when the specimen width is smaller than the box dimensions.

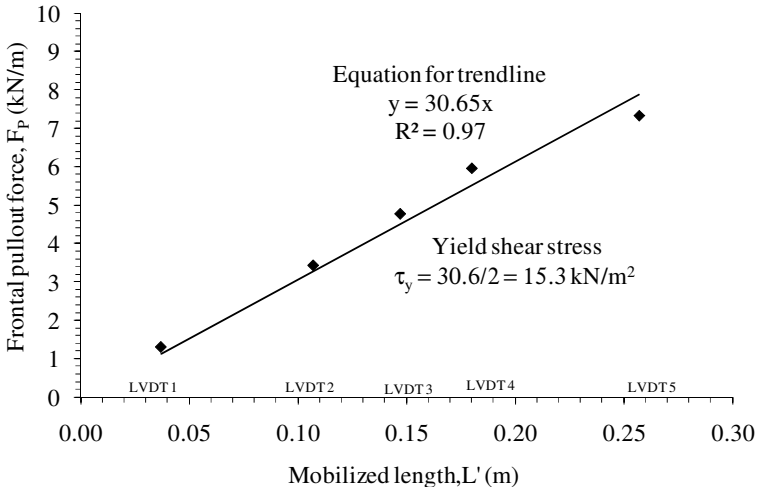

Figure 4.32 Yield shear stress calculation for test I-5

The value of τ_y was used to compute the confined force at all the LVDT locations. The comparison of K_{SGI} value for tests I-4 and test I-5 is as shown in Figure 4.33. It can be observed that the response of the geosynthetic is stiffer in test I-5 when compared to that of test I-4.

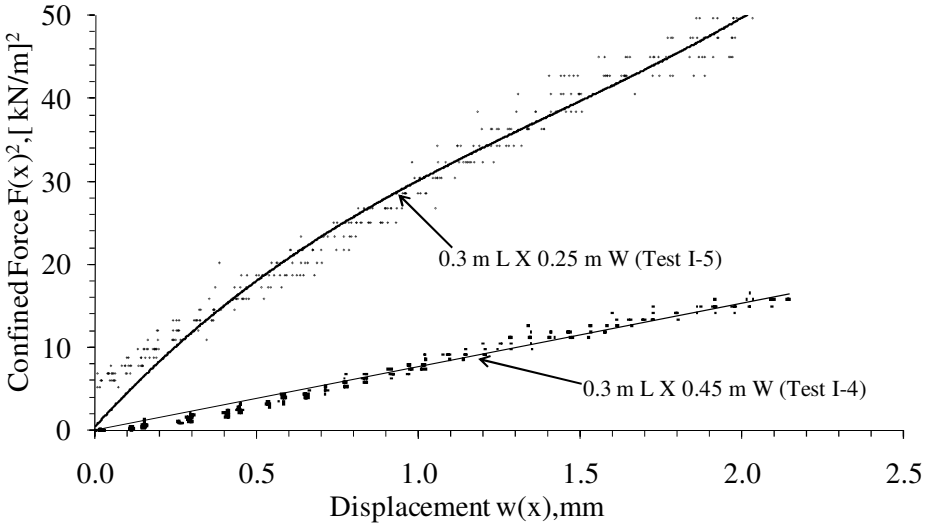

Figure 4.33 Comparison of K_{SGI} values for test I-4 and test I-5

The above plot was used to compute the values of J_c and K_{SGI} for test I-5. The comparison of test results for test I-4 and test I-5 is shown in Table 4.9. It can be seen that reducing the width of the specimen led to increase in the value of yield shear stress and K_{SGI} significantly (> 250%).

Table 4.9 Effect of specimen width on K_{SGI}

Test	**Specimen dim.**		**Pullout parameters**		**Model parameters**		**Constant**	
	L	**W**	F_{max}	τ_{max}	J_c	τ_y	K_{SGI}	$M_{SGI,1mm}$
	m	**m**	**kN/m**	**kN/m²**	**kN/m**	**kN/m²**	**(kN/m)²/m**	**kN/m²**
I-4	0.30	0.45	7.4	12.3	585	4.0	9360	3059
I-5	0.30	0.25	8.7	14.5	550	15.0	33000	5745
% Increase		**-44**	**18**	**18**	**-6**	**275**	**250**	**88**

4.4.1.5 Effect of normal pressure

Test I-1 was established as the baseline test and conducted at normal pressure of 21 kPa. To evaluate the effect of normal pressure same test setup and specimen dimensions as used in test I-1 were adopted. The normal pressure on the top of the specimen was changed from 21 kPa in test I-1 to 7 kPa in test I-6 and 35 kPa in test I-7. The frontal pullout forces vs. displacement curve for each test were obtained as shown in Figure 4.34. The maximum pullout force obtained in test I-6 was 11 kN/m and for test I-7 was 22 kN/m indicating the increase in normal pressure on the soil-geosynthetic interface led to increase in the maximum pullout resistance of the system.

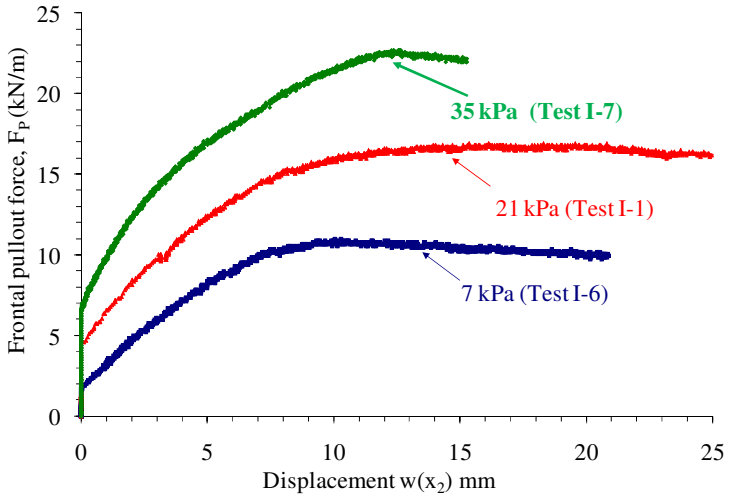

Figure 4.34 Frontal pullout force vs. displacement for test I-1, I-6 and I-7 for LVDT 2

The yield shear stress based on the test data was calculated for both the tests as shown in Figure 4.35. The value of yield shear stress for tests I-6 and I-7 was 4.5 kN/m^2 and 14.5 kN/m^2 respectively. These were then used to compute J_c and K_{SGI} values. The confined force and displacement plots for all three tests for LVDT 1 and LVDT 2 are as shown in Figure 4.36. These were used to compute the K_{SGI} value for each test. The comparison of K_{SGI} value obtained from LVDT 2 for all the three tests is as shown in Figure 4.37.

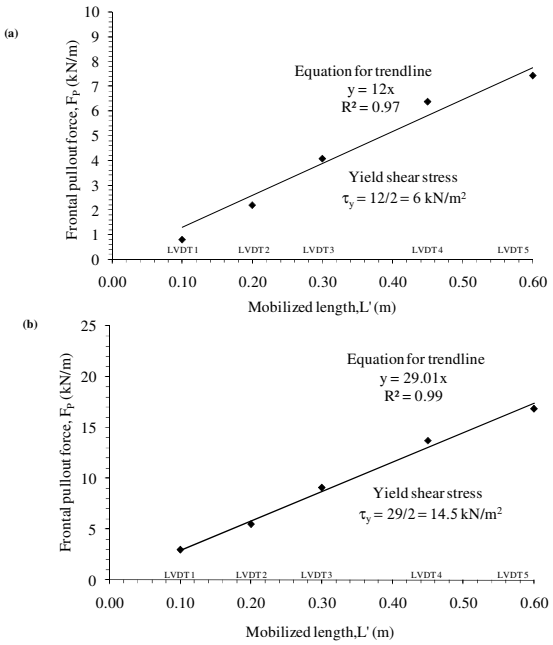

Figure 4.35 Yield shear stress for (a) Test I-6 at 7 kPa (b) Test I-7 at 35 kPa normal pressure

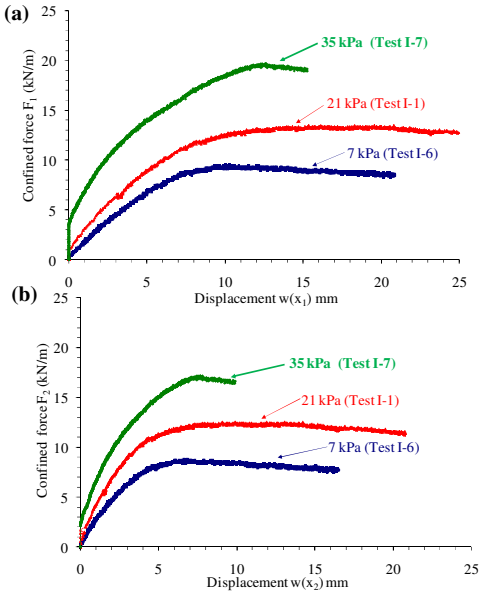

Figure 4.36 Confined force vs. displacement for Test I-1, I-6 and I-7 (a) LVDT 1 (b) LVDT 2

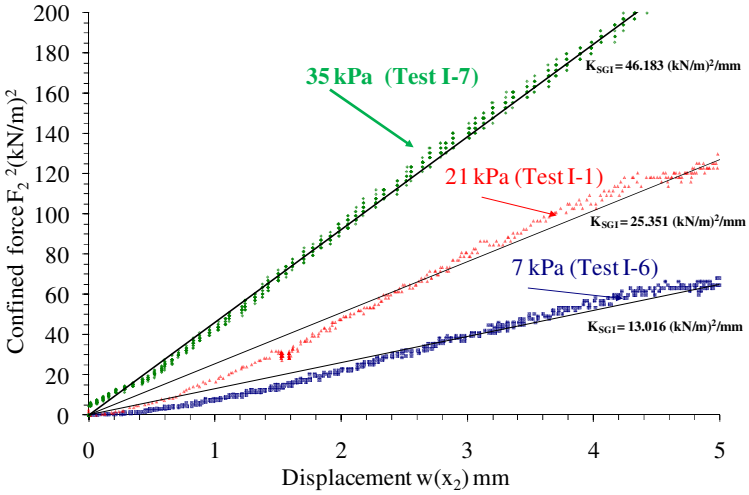

Figure 4.37 Comparison of K_{SGI} for test I-1, I-6 and I-7 to quantify effect of normal pressure

The above plot for LVDT 2 was used to compute the K_{SGI} and J_c. value for test I-6 and I-7. The comparison for average value of parameters based on all the LVDT's for three tests conducted at normal pressure of 7, 21 and 35 kPa are as shown in Table 4.10. The results indicated that increasing the normal pressure led to increase in the stiffness response of the soil-geosynthetic system. The higher the normal pressure applied to the specimen during the test, the higher was the value of both τ_y and J_c for that test. . Also, it was observed that value of τ_y was less than the value of τ_{max} calculated based on the maximum pullout force. Finally, based on the test results it was concluded that the increase in the normal pressure led to increase in the K_{SGI} value of the system.

Table 4.10 Effect of normal pressure on K_{SGI}

Test	**Specimen dim.**		**Normal pressure**	**Pullout parameters**		**Model parameters**		**Constant**	
	L	**W**	**NP**	**F_{max}**	**τ_{max}**	**J_c**	**τ_y**	**K_{SGI}**	**$M_{SGI,1mm}$**
	m	**m**	**kPa**	**kN/m**	**kN/m²**	**kN/m**	**kN/m²**	**(kN/m)²/m**	**kN/m²**
I-6	0.60	0.45	7	11.0	9.2	500	6.0	12000	3464
I-1	0.60	0.45	21	14.5	12.1	590	10.5	24780	4978
I-7	0.60	0.45	35	22.0	18.3	773	14.5	44834	6696

4.4.1.6 Effect of orientation

The geosynthetic has two principal directions i.e., longitudinal or machine and transverse or cross-machine direction. The testing direction of a geosynthetic in the pullout test is one in which force is applied, similar to conducting a tensile test on it. Therefore one pullout test was run to evaluate the interaction properties of change in orientation by pulling the specimen in the longitudinal (or machine) direction.

The test results were used to characterize and compare the properties of geosynthetic G3 with the baseline test I-1. The effect of change in specimen direction was quantified by conducting a test similar to the baseline test, but reversing the principal directions of the specimen. The specimen was prepared for confined length of 0.6m and width of 0.45m and then subjected to a normal pressure of 21 kPa. The frontal pullout force values corresponding to displacements for the five LVDT locations were obtained. The comparison for the frontal pullout force values obtained from LVDT 2 for test I-1 and test I-8 are shown in Figure 4.38a. The maximum pullout force value obtained in test I-8 was 18 kN/m as compared to value of 14.5 kN/m obtained for test I-1. Furthermore, the yield shear stress value was obtained for this tests based on LVDT movement was 16 kN/m as shown in Figure 4.38b. Finally, using the yield shear stress value, the K_{SGI} value for the test was computed as shown in Figure 4.38c.

The average values of parameters obtained for both the tests are shown in Table 4.11. The value of K_{SGI} was lower in test 8 than that obtained in Test I-1 as the area of stronger longitudinal ribs was reduced when specimen was tested in machine direction.

Table 4.11 Effect of specimen direction on K_{SGI}

Test	Specimen dim.		Pullout parameters		Model parameters		Constant	
	L	W	F_{max}	τ_{max}	J_c	τ_y	K_{SGI}	$M_{SGI,1mm}$
	m	m	kN/m	kN/m^2	kN/m	kN/m^2	(kN/m)^2/m	kN/m^2
I-1	0.60	0.45	14.5	12.1	590	10.5	24780	4978
I-8	0.60	0.45	18.5	15.4	220	16.0	14500	3808

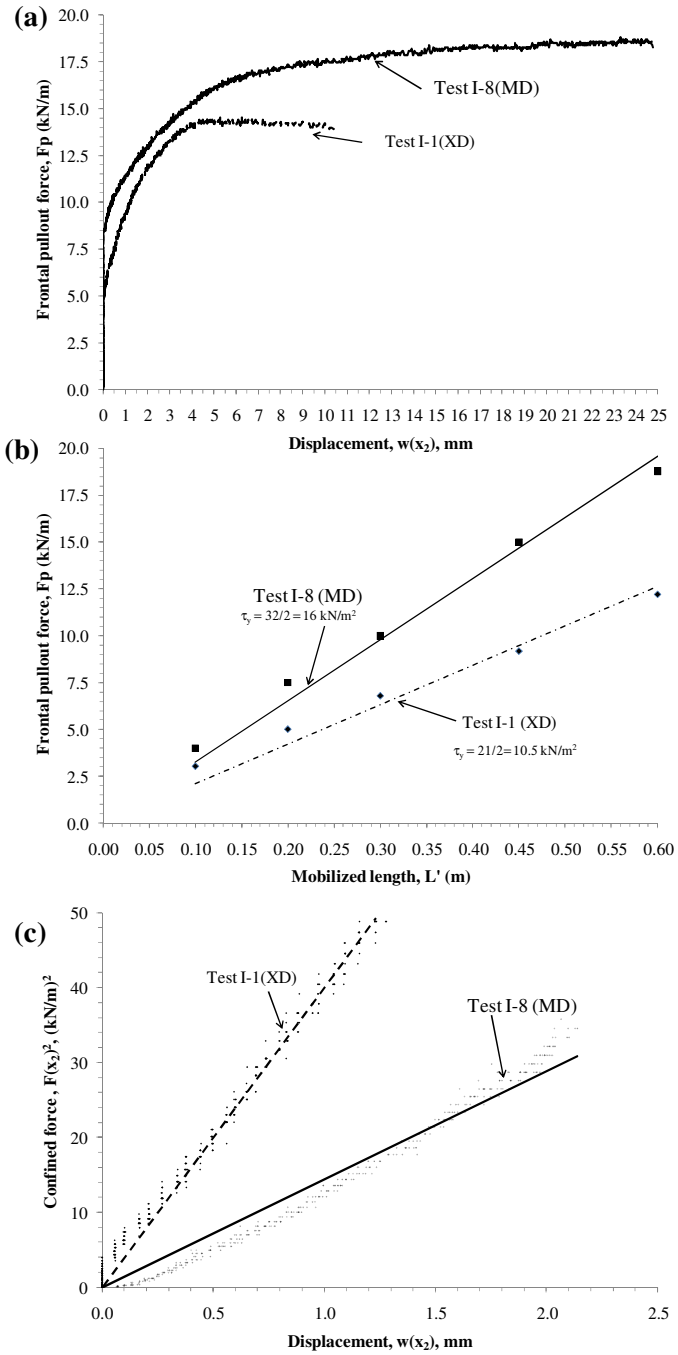

Figure 4.38 Comparison of tests (I-1 and I-8) conducted to evaluate effect of specimen direction on parameters: (a) Maximum pullout force (b) Yield shear stress (c) K_{SGI}

4.4.1.7 Discussion

The test conducted under series-I helped to calibrate the proposed model using the new pullout equipment. A standardized procedure was established for conducting the pullout test for geosynthetics and the data obtained from these tests was interpreted to obtain model parameters τ_y and J_c. The value of soil-geosynthetic interaction coefficient (K_{SGI}) was calculated for each test and it was shown that the proposed constant was able to quantify the low displacement interaction behavior of the geosynthetics.

The tests were conducted to establish the repeatability of data obtained from the equipment. Based on the test results, it was found that the model parameters were less sensitive to geosynthetic specimen and soil used as compared to maximum pullout force. They could be obtained in consistent manner for a given soil-geosynthetic system subjected to normal pressure in the pullout box equipment. Furthermore, bounds on value of K_{SGI} were calculated. For values to be in 95% interval, the upper and lower bounds were in the range of ±1000 $(kN/m)^2/m$ interval of the mean value.

The tests were conducted to quantify the effect of specimen dimensions on the model parameters. It was found that the increasing the length of the specimen from that used in the baseline test led to extensibility of the geosynthetic when high pullout force (close to maximum force) were mobilized during the tests. On the other hand reducing the length of the specimen led to significant drop in yield shear stress value as the specimen was mobilized fully at low magnitudes of frontal pullout force. Also, the effect of specimen width on the pullout results was evaluated. It was found that reducing the width of specimen in a comparison to the box dimensions led to development of dilatancy at the soil-geosynthetic interface. This led to increase in the pullout resistance of the specimen. The yield shear stress of the soil-geosynthetic system also increased whereas the confined stiffness of the geosynthetic did not change significantly with change in specimen width.

Both the model parameters had different response to change in specimen dimensions i.e. length and width. Where the yield shear stress was sensitive to change in the specimen dimension, the confined stiffness value was found independent of these changes. However, change in either of them led to change in the value of K_{SGI} for the given soil-geosynthetic system. Therefore, to provide a common basis for comparison of performance, the dimension adopted for baseline test were used for pullout tests conducted on different geosynthetics in later part of the study.

The effect of change in normal pressure on the response of soil-geosynthetic system was evaluated by conducting two tests. The normal pressure was changed by ±14 kPa from that used in the baseline test. It was found that increase in the normal pressure led to increase in the maximum pullout resistance of the system. Both the model parameters also had higher value for higher pressure used in the test. Thus, K_{SGI} value was found to be a function of normal pressure for the soil-geosynthetic system.

The effect of orientation of specimen was evaluated by conducting the test similar to the baseline test but reversing the principal specimen direction. It was found that the ribs perpendicular to the pullout force direction had significant effect on the interaction properties of the geosynthetic. The value of model parameters for the same normal pressure was different in both the tests. For pavement application, loading conditions are multi-dimensional in nature. The tires travel direction is parallel to the machine direction of the geosynthetic when a vehicle is driven over a roadway. This leads to localized shear forces in the cross-machine ribs of the geosynthetic causing mobilization of lateral restraint mechanism in the system. The cross-machine direction response is considered critical for geosynthetic reinforced pavement application. However, tests were done in both machine and cross-machine direction for geosynthetics tested in the study as it was found that the combined response and interaction between junctions of geogrids would govern the final performance of the reinforced pavement system. The results of tests conducted on geogrids are discussed in 4.4.2.

4.4.2 Series II: Comparison between two geogrids of same material

4.4.2.1 Materials used

The two geogrid products used in this test series (Tensar BX-1100 (G1) and Tensar BX-1200 (G4), Figure 4.39) were obtained from Tensar Earth Technologies. Geogrid G1 was used in the preliminary series of the testing program as described in Chapter 3. It was decided to compare its performance with another geogrid product which had similar physical properties but was reportedly used for conditions that require better performance. Therefore, geogrid G4 was obtained from the same manufacturer to evaluate the properties of both geosynthetics under pullout conditions to validate the proposed model. These geogrids are marketed for the pavement reinforcement purposes, with geogrid G4 being considered superior in performance to G1. Evaluation of the K_{SGI} value for these a product reportedly of better performance (G4) was expected to lead to a higher value of K_{SGI}.

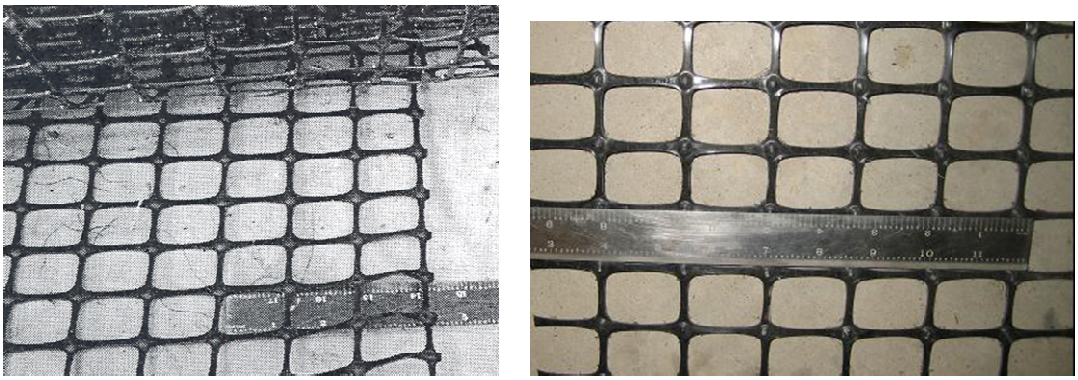

Figure 4.39 Geogrids: (a) Tensar BX-1100 (G1); (b) Tensar BX 1200 (G4) (adapted from Finnefrock, 2008)

The two geogrids have similar physical properties. Both these geogrids are integrally formed, punched-and-drawn polypropylene (PP) grids featuring raised protrusions at each rib intersections to provide a structural abutment when placed between soil layers. They have similar physical dimensions i.e., aperture size and rib

shape. The major difference between the two geogrids is the unconfined tensile strength, with the BX-1200 having a higher tensile strength in both machine and cross-machine directions than BX-1100. The index values of both the products as reported by Tensar (2002) are listed in Table 4.12.

Table 4.12 Properties of geogrids G1 and G4 (Tensar, 2002)

Property	**Test Method**	**Units**	**G1**	**G4**
Rib Shape	Observation	N/A	Rectangular	Rectangular
Rib Thickness	Calipers	mm	0.76	1.27
Nominal Aperture Size	I.D. Calipers	mm	25	33
Junction Efficiency	GRI-GG2-87	%	93	93
Flexural Rigidity	ASTM D1388-96	mg-cm	250,000	750,000
Aperture Stability Modulus at 20 cm-kg (2.0 m-N)	Kinney (2001)	m-N/deg	0.32	0.65
Minimum True Initial Modulus	ASTM D6637-01			
- MD		kN/m	250	410
- XD		kN/m	400	620
Tensile strength at 5% strain				
- MD		kN/m	7	13
- XD		kN/m	11	19

4.4.2.2 Scope of testing program

A total of eight tests were conducted in this series of pullout testing as shown in Table 4.1. Each test was setup similar to the test I-1 in terms of specimen dimensions i.e., 0.6 m confined length and 0.45 m width, LVDT locations i.e., 100 mm, 200 mm, 300 mm, 450 mm and 600 mm from the front end of the specimen and soil used i.e., Monterey No.30 sand. Each geosynthetic was tested in the cross-machine direction at three normal pressures of 7 kPa, 21 kPa and 35 kPa and in machine direction at normal pressure of 21 kPa. The comparison of results obtained for both the geogrids at each applied normal pressure magnitude are discussed in Section 4.4.2.3.

4.4.2.3 Pullout Test results

The tests II-1, II-2 and II-3 were done on geogrid G1 and II-4, II-5 and II-6 were done on geogrid G4 in cross-machine direction at normal pressure of 7, 21 and 35 kPa on the top of the specimen as listed in Table 4.1. The frontal pullout forces vs. displacement curve for each test are as shown in Figure 4.40. Based on the results, it was observed that at each normal pressure level the value of maximum pullout force obtained for geogrid G4 was greater than that for geogrid G1.

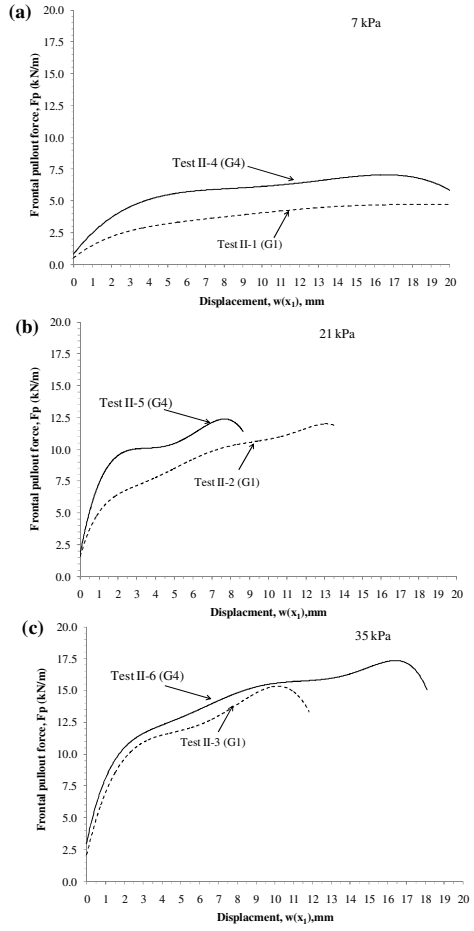

Figure 4.40 Frontal pullout force vs. displacement for G1 and G4: (a) 7kPa; (b) 21kPa; (c) 35 kPa

The model parameters τ_y and J_c were calculated based on these tests. The comparison of yield shear stress value obtained at given normal pressure for both the geogrids is shown in Figure 4.41. It was observed that the geogrid G4 had higher yield shear stress than G1 at each normal pressure. This is primarily attributed to the higher thickness of ribs in G4 than G1. This led to better shear stress development at its surface during the pullout test when compared with geogrid G1.

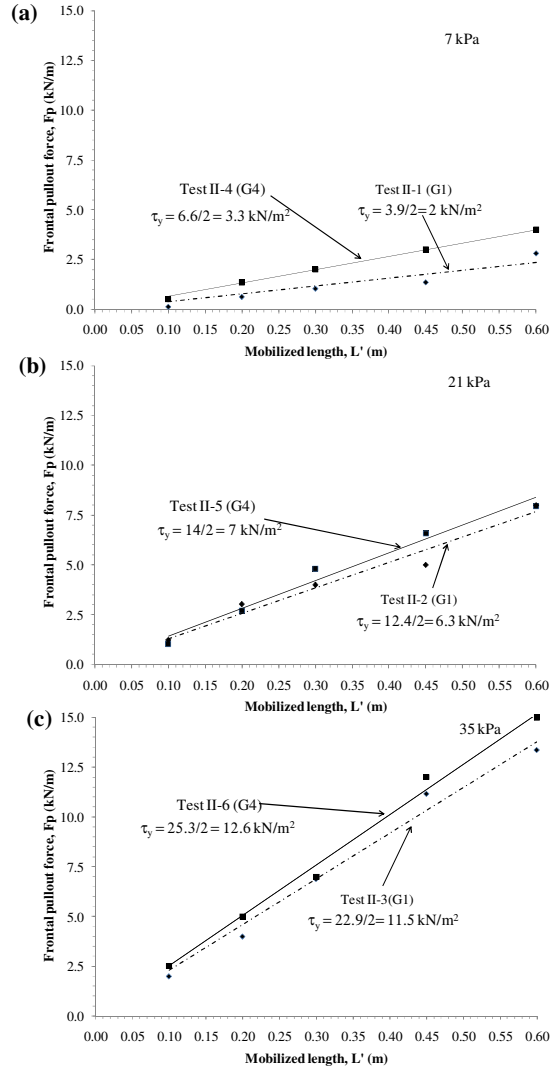

Figure 4.41 Yield shear stress for G1 and G4: (a) 7kPa; (b) 21kPa; (c) 35 kPa

The test results were used to compute the K_{SGI} value for each test by plotting the square of confined force value with displacement at LVDT 2. The comparison of K_{SGI} value for each normal pressure level for two geogrids is shown in Figure 4.42. It was observed that G4 had higher K_{SGI} value at each normal pressure level than G1. The difference in performance was greatest at low confining pressure, but the differences were less significant for higher normal pressure. For reinforced pavement, the performance under low normal stresses is the most important, so G4 was consider better suited than G1 for pavement reinforcement.

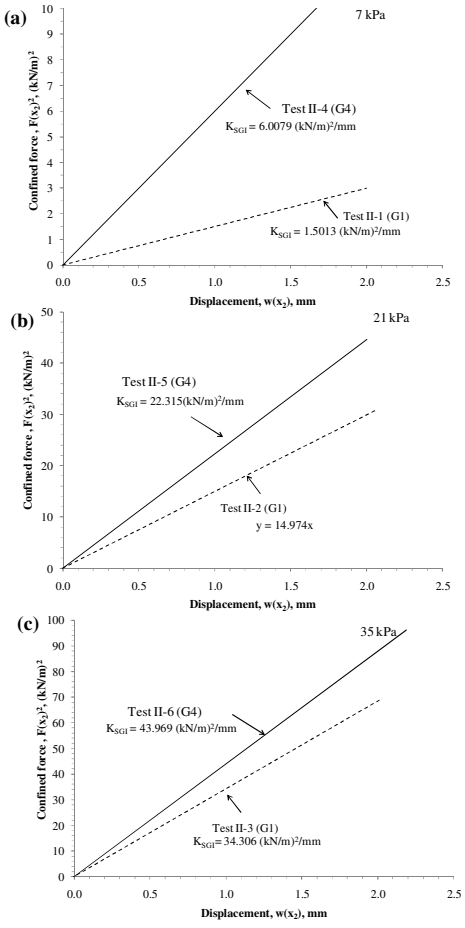

Figure 4.42 K_{SGI} for G1 and G4: (a) 7kPa; (b) 21kPa; (c) 35 kPa

The values of J_c were back calculated for all the tests as shown in Table 4.13. Based on the results it was observed that an increase in normal pressure leads to increasing values of J_c for both the geogrids. Furthermore, for each normal pressure, G4 showed higher J_c value than G1 indicating better performance under confined conditions. This trend was similar to that observed for unconfined tensile strength of these geogrids, where G4 had higher strength than G1 in the cross-machine direction.

Table 4.13 Effect of geogrid type on K_{SGI}

Test	Abbreviation	Specimen dim.		Normal pressure	Pullout parameters		Model parameters		Constant	
		L	W	NP	F_{max}	τ_{max}	J_c	τ_y	K_{SGI}	$M_{SGI,1mm}$
		m	m	kPa	kN/m	kN/m^2	kN/m	kN/m^2	$(kN/m)^2/m$	kN/m^2
II-1	G1-XD-7	0.60	0.45	7	5.0	4.2	188	2.0	1501	1225
II-2	G1-XD-21	0.60	0.45	21	12.2	10.2	594	6.3	14974	3870
II-3	G1-XD-35	0.60	0.45	35	15.5	12.9	745	11.5	34306	5857
II-4	G4-XD-7	0.60	0.45	7	7.5	6.3	500	3.0	6007	2451
II-5	G4-XD-21	0.60	0.45	21	12.7	10.5	796	7.0	22315	4723
II-6	G4-XD-35	0.60	0.45	35	17.5	16	872	12.6	43969	6630

The tests II-7 and II-8 were done on geogrid G1 and G4 in machine direction at normal pressure of 21kPa on the top of the specimen as listed in Table 4.1. The frontal pullout forces vs. displacement curve for each test are as shown in Figure 4.43a. Furthermore, the yield shear stress value was computed for both the geogrids as shown in Figure 4.43b. Finally, the results obtained were used to compute the K_{SGI} value for each test as shown in Figure 4.43c. The values of J_c were then back calculated for all the tests and are as shown in Table 4.16.

Table 4.14 Effect of geogrid testing orientation on K_{SGI}

Test	Abbreviation	Specimen dim.		Normal pressure	Pullout parameters		Model parameters		Constant	
		L	W	NP	F_{max}	τ_{max}	J_c	τ_y	K_{SGI}	$M_{SGI,1mm}$
		m	m	kPa	kN/m	kN/m^2	kN/m	kN/m^2	$(kN/m)^2/m$	kN/m^2
II-7	G1-MD-21	0.60	0.45	21	11.5	9.6	660	7.6	20145	4488
II-8	G4-MD-21	0.60	0.45	21	14	10.0	690	8.5	23500	4850

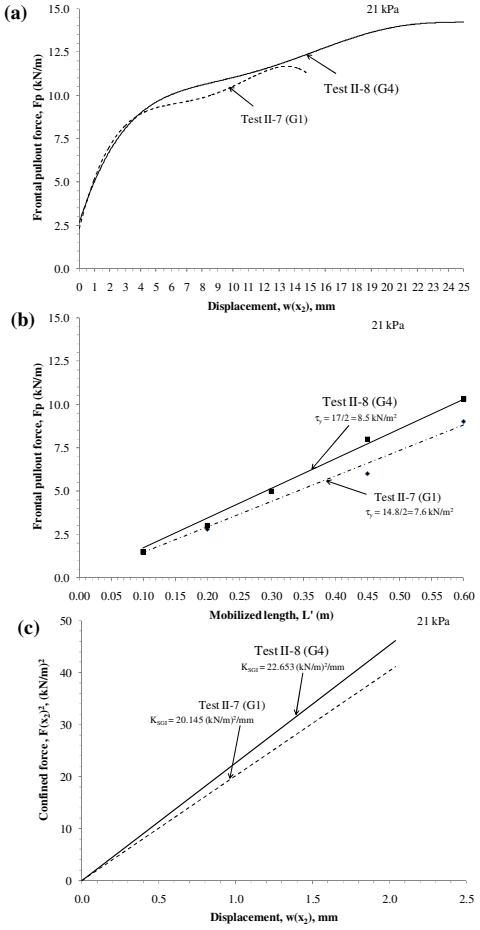

Figure 4.43 Comparison of tests conducted to evaluate effect of specimen orientation on parameters for geogrid G1 and G4: (a) Maximum pullout force (b) Yield shear stress (c) K_{SGI}

Based on the results, it was observed that the geogrid G4 had slightly higher value for K_{SGI} than geogrid G1 in the machine direction. The contrast in performance properties of both geogrids was not as significant as observed for tests in cross-machine direction. This trend was compared with physical properties of both geogrids and it was found that both geogrids had similar properties in machine direction whereas different properties in cross-machine direction, thereby establishing accuracy of the proposed method to predict confined properties of these geogrids.

4.4.2.4 Discussion

The pullout tests conducted under series-II as explained in Section 4.4.1.4 helped to compare the properties of geogrids with similar physical properties but slightly different tensile strengths. The procedure established for pullout testing of geosynthetics as explained in test series-1 was adopted. The tests helped in establishing the applicability of SGI model to predict performance of geogrids.

The pullout test results where the unconfined properties of the geogrids were known were analyzed based on this model. The order of performance predicted based on the K_{SGI} value was similar to that predicted by laboratory and field studies conducted on these geosynthetics earlier. The behavior predicted based on these tests showed good agreement with the physical characteristics of these products. Specifically, G4 consistently had higher coefficient value than G1 at the three confining pressure levels and in both directions of testing. This indicated that G4 would perform better than G1 under confined conditions for reinforced pavement application.

4.4.3 Series III: Test on geogrid made of different material

4.4.3.1 Material used

Field test sections were constructed to monitor the performance of geosynthetics as described in Chapter 5. The geosynthetics G1, G2 and G3 were used in these sections. The geogrid G2 used in initial phase of testing as described in Chapter 3 was thus evaluated in this phase of pullout tests. This helped in assessing the quantitative performance of geosynthetics predicted based on the laboratory pullout tests to qualitative performance of geosynthetics in the field study.

The geosynthetic G2 is a Mirafi BasX-11 geogrid as shown in Figure 4.4 with index properties as explained in Chapter 3. The geogrid has an aperture size of 25 mm in both machine and cross-machine direction. The manufacturer reported similar tensile strength in the machine and cross-machine direction for geogrid G2 (29 kN/m). The manufacturing process involved in this geogrid is different from geogrids used in test series-II of this research.

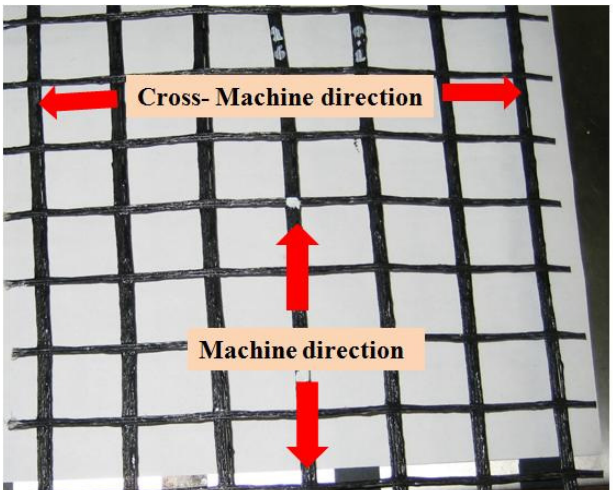

Figure 4.44 Geogrid G2 with machine and cross-machine direction

The geogrid G2 differs from geogrid G1 as it has no distinct protrusions at the junction of longitudinal and transverse ribs. The geogrid G2 has similar properties in both principal directions whereas G1 had stronger cross-machine direction than machine direction. However, the unconfined tensile strength of geogrid G2 was greater than G1 in both directions. The similar array of pullout tests was done on this geogrid as G1 and is discussed in Section 4.4.3.2.

4.4.3.2 Scope of testing program

A total of four tests were conducted in this series of pullout testing as shown in Table 4.1. Each test was setup similar to the test I-1 in terms of specimen dimensions i.e., 0.6 m confined length and 0.45 m width, LVDT locations i.e., 100 mm, 200 mm, 300 mm, 450 mm and 600 mm from the front end of the specimen and soil used i.e., Monterey No.30 sand. The geosynthetic was tested in the cross-machine direction (III-1, III-2, and III-3) at three confining pressures of 7 kPa, 21 kPa and 35 kPa and in machine direction (III-4) at confining pressure of 21 kPa. The results obtained for the geogrid at each confining pressure are discussed in Section 4.4.3.3.

4.4.3.3 Test results

The tests III-1, III-2, and III-3 were conducted in cross-machine direction at normal pressure of 7, 21 and 35 kPa on geogrid G2 as listed in Table 4.1. The frontal pullout forces vs. displacement curve for each test are as shown in Figure 4.45a. Furthermore, the yield shear stress value was computed at each normal pressure level for the geogrid as shown in Figure 4.45b. Finally, the results obtained were used to compute the K_{SGI} value for each test as shown in Figure 4.45c. The values of J_c back calculated for each test and are listed in Table 4.15. Based on the test results, it is observed that an increase in normal pressure leads to increasing value of these parameters.

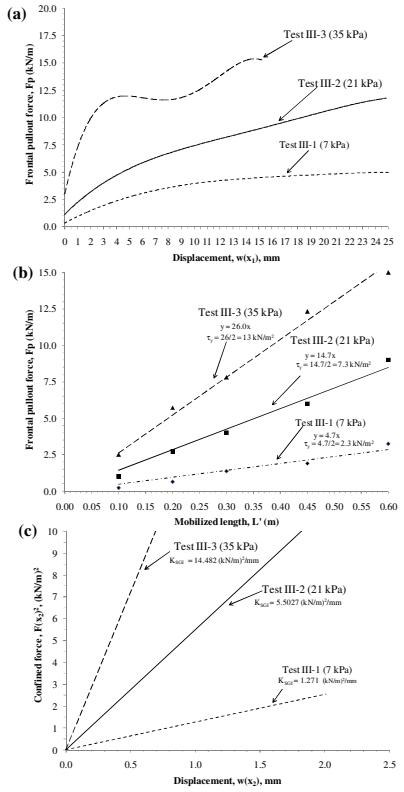

Figure 4.45 Tests conducted to evaluate effect of confining pressure on parameters for geogrid G2 in cross machine direction: (a) Maximum pullout force (b) Yield shear stress (c) K_{SGI}

Test III-4 was conducted in machine direction at normal pressure of 21 kPa using geogrid G2. The test helped to quantify the effect of change in specimen direction on model parameters. This test was conducted in similar manner as Test III-2, but by reversing the principal directions of the specimen. The frontal pullout force values corresponding to displacements for the five LVDT locations were obtained. The test results were analyzed to obtain the parameters as described in SGI model and is listed in Table 4.15.

Table 4.15 Results for geosynthetic G2 testing

Test	Abbreviation	Specimen dim.		Normal pressure	Pullout parameters		Model parameters		Constant	
		L	W	NP	F_{max}	τ_{max}	J_c	τ_y	K_{SGI}	$M_{SGI,1mm}$
		m	m	kPa	kN/m	kN/m^2	kN/m	kN/m^2	$(kN/m)^2/m$	kN/m^2
III-1	G2-XD-7	0.60	0.45	7	5.1	4.3	159	2	1271	1127
III-2	G2-XD-21	0.60	0.45	21	12.0	10.0	189	7.3	5502	2345
III-3	G2-XD-35	0.60	0.45	35	15.5	12.9	279	13	14482	3805
III-4	G2-MD-7	0.60	0.45	7	17	14	185	14.5	10751	3275

The comparison of results for tests III-2 and III-4 are shown in Figure 4.46. The frontal pullout force obtained from LVDT 2 for test III-2 and test III-4 is shown in Figure 4.46a. The geogrid (G3) shows higher pullout resistance in machine direction than cross-machine direction. The average yield shear stress value calculated based on initial displacement of five LVDT's for both tests is shown in Figure 4.46b. The specimen has twice the yield shear stress in cross-direction when compared with machine direction for same applied normal pressure. This was attributed to manufacturing of the geogrid, where the longitudinal ribs are thicker when compared to transverse ribs.

The comparison between K_{SGI} values for both the tests was conducted and is shown in Figure 4.46c. Based on the results shown in this figure, J_c values for both the tests were back calculated as shown in Table 4.15. It was observed that the specimen had similar J_c values in both the directions. This was similar to the unconfined tensile strength characteristics of this geosynthetics where it had same strength in both directions.

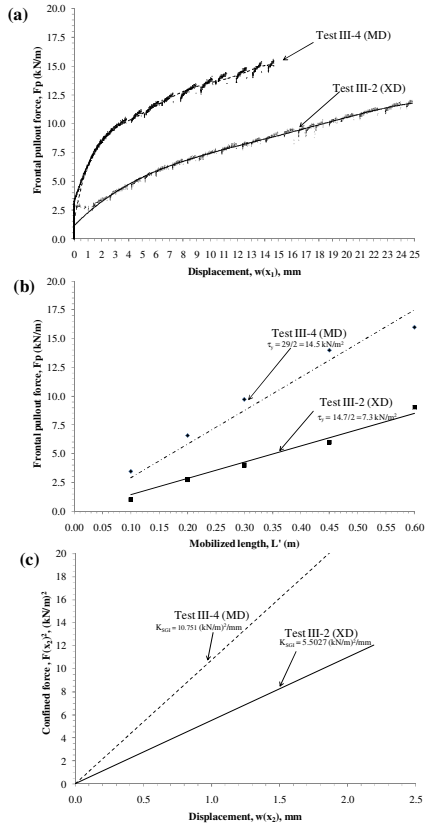

Figure 4.46 Comparison of tests conducted to evaluate effect of specimen direction on parameters for geogrid G2: (a) Maximum pullout force (b) Yield shear stress (c) K_{SGI}

4.4.3.4 Discussion

The pullout tests conducted in Series III as explained in Section 4.4.3.3 helped to obtain the confined properties for geogrid G2 which was also used in the field test sections as discussed in the Chapter 5. The data obtained from these tests was interpreted to obtain K_{SGI} value for each test. This geogrid was manufactured using a different process as compared to the geogrids G1 and G4. Therefore, it had better confined properties in machine direction as compared to cross-machine direction, which was opposite of what was observed for geosynthetics G1, G3 and G4. Finally, the results obtained were useful in comparing the performance of this geosynthetics with other geosynthetics tested in series I and II.

4.5 DISCUSSION OF RESULTS FROM PULLOUT TESTS ON GEOSYNTHETICS

The pullout tests were conducted on four geosynthetics and results were analyzed based on SGI model developed in Chapter 3. Out of these geosynthetics, G3 was a geotextile whereas G1, G2 and G4 were geogrids. Geogrids G1 and G4 were manufactured using polypropylene (PP) whereas G2 was manufactured using polyethylene (PET). Three of these geosynthetics G1, G2 and G3 were also used in the field test sections, as explained in Chapter 5. The unconfined tensile strength of all these geosynthetics was evaluated in machine and cross-machine directions.

This section describes the comparison of model parameters and K_{SGI} values for these four geosynthetics. A total of eight tests, four in each direction (machine and cross-machine) are compared, as they were conducted using the same specimen dimensions and confining soil at normal pressure of 21 kPa. In other words, two tests one in machine and cross machine direction for the four geosynthetics are discussed. Also, comparison is made between the unconfined stiffness of these geosynthetics at 5 % strain with confined stiffness parameter value calculated based on the SGI model. Finally, the applicability of the present model to reinforced pavement design is discussed.

4.5.1 Machine direction

The four tests in machine direction for geosynthetics G1, G2, G3 and G4 at 21 kPa as listed in Table 4.1 were test numbers II-7, III-4, I-8 and II-8 respectively. The comparison was made based on data obtained from pullout test for maximum pullout force, yield stress, and K_{SGI} values for these tests as shown in Figure 4.47a, 4.47b and 4.47c respectively. The value of confined stiffness J_c was back calculated from the K_{SGI} values for each of these tests. The value of these parameters for four tests is listed in Table 4.16.

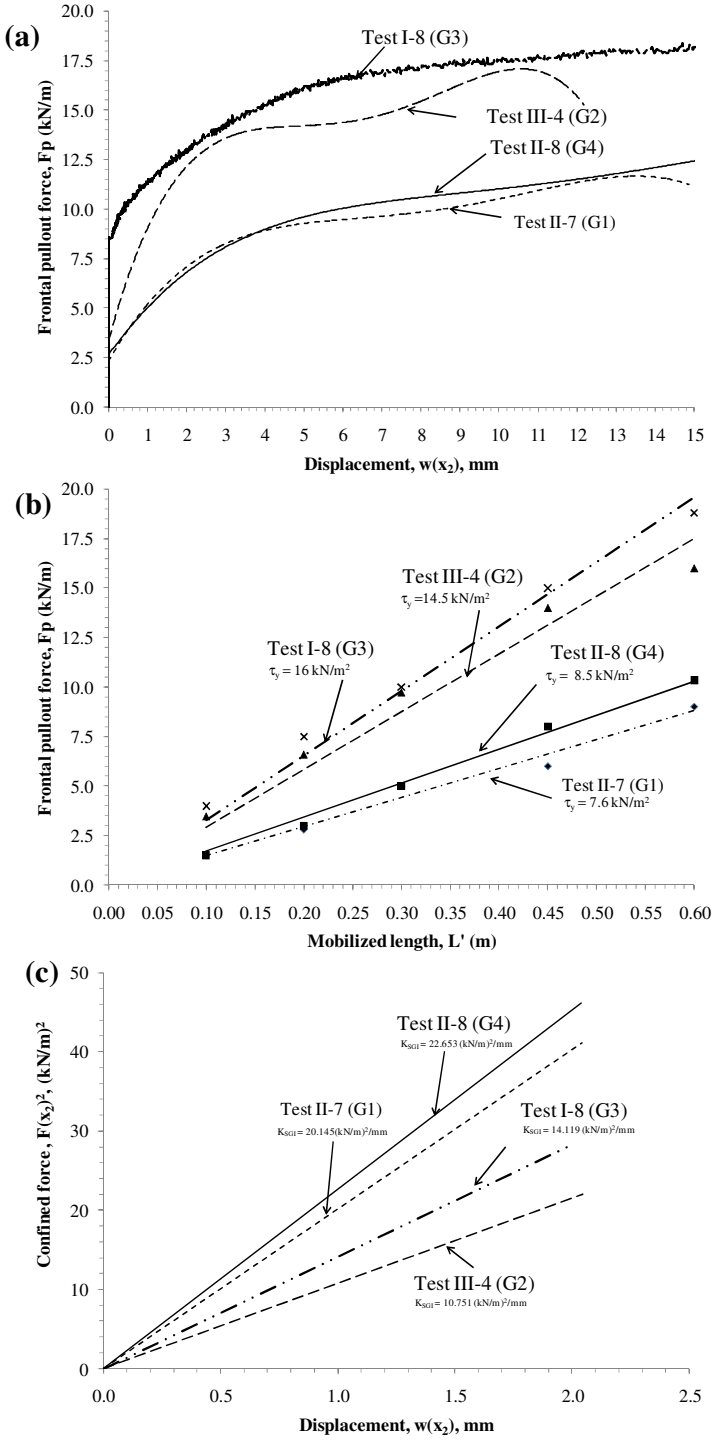

Figure 4.47 Comparison of tests conducted in machine direction for geosynthetics G1, G2, G3 and G4: (a) Maximum pullout force (b) Yield shear stress (c) K_{SGI}

Table 4.16 Comparison of K_{SGI} for geosynthetics in machine direction

Test	Abbreviation	Specimen dim.		Normal pressure	Pullout parameters		Model parameters		Constant	
		L	W	NP	F_{max}	τ_{max}	J_c	τ_y	K_{SGI}	$M_{SGI,1mm}$
		m	m	kPa	kN/m	kN/m^2	kN/m	kN/m^2	$(kN/m)^2/m$	kN/m^2
II-7	G1-MD-21	0.60	0.45	21	11.5	9.6	660	7.6	20145	4488
III-4	G2-MD-21	0.60	0.45	21	17	14	185	14.5	10751	3275
I-8	G3-MD-21	0.60	0.45	21	18.5	15.4	220	16.0	14500	3808
II-8	G4-MD-21	0.60	0.45	21	14	10.0	690	8.5	23500	4850

Based on the results it was concluded that the geosynthetic G3 had the maximum pullout resistance (see F_{max} in Table 4.10) followed by geosynthetic G2, G4 and then G1 in decreasing order. However, the focus of the present research is to characterize the interaction behavior under low displacement of soil-geosynthetic systems. Therefore, K_{SGI} values of these geosynthetics were compared and it was found that G4 had highest value of all the geosynthetics followed by G1, G3 and then G2. The difference in K_{SGI} values for these geosynthetics can be explained by examining the model parameter (τ_y and J_c) values for these geosynthetics. It was observed that products G1 and G4 (geosynthetics with same material) had higher confined stiffness J_c and lower yield shear stress τ_y when compared to G2 and G3 (geosynthetics from another manufacturer) for similar testing conditions. The geotextile G3 showed the highest value of yield shear stress when compared to other three geosynthetics (geogrids). Therefore, G3 would be product of choice if only the shear stress of the system was of concern as is the case for tensioned membrane effect in unpaved roads which is mobilized at high displacement magnitudes. The flexible (paved) pavements require that the geosynthetic be mobilized under low displacements, as lateral restraint is the governing mechanism. Thus, not only shear stress but also confined stiffness of the geosynthetics is important. Therefore, geosynthetic G4 which had the highest value of K_{SGI} was considered the best suited geosynthetic, among those tested in this study, for this application.

In summary, the proposed model allowed the dissimilar properties of these geosynthetics to be combined into a single framework and used for comparing their performance at low displacements using the K_{SGI} value.

4.5.2 Cross-Machine direction

The four tests in cross-machine direction for geosynthetics G1, G2, G3 and G4 at 21 kPa as listed in Table 4.1 were test numbers II-2, III-2, I-1 and II-5 respectively. The comparison was made based on data obtained from pullout test for maximum pullout force, yield stress, and K_{SGI} values for these tests as shown in Figure 4.48a, 4.48b and 4.48c respectively. The value of these parameters for four tests is listed in Table 4.17.

Table 4.17 Comparison of K_{SGI} for geosynthetics in cross-machine direction

Test	Abbreviation	Specimen dim.		Normal pressure	Pullout parameters		Model parameters		Constant	
		L	W	NP	F_{max}	τ_{max}	J_c	τ_y	K_{SGI}	$M_{SGI,1mm}$
		m	m	kPa	kN/m	kN/m^2	kN/m	kN/m^2	$(kN/m)^2/m$	kN/m^2
II-2	G1-XD-21	0.60	0.45	21	12.2	10.2	594	6.3	14974	3870
III-2	G2-XD-21	0.60	0.45	21	12.0	10.0	189	7.3	5502	2345
I-1	G3-XD-21	0.60	0.45	21	14.5	12.1	590	10.5	24780	4978
II-5	G4-XD-21	0.60	0.45	21	12.7	10.5	796	7.0	22315	4723

Based on the results it may be concluded that the geosynthetic G3 (geotextile) has the maximum pullout resistance and yield shear stress values in cross-machine direction as compared to the other geosynthetics (geogrid). This trend is similar to that observed in machine direction for these geosynthetics. The yield shear stress value for three geogrids was in the range of 6-7.5 kN/m^2. Therefore, their performance could be distinguished by comparing the confined stiffness directly. Based on this parameter it is observed that geogrid G4 performed better than G1 followed by G2.

When K_{SGI} values for all the four geosynthetics was compared, similar trend in performance was observed for three geogrids (G4>G1>G2) as in the machine direction. However, in cross-machine direction the geotextile G3 had the highest K_{SGI} value. This may be attributed to stronger cross-machine direction fibers than machine direction fibers for this geosynthetic. When the confined stiffness value of G3 was compared with geogrids, it had value which was lower than that obtained for G4, equal for G1 and higher for G2 in this case.

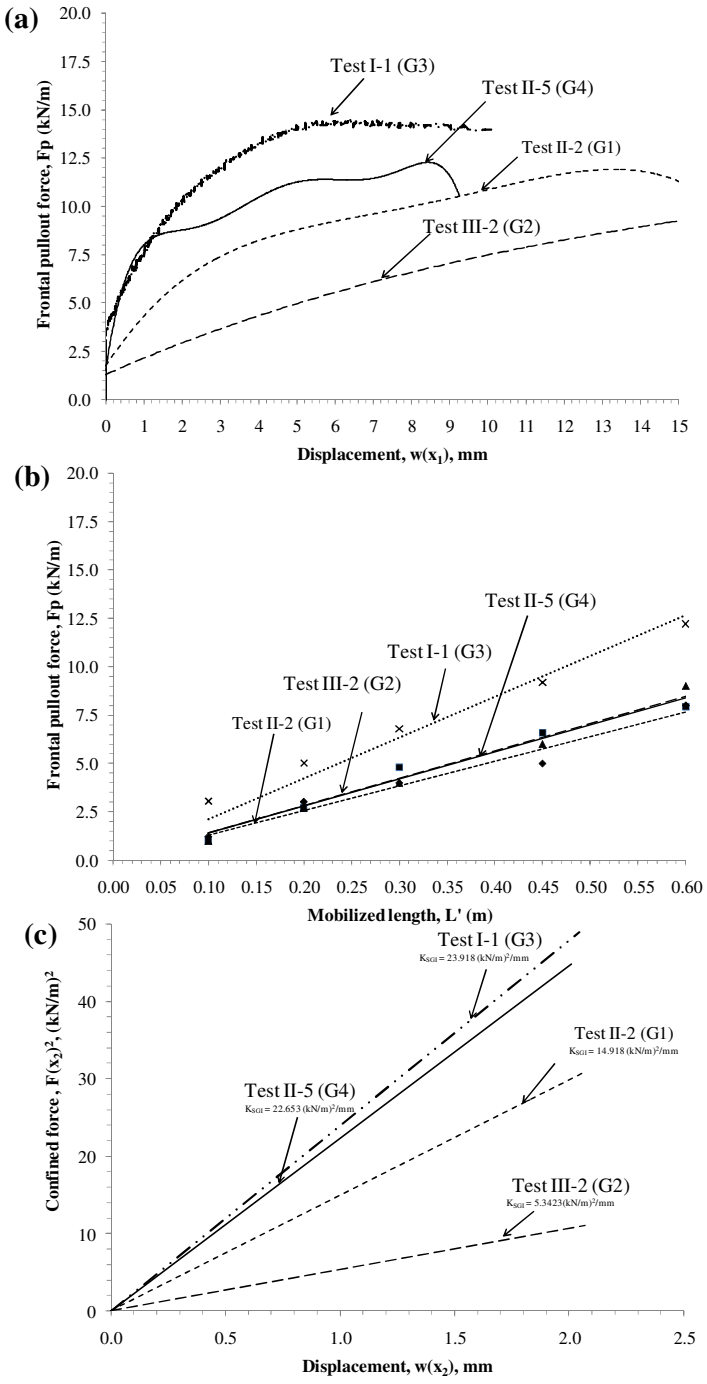

Figure 4.48 Comparison of tests conducted in cross-machine direction for geosynthetics G1, G2, G3 and G4: (a) Maximum pullout force (b) Yield shear stress (c) K_{SGI}

4.5.3 Unconfined and Confined stiffness

The unconfined tensile stiffness (J_u) was determined based on wide-width tensile tests conducted on three geosynthetics. The comparison was made between unconfined tensile stiffness obtained using wide width tensile test at 5% strain (J_u) with confined stiffness parameter (J_c) obtained using pullout test for the four geosynthetics used in this study. The difference in values of unconfined tensile stiffness with confined stiffness of these geosynthetics in machine-direction (MD) and cross-machine direction (XD) is shown in Table 4.18

Table 4.18 Comparison of unconfined and confined stiffness of geosynthetics

	Unconfined stiffness at 5% strain, (J_u)		**Confined stiffness from model, (J_c)**	
Geosynthetic	**MD kN/m**	**XD kN/m**	**MD kN/m**	**XD kN/m**
G1	194	323	660	594
G2	278	282	185	189
G3	469	487	220	590
G4	260	380	690	796

The data shown in Table 4.18 indicates higher values for J_c as compared to J_u for three geosynthetics (G1, G3 and G4). These results support the model assumption (Section 3.5.2.1) that use of geosynthetics under confined conditions leads to the increase in their stiffness. When a geosynthetic is subjected to loads under confinement, the interaction between the soil particles and the geosynthetics helps in activating additional mechanisms. Specifically, the ribs perpendicular to the loading direction get mobilized thereby sharing the applied load and leading to lesser strains in the parallel ribs for the same force magnitude under unconfined conditions (Figure 3.25).

For geotextile G3, the primary mechanism affecting its performance for flexible pavement is yield shear stress. When the performance of geogrids G1, G2 and G4 were compared in terms of model parameters they had similar yield shear stress values (Section 4.5.2). Also these geogrids had comparable unconfined tensile stiffness (±100 kN/m) in both machine and cross-machine direction (Table 4.18). However, when

confined stiffness values for these geosynthetics were compared, it was observed that G2 showed no improvement in confined stiffness whereas the geogrids G1 and G4 had higher confined stiffness values. This improved performance in geogrids G1 and G4 was attributed to the strength of the junctions at crossing of their longitudinal and transverse ribs The ability of geosynthetic to perform (interlock) under confined conditions does not depend solely on its unconfined stiffness but also on the ability of its junction to transfer load from one direction to another at low strains thereby mobilizing the entire geosynthetic under given traffic load.

4.5.4 Discussion

The SGI model provided a methodology to interpret the results of pullout tests for various geosynthetics under a single framework. Based on the comparison of results for four geosynthetics, it was concluded that geogrids G1 and G4 had similar properties in both directions under confined conditions. The geogrid G4 had slightly higher confined stiffness value than G1. When compared with geogrid G2, both geogrids G1 and G4 consistently showed better K_{SGI} value in machine and cross machine direction. However, when results were compared with geotextile G3, it had contrasting properties in both directions. In machine direction it had lower value whereas in cross- machine direction it had higher value for K_{SGI} than these geogrids.

The actual stress developed in pavement under wheel loading is biaxial in nature. Thus, it was assumed that geosynthetic which can work as a combined unit would perform better under these circumstances rather than products which had preferential direction of improved performance. Based on the analysis it was concluded that performance in descending order for the four geosynthetics would be G4 followed by G1, then G3 and finally G2. This performance order for geosynthetics was obtained for tests on Monterey No. 30 sand and thus is preliminary in nature. For actual pavement design, the geosynthetics are recommended to be tested in the project specific soil to determine the constant K_{SGI}.

4.6 CONCLUSIONS

The suitability of the SGI model proposed in Chapter 3 for the analysis of the geosynthetic reinforced pavements was evaluated by conducting pullout tests. In the initial phase, pullout test equipment was designed with capability of measuring small displacement magnitudes at low normal pressures. A series of pullout tests were carried out using a geotextile and sand as baseline materials to calibrate the equipment. The consistency in the test results was established by running tests under similar conditions. The effect of model assumptions on the calculated constant was investigated by performing a parametric study of relevant variables. These studies included effect of specimen dimensions, normal pressure, and specimen direction on the parameter magnitude.

A good agreement was obtained between the proposed model and the experimental results. The good agreement included the uniform distribution of shear stress throughout the geosynthetic specimen and unique force-displacement relation for a given system. Moreover, the boundary conditions were found to affect the results from displacement LVDT's placed close to the specimen edges. Based on the results obtained a standardized procedure was established for the future testing.

The prediction of the performance was evaluated by comparing the pullout tests results of various geosynthetics. An extensive testing program was performed in order to evaluate the K_{SGI} value for the geosynthetics in machine and cross machine direction at various confining pressures. The current state of practice involves evaluating the unconfined tensile strength of the geosynthetic and using it as a design input. It is assumed that the higher the unconfined tensile strength of the geosynthetic the better it will perform under confinement. Contrary to the current design assumption, it was shown that the geosynthetic capable of interlocking with soil and mobilizing its junctions and transverse ribs at low displacements would perform better in pullout tests (under confinement), independent of its unconfined tensile strength.

The results showed that the pullout testing is a useful tool to investigate the soil-geosynthetic interaction mechanisms for the reinforced pavements. In this particular study, pullout testing provided much needed evidence that the soil-geosynthetic interaction under low displacements can be adequately captured in the laboratory setup. However, additional testing would be required with project specific soils and measured against the field performance of geosynthetics to establish the validity of the approach proposed in this chapter.

Chapter 5: Geosynthetic Reinforced Pavements - A Field Study

"By three methods we may learn wisdom: First, by reflection, which is noblest; second, by imitation, which is easiest; and third by experience, which is the bitterest."
-Confucius-

5.1 INTRODUCTION

According to Zornberg (1994), "Field case studies involving instrumentation and monitoring of structures to evaluate their performance are vital to the practice of geotechnical engineering. This is in contrast to the most other branches of engineering in which people have greater control over the materials with which they deal. Although adequate field instrumentation is costly, examination of the performance of full-scale structures constitutes the only true confirmation that the design of reinforced soil structures is, in fact, satisfactory." This chapter discusses the evaluation of field performance of geosynthetics used in a flexible pavement with primary function of reinforcement. The aim of this field study was to correlate the field performance of test sections with the laboratory test results obtained in Chapter 4.

Geogrids and geotextiles have been used for more than 30 years as reinforcement in the base course layer of flexible pavements. Based on the review of field case histories as reported in Chapter 2, it was found that the primary aim of field studies until now has been to characterize behavior of reinforced pavements under traffic loads. The advantages are generally quantified in terms of reduction in base course thickness for same design life or extended service life for same structural composition of the pavement. However during its lifetime the pavement has to resist the stresses applied to it due to combined effect of traffic and environmental loading in the field conditions. Therefore, while setting up the field test sections in the present study, effort was made to quantify the pavement distress when subjected to environmental and traffic loading conditions. Thus the aim of this study was to obtain a realistic measure of pavement improvement by evaluating its behavior for traffic and environmental loads when geosynthetics were used to reinforce it.

5.2 TYPES OF DISTRESS IN FLEXIBLE PAVEMENTS

The field case study evaluated as part of this research was conducted with assistance from Texas Department of Transportation (TxDOT) at a Low Volume Road (LVR). Since LVR's are constructed in rural areas, they are also known as Farm to Market (FM) roads. They are characterized by thin asphalt seal-coat layer and generally carry low-volume high-intensity traffic. These roads develop distress conditions due to two main reasons which are traffic loads and environmental conditions as discussed in Chapter 2. The thin pavement structure leads to severe cracking under traffic loads. Due to their location (rural/agricultural areas of Texas), they are also subjected to environmental loads caused by extreme variations in temperature and moisture values at the pavement site. Along with above two factors the construction practices adopted also influence the distress in these pavements during their service life.

The primary goal for conducting this study was to obtain information regarding the field performance of various geosynthetics and compare it with their laboratory obtained coefficient values as discussed in previous chapter. The initial discussion in this research focused on understanding lateral restraint mechanism developed in reinforced pavements with specific application to traffic loads. Along with this benefit, as the part of the present research new application of geosynthetic reinforcement was studied for improving pavement performance when subjected to environmental loading.

The subgrade soils in Texas are generally clays of high plasticity, which experience volumetric expansion and shrinkage due to moisture fluctuation below the pavement. This leads to longitudinal cracks over thin pavement sections (FM roads) constructed over these soils. Geosynthetics were used with the purpose of mitigating the development of longitudinal cracks in these pavements. As discussed in Section 5.2.1, it is shown that the primary criteria governing the geosynthetic performance is similar to that for traffic loading i.e. its ability to develop lateral restraint and thus prevent crack propagation when subjected to bottom-up loading due to environmental factors.

5.2.1 Mechanism of longitudinal crack development

The construction of pavements over expansive clays in regions such as central Texas has often led to distress due to the development of longitudinal cracks induced by moisture fluctuations. Environmental loading such as that caused by moisture fluctuations are rarely evaluated as part of the design of pavements, where central focus is on traffic conditions. Yet, volumetric changes associated with seasonal moisture variations have led to pavement heave during wet seasons and shrinkage during dry seasons. The mechanisms leading to the development of the longitudinal cracks are eatributed to tensile stresses induced by flexion of the pavement due to settlements caused during dry seasons. Figure 5.1 illustrates the envisioned mechanism that leads to the development of longitudinal cracks (Gupta et.al 2008).

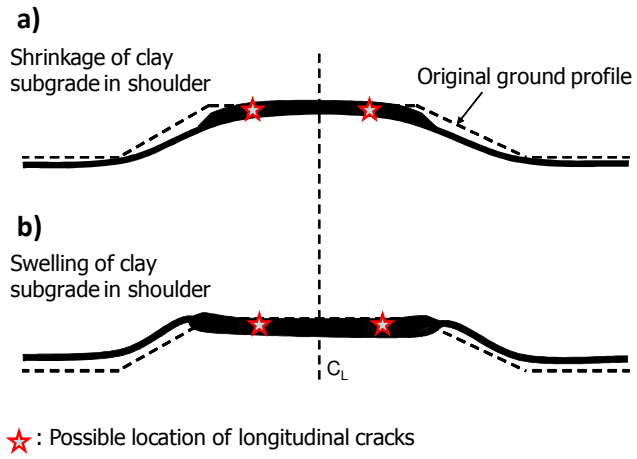

Figure 5.1 Mechanisms of pavement deflection over expansive clay subgrades: (a) settlements during dry season, (b) heave during wet season.

During the dry season, there is decrease in the moisture content of the soil in the vicinity of the pavements shoulder (Figure 5.1a). This leads to settlements in the shoulder area, but not in the vicinity of the central line of the pavement, where the moisture content remains approximately constant throughout the dry season. On the other hand, during the wet season, the moisture content in the soil in the vicinity of the shoulder

increases (Figure 5.1b). In this case, heave occurs in the vicinity of the shoulder area, but not in the vicinity of the pavement central line. As shown in Figure 5.1, the cracks are developed in the region where the moisture front advancing and retreating from the shoulders reaches its maximum penetration under the pavement.

Longitudinal cracks have been reported to occur towards the end of dry seasons, which is consistent with this envisioned mechanism. The development of a longitudinal crack on a farm-to-market road (a low traffic volume road) in central Texas is shown in Figure 5.2. This pattern of cracking is typical of volumetric changes associated with expansive clays found thorough the state of Texas.

Figure 5.2 Typical longitudinal crack developed on pavements over expansive clays

5.2.2 Remedial measures adopted

The experience within TxDOT has indicated that the cyclic movements caused due to moisture fluctuation led to considerable damage in the form of longitudinal cracks. Stabilization of the pavements over such subgrades in Texas has often been remediated using lime-treatment of the soils and more recently by reinforcing the base course layer with geosynthetics.

Lime stabilization has often been used to mitigate such longitudinal cracking in expansive soils. The addition of lime to the subgrade or base course layer helps to reduce the swelling potential of the soil and stiffening the pavement thereby improving its resistance against potential crack development. However, they are not effective in subgrades having high sulphates content, as it inhibits the reactivity of the lime thereby

reducing its impact. Furthermore, homogeneity of treatment is difficult and the lime stabilization method tends to wear out before the pavement service life is over thereby either requiring costly maintenance or resulting in severe distress in term of cracks thereby reducing the serviceability of the road.

Recently, geosynthetic reinforcement has been used in combination with lime-treatment o provide a solution for the problem of longitudinal cracking in pavements. A typical cross-section of a geosynthetic reinforced and lime stabilized pavement system as used by the TxDOT in the case of expansive clay sub grades is shown in Figure 5.3.

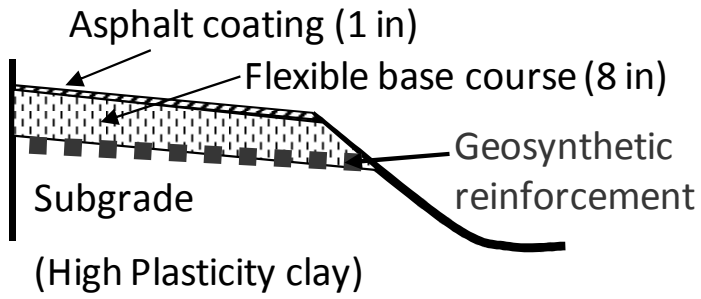

Figure 5.3 Typical pavement cross-section of a low-volume road in Central Texas using reinforcement for mitigation of cracks induced by expansive subgrades

The addition of geosynthetic helps in preventing the propagation of cracks developed in the subgrade into the base course layer thereby maintaining integrity of the pavement structure. The tensile stresses are induced in the geosynthetic when this environmental load is applied to it and its ability to laterally restraint the base course movement helps in preventing the crack propagation in the top layers. Therefore, governing criteria for geosynthetic performance under these loading conditions is similar to one required for resisting traffic loads i.e. ability to interlock with base material (develop lateral restraint). A field study was thus setup to monitor the pavement performance for both traffic and environmental loading conditions.

5.2.3 Discussion

Pavements are subjected to traffic and environmental loading during their service life. For adequate performance, the pavement should be able to resist stresses due to both these loading conditions. The distress caused under both of these loading condition influences the performance of pavement. For example, the moisture fluctuation below the pavements due to environmental loading leads to weakening of the subgrade thereby causing the longitudinal cracks. This distress affects the pavements ability to perform under traffic loads. It is difficult to isolate pavement performance under one of these loading conditions in field setting. Therefore, in the present field study the attempt was made to monitor the pavement performance and measure the distress cause under field conditions from both factors.

Cracking or distress caused due to traffic and environmental loads can be minimized in pavements by reinforcing them with geosynthetics. The primary mechanism governing the performance of geosynthetic reinforced pavements for both these loading conditions is their ability to contribute to lateral restraint. Therefore, the qualitative measurement of response obtained from field sections can be compared with quantitative measure obtained in the laboratory for measuring the confinement (in terms of lateral restraint) provided by geosynthetics in both cases.

Various remedial measures can be adopted to prevent distress due to the combined effect of traffic and environmental loads in the field. These include constructing pavement using geosynthetic-only, lime-only and combined (geosynthetic and lime) sections. However, currently the performance of these sections has neither been compared among each other nor against a control section. Therefore, in the present field study test sections were constructed (control, geosynthetic only consisting of two geogrids and a geotextile, lime only, geosynthetic and lime combined) to quantify performance of a flexible pavements. The relative performance of these test sections was compared and the best alternative was suggested.

The present research study included a survey of TxDOT projects to determine the present state of practice on use of geosynthetics as reinforcement. Based on the responses

obtained, the three case studies which were most relevant to the present research were selected for future monitoring. The case studies provided insight not only into the mechanism of longitudinal cracking but also the deficiencies in the current methods used to evaluate the performance of the geosynthetic reinforced pavements. Then based on the lessons learned from these case histories, a full scale field instrumentation and monitoring study was conducted to evaluate the performance of geosynthetic reinforced pavement having test sections which involved various combinations of lime stabilization and geosynthetic reinforcement. The performance evaluation of these test sections was done for their response under environmental and traffic loads. A qualitative analysis was then conducted for their field response and compared with the laboratory test results for geosynthetics, as discussed in the previous chapter. Overall this field study provided evidence for the effectiveness of geosynthetics in improving the pavement performance and it also provides preliminary basis for validating the laboratory method used for comparing various geosynthetics.

5.3 CASE STUDIES

A survey of TxDOT projects was conducted to determine the state of practice among various districts of Texas on use of geosynthetics as reinforcement. The survey was written in such a manner that it complemented the information on use of geosynthetics as reinforcement in flexible pavements with their use to prevent longitudinal cracking. The survey form was distributed to the district engineers associated with relevant projects. Survey responses for 35 projects were obtained from 16 TxDOT districts. The districts which responded to survey are shown in Figure 5.4. Analysis of the survey responses indicated important gaps in the current state of practice for the geosynthetic reinforced pavement design in Texas, as summarized in Table 5.1.

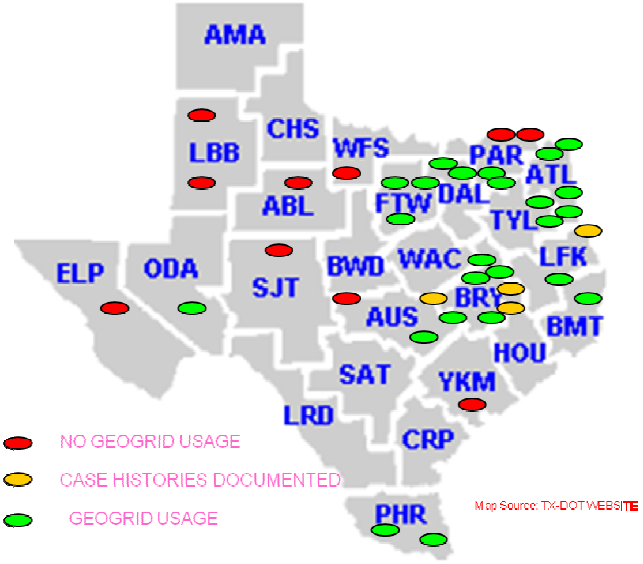

Figure 5.4 Map showing usage of geosynthetics in Texas based on districts which responded to the survey

Table 5.1 Summary of survey response of TxDOT districts

	Yes	*No*
Cracking problems were observed on pavements over high PI subgrades	88%	12%
Additional problems were observed due to the low bearing capacity	94%	6%
Geosynthetic reinforcements were used in recent projects or repairs	73.5%	26.5%

Based on the survey responses obtained, it was found that most of the subgrade soils in Texas that proved problematic consisted of high PI clays (PI > 25). Longitudinal cracking was the major source of distress for pavements constructed over such soils. The field district engineers attributed most of the cracking in pavements to the low bearing capacity of the subgrade. Geosynthetics had been effectively used to delay the onset of such cracking. Both geogrids and geotextiles had been used; though geogrid were more widely used as compared to geotextiles.

For the majority of the projects, the geosynthetics were placed in the pavement during construction and no post-construction performance evaluation was conducted making it difficult to quantify the benefits of the use of geosynthetics in pavements. The geosynthetic products used uniaxial geogrids, biaxial geogrids (from various manufacturers), woven geotextiles and glass fiber grids. The geosynthetics were also used at various locations within the pavement (i.e. at the base-subgrade interface, within the base and within the asphalt). The engineers only had specifications on conducting rib tensile strength for geogrids to be used in pavement for reinforcement purposes, but no such specification existed for geotextiles. Based on the comments received on the survey forms, it was found that there was no standard practice for designing a geosynthetic reinforced road. Therefore, it was concluded from the survey that even though there was a significant experience with usage of geosynthetics in pavements within the TxDOT, there was no clear design methodology or post-construction performance evaluation procedure which could be adopted in the field for this application.

Three sites were selected for post-construction field monitoring based on the preliminary survey conducted above, to establish their performance Zornberg et al.., (2008). The location of three sites (i.e., FM 542, FM 1774 and FM 1915) relative to Austin, Texas is shown in Figure 5.5. In the first project, immediately after construction of the geogrid reinforced pavement, the longitudinal cracks were observed even before it was open to traffic. In second project, contrastingly different performance was observed after using two different geosynthetic products selected using project-specific specifications. The third project showed consistently good performance in various sections, but the good performance was not consistent with the results of dynamic field monitoring tests. The observations from these field studies indicated discrepancies in current design methods for geosynthetic reinforced pavements.

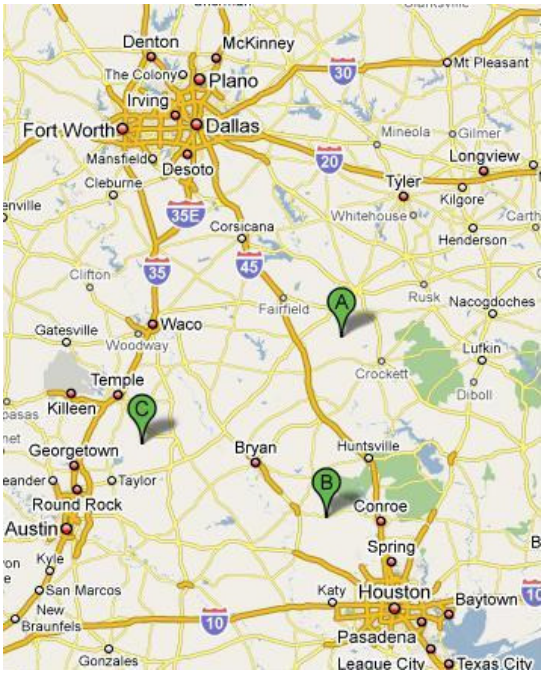

Figure 5.5 Map showing location of the three site a) FM 542 b) FM 1744 c) FM 1915

5.3.1 Case History 1

FM 542 is located in Leon county of Bryan district, Texas. In March 2005, the main section of the road was closed for reconstruction and the shoulder road was used as an alternative route for traffic. For this, the shoulder was constructed using lime stabilized subgrade, flexible base and one course of surface treatment with a layer of geogrid provided at the subgrade-base interface as shown in Figure 5.6.

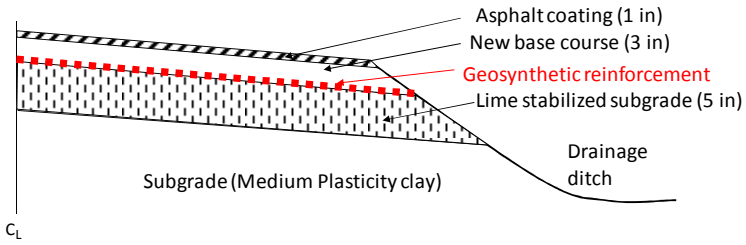

Figure 5.6 Typical cross-section of pavement at FM 542

Longitudinal cracks were observed in the pavement section even before it was open to the traffic. Accordingly a forensic investigation of the site was conducted to establish the reasons for premature failure of the road. This involved visual inspection of the site followed by trenching with a backhoe at the location of crack propagation. Longitudinal cracks, 50 mm (2 inches) wide were observed close to the junction of the recently constructed shoulder and previous main road section. The backhoe was then used to excavate the top portion and expose the cracked portion of the pavement. It was observed that there was no geogrid below the cracked portion of the pavement. Most of the cracks were observed at the junction of the unreinforced and reinforced section as shown in Figure 5.7

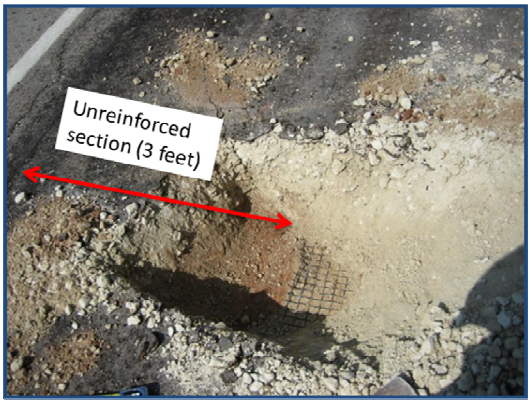

Figure 5.7 Longitudinal cracks in the unreinforced section of FM 542 pavement

The geogrid rolls supplied by the manufacturer were 3m (9.8 ft) wide but the proposed lane was 4.2 m (14 ft) wide. The contractor had placed only one roll of the geogrid below the pavement which left 1.2 m (4.2 ft) of the pavement unreinforced. While the section consisting of the geogrid reinforcement was performing adequately, the cracks developed in the unreinforced section of the pavement. This case study provides field evidence that the geogrid reinforced pavements in expansive subgrade soils are less susceptible to cracking induced due to environmental loads than the unreinforced pavements.

5.3.2 Case History 2

FM 1774 is located in Grimes county of Texas. In August 2002 as part of restoration of existing road, 9.120 miles (14.68 km) of the FM 1774 road from SH 90 to FM 2445 i.e., from station 993+34 to 1474+90 was reconstructed. During construction, the existing road was excavated and leveled in order to install 10 inches (0.25 m) of cement and lime stabilized subgrade, 7 inches (0.18 m) of flexible base and one course of surface treatment. Site investigation and soil testing indicated presence of clay of high plasticity (PI=40) from stations 1289+00 to 1474+90. To reinforce the pavement at these locations an additional layer of geogrid was provided at subgrade-base interface. Two different geogrid types available in the market were found to satisfy the project specifications. To evaluate the field performance both the geogrids were used i.e. geogrid type 1 (polypropylene) from station 1299+58 to 1315+42 and geogrid type 2 (polyester) from station 1362+94 to 1474+90. The typical section of the geogrid reinforced pavement constructed at site was as shown in Figure 5.8.

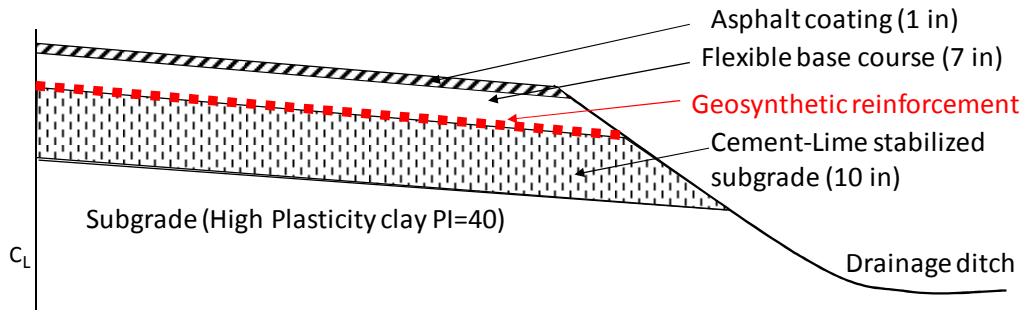

Figure 5.8 A typical geogrid reinforced pavement section at FM 1774

During the 2004 summer, longitudinal cracks were observed in section reinforced with geogrid type 2 while the sections reinforced with geogrid type 1 did perform well. After excavating the cracked road sections of the pavement reinforced with geogrid type 2, it was found that there was no longer bond between the longitudinal and transverse elements of the geogrid (at the junction of geogrids). Longitudinal cracks and slippage at

junction of geogrids in section reinforced with geogrid 2 are as shown in Figures 5.9a and 5.9b respectively. The material properties of both the grids were evaluated and compared with the project recommended specifications. These are as listed in Table 5.2.

(a) (b)

Figure 5.9 (a) Longitudinal crack on the pavement reinforced with geogrid type 2 (b) Slippage between longitudinal and transverse ribs at junction of geogrid type 2

Table 5.2 Comparison of Geogrid (type 1 and 2) properties with project specifications given by TxDOT

	Geogrid A	*Geogrid B*	*Recommended*
Aperture size, mm	35	43	25-50
% Open area	75 %	74 %	70% min.
Tensile Modulus at 2% strain, kN/m	215	385	200-300
Ultimate strength, MD, kN/m	26	44	-
CMD, kN/m	21	25	-
Junction, kN/m	22.5	11	-
Junction efficiency	93 %	35 %	70% min.

Geogrid type 2 had higher strength in machine and cross machine direction but lower strength of the junctions when compared to geogrid type 1. TxDOT specifications for geogrid products include both index properties (e.g., aperture size, % open area) and performance properties (e.g. tensile modulus, junction efficiency, ultimate strength in machine and cross-machine direction). A preliminary review of geogrid test results in well performing section showed junction efficiency (i.e., the ratio between the strength of the junction and the rib tensile strength) of 94% while the geogrid test result in a poorly-performing section shows a junction efficiency of only 50 %. Since current specifications require 90% junction efficiency, the inadequate junction efficiency value could be inferred as being the potential cause for the difference in pavement performance.

Closer inspection of the available test results indicated that the tensile modulus (at 2% strain) in the poorly-performing section is approximately twice as high as that in the well-performing section. Since the tensile modulus is a key property in current design methods, the need for additional material characterization to provide insight into the actual causes of the differences in pavement performance is required. For example, the tensile modulus in the cross-machine direction is rarely specified, but it is not less relevant than the tensile modulus in machine direction which is typically specified. Also the time -dependent response of polymeric material may lead to different results if tensile tests are conducted at different strain rates. The results from this case study emphasized the need for having additional laboratory tests that will capture the geosynthetic mechanism and provide independent verification of its properties that can better predict its performance in the field.

5.3.3 Case History 3

FM 1915 is located in Milam County, Texas. In 1996, longitudinal cracks were observed in the pavement section starting from Little River Relief Bridge to 2.5 miles (4 km) west of it. The subgrade in the entire pavement section had plasticity index in excess of 35. Accordingly, the pavement was reconstructed such that all sections had 10 inches (0.25 m) of lime treated subgrade with a seal coat at top. Due to presence of clays of high

plasticity at site, the pavement was reinforced with a layer of geogrid at the base and subgrade interface. The effect of base course thickness was evaluated on this pavement by constructing three different pavement cross-sections as shown in Figure 5.10.

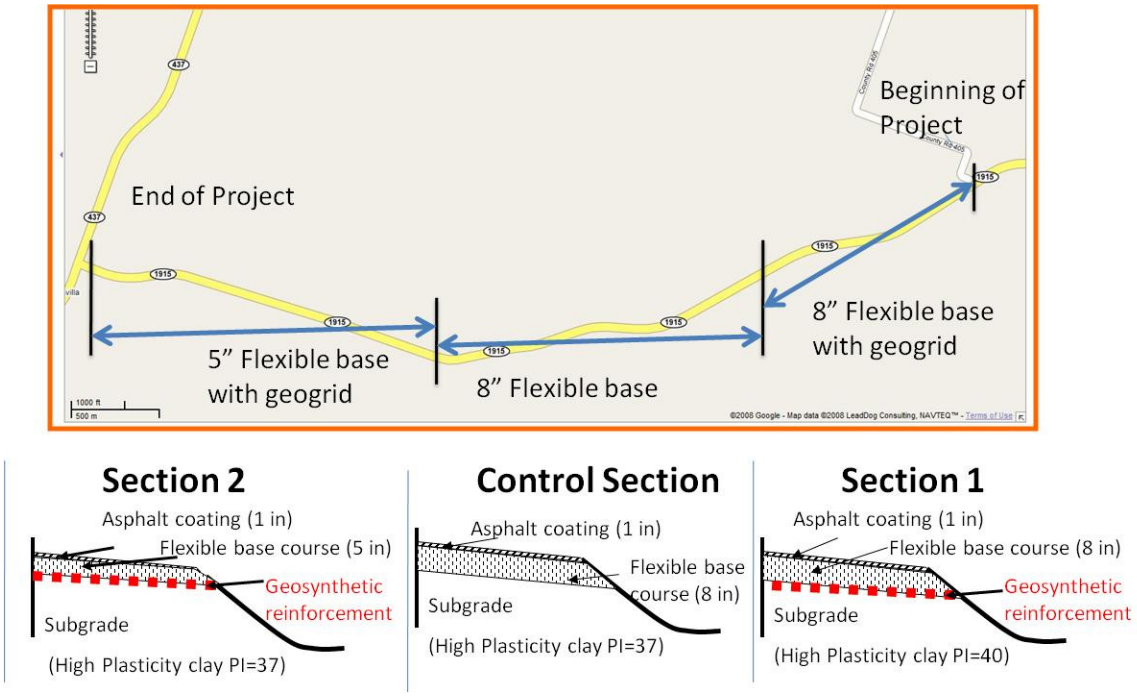

Figure 5.10 Project details and cross section of test sections at FM 1915 site

Thus, to evaluate the geogrid performance, two geogrid reinforced sections were constructed such that Section 1 had a base course thickness of 8 inches (0.20 m) and Section 2 had a base course thickness of 5 inches (0.127 m) along with a control section having base course thickness of 8 inches (0.20 m). The length of each section along with the plasticity index of subgrade for each test section is listed in Table 5.3.

Table 5.3 Details of test section at FM 1915

	Section 1	*Control section*	*Section 2*
Reinforcement	Geogrid	No Geogrid	Geogrid
Base course thickness, m	0.20	0.20	0.127
PI	49	37	37
Total length of section, km	1.26	1.34	1.31

In July 2001, TxDOT performed falling weight deflectometer (FWD) testing on the entire 2.5 miles (4 km) of the pavement section. The tests were conducted at every 100 ft (30.48 m) interval starting from Section 1. The FWD deflection data thus obtained was analyzed using the Modulus 6.0 software program developed by the Texas Transportation Institute (Scullion, 2004) and the elastic modulus for each pavement section layer was then back calculated. Table 5.4 summarizes the average values of modulus obtained for pavement layers of each section.

Table 5.4 Mean values for pavement modulus obtained using Modulus 6.0, for various pavement layers of the three test sections at FM 1915

MODULUS	**Section 1**	**Control**	**Section 2**
(MPa)	**Mean**	**Mean**	**Mean**
Seal coat	2068	2063	2020
Base course	1724	1660	1451
Sub base	443	380	302
Sub grade	139	134	132

The results from the FWD testing showed higher values of the modulus for the base-course and subgrade layer when geogrid reinforcement was used with 8 inches (0.20 m) thick flexible base course as compared to the control section. But the third section having geogrid reinforcement with 5 inches (0.127 m) base course thickness had lower base and sub base modulus as compared to the other two sections. These results lead to conclusion that the geogrid reinforcement would improve the performance of the

pavement when used over the same base course thickness but the benefits would not be realized if the base course thickness was reduced.

When the FWD results were compared with the field visual assessment of the pavement, longitudinal cracks were observed in the control section. On other hand the two geogrid reinforced sections were found to be performing well without any surface cracking of pavement. The anomaly between the field observations and FWD testing is mainly due to the current pavement analysis procedures for FWD loading which do not appropriately consider the effects of geogrid reinforcement layer. Presently the analysis is done by neglecting the geogrid layer and directly computing the modulus values for various pavement layers in the given section. These values are then compared to the modulus values for various pavement layers of a control section. The increase in the base course, sub base course and subgrade modulus is attributed to the presence of the geogrid layer for a reinforced section when compared with a control section. This method of analysis can quantify the benefits for the same base course thickness but can be misleading if the base course thickness is varied. The case study pointed out the drawbacks in current methods and emphasized the need for a better analysis method to quantify the benefits of geogrid reinforcement in the pavement which can adequately predict its field performance.

5.3.4 Discussion

The three case studies discussed above provided insight into the current state of practice with geosynthetic reinforced pavement design in Texas. In the first study, forensic investigation conducted at a newly constructed pavement on FM 542 was reported. The longitudinal cracks were observed in the geogrid reinforced pavement before it was open to traffic. But when site was excavated near the cracks, no geogrid was found below the pavement section. Further investigation revealed that the contractor had laid 9.8 ft (3 m) roll of geogrid and the pavement being 14 ft (4.2 m) long, remaining 4.2 ft (1.28 m) section was unreinforced and was cracked. This study showed that use of geogrid can prevent cracking in the pavements.

Field performance of two geogrid reinforced pavement consisting of subgrade having clay of high plasticity were reported. The pavement had two different types of geogrid. Both the geogrids meet the project specifications set by TxDOT. Although one section reinforced with geogrid type 1 (polypropylene) was found to be performing well, the other section reinforced with geogrid type 2 (polyester) showed longitudinal cracking. The review of the material properties lead to the preliminary conclusion that poor performance in the geogrid type 2 sections is due to inadequate junction efficiency but closer inspection indicated the higher tensile modulus of geogrid in this section. Since tensile modulus is an important property of geogrid, the need for better material characterization is stressed to predict the actual cause of difference in field performance.

In the third pavement, three sections were constructed. The two geogrid reinforced sections i.e., section 1 and 2 had base course thickness of 8 inches (0.20 m) and 5 inches (0.127 m) respectively; whereas control sections (no geogrid reinforcement) had 8 inches (0.20 m) thick base course layer. FWD testing showed higher pavement modulus for the geogrid reinforced section with 8 inches (0.20 m) thick base course layer over the control section whereas lower modulus value were predicted for geogrid reinforced section having 5 inches (0.127 m) thick base course layer . This indicates better performance for the section 1 and poor performance of section 2 when compared with the control section. But field visual assessment showed cracking in the control section and the two geogrid reinforced section were performing well. The geogrid reinforced sections outperform the unreinforced sections though the FWD testing indicates otherwise. This shows the inadequacy in the present analysis technique for non destructive testing to quantify the geogrid benefit in pavements.

In summary, there is good field evidence that the geosynthetic reinforcement provides benefits by stabilizing pavement over clays of high plasticity. But still there is need for new laboratory tests which can provide insight into field performance of these reinforced pavement sections. Furthermore, new methods for the analysis of FWD testing need to be developed which can better predict the field performance of geogrid reinforced and unreinforced section.

5.4 FIELD TEST SECTION

The lessons learned from the field case studies, formed the basis for a field monitoring program to evaluate the performance of geosynthetic reinforced pavements in Texas. As part of a highway maintenance and rehabilitation project, TxDOT supervised the construction of a geosynthetic reinforced farm-to-market road (FM-2) which was a low volume road in Bryan district of Texas.

For comparative evaluation, the reinforced pavement was reconstructed using 8 different reinforcement schemes (i.e. 3 reinforcement products and unreinforced control section, with/without lime stabilization). Furthermore to account for variation in field due to environmental, construction and site factors, a total of 4 repeats of each test section were constructed at the site. Therefore, a total of 32 test sections (4 reinforcement types x 2 stabilization approaches x 4 repeats) were constructed in FM-2. Significant features of the field monitoring program were:

1. Test sections with different geosynthetic types i.e. geogrid and geotextiles
2. Test sections with two different type of geogrids
3. Control sections with no geosynthetic to provide baseline for the study
4. Test sections having lime and no lime treatment
5. Multiple test sections with similar construction materials and geosynthetics

Due to unique characteristics of this field study, the reinforced pavement was considered experimental and an extensive program of instrumentation for monitoring its post construction performance was implemented. In addition, instrumentation in the form of thirty-two moisture sensors was implemented in order to characterize the patterns of moisture migration under the pavement. A total of eight horizontal moisture and vertical moisture sensor profiles each containing an array of four sensors was installed below the pavement.

Field monitoring involving visual inspection, surveying and falling weight deflectometer was conducted before reconstruction and immediately after reconstruction

of the road. The final construction of the reinforced pavement was completed in January 2006 and performance evaluation of the newly reconstructed road was conducted on regular basis for the next three years. The results obtained from the field study provided understanding of the underlying fundamental mechanisms governing the performance of the geosynthetic reinforced pavement in field. Furthermore, they helped in quantify the mechanisms of longitudinal cracking and effectiveness of the geosynthetic reinforcements in mitigating such distresses.

5.4.1 Site Details

Texas Farm-to-Market Road No.2 (FM 2) is located in the Grimes County (i.e. in southeast part of Texas). Figure 5.11a below shows FM 2 relative to major metropolitan areas in Texas. The total length of the road is 6.4 miles of which 2.4 miles lie towards the west of State Highway 6 (SH 6) at Courtney and rest 4 miles continues eastward and ends at FM 362 as shown in Figure 5.11b. The test sections were constructed in the portion of the road lying between SH6 and FM 362.

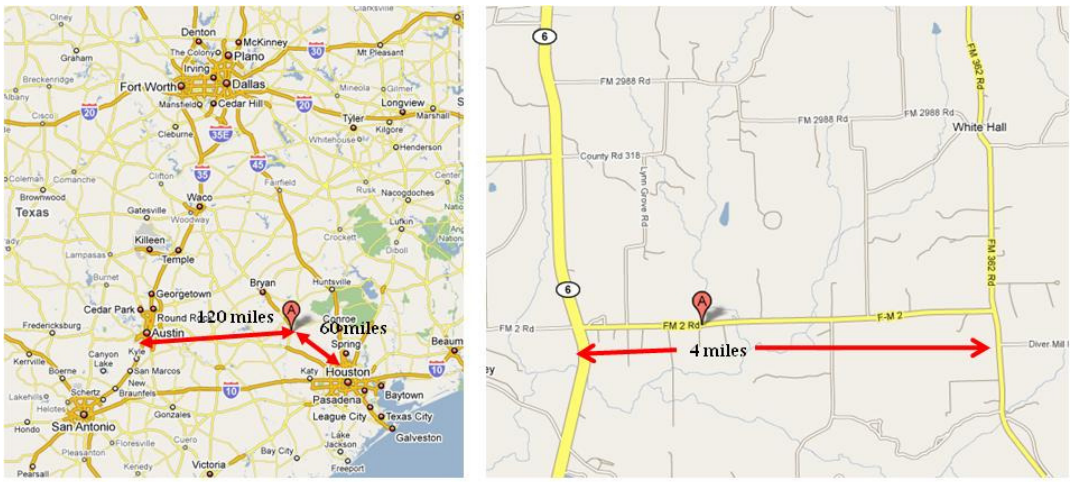

Figure 5.11 (a) Location of FM 2 relative to Houston and Austin; (b) Layout of FM 2

5.4.2 Average Annual Daily Traffic

Based on the traffic information provided by the TxDOT for the FM 2 road, the average daily traffic (ADT) was 800 in 2002 and is expected to increase to 1300 vehicles by 2022. Of this, trucks account for 6.6 percent of the ADT. The expected total number of equivalent 18-kip single axle load (ESAL) is 91,000 in one direction of the flexible pavement for a 20 year period from 2002 to 2022. The speed limit on FM 2 was 55 miles per hour.

5.4.3 Weather Conditions

FM 2 is located on the outskirts of the city of Navasota in the Grimes county of Texas. The closest weather station to the site for which weather information is available for 2004 is located in College Station, Bryan district of Texas. Weather conditions at the site and surrounding areas, the weather information was gathered for this station. The record for the average monthly temperature and precipitation for last 30 years in Navasota (WSI Corporation, 2005) were obtained and are as shown in Table 5.5.

Table 5.5 Navasota 30 Year Climate Averages and Records

Month	1	2	3	4	5	6	7	8	9	10	11	12
Temp. High (°F)	58	63	71	79	85	91	95	96	89	81	71	62
Temp. Low (°F)	37	40	48	57	64	69	72	71	66	56	48	39
Record High (°F)	88	90	99	95	101	104	108	110	106	100	91	85
Record Low (°F)	9	16	19	30	42	52	56	55	43	28	21	3
Mean Temp. (°F)	48	52	60	68	75	80	83	84	78	69	60	51
Rainfall (in.)	3	2.9	3	3.1	4.5	3.9	2.3	2.8	4.8	3.7	3	2.9

Based on the climate data, two dry periods can be observed at the site in a year, with two wet seasons as shown in Figure 5.12. That is on an average, the site had two annually occurring wet-dry cycles.

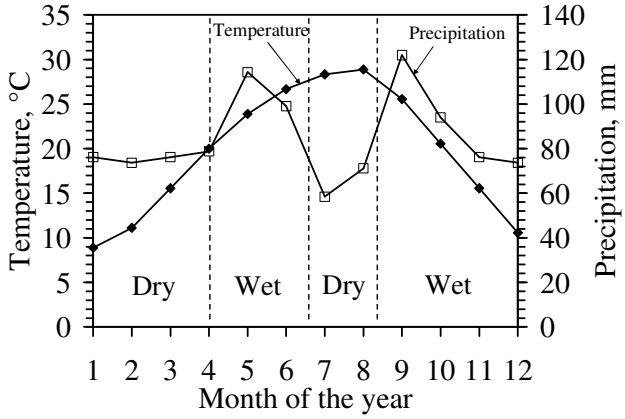

Figure 5.12 Wet and dry season at the site based on 30 year average climate data

5.4.4 Pre-construction field evaluation

Before reconstruction of the FM 2 road, a field survey was conducted in January 2005 to evaluate the structural section of the in-situ pavement. This survey is aimed at quantifying the existing damage by documenting the type of cracking present due to environmental and traffic loading at the site. Furthermore, it allowed assessment of the improvement in the pavement after construction. Finally, the condition of the subgrade, the existing base course and the asphalt layer were assessed with the aim of choosing a site for field test sections over similar ground conditions.

The first step in the site characterization was the placement of markers at the edge of the pavement. The markers, (wooden pegs) were placed every 0.5 miles starting from the west end of the road (FM 362). GPS marking were then made for notable features such as traffic signs, culverts and minor roads close to the site. As shown in Figure 5.13, the important features are marked for a section of pavement close to FM-362 end of the FM-2 road. These identified points of interest were used as reference for non-destructive testing before and after construction of the pavement. The nature and extent of vegetation adjacent to the pavement was also noted.

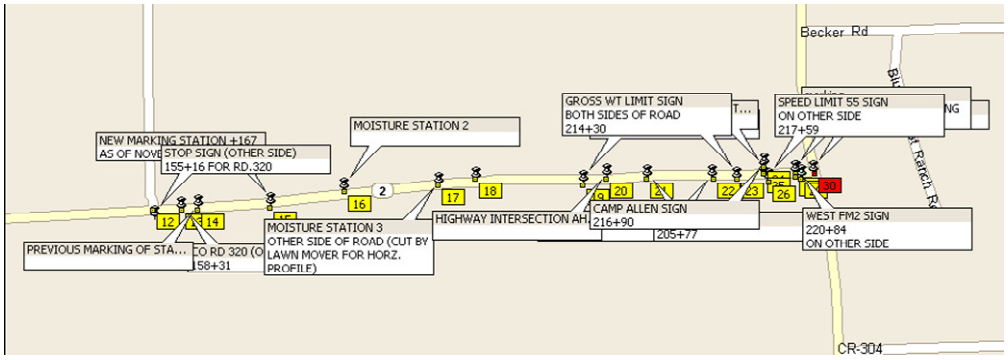

Figure 5.13 GPS marking for FM 2 road close to FM-362 end

Non- destructive testing was done using Rolling Dynamic Deflectomer (RDD) and Falling Weight Deflectomer (FWD) on FM-2 road. A total of 3.84 miles of section of west bound lane, also labeled as K6 was tested starting from FM-362 end of the road and going towards SH-6. FWD testing was performed at 300 feet intervals using four load levels of 6, 8, 11 and 15 kip. Simultaneously, RDD testing was done using two static load levels of 8 kips and 13 kips. The data obtained by FWD testing was processed using Modulus 6.0 software to obtain equivalent modulus of the existing pavement. The average deflection values obtained by RDD testing and equivalent modulus obtained by FWD methods are plotted as shown in Figure 5.14.

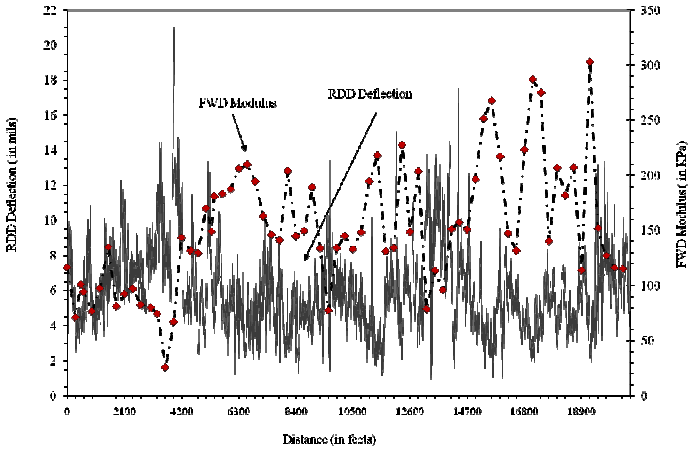

Figure 5.14 Preliminary results of non-destructive testing at FM 2

Both the tests showed similar behavior in terms of pavement performance. Specifically, the sections with high deflection during RDD test showed lower equivalent modulus as obtained by FWD test, thereby indicating the weak spot in the pavement. The results obtained by these tests were used to plan the layout of the test sections. This was done to minimize the bias from the test sections in terms of their location on the site assuming uniform construction procedures were followed throughout the project. Finally, a field visual inspection of the site in accordance with FHWA distress identification manual (Miller and Bellinger, 2003) starting from FM-362 westward to SH-6 was conducted. Based on the visual survey, the pavement was classified as severely distressed and thus in need of immediate repair and maintenance.

The soil at the edge of the pavement was excavated and the samples were collected up to a depth of 2 feet. These samples were not found to be representative of the actual subgrade soil as they contained debris which was a mixture of asphalt and other construction material left at site from previous rehabilitation and maintenance operations. Accordingly, in order to characterize the site cores of the pavement cross section were obtained from the middle of the pavement. Based on the data collected it was established that the pavement had an asphalt seal coat layer 1.0 inch thick followed by a base course layer with an average thickness of 15 inches above the clay subgrade as shown in Figure 5.15.

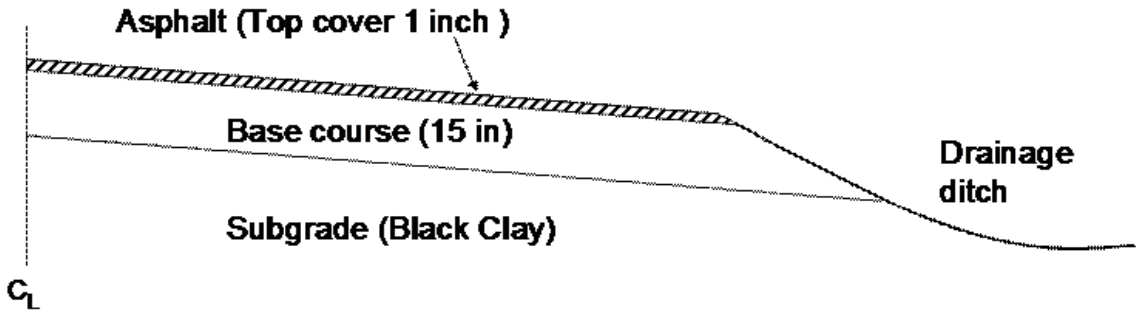

Figure 5.15 Cross section of the FM 2 pavement before reconstruction

5.4.5 Reconstruction of FM-2 site

During reconstruction the original pavement layer was scarified, such that the top 10 inches of existing base course layer were removed. The material that was removed during this process was re-compacted to relative compaction of 95% of the standard proctor density. For treated sections, this material was stabilized with lime to act as the sub-base layer for the new pavement. An additional new base course layer 7 inches thick was then placed on the recompacted over sub-base layer followed by 1.0 inch thick asphalt layer at the top of the pavement. The cross section of the scarified pavement is shown in Figure 5.16.

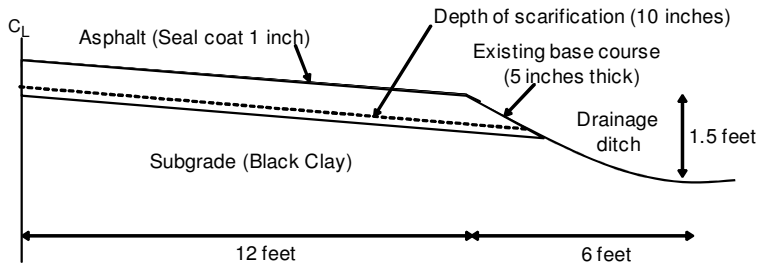

Figure 5.16 Cross section of the FM-2 pavement during scarification

For the field monitoring study, the following four basic test section as shown in Figure 5.17 were proposed.

(a) Unreinforced section without lime stabilization, (Figure 5.17a), to act as a control section.

(b) Unreinforced section in which the scarified existing base course is lime stabilized (Figure 5.17b), to evaluate effect of lime –treatment only.

(c) Geosynthetic reinforced section in which the scarified existing base course is not lime stabilized (Figure 5.17c), to evaluate effect geosynthetic reinforcement only.

(d) Geosynthetic reinforced section in which the scarified existing base course is lime stabilized (Figure 5.17d), to evaluate combined effect of both treatments.

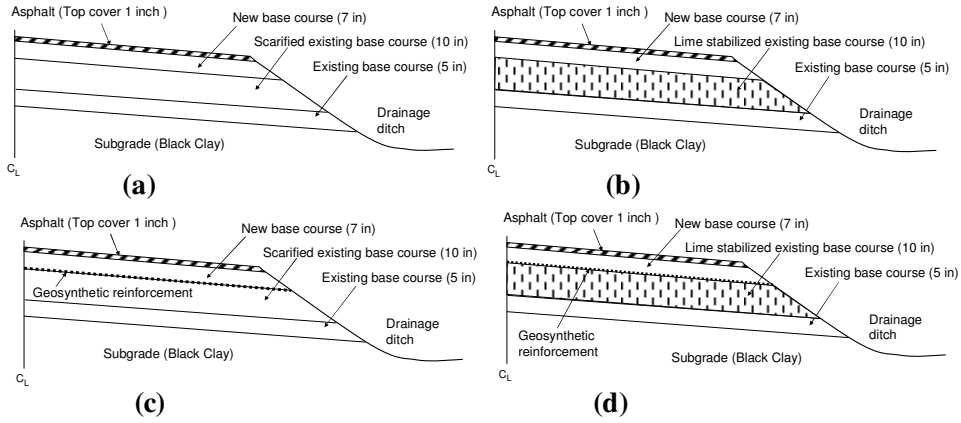

Figure 5.17 Pavement test sections at FM- 2: (a) Unreinforced without lime stabilization; (b) Unreinforced with lime stabilization; (c) Reinforced without lime stabilization; (d) Reinforced with lime stabilization

The unreinforced section with no reinforcement was labeled as G0.The reinforced sections consisted of one of the three types of geosynthetic reinforcements i.e., geogrid type 1 (G1) or geogrid type 2 (G2) or a geotextile (G3). The properties of geosynthetics were discussed in the previous chapter. Further, each of the above sections would be constructed over lime-treated and non lime-treated base course as listed in Table 5.6. The numbers 1 to 4 represent sections with no-lime treatment whereas 5 to 8 represent sections with lime treatment. Therefore, 8 such profiles were constructed in the field using four reinforcement combinations along with two stabilization options.

Table 5.6 Profiles used in field monitoring study at FM-2

Profile No.	Stabilization	Reinforcement type	Reinforcement Label
1	No-lime treatment	No reinforcement	G0
2		Geogrid 1	G1
3		Geogrid 2	G2
4		Geotextile	G3
5	Lime Treatment	No reinforcement	G0
6		Geogrid 1	G1
7		Geogrid 2	G2
8		Geotextile	G3

5.4.6 Layout of Test Sections

The field layout and the numbering system adopted to distinguish various test sections is as shown in Table 5.7. The four repeats were constructed at the site for each of the eight profiles (Table 5.8). Therefore, to provide a unique identity to each profile, they were further divided based on the driving lane (east bound, E or west bound, W) and their occurrence in each lane based on their distance from FM362 end (a or b).Thus, each of the eight profiles had four prefixes (Ea, Eb, Wa or Wb). For example, the section 2Ea indicated profile type 2 as listed in Table 5.6 in east bound lane with first repeat which is closer to FM 362 end of the pavement.

Table 5.7 Numbering system adopted to identify individual test section

Section No.	Profile type	Lane	Repeat	Test Section
1	1	K1- East Bound (E)	a	1Ea
2	2			2Ea
3	3			3Ea
4	4			4Ea
5	5			5Ea
6	6			6Ea
7	7			7Ea
8	8			8Ea
9	1		b	1Eb
10	2			2Eb
11	3			3Eb
12	4			4Eb
13	5			5Eb
14	6			6Eb
15	7			7Eb
16	8			8Eb
17	1	K6- West Bound (W)	a	1Wa
18	2			2Wa
19	3			3Wa
20	4			4Wa
21	5			5Wa
22	6			6Wa
23	7			7Wa
24	8			8Wa
25	1		b	1Wb
26	2			2Wb
27	3			3Wb
28	4			4Wb
29	5			5Wb
30	6			6Wb
31	7			7Wb
32	8			8Wb

The reconstruction of FM-2 involved constructing a 30 feet wide pavement with two lanes of 15 ft width each. The east bound lane was labeled as K1 and west bound lane as K6. Further, based on the contract restrictions the research team was given permission to construct test sections between stations 223+39 and 162+83, and stations 98+19 and 78+35. Thus, to incorporate the above requirements it was decided to construct 450 ft (~150 m) long test sections with first set of 24 test sections between station 221+00 and 167+00 and the second set of 8 test sections between stations 98+00 and 80+00. The details of each test section with their labels and location of moisture sensors as discussed in previous table are shown in Figure 5.18. The field test sections were successfully constructed as per the layout detailed below in January 2006.

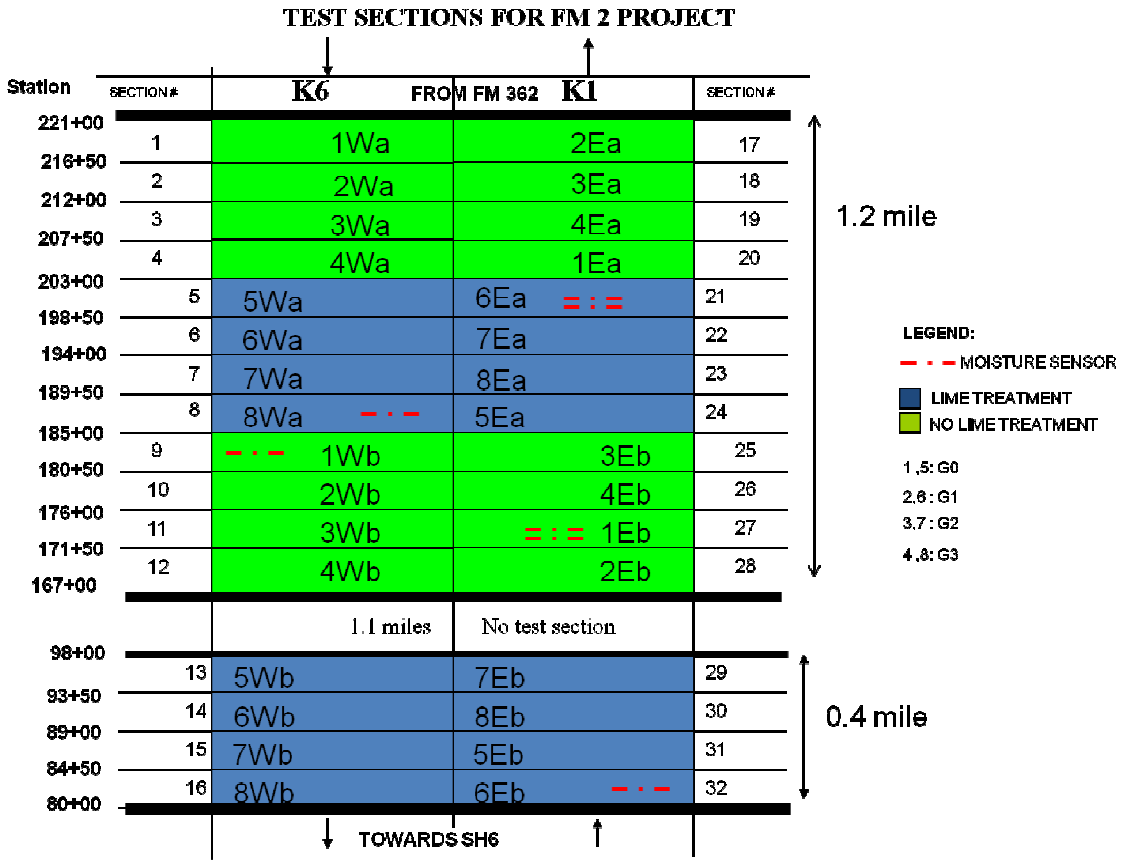

Figure 5.18 Schematic layout of the test section as per station number on FM 2 site

5.4.7 Post-construction field evaluation

The field test sections were constructed using the layout (as shown in Figure 5.18) and the geosynthetics were placed at the interface of sub-base and base course layer. After the rehabilitated road was reopened to traffic a field monitoring program was implemented to document the pavement response under traffic and environmental loading. Various techniques including moisture sensors, visual inspection and falling weight deflectometer were used to measure its performance. The weather conditions at the site were monitored from a new weather station installed at a distance 5 miles from the site in January 2006 at Hempstead, Texas as shown in Figure 5.19. The weather data from this station was used for day-to-day assessment of the environmental conditions at the FM-2 site. Furthermore, the information obtained from this weather station was used to calibrate and check the response measured by the moisture sensors installed in the field test sections.

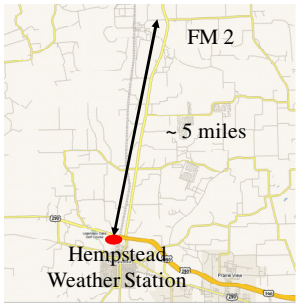

Figure 5.19 Distance of weather station from the site

The precipitation data for the year 2006 and 2007 obtained from the weather station is as shown in Figure 5.20a. This figure indicates that periods of intense rain occurred between October and February of 2006, while periods of little rainfall were observed in the late spring and late summer of the year 2007. The temperature and relative humidity at Hempstead are shown in Figure 5.20b. This figure indicates that the relative humidity fluctuates between 50 and 92%, while the temperature ranges from 0 to 31 °C.

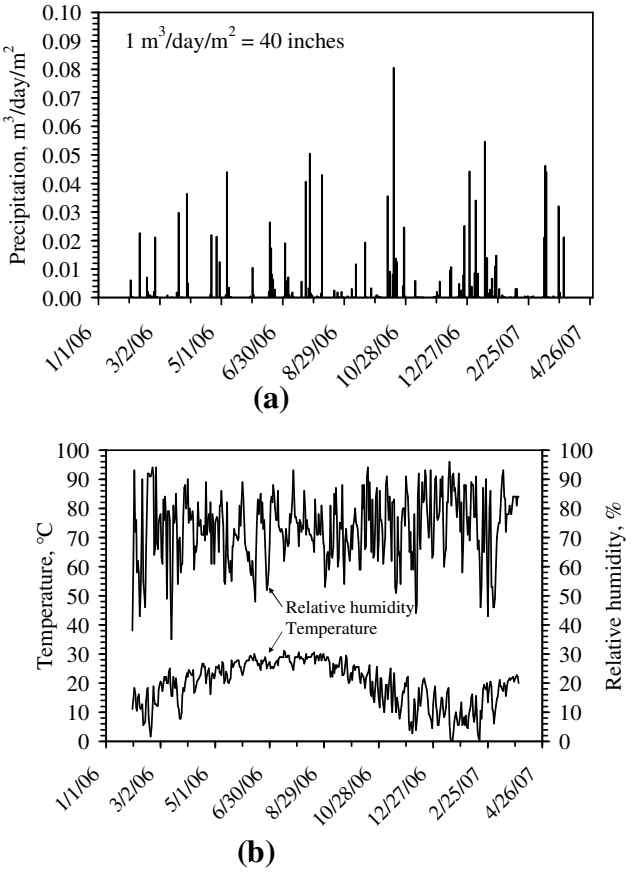

Figure 5.20 Data collected from Hempstead weather station for (a) Precipitation (b) Relative humidity and temperature

The bore hole sampling was conducted at the site to characterize the subgrade soil. The samples were obtained from locations close to the installed moisture stations 184 and 199. The steps involved in taking a borehole specimen at station 184 are shown in Figure 5.21. The bore-hole rig was placed at the marked location (Figure 5.21a). Then the auger and the sampling tube were assembled (Figure 5.21b) and driven into the ground (Figure 5.21c). Finally, the split spoon sampler was retrieved (Figure 5.21d) and the continuous sample was obtained till the required depth. The top 5 feet of sample obtained at station 184 consisted of black clay (Figure 3.21e) followed by another 3 feet of similar clay and 2 feet of sandy clay (Figure 5.21f).

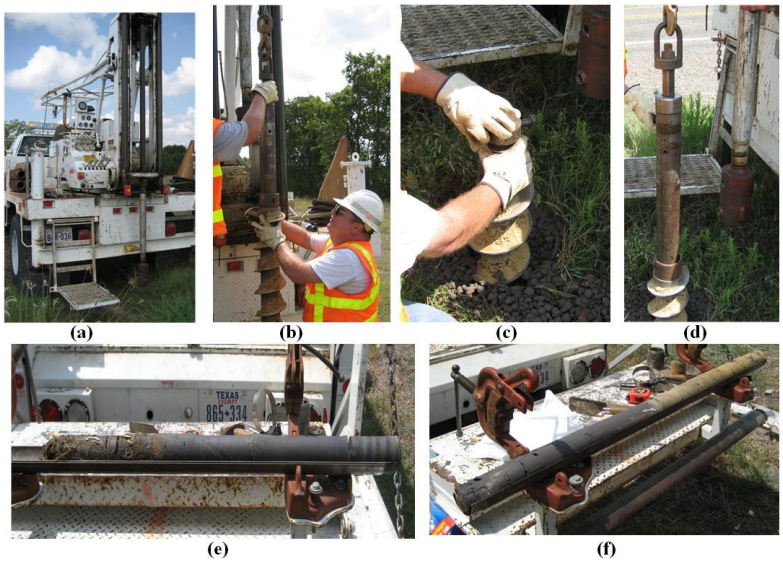

Figure 5.21 Details of borehole sampling operation (a) Rig placed at marked location (b) Auger and split spoon being assembled (c) Auger driven into the soil (d) Sampler retrieved from the borehole (e) 0-5 feet of sample obtained (f) 5-10 feet of sample obtained consisting of black clay followed by sand clay

The borings were conducted at similar locations in January and August 2006 to determine the in-situ water content profiles at these times of the year. The gravimetric water content profiles for Station 184 and 199 for the above months in year 2006 are as shown in Figure 5.22a and 5.22b respectively. The top soil had relatively dry surface layer as it was exposed to the atmosphere. The moisture profile at Station 184 indicated change in moisture content below a depth of 1m wherein the water content increased from January to August 2006. Similarly for station 199, the moisture profile showed increase in water content from January to August 2006. However, no significant change in field moisture content was observed for the two sites below the depth of 2m for both the stations. This data indicated that the zone of moisture fluctuation was limited to the top 1m of the subgrade layer. The moisture profiles from January 2006 were representative of relatively dry conditions, while the profiles from August were representative of relatively wet conditions. This observation from the borehole moisture profiles matched the data obtained from the weather station for the same duration.

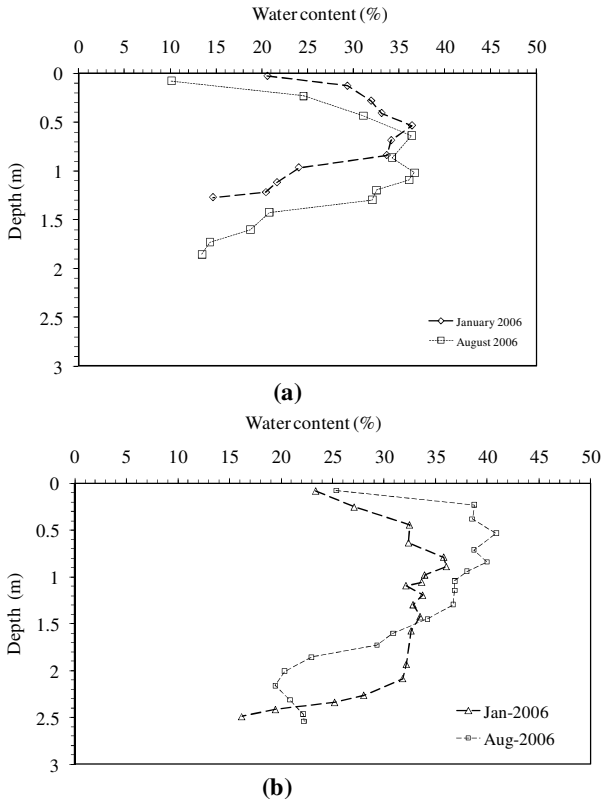

Figure 5.22 Gravimetric water content profiles from the boreholes for January and August 2006 at: (a) Station 184; (b) Station 199

The cores obtained from the borehole sampling above were also used to obtain the shrinkage curve of the soil. This was done by air drying the core in the lab and calculating the volume of the sample over time till no further change was observed. Then, based on the water content reading taken at the beginning and end of the test, the shrinkage limit of the soil was computed. The shrinkage limit for this soil was found to be 13% at void ratio of 0.46 as shown in Figure 5.23. The value of shrinkage limit of the soil obtained using this method is approximate because as the sample dried, it cracked leading to higher total volume than actually expected in field.

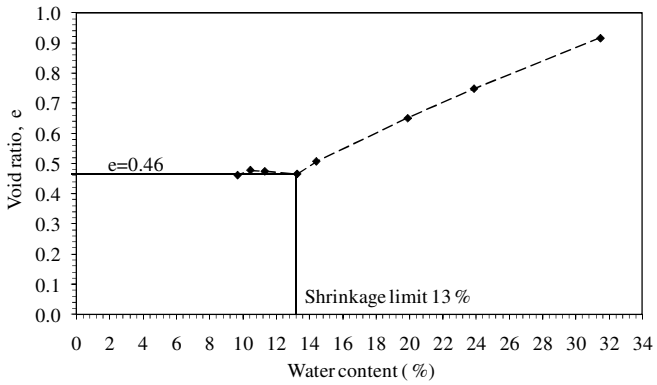

Figure 5.23 Shrinkage limit of the soil based on drying of cores

The typical soil profile for the site based on borehole investigation indicated a top soil zone of 0.2 m followed by subgrade clay layer of 2.7 m thickness with plasticity index between 35 to 50 (PI > 25, highly plastic soil) and a layer of sandy clay with thickness of 0.1 m as shown in Figure 5.24a. Then, the elevation survey at the site was conducted using total station immediately after construction. The results indicated a steeper slope on the east side as compared to the west side of the pavement as shown in Figure 5.24b. The effect of this feature on the pavement performance is discussed in Section 5.6. Finally, the data from borehole survey was combined with the elevation survey to obtain a representative profile at Station 184.

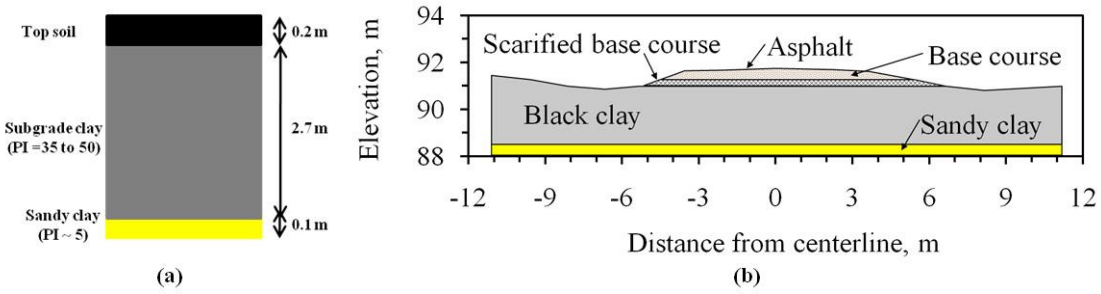

Figure 5.24 Profile at FM-2 for (a) subgrade cross-section based on borehole survey (b) pavement cross-section based on elevation survey

5.4.8 Discussion

A field study to investigate the performance of geosynthetic reinforced pavement was designed based the lessons learned from the survey of already constructed pavements in Texas. The site had a control section and three different geosynthetic reinforced sections which were either lime stabilized or non-lime stabilized. A total of 32 test sections were constructed with four repeats for each of the eight profiles. The site conditions were investigated during its rehabilitation and immediately after construction to obtain the baseline data for future investigation. This included non-destructive testing in form of FWD and RDD tests, borehole coring at two locations and elevation survey of the site. The environmental conditions were monitored using a weather station located at a distance of 5 miles from the site.

During the service life of a pavement it is subjected to both environmental and traffic loads. It is difficult to separate one effect from another as they are interrelated and distress caused by one form of loading influences performance under another other form of loading. Therefore, a comprehensive plan for post construction field monitoring was drawn which incorporated both of these factors.

The effect of environmental loading was monitored in terms of moisture variation below the pavement. The monitoring of moisture migration below pavement involved installing the sensors with an onboard data logger to store the data. In addition to this, to evaluate the effect of traffic loading, FWD tests were planned to be conducted at regular intervals such that they coincided with extreme environmental conditions i.e., peak in summer season or after a heavy rainfall event at the site. Finally, the field visual inspection survey was conducted at the end of these wet and dry seasons wherein the site was inspected for longitudinal cracks. Thus the data collected from these sources allowed for a comparison of the performance of the different tests sections and thus the effectiveness of geosynthetics in their role of mitigating the environmental and traffic loads.

5.5 EVALUATION OF MOISTURE SENSOR INFORMATION

The seasonal moisture variation below the pavement leads to longitudinal cracks on its shoulders. These cracks occur parallel to the roadway and can extend a significant distance, as explained in Section 5.2. These cracks are undesirable, as they provide a pathway for moisture infiltration and increased ease of base course particle migration, ultimately accelerating the roadway degradation.

A mechanism of longitudinal cracking relevant to flexible pavements atop expansive clay subgrades was envisioned earlier which involved differential volume change across the width of the roadway. This differential movement between the shoulders and the centerline of the road often leads to longitudinal cracks that are closer to the edge of the pavement. As this mechanism is independent of vehicle loading, it may be used to explain several pavement failures observed by TxDOT before opening to traffic. An improved understanding of the migration of moisture in highway subgrades will enhance implementation of strategies for prevention of longitudinal cracking in pavements.

A strong correlation between moisture migration and longitudinal cracking has not been well established in the literature. Accordingly, it was decided to investigate the migration of moisture under the pavement in order to assess the likelihood of differential shrinkage and swelling between the center and edges of the pavement. Thus, four horizontal and vertical profiles of moisture sensors were installed below the subgrade during the rehabilitation of FM-2 road.

This section describes the details of the moisture sensor used, the calibration and installation procedure adopted and then presents result from moisture sensors installed into the subgrade component of several pavement profiles at FM-2. Finally the trends in the moisture data useful for investigation of the mechanism of longitudinal cracking are evaluated.

5.5.1 Moisture sensor details

The moisture sensors used in this study to infer the gravimetric water content at particular locations in the subgrade were ECH_20 sensors, obtained from Decagon, Inc., as shown in Figure 5.25a below. They were attached to the Decagon EM50 data logger which was powered by standard alkaline batteries as shown in Figure 5.25b.

Figure 5.25 Instruments used in field study (a) Moisture sensor (b) Data logger

These sensors consist of a capacitor circuit embedded within a protective resin. The sensors measure the time required for the capacitor to charge upon application of a potential difference (Decagon, 2006). The soil acts as the dielectric material between the capacitor plates, so the time required to charge the capacitor is sensitive to the dielectric permittivity of the soil. Changes in the relative amounts of air and water in the soil during wetting and drying, as well as changes in density during shrinkage/swelling, result in changes in dielectric permittivity. The charge time of the capacitor is correlated with the gravimetric water content of the soil, as this parameter is only sensitive to changes in the mass of water (assuming that the mass of solids is constant). The ECH_20 sensors have low power requirements compared to other moisture sensors (time domain reflectometry, neutron gauge), are relatively small, are inexpensive, and can be used with conventional data loggers such as the Decagon EM50 or the HOBO data loggers.

5.5.2 Moisture sensor calibration

The moisture sensors were calibrated for subgrade soil or FM-2 clay in the laboratory. A rectangular mould which could accommodate the shape of the sensor was constructed to act as the calibration chamber as shown in Figure 5.26a. The mould was designed to provide a clearance of 30 mm on each side of the sensor to avoid the interference of signal due to reflection from the side walls of the chamber. A bellofram piston compactor as shown in Figure 5.26b was used to control the energy imparted to the soil during compaction. A total of four lifts each 30mm in height were used to compact the soil and the moisture sensor was placed at the end of first two lifts. A barrel of subgrade soil was dried in the lab and several 3 kg samples were conditioned to a range of gravimetric water contents expected in the field (5 to 35%). The specimens of the subgrade soil were compacted to dry density of 15.5kN/m^3 in a rectangular mold using a piston compactor. After compaction, a measurement was made with the moisture sensor to obtain a correlation between the sensor voltage output and gravimetric water content.

(a) (b)

Figure 5.26 Devices used for calibration of moisture sensors (a) Rectangular mould (b) Piston compactor

The relationship between the gravimetric water content of the remolded subgrade soil and the sensor reading is shown in Figure 5.27. The observed calibration curve was a straight line parallel to the 45^0 line. It was assumed that this calibration will not provide the exact water content for the clay after swelling or shrinkage occurs, but will give an indication of the preliminary estimate of the water content in the subgrade.

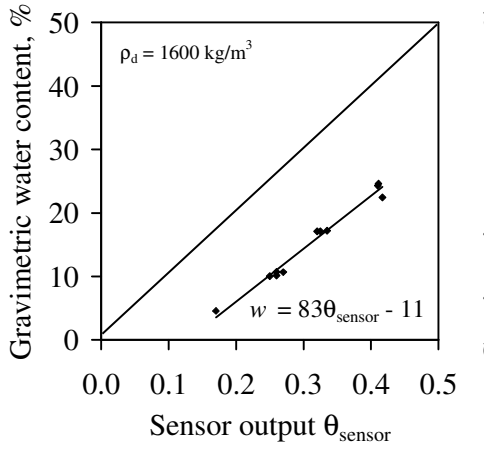

Figure 5.27 Moisture sensor calibration for subgrade soil

5.5.3 Moisture sensor installation

The moisture fluctuation below the pavement cross-section was quantified by installing moisture sensors below the pavement during its construction. The low hydraulic conductivity of the asphalt seal coat ($<10^{-9}$ m/s) indicated that the precipitation falling onto the pavement surface will runoff into the drainage ditch. Therefore, the drainage ditch was assumed to be the primary infiltration pathway into the subgrade. Furthermore, the secondary source of water entry into the subgrade was identified as the seepage through the slope of the pavement during runoff. Both these sources of water entry along with cross-section of pavement are shown in Figure 5.28a.

Based on above sources, four possible pathways of moisture migration into the subgrade were envisioned as: (1) Horizontal seepage through the slope, (2) vertical seepage through the slope, (3) horizontal seepage through the pheratic surface and, (4) vertical seepage through the ditch in the ponded water as shown in Figure 5.28b. Thus, it was decided to install horizontal and vertical moisture profiles along the pavement cross section to capture the above pathways. The horizontal array of sensors would be useful to assess the lateral migration of water under the pavement, while the vertical array would be useful to assess moisture fluctuations in the soil profile without the influence of the pavement boundary.

The seepage through the slope both in horizontal and vertical direction was assumed as the flux boundary condition whereas the flow through the ditch was assumed as a constant head boundary condition. Furthermore, the centre line of the pavement was assumed as the no flow boundary condition for design purposes. Thus it was decided to limit the horizontal array of sensors to the center line of the pavement and the vertical array of sensors to the depth of two feet below the pavement. The procedure adopted to install horizontal and vertical moisture sensors are explained in the subsequent section.

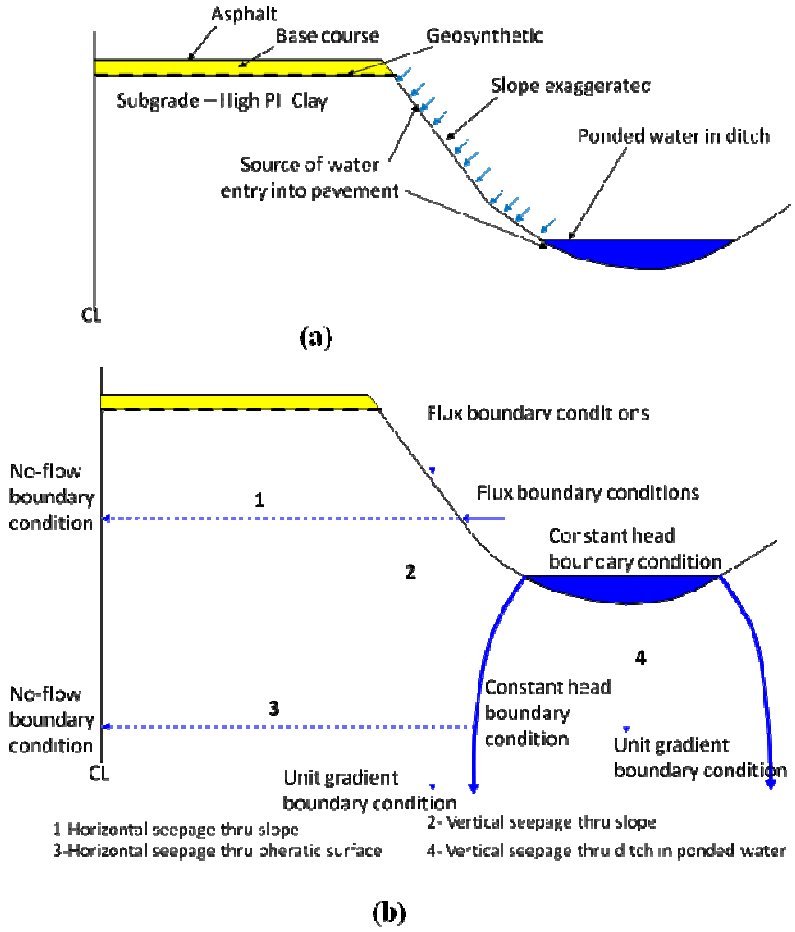

Figure 5.28 Moisture migration below pavement (a) Sources of water entry (b) Flow boundary conditions

5.5.3.1 Horizontal moisture sensor installation

An array of four moisture sensors was installed at a given cross-section below the pavement. The moisture sensors were placed at a distance of 2m from each other beginning from the center of the pavement leading towards the edge of the pavement. A typical horizontal moisture sensor profile below the pavement at Station 84 is shown in Figure 5.29 below. The sensors were placed at a distance of 150mm below the subgrade layer in remolded clay layer which had calibration curve consistent with the one obtained in the laboratory.

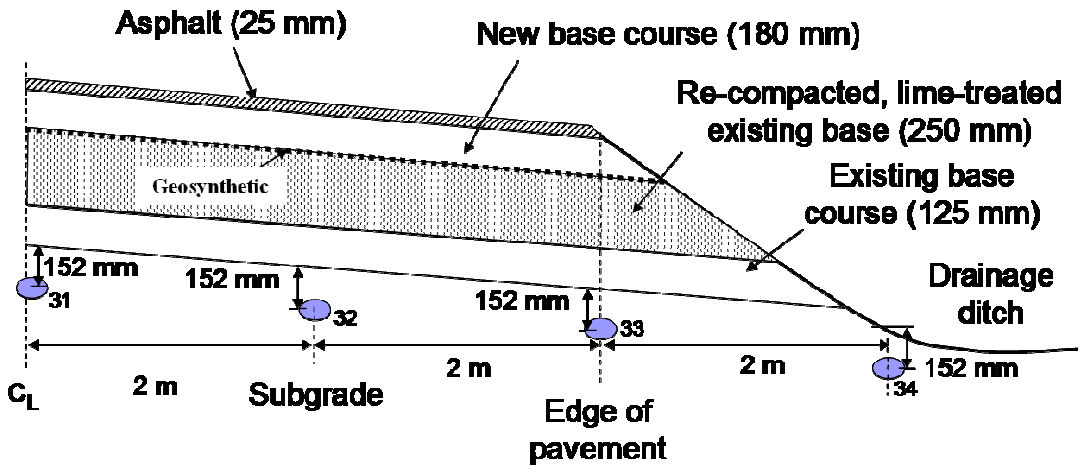

Figure 5.29 Horizontal array of moisture sensors

For this location, a trench perpendicular to the direction of the road was excavated through one of the lanes using a backhoe (Figure 5.30a). Care was taken to separate the base course and the subgrade layer by placing them on different sides of the excavation, for their later replacement in the road section (Figure 5.30b). The soil was then leveled at the sensor locations (Figure 5.30c). Using the saw blade and rubber mallet (Figure 5.30d), a slit was made on the exposed edge of the subgrade soil (Figure 5.30e). The saw blade was carefully removed as to cause minimum disturbance to the surrounding soil. Then the moisture sensor was inserted into the slit (Figure 5.30f), and soil was backfilled over the sensor end. The subgrade was then backfilled into the hole and compacted by

hand using the hammer (Figure 5.30g). The cables were connected to a data logger inside the mailbox containment system for easy access (Figure 5.30h). The sensor cables were passed through a corrugated plastic tube to a mailbox (Figure 5.30i). Similar procedure was followed at four locations along the pavement to install the array of horizontal moisture sensors. The data loggers were programmed to take moisture content reading every four hours. The moisture data was stored on-board of the logger and was retrieved using Decagon software and a laptop computer during the subsequent field visits.

Figure 5.30 Horizontal Moisture sensor installation procedure: (a) Trenching; (b) Separation of base and subgrade layer; (c) Leveling of installation site; (d) Tools for insertion of sensor; (e) Pre-insertion slit into the subgrade; (f) Installed sensor; (g) Compaction near sensor head; (h) Data logger; (i) Protective tube and casing for data logger

5.5.3.2 Vertical moisture sensor installation

Vertical moisture sensors were installed in the ditch, close to the edge of the pavement. An array of four moisture sensors was used at a given cross-section adjacent to the pavement which was placed at a distance of 150mm, 300mm, 450mm and 600mm below the pavement in the subgrade layer. A typical vertical moisture sensor profile below the pavement at Station 184 is shown in Figure 5.31 below.

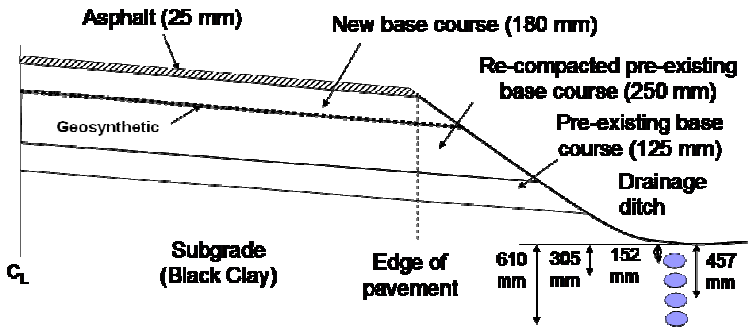

Figure 5.31 Vertical array of moisture sensors

The moisture sensors in the vertical array at a given station were installed by digging a trench 0.75m (2 feet) deep (Figure 5.32a). The four sensors with the wiring were passed through a protective tube (Figure 5.32b) at the marked locations. A slit was made using a saw blade and rubber mallet on the edge of the trench (Figure 5.32c) and the sensors were inserted into it, while trying to minimize disturbance to the adjacent soil. The tube with the wiring was then lowered into the trench (Figure 5.32d) and the trench was recompacted using the excavated soil. The data logger was then attached to the sensor wiring (Figure 5.32e) and placed on the top of the protective tube (Figure 5.32f) which was sealed using a top plastic cap to provide a secure encasement to the setup. The installation procedure discussed above was followed at four other locations along the pavement to install the array of vertical moisture sensors. The data loggers were then programmed to take moisture content reading every four hours. The moisture data was stored on-board of the logger and was retrieved using Decagon software and a laptop

computer during the subsequent field visits. Initially, the data logger was placed close to the ground surface. In subsequent field visit, ponding of water in the protective tubing was observed. Therefore, an additional length of protective tube was added thereby raising the level of the data logger. This was done to mitigate the potential damage which could be caused by water entry into the circuitry of the logger and also provide easy access to the data logger for data retrieval.

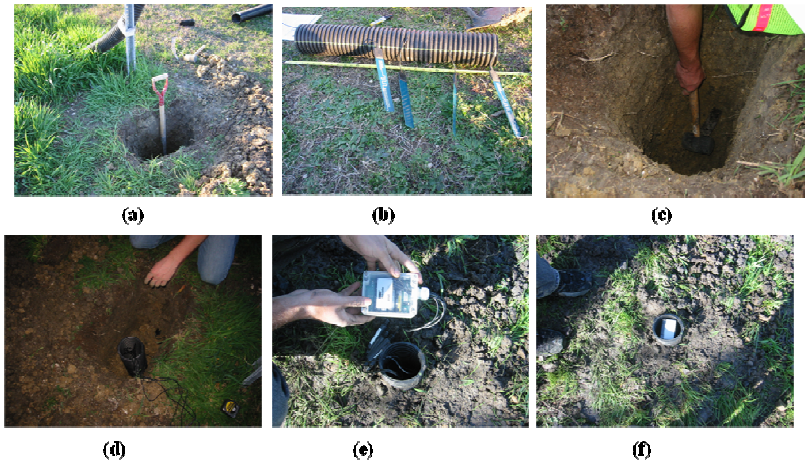

Figure 5.32 Vertical Moisture sensor installation procedure: (a) Trenching; (b) Placing sensors in protective tubing; (c) Pre-insertion slit into the soil; (d) Placing the protective tube in the trench; (e) Data logger; (f) Backfilling the trench

5.5.4 Moisture sensor results

The horizontal and vertical moisture sensor profiles were installed Section 5.5.3. The data logger for horizontal moisture profile at Station 84 started logging data on May 26, 2005, which was before the roadway had been fully rehabilitated as construction finished in June 2005. Horizontal moisture sensor arrays were also installed under the road at three other locations, but the installations were damaged by lawnmowers and rodents. Accordingly vertical arrays of sensors were installed in the drainage ditch at Stations 184 and 199 one year after the installation of the sensors at Station 84. The data obtained from these profiles is discussed in Section 5.5.4.1.

5.5.4.1 Horizontal Moisture Profile Results from Sensors

The monitoring results for the horizontal array of sensors at Station 84 are shown in Figure 5.33. The initial readings obtained from moisture sensors were discarded as immediately after its installation in May 2005, the data logger malfunctioned due to overheating and subsequent leaking of their batteries. The problem was fixed by cleaning the circuit board and replacing the batteries in July 2005. Based on the discussion with the construction manager it was found the site was relatively dry during construction in the summer of 2005. This dry period was reflected by the significant drop in gravimetric water content measured by sensor closest to the edge of the pavement i.e., sensor 34. After December 2005, the moisture sensor 34 showed significant fluctuations in water content, ranging from 16% to 46% whereas the water content inferred by the three sensors under the road did not vary and was close to 30%. A slight increase in water content was observed by the sensors under the pavement at the end of construction which was attributed to equilibration of gravimetric water content in the subgrade.

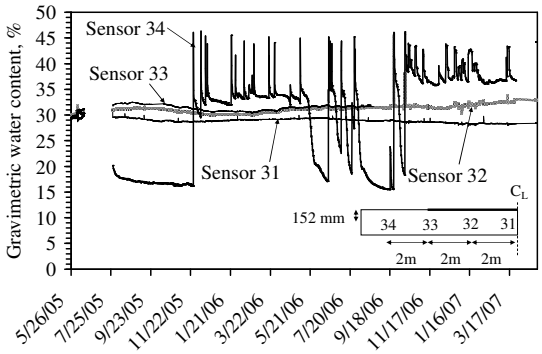

Figure 5.33 Time series of moisture data for each sensor at Station 84

A comparison between the precipitation data obtained from the weather station close to the site and the gravimetric water content readings from sensor 34 at the shoulder of Station 84 are shown in Figure 5.34. The spikes in water content in the subgrade layer at the edge of the pavement were found to be consistent with the timing of rainfall events at Hempstead weather station located at distance of 5 miles from the site.

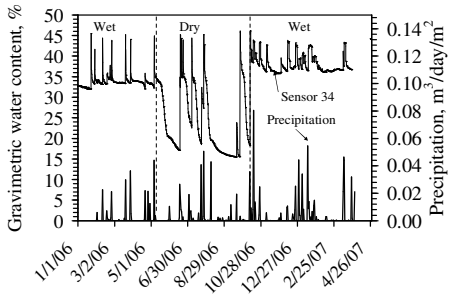

Figure 5.34 Comparison of data obtained from weather station and edge moisture sensor

The isochrones were drawn for moisture time histories for all the four sensors as shown in Figure 5.35. This graph indicated that the moisture variation was limited to the edge of the pavement while the center of the pavement remained at the constant moisture content. The zone of moisture fluctuation was limited to the first 2 m close to the edge of the pavement.

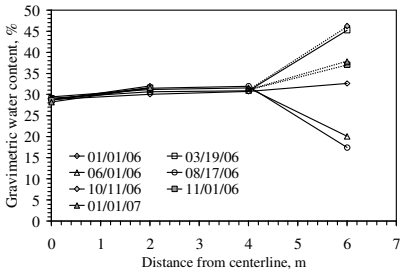

Figure 5.35 Isochrones of moisture data for each sensor at Station 84

Despite the difference in moisture fluctuations between the subgrade in the drainage ditch and that under the pavement, no longitudinal cracks were observed near the station location. As this location i.e., Section 6Eb was lime treated and reinforced with geosynthetic G1, the pavement was relatively stiff. This indicated that reinforcing the pavement helped in mitigating the onset of longitudinal cracking due to moisture variation below the pavement. These results are correlated with field visual inspection survey and discussed in Section 5.6.

5.5.4.2 Vertical Moisture Profile Results from Sensors

The vertical arrays of sensors were installed in the drainage ditch at Stations 184 and 199 one year after the installation of the horizontal array of sensors at Station 84. These profiles were installed to measure the range of water contents in the field, as well as the rate of movement of wetting or drying fronts from the drainage ditch to the subgrade under the shoulder. The time series for the moisture sensors at Station 184 are shown in Figure 5.36.

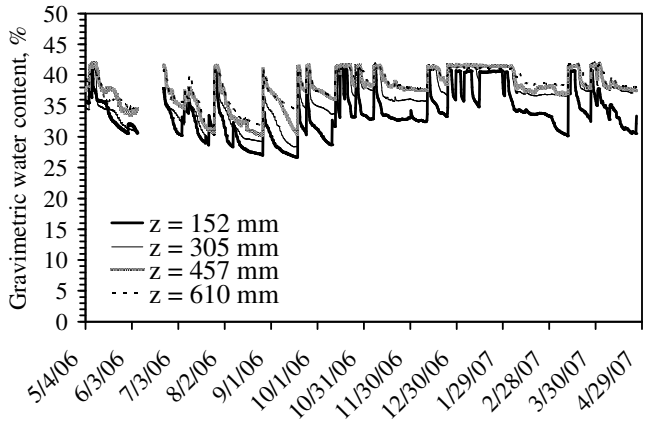

Figure 5.36 Time series of gravimetric water content data for Station 184

The water content at this location was observed to vary between 26% and 43%. These results showed water content above the shrinkage limit of soil (13% as shown in Figure 5.23) thereby indicating wet conditions prevailed at the location for the duration of monitoring. All the sensors showed change in water content over time. Based on the results it was concluded that the depth of moisture fluctuation was greater than the depth of sensor installation at site. Therefore, the minimum depth of moisture fluctuation at site was assumed equal to depth of bottommost sensor (610 mm). When comparing results among the four installed sensors, it was observed that the topmost sensor had the maximum daily fluctuation in readings. This indicated that the surface of the soil had wider variation in water content than deeper profile of the soil.

The gravimetric water content time series for the vertical array of sensors at Station 199 is shown in Figure 5.37. All the sensors showed similar trend in gravimetric water content with time. The gravimetric water content was observed to vary between 30% and 43%. This location had vegetation in form of trees and ponded water was routinely observed in the drainage ditch during most field trips to the site. This site had higher water content than station 184 which had no shade from trees, and so the water dried out due to exposure to sun leading to drier conditions.

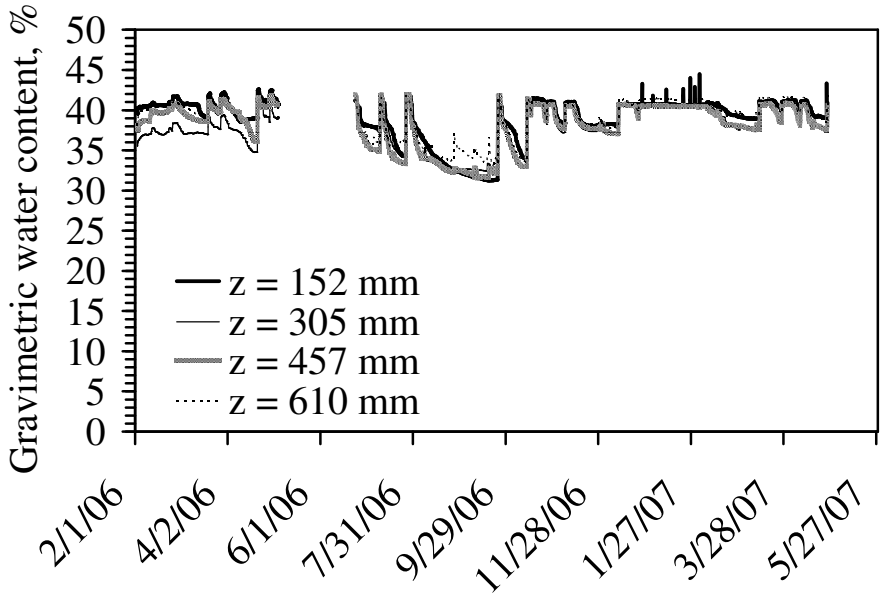

Figure 5.37 Time series of gravimetric water content data for Station 199

The isochrones of vertical array of sensors at station 184 and 199 were plotted as shown in Figures 5.38a and 5.38b respectively. The top two sensors located at 150 mm and 300 mm at both of these stations showed more variation in moisture readings when compared to the bottom two sensors located at 450 mm and 600 mm. This indicated that the top 300 mm (1feet) of the subgrade layer was more susceptible to moisture fluctuation than the bottom part.

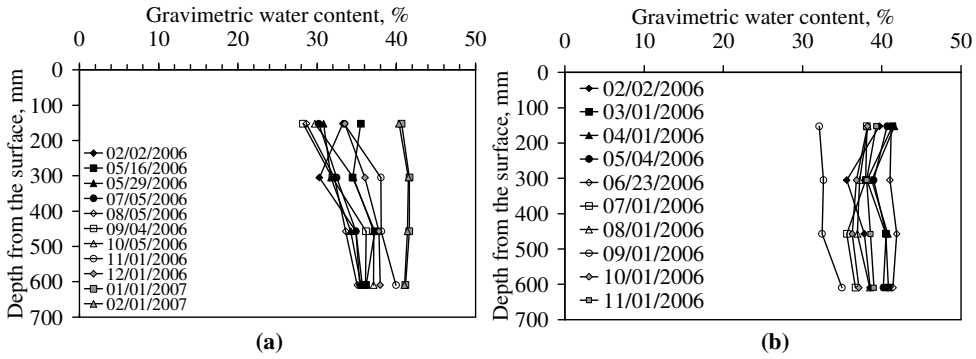

Figure 5.38 Isochrones for vertical moisture sensor array at stations (a) 184 (b) 199

A comparison between the gravimetric water content measured by the sensors closest to the ground surface in the drainage ditch at horizontal moisture stations 84 and the vertical moisture station 199 is shown in Figure 5.39. Both the sensors indicated similar trend in the moisture variation, though they were installed at different locations. This data helped in verifying the accuracy of the installed sensors both in horizontal and vertical direction in predicting moisture fluctuation trends at the site. Furthermore, the magnitude of moisture variation was similar for the two sites, with large changes in gravimetric water content occurring over the period of several days indicating uniformity of weather conditions over the entire section of the pavement.

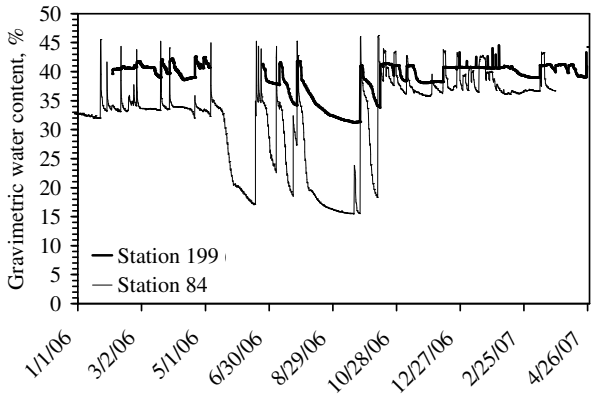

Figure 5.39 Comparison of top moisture sensors located at station 84 and 199

The daily changes in gravimetric water content for Stations 184 and 199 are shown in Figures 5.40a and 5.40b respectively. The positive increase of up to 14% in water content was observed during the course of a day during a heavy rainfall event which occurred after a relatively dry period, causing ponding of water at the site. However, no significant decreases in gravimetric water content were observed (i.e., less than 3% changes in water content was observed in a given day) which can be attributed to the lower hydraulic conductivity of unsaturated soils. This indicated that since the construction the site has maintained a baseline moisture profile and all the moisture gained due to rainfall events is subsequently lost over dry periods.

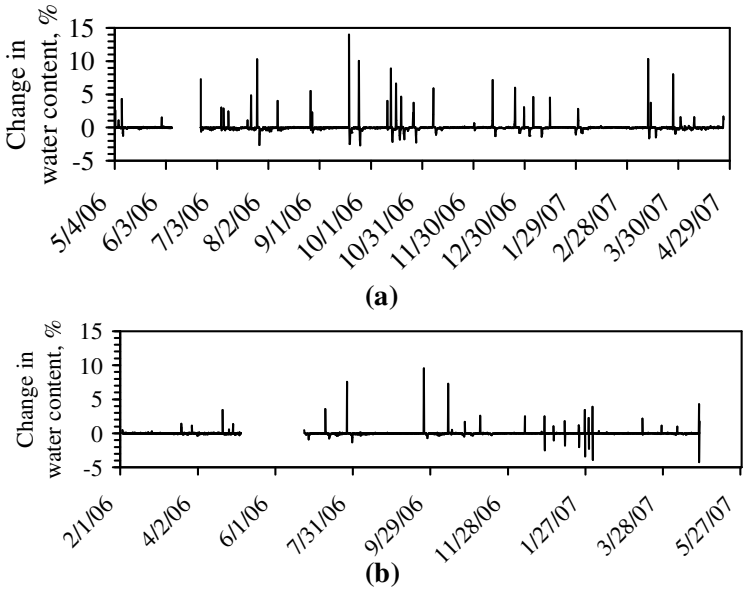

Figure 5.40 Change in water content of the surface sensor (152 mm): (a) Station 184; (b) Station 199

Based on the graphs it can be seen that there was a relatively dry period from May to July 2006, followed by a wet season from July through November 2006. In the next year, the dry season continued till March, 2007 followed by rainfall event in April, 2007. Thus, data obtained from moisture monitoring indicated that the site was subjected to seasonal moisture fluctuation in this period.

5.5.5 Discussion

Field moisture monitoring was performed by installing an array of sensors in horizontal and vertical direction below the pavement subgrade. The water content readings from the horizontal and vertical array of sensors indicated that the moisture variation occurred mostly near the edge of the pavement whereas the center of the pavement remained at a constant level. The zone of at least 1m below the pavement was susceptible to moisture change due to these seasonal fluctuations. These results obtained helped in understanding the moisture variation pattern below the pavement.

Based on the field moisture migration study it was concluded that there is seasonal moisture fluctuation below the pavement, but it is primarily limited to the edge of the pavement. Further, the top 1m zone of the subgrade soil is critical for vertical moisture migration. Therefore, the edge of the pavement is the most stressed zone due to these horizontal and vertical moisture fluctuations. Extending the geosynthetic towards the edge can be an effective strategy to prevent the longitudinal cracking of pavements.

5.6 FIELD MONITORING USING CONDITION SURVEY

The moisture content variation below the pavement was found to be cyclic in nature causing it to crack in the longitudinal direction by concentrating the stress at the edges. The sensors installed to measure the water content below the pavement indicated the above pattern of moisture fluctuation. Then, to establish the linkage between the moisture content variation as shown by the moisture sensors and appearance of field longitudinal cracks, visual inspection of the pavement was done. The motivation for this component of the research study was to obtain field evidence for longitudinal cracking and also determine the difference in performance obtained by sections having lime stabilization and geosynthetic reinforcement compared to the control sections.

5.6.1 Field surveying details

The distress due to environmental loading on the pavement was visually documented using the field condition surveying. The field visual inspection surveying

procedure involved walking the entire length of the test sections with a distance measurement wheel and datasheet to track the nature of cracks on the pavement. The tools used during the field visual inspection were a measuring tape to know the distance of the crack from the shoulder white line and a measuring scale to establish the depth of crack as shown in Figure 5.41. The photographs were taken using digital camera for each field trip and analyzed to understand the mechanism of crack formation, establish the origin of the crack and its propagation over the period of time.

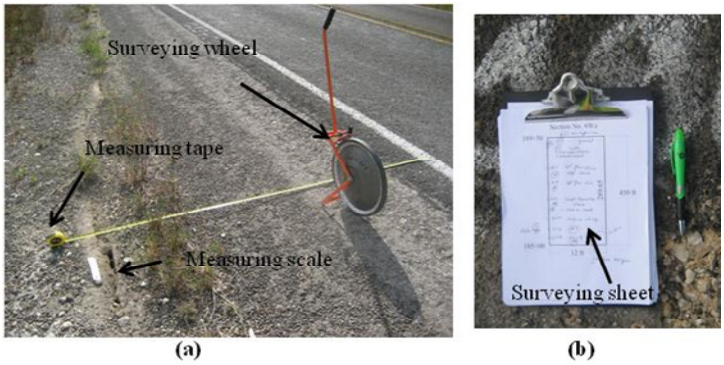

Figure 5.41 Tools used during field visual inspection of the FM-2 pavement: (a) Measurement devices, (b) Surveying datasheet

A total of nine field condition surveys were performed since reconstruction of FM-2 road. The surveys were performed in August and November of 2006; February, May and November of 2007; April and August of 2008; May and August of 2009. There were no signs of major distress from the first survey, conducted in May 2006 to the fifth survey conducted in November 2007. This absence of longitudinal cracks in the pavement was attributed to its few exposures to seasonal moisture variation and its relatively new construction. However, since the survey in April 2008, incipient longitudinal cracks were noticed. Initially, the cracks developed in the unpaved portion of the pavement close to the shoulder region. Most of the cracks were of hairline thickness and widened over time. A typical progression of crack observed over the subsequent field trips is as shown in Figure 5.42. The nature of cracks formed in different test sections is

then discussed. Furthermore, the comparison is made between the progression of cracks in base line section when compared sections which had lime treatment or geosynthetic reinforcement or both. Finally, the nature of preferential cracking observed on one side of pavement and effect of location of test sections on crack formation is also discussed.

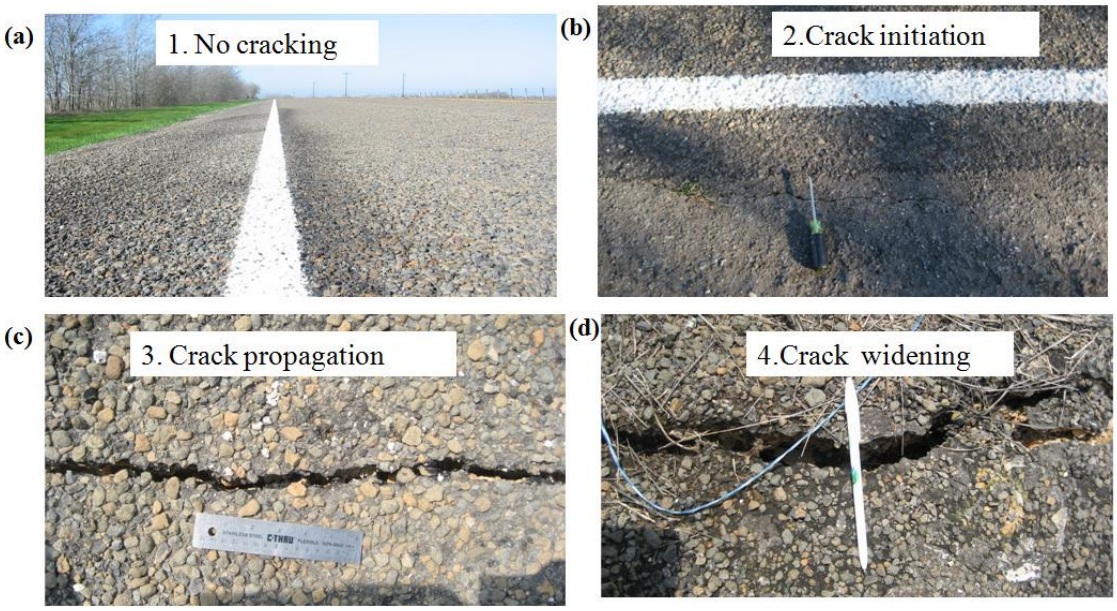

Figure 5.42 Development of crack at a location over time (a) November 2006; (b) November 2007; (c) August 2008; (d) August 2009

5.6.2 Performance of test sections

The test sections were surveyed using visual inspection. The details of test section are described in Section 5.4.6. For the present performance evaluation, the thirty two test sections were divided into four main groups: control section (four in number), no reinforcement section with lime treatment (four in numbers), geosynthetic reinforced section with no lime treatment (twelve in number) and geosynthetic reinforced lime treated sections (twelve in numbers).

During the field survey, preferential cracking was observed at east side of the pavement as compared to the west side. This was ascribed to the steeper slope of the pavement on this side. Furthermore, three test sections on east side (6Ea, 7Ea, and 8Ea)

showed severe distress, due to their location close to the culverts as shown in Figure 5.43. The cracks observed in these sections were considered independent of the parameters under scope of the present study i.e., lime treatment and geosynthetic reinforcement and are not discussed in this research.

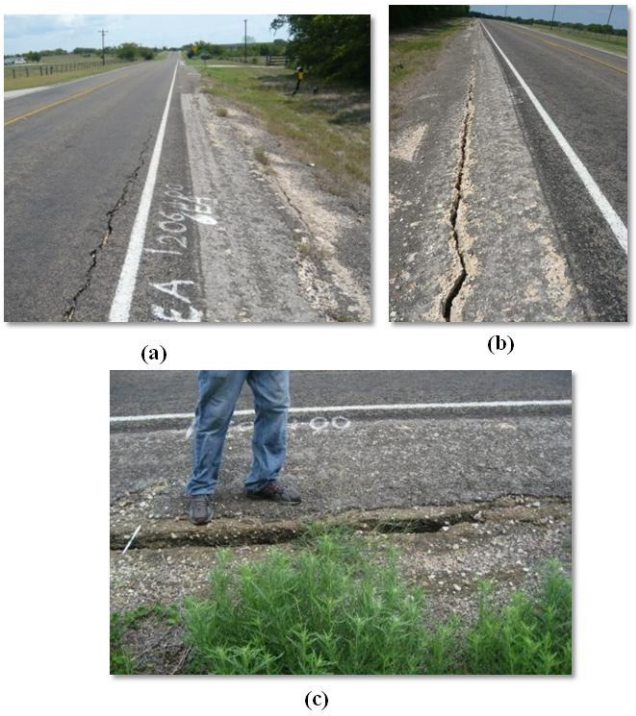

Figure 5.43 Continuous cracks through three section due to steep slope on east side of the pavement; (a) 6Ea (b) 7Ea, (c) 8Ea

5.6.2.1 Control test section

The control section consisted of no geosynthetic reinforcement or lime treatment. The location of four control sections (1Wa, 1Wb, 1Ea, 1Eb) is as shown in Figure 5.44.

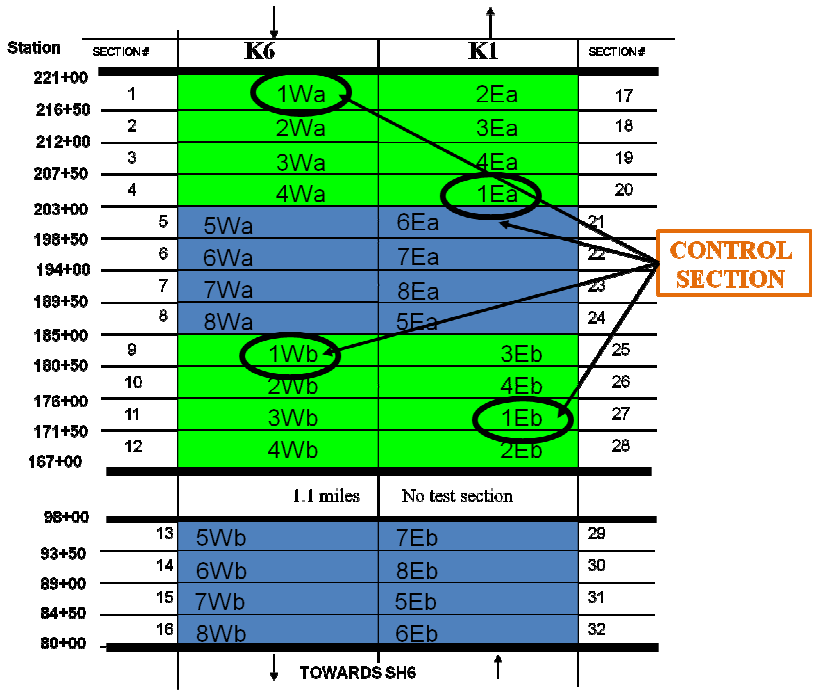

Figure 5.44 Location of control section on FM-2 road

The evidence of longitudinal cracking was seen in all the four control sections. The longitudinal cracks were observed to originate in the shoulder region of the pavement. Then, they spread such that the cracks ran parallel to the pavement or split into two or three branches. These cracks then ended up entering the main pavement structure and causing it to break as shown in Figure 5.45.

Figure 5.45 Longitudinal crack in different stages in sections (a) 1Ea, (b) 1Eb, (c) 1Wa, and (d) 1Wb

Besides the longitudinal cracks observed in these sections, other forms of distress were also observed. The control section, 1Ea was observed to be severely distressed with secondary type of cracks which occur due to traffic loading as shown in Figure 5.46. The survey of this pavement section showed that the absence of reinforcement and lime-treatment not only led to longitudinal cracking but rapid deterioration of the pavement under traffic loading. Also, the pavement response was linked. The poor performance under one form of loading led to deterioration under other form of loads.

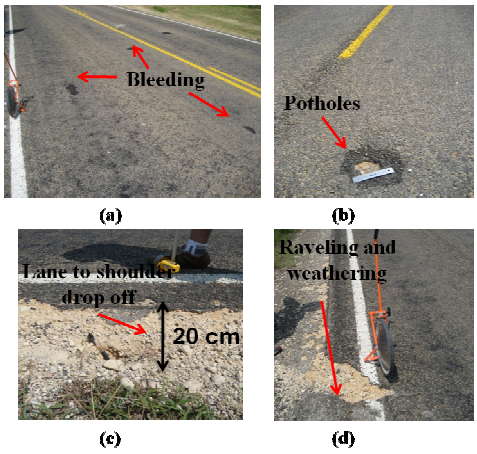

Figure 5.46 Type of distress observed in the control section (a) Bleeding; (b) Potholes; (c) Lane to shoulder drop off; (d) Raveling and weathering

5.6.2.2 Lime treated unreinforced test sections

The four unreinforced lime-treated test sections (5Wa, 5Wb, 5Ea, 5Eb) were located at stations as shown in Figure 5.47. The sections were surveyed for signs of longitudinal cracking in each field investigation. Based on the analysis of the field survey data, no major distress signs were observed in these sections till May 2009.

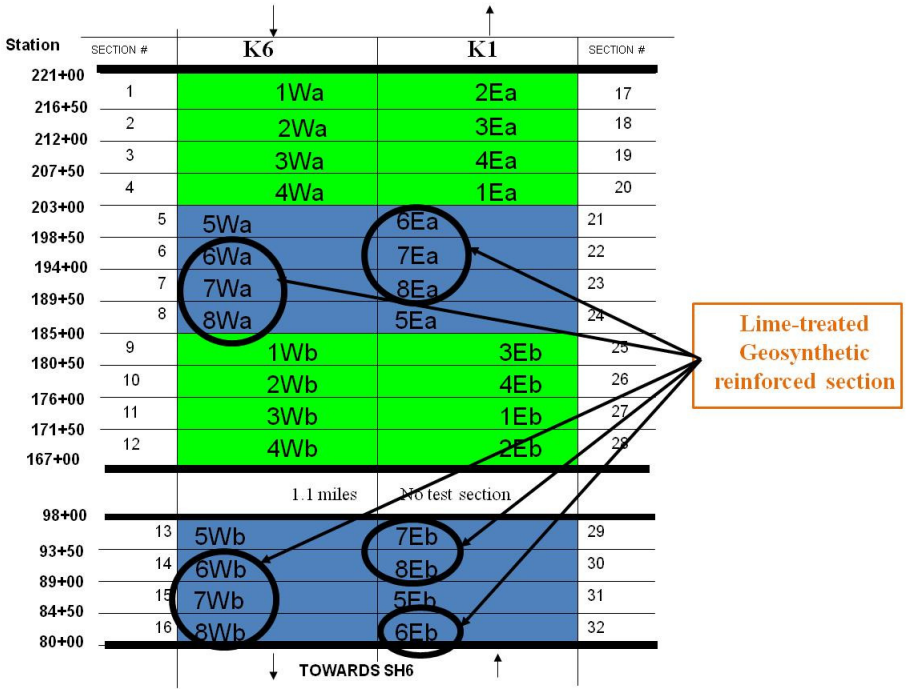

Figure 5.47 Location of lime treated no-reinforcement sections on FM-2 road

In the field survey conducted in August 2009 minor cracks were observed in the pavement sections as shown in Figure 5.48. Section 5Eb was found to have most distress of the entire four test sections as shown in Figure 5.49. Based on the observations, it was concluded that lime treatment is an effective method to mitigate cracking in the expansive subgrades but its depletion overtime reduces its effectiveness as a long term rehabilitation strategy. Furthermore, the non-uniform mixing of lime with the subgrade soil leads to localized failures when this method is adopted in the field.

Figure 5.48 Longitudinal crack in section 5Ea (a) No cracking till May 2009 (b) Appearance of cracks in August 2009

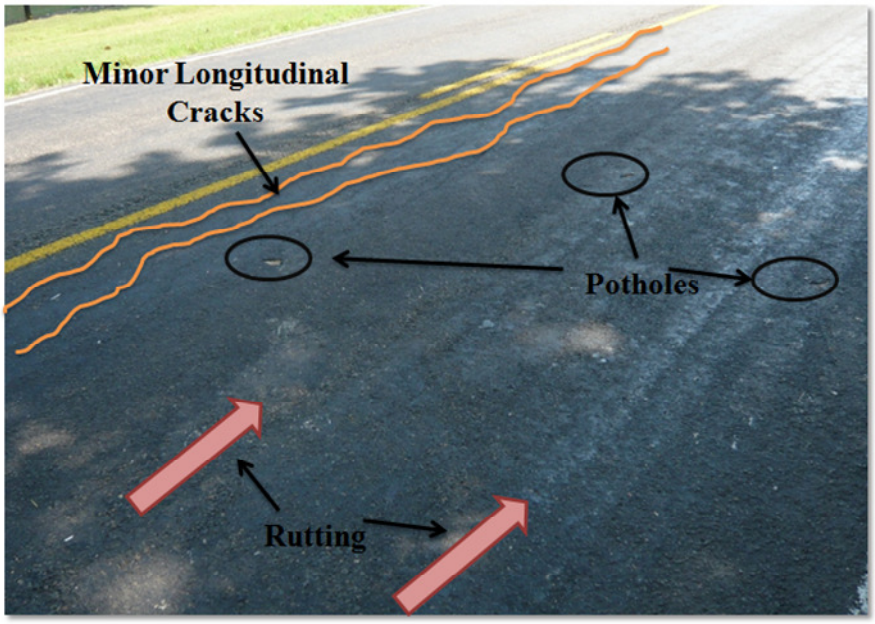

Figure 5.49 Distress cracking in test section 5Eb

5.6.2.3 Reinforced non lime-stabilized test sections

The twelve reinforced test sections with no lime treatment are as shown in Figure 5.50. These sections consisted of geosynthetic reinforcements G1, G2 and G3 as explained in section 5.4.6 of this chapter.

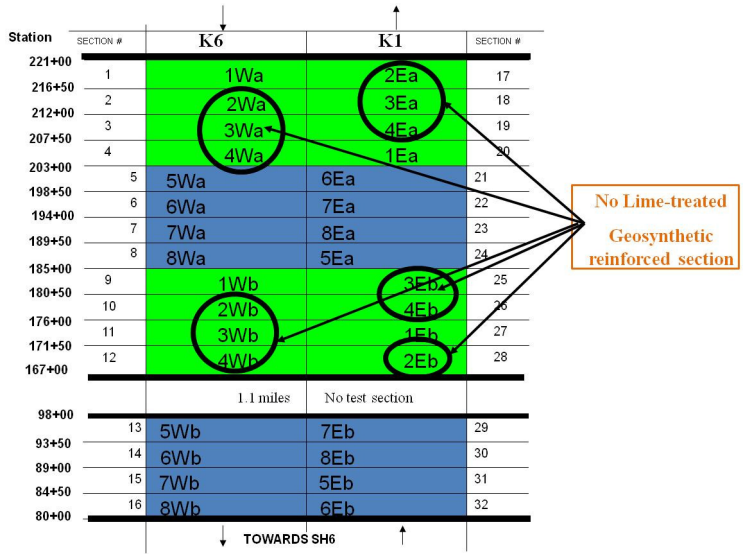

Figure 5.50 Location of no-lime treated geosynthetic reinforced sections on FM-2 road

The sections were surveyed for signs of longitudinal cracking in each field investigation. Based on the analysis of the field survey conducted till May 2009, no major distress signs were observed in these sections. Most of the hairline cracks were observed parallel to the outer edge of the paved reinforced zone. These cracks were seasonal in nature i.e., opening in summer and closing in the rainfall. In the field survey conducted in August 2009, these minor hairline cracks were observed to enter in the pavement sections reinforced with geosynthetic reinforcements G2 and G3 whereas the sections reinforced with geosynthetic G1 were observed to perform well as shown in Figure 5.51. In general, the performance of the geosynthetic reinforced sections was found to be satisfactory without any major evidence of severe distress cracking as observed in previous two test sections.

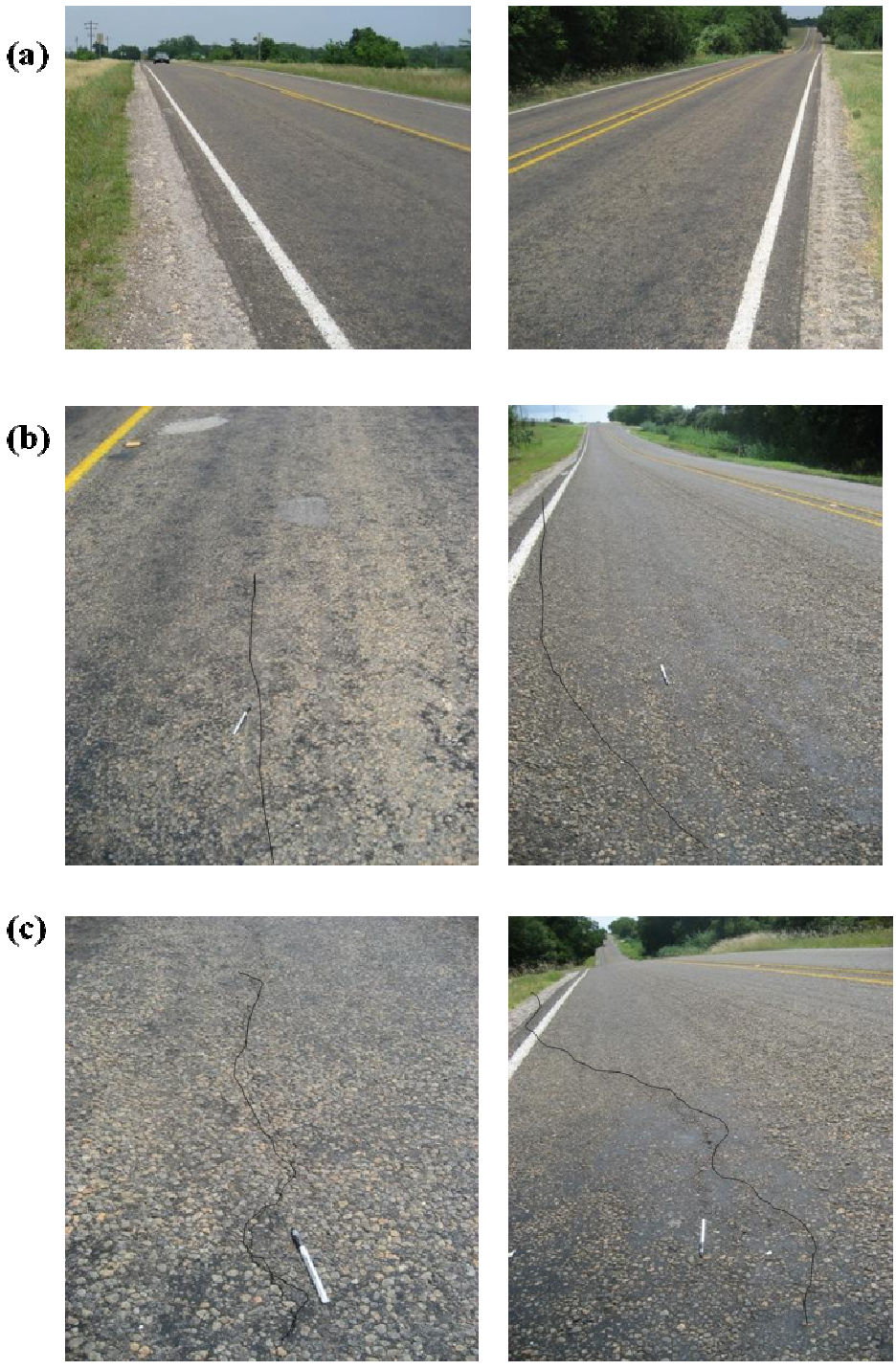

Figure 5.51 Performance of geosynthetic reinforced non-lime treated test sections (a) G1 (b) G2 (c) G3

During the field survey conducted in August 2009, the edge of the geosynthetic reinforced sections was excavated to check for the integrity of the reinforced geosynthetics. The observations indicated that the geosynthetic G1 had the continuous longitudinal and transverse rib configuration and acted as a single unit as shown in Figure 5.52a. Moreover, the integrity of junctions in geosynthetic G2 was compromised causing the longitudinal and transverse ribs to slip as shown in Figure 5.52b. Finally, the section reinforced with geosynthetic G3 was observed to have folds causing localized slacking of the reinforcement as shown in Figure 5.52c. This was attributed to the improper installation of the geosynthetic while constructing the pavement thereby reducing its effectiveness during working conditions. Overall, the sections reinforced with geosynthetic G1 were found to perform better than those reinforced with geosynthetic G3 followed by geosynthetic G2.

Figure 5.52 Checking integrity of geosynthetic reinforced non-lime treated test sections (a) G1; (b) G2; (c) G3

5.6.2.4 Reinforced lime-stabilized test sections

The twelve reinforced test sections with lime treatment and geosynthetic reinforcements (G1, G2 and G3) are as shown in Figure 5.53. The sections were performing satisfactorily, with no major signs of distress with exception of sections 6Ea, 7Ea and 8Ea which showed preferential cracking due to their location as discussed earlier.

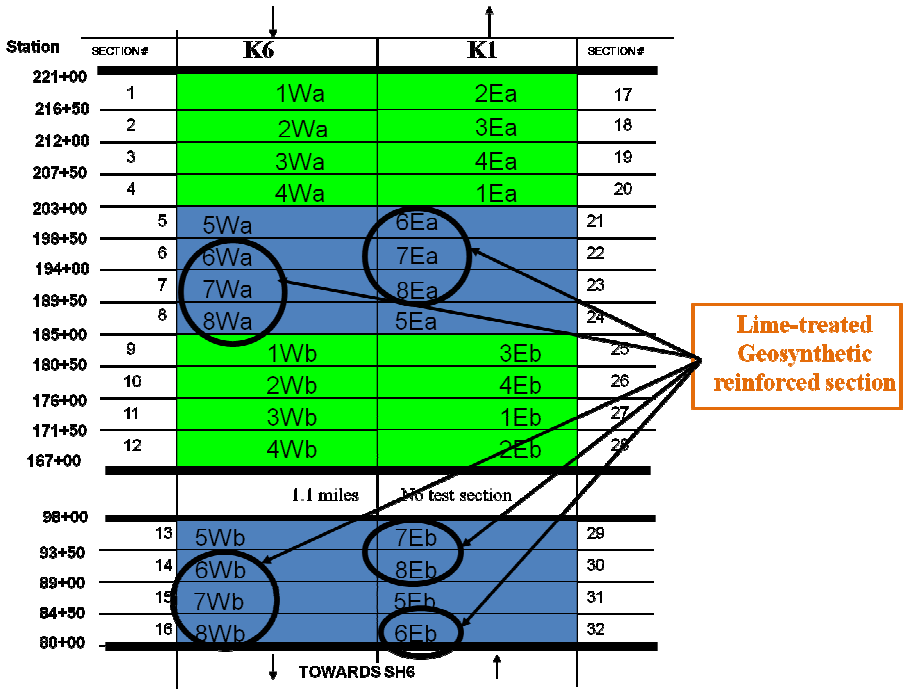

Figure 5.53 Location of lime treated geosynthetic reinforced sections on FM-2 road

Out of these twelve sections, six sections were located in between stations 185+00 and 203+00 whereas the second series of section was located between stations 80+00 and 98+00. The soil profiles at these locations based on the borehole survey are shown in Figure 5.54. Based on the borehole survey it was observed that the six sections (6Wb, 7Wb, 8Wb, 6Eb, 7Eb and 8Eb) were located over clay of relatively low plasticity as compared to rest of the test sections. Therefore, for discussion purposes their performance was not compared with rest of the test sections. Thus, sections 6Wa, 7Wa and 8Wa were checked for sign of distress and no major cracking was observed till date.

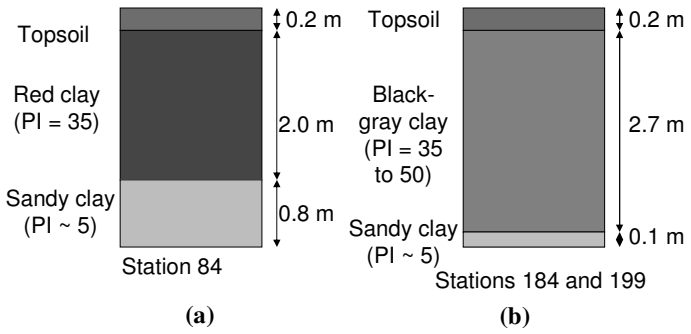

Figure 5.54 Soil profiles at two lime treated geosynthetic reinforced sections based on the borehole survey (a) Station 84 (b) Station 199

5.6.2.5 Comparison of test sections performance

The performance of four categories of test sections was compared. When the performance of non-lime treated unreinforced sections i.e., control sections was compared with non-lime treated reinforced sections a clear distinction in the crack propagation mechanism was observed as shown in Figure 5.55. In both cases, the cracks were observed to originate from the unpaved shoulder region of the pavement. In the unreinforced test sections these cracks were found to increase in size over subsequent seasonal cycles and eventually entering the paved portion of the pavement and causing it to develop distress. The major form of distress was observed in form of longitudinal cracks followed by secondary cracking in form of potholes, lane to shoulder drop off and bleeding of the pavement. In the geosynthetic reinforced pavements, these cracks either closed over subsequent seasons or ran parallel to the edge of the pavement at the boundary of unpaved and paved portion. Thus, geosynthetic reinforced test sections were observed to perform better than the unreinforced test sections.

On the other hand, the lime treated sections with or without geosynthetic reinforcement performed adequately with signs of localized distress. This variability in the performance was attributed to non-uniform mixing of lime with field soils and its depletion with time leading to its reduced effectiveness. In general, the lime treated reinforced test sections performed better than unreinforced lime treated test section. When the performance of these sections was compared to the geosynthetic reinforced

section without any lime treatment, no significant reduction in cracks was observed. Therefore, given the difficulty of lime stabilizing the subgrade compared to installing the geosynthetics in the field, no clear advantage was observed in terms of performance for the lime stabilized test sections. Overall, the control sections were found to have the highest severity of distress in terms of longitudinal cracks. The use of geosynthetic reinforcement and lime-treatment were observed to help in mitigating the development of such cracks into the main pavement section.

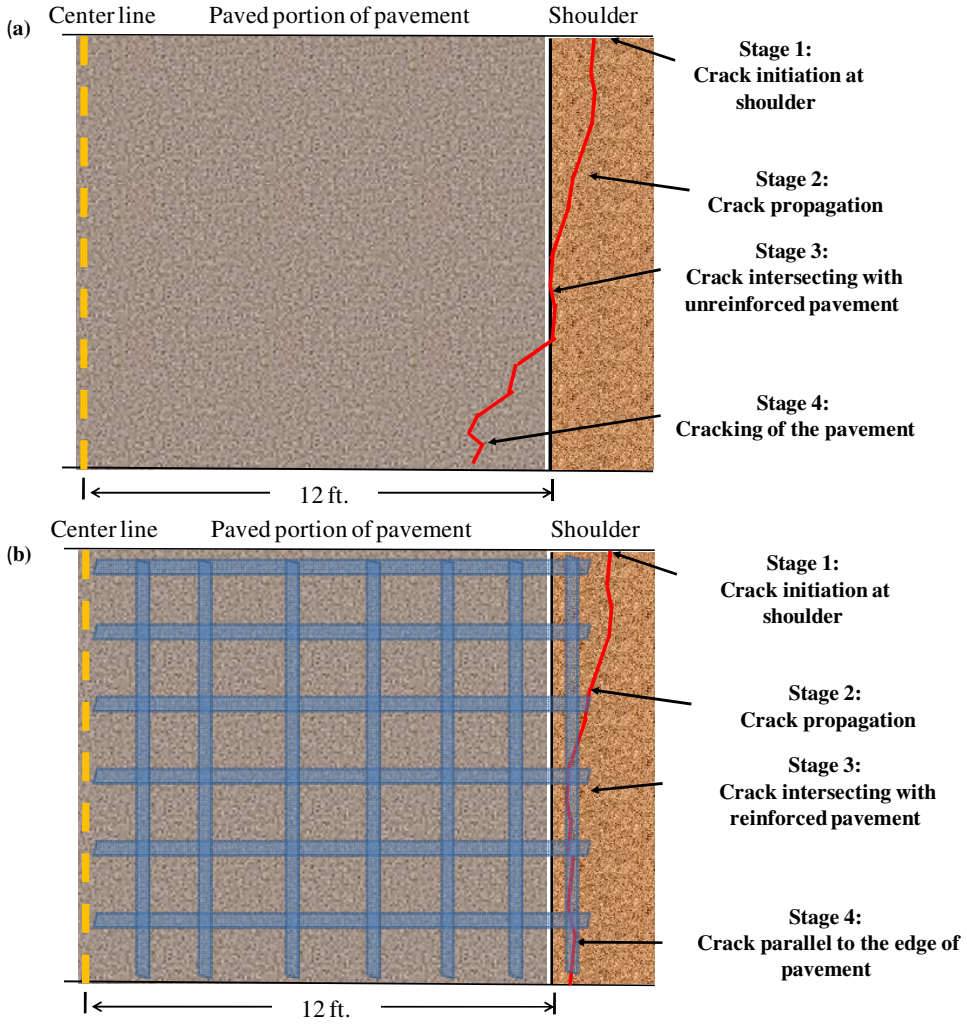

Figure 5.55 Stages in crack propagation (a) Unreinforced section (b) Reinforced section

5.6.3 Discussion

The field visual inspection was carried out to document the cracking pattern (origin and spreading) at the site. The longitudinal cracks were observed to originate from the edge of the pavement. Furthermore, the increased evidence of longitudinal cracking was found in the summer seasons. It was envisioned that as the dry front progressed from the edge of the pavement towards the center, the water content in the subgrade below was reduced causing it to shrink thereby opening the cracks. The results obtained by field visual inspection were related with the field moisture data collected from the installed sensors. Both the methods indicated that the zone of one meter close to the pavement edge was exposed to the maximum moisture fluctuation, causing severe distress and its subsequent cracking.

The comparative analysis for various categories of test sections was done. It was observed that in unreinforced sections the longitudinal cracks travelled inside the pavement causing it to crack whereas they remained parallel to the boundary of unpaved and paved portion of the road in the geosynthetic reinforced test sections. The cracking in the unreinforced sections was observed primarily in the edge portion of the pavement whereas the center of the pavement remained intact. It was concluded that the presence of geosynthetic prevented the cracks to enter the pavement. In the test sections, where lime treatment was used satisfactory performance was observed with localized distress zones. This was attributed to the non-uniform mixing of lime during the construction of the pavement and its depletion over time.

Therefore, based on the field visual inspection study it was concluded that there is seasonal moisture fluctuation below the pavement, but it is primarily limited to the edge of the pavement. Therefore, extending the geosynthetics towards the edge of the pavement was considered as a solution to prevent the spreading of such cracks. Finally, the geosynthetic reinforced test sections were found to be most effective in mitigating the longitudinal cracks than unreinforced and lime-stabilized test sections.

5.7 FIELD MONITORING USING FALLING WEIGHT DEFLECTOMETER

The use of geosynthetics in the flexible pavements not only helps to mitigate the longitudinal cracking due to environmental factors but also helps to reduce the maintenance cost of the pavement by reinforcing it structurally against traffic loading. During field visual inspection, distress due to traffic loading was observed in control sections having no geosynthetic reinforcement. Therefore, an attempt was made to quantify the benefits achieved by addition of geosynthetics and lime-stabilization to prevent distress caused in the flexible pavements by traffic loads. The performance of the test sections was compared with control section against the measured deflection for a known load applied to it using falling weight deflectometer (FWD). Therefore, FWD tests were done periodically at the site and the test sections response in terms of total deflection was documented.

Thus, this component of research study helped to obtain the field evidence in terms of difference in performance obtained by sections having lime stabilization and geosynthetic reinforcement compared to the control sections when they are subjected to traffic loads.

5.7.1 FWD testing details

FWD testing was conducted at FM 2 site to monitor the structural deterioration of the pavement over time. A total of eight field surveys were conducted after construction of the pavement. The surveys were conducted in February 2006, August 2006, November 2006, February 2007, April 2007, June 2007, May 2008, and February 2009. During each field trip all the test sections in both lanes of the pavement were tested. Each test section was 450 ft long and test was done at 50 ft interval thereby providing nine readings for each test section. Furthermore, the deflection readings were obtained for four load values of magnitude 6000 lbs, 9000 lbs, 11000 lbs and 15000 lbs at each point. These four readings were normalized to equivalent single axle load reading of 9000 lbs as shown in Figure 5.56a. The present analysis of the pavement was done assuming it as a linear system. The first deflectometer reading i.e., the deflection from the sensor closest to the

dropped weight is reported in the present analysis as it represented the response of the entire pavement section for the given load. The average readings for a group of four sections are as shown in Figure 5.56b. The section with lowest deflection for a give load was considered the stiffest and thus performing better than other sections. The details of the deflection profiles observed for different sections over time and their relative performance to each other are discussed.

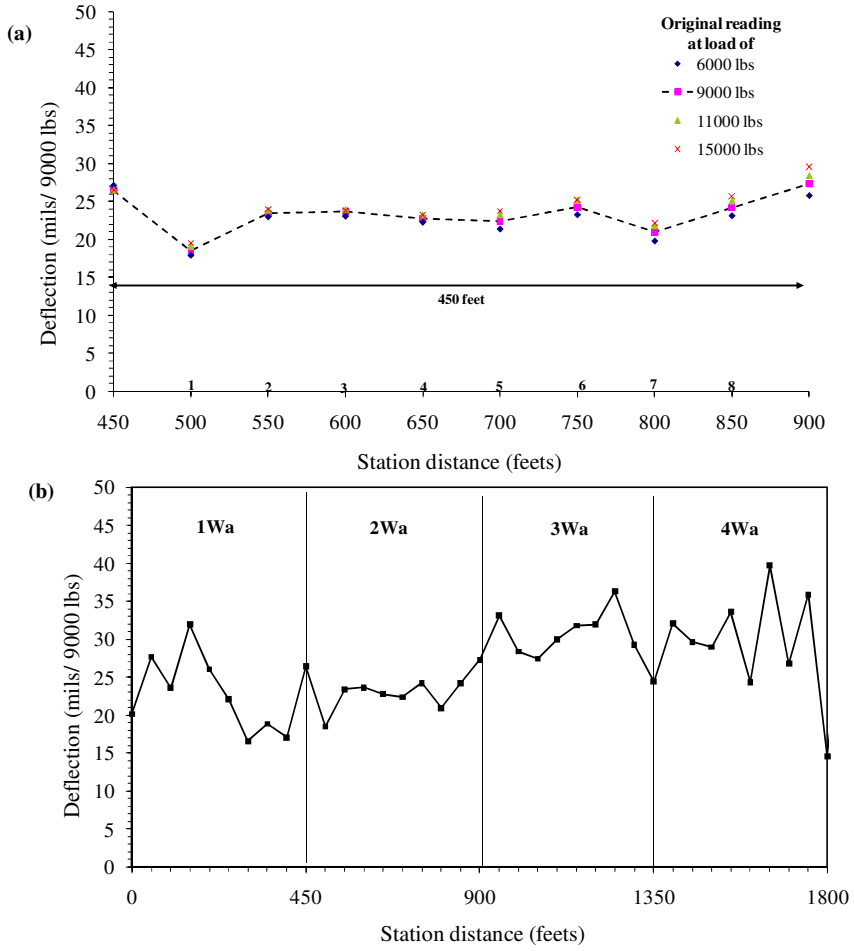

Figure 5.56 Analysis procedure adopted for FWD data analysis of a given field trip (a) Four load levels used at a section (b) Average deflection value for a series of test sections used to compare their relative performance

5.7.2 Performance of test sections

The response of the pavement sections for a given load in terms of deflection was measured using FWD tests. The details of test section were described in Section 5.4.6. During the field survey, preferential cracking was observed at east side of the pavement as compared to the west side of the pavement due to the location of the test sections. Furthermore, the sections located in the stations from 80+00 to 98+00 had different soil conditions than the main test sections located between stations 185+00 and 203+00. The deflections observed in these sections were considered to be influenced by the parameters not under the scope of the present study i.e., lime treatment and geosynthetic reinforcement and are not discussed in this research.

Therefore, for the present analysis, the performance of first eight sections i.e. 1Wa to 8Wa as shown in Figure 5.57 is discussed as they were supposed to have the uniform construction and traffic conditions. The sections were divided into four main groups: control section, no reinforcement section with lime treatment (three in numbers), and geosynthetic reinforced section with no lime treatment and geosynthetic reinforced lime treated sections (three in numbers).

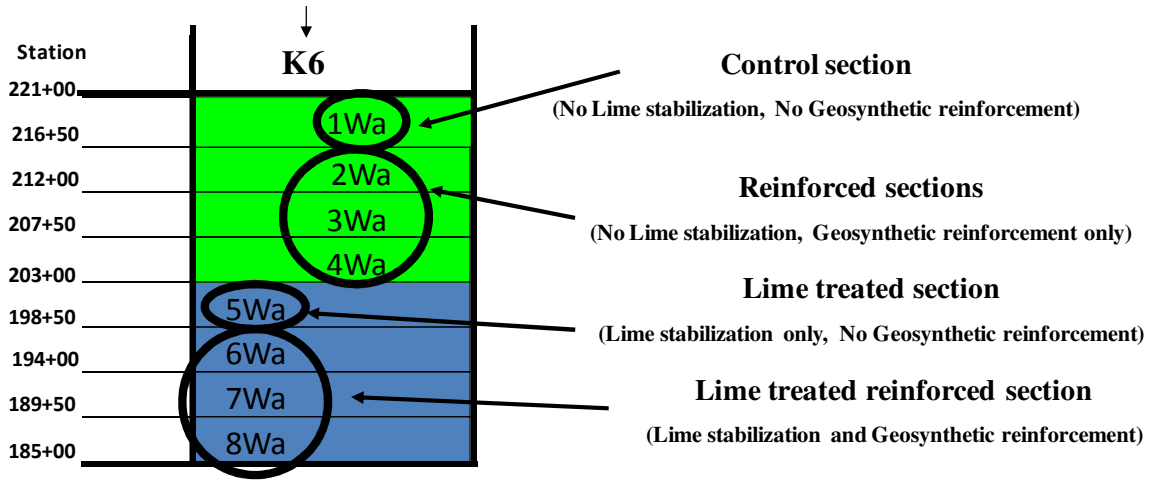

Figure 5.57 Test sections used in FWD analysis

Finally, for discussion purposes the data obtained from the field trips conducted in February 2006, i.e., immediately after construction of the pavement and the latest one conducted in February 2009 are reported. The deflection profiles for all the above four categories of test section are shown in Figure 5.58a through 5.58d. The deflections increased for all the test sections in the span of three years indicating the structural deterioration of the pavement with time. The test sections where the lime-treatment was used along with geosynthetic reinforcement, no significant change in deflections was observed over the given duration. Thus, for the given pavement this was considered as the best remedial measure to prevent its deterioration due to traffic loading. The performances of test sections relative to each other are compared in subsequent sections.

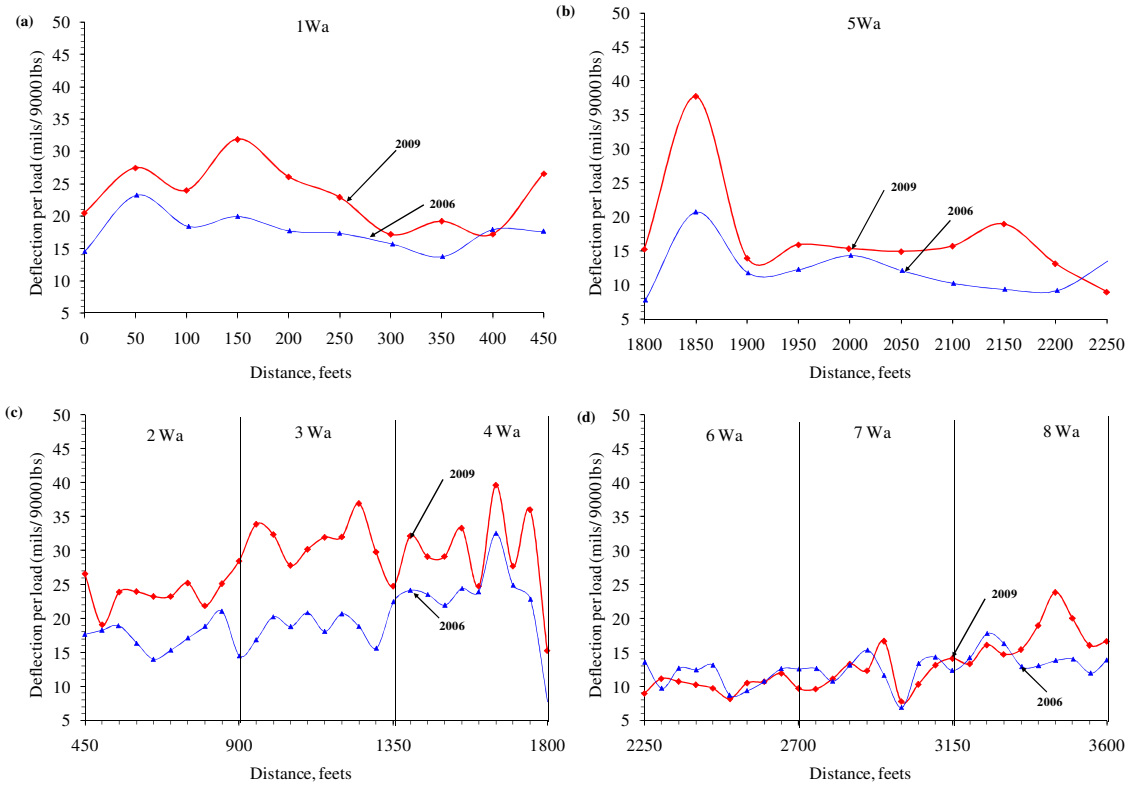

Figure 5.58 Deflection profile in February 2006 and 2009 (a) Control (b) Geosynthetic reinforced non lime stabilized (c) Lime stabilized unreinforced (d) Lime stabilized geosynthetic reinforced test sections

5.7.3 Comparison of test sections

The data obtained from the two field trip discussed above was compared among different test sections to quantify the benefit of using lime stabilization and geosynthetic reinforcement. Each test section of 450 feets was divided into 50 feet segment and the nine readings for each test section were plotted on the same scale. Moreover, the three readings in the middle of a given test section from 150 to 300 feets were considered to be the most representative of the test section as they were away from the overlapping boundary between different test sections. This system was used for the comparative analysis throughout this section.

5.7.3.1 Effect of lime stabilization

The performance of control section (1Wa) and lime stabilized section with no reinforcement (5Wa) was compared for field trips conducted in February 2006 and February 2009 as shown in Figure 5.59a and 5.59b respectively. The data indicated that the deflection obtained for section 5Wa were lower than section 1Wa for both the field trips. This indicated effectiveness of lime treatment in stiffening the pavement thereby reducing the deflection under traffic loading as compared to the control section.

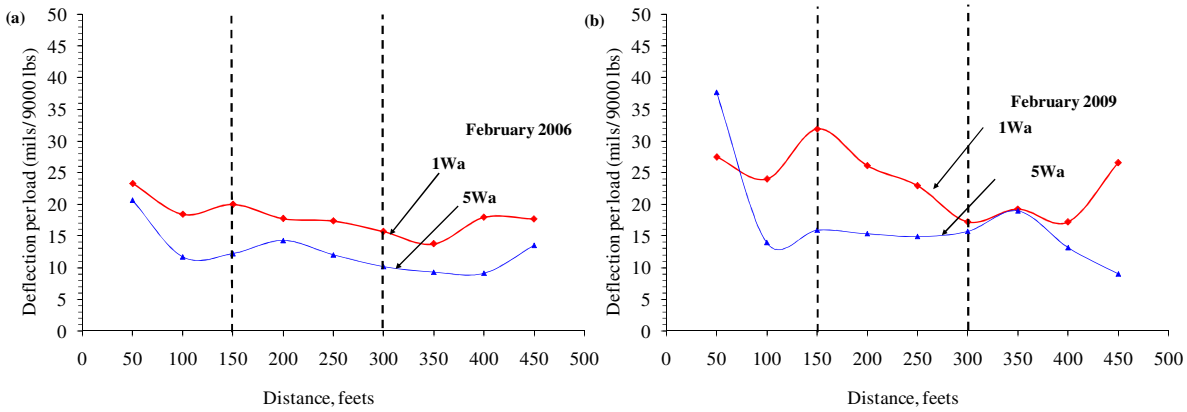

Figure 5.59 Deflection profile for control and lime stabilized unreinforced section for (a) February 2006 (b) February 2009

5.7.3.2 Effect of geosynthetic reinforcement

The performance of three geosynthetic reinforced non-lime treated test sections was compared for field trips conducted in February 2006 and February 2009 as shown in Figure 5.60a and 5.60b respectively. The data indicated that the total deflection obtained for section 2Wa reinforced with geosynthetic G1 was consistently lower than that for section 3Wa and 4Wa reinforced with geosynthetics G2 and G3 for both the field trips. The preliminary results based on limited field data obtained for first three years of monitoring the site has shown that the three geosynthetics have performed differently for a given pavement under similar traffic conditions. Still, more field data in terms of FWD deflections is required to make a final assessment of performance for these three test sections and identify the governing distress mode.

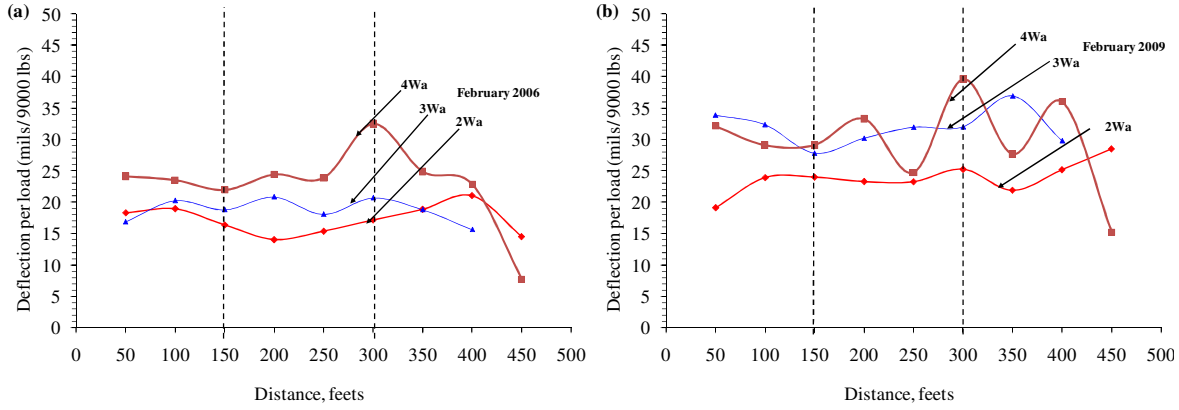

Figure 5.60 Deflection profile for three geosynthetic reinforced and non- lime stabilized sections for (a) February 2006 (b) February 2009

The notion of reinforcing pavement with any geosynthetic and achieving the desired benefits is incorrect. Furthermore, the field tests are expensive and time consuming, thus not conducted at regular basis in most of the reinforced pavement projects. Moreover, installing different geosynthetics and observing their performance for a year before constructing the pavement is not a feasible solution.

5.7.3.3 Effect of geosynthetic reinforcement and lime stabilization

The performance of three geosynthetic reinforced and lime-treated test sections was compared for field trips conducted in February 2006 and February 2009 as shown in Figure 5.61a and 5.61b respectively. The data indicated that the deflection obtained for these sections was lowest for all the given test sections as discussed earlier. Furthermore, all the three test sections had similar deflection profile immediately after the construction in February 2006. This indicated that in the initial part of the project significant benefit can be obtained by lime treating the pavement. Over the span of three years, the deflection of the pavement increased as indicated by results obtained in February 2009.

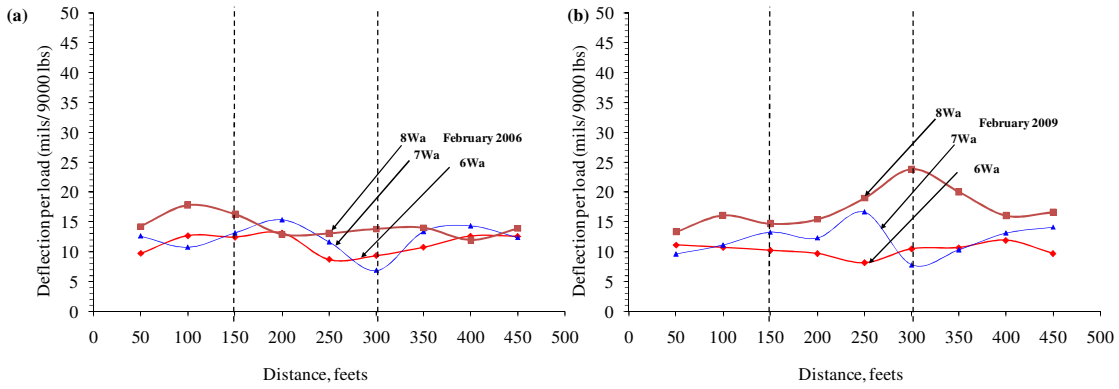

Figure 5.61 Deflection profile for three geosynthetic reinforced and lime stabilized sections for (a) February 2006 (b) February 2009

Furthermore, it was observed that the lime treated test section 6Wa reinforced with geosynthetic G1 had lower deflection than for section 7Wa and 8Wa reinforced with geosynthetics G2 and G3. The similar trend in the performance of three geosynthetics was observed when they were used without lime treatment as discussed in the previous section. However, as observed during the visual inspection the present results indicate that the lime treatment reduces in effectiveness over time and cannot be used as long term remediation strategy by itself. Thus, using lime stabilization along with geosynthetic reinforcement is an effective technique to increase the stiffness of the pavement thereby reducing its deflection under the traffic loads especially over expansive soils.

5.7.4 Discussion

The FWD testing was carried out to quantify the pavement response when it is subjected to traffic loads for the duration of the field study. The results obtained from FWD test done immediately after construction of the pavement in February 2006 were used as the baseline and compared with the latest field test done in February 2009. The results indicated increase in deflection for all the test sections over the span of three years. This showed that the pavement had structurally deteriorated under traffic loads.

The control section had the highest deflection of all the test sections. The lime-treated sections were observed to have stiffer response than non-lime treated sections, immediately after construction. Further, the effect of lime treatment reduced over the three years and increase in deflections was observed, though they were still less than the control section. When the lime treatment was used with geosynthetic reinforcement, the lowest deflections were observed in these test sections indicating it to be a better strategy for reinforcing the expansive soils. In addition to the above study, effect of geosynthetic reinforcement on pavement response was also evaluated. The three geosynthetic reinforced test sections had dissimilar response. Based on preliminary evidences collected so far, it was observed that the test sections reinforced with geosynthetic reinforcement G1 performed better than G2 and G3 independent of the use of lime stabilization in these test sections. The similar order of performance was observed based on laboratory pullout tests reported in terms of coefficient of soil-geosynthetic interaction for these geosynthetics as reported in Chapter 4.

Based on the field FWD testing it was concluded that there is deterioration of the pavement for traffic loading over the last three years. The lime stabilization may be used as a temporary measure but the geosynthetic reinforcement leads to increase in pavement stiffness over long duration of time. Moreover, different geosynthetics had different response and thus merely using reinforcement would not lead to desired results. Therefore, proper design is required while deciding to use lime stabilization or geosynthetic reinforcement or both for given traffic loads to increase the life span and reduce the maintenance cost for the flexible pavement.

5.8 CONCLUSIONS

The effectiveness of geosynthetics when they are used as reinforcement in base course of flexible pavements was evaluated in the present research study. The use of geosynthetics was also evaluated for their potential to mitigate the longitudinal cracks induced in the expansive subgrades. In the initial part, a hypothesis for mechanism of longitudinal crack formation and subsequent stress zone due to seasonal moisture fluctuation was proposed. Specifically, it was envisioned that cyclic wetting and drying of the pavement caused the swelling and shrinkage of the subgrade. This volumetric strain then imposed tensile and bending stresses under the pavement. The zone of increased stress was concentrated from the shoulder of the pavement till the point beneath the pavement at which moisture does not fluctuate. Therefore, differential movement occurred between the shoulders and the center of the road leading to longitudinal cracking that was closer to the edge of the pavement. This mechanism was independent of traffic loading and result in several pavement failures before their opening to traffic.

A comprehensive field investigation was done to gain evidence for the above proposed mechanism. A low volume farm to market road, FM-2 was used to construct 32 test sections consisting of control section and three different geosynthetic reinforced sections with and without lime stabilization with four repeats for each profile. The site was monitored for both environmental and traffic loading in the post construction phase. The site moisture monitoring involved installing sensors below the pavement to document the seasonal moisture fluctuations which was considered as an environmental load on the pavement. Furthermore, to document the pavement response for the traffic loading periodic FWD testing was done at the site. The data obtained from these sources was combined with field visual inspection observations to obtain the comprehensive picture of the pavement performance.

The results indicated a zone of 1m located both horizontally and vertically near the edge of the pavement which was most susceptible to the moisture fluctuation. Moreover, the cracks were observed to originate in the unpaved portion of the pavement. These cracks over the duration of three years slowly travelled towards the paved end of

the road. In case of unreinforced sections, they eventually entered the main pavement sections causing it to crack. For the geosynthetic reinforced sections these cracks were observed to remain parallel to the boundary of unpaved and paved portion. The lime stabilized sections also showed no significant signs of cracking. Furthermore, the FWD results indicated increased stiffness in all the lime stabilized sections when compared with the control section. Thus, lime treatment stiffened the pavement, but localized stress zones could still exist due to non-uniform mixing of the lime with the pavement soils. Since, it is easier to install geosynthetics in field than to place a lime-stabilized base course, it was considered as better alternative for improving pavements performance under traffic and environmental loading with same performance.

The three geosynthetics used in the case study were observed to have different performance under the given traffic loading. Based on the preliminary data obtained, the pavement sections reinforced with geosynthetic G1 were observed to perform better than those reinforced with geosynthetic G2 and G3. A laboratory pullout test was proposed to evaluate the performance of geosynthetics under confined conditions in Chapter 4. The coefficient of soil geosynthetic interaction (K_{SGI}) was evaluated for geosynthetics G1, G2 and G3. The performance order indicated in terms of K_{SGI} shows better correlation with preliminary field data than that predicted based on unconfined tensile strength values for these geosynthetics. The current state of practice when recommending a geosynthetic for pavement application involves evaluating its unconfined tensile strength. This practice does not necessarily quantify the geosynthetic performance under confined conditions in pavement. Therefore it is recommended that the behavior of geosynthetics under confinement and its interactions with surrounding soil should be evaluated to get an idea of its field performance.

Chapter 6: Summary and Conclusions

"If you want a happy ending, that depends, of course, on where you stop your story!"
Orson Welles

6.1 SUMMARY OF RESEARCH COMPONENTS

The goal of this study was to evaluate the primary mechanism of lateral restraint provided by geosynthetics when used for reinforcement purposes in the base course layer of flexible pavements. Analytical, experimental and field studies were conducted as part of this investigation in order to understand the variables governing the behavior of geosynthetics in reinforced pavements. Each component of research provided lessons which were useful for evaluating the performance for geosynthetics in the flexible pavements. These components complimented each other in providing a good understanding of reinforced flexible pavements which would be difficult to characterize using a single method of analysis.

Based on these research components, a new analytical model for determining the soil geosynthetic interaction at low displacement magnitudes and under pavement loading conditions was developed. This was followed by a new approach for conducting laboratory pullout test to measure soil-geosynthetic interface properties. The results of laboratory tests were then used to evaluate the proposed parameter values for various geosynthetics (geotextiles and geogrids). Finally, a field study was conducted to compare the performance of geosynthetics with the experimentally obtained parameter using the analytical model suggested in this research.

This study is expected to contribute towards a better understanding for the use of geosynthetics in reinforced flexible pavements by capturing the governing mechanism realistically using laboratory tests to provide a reasonable estimate of their field performance. The specific objectives of this study stated in the introduction were achieved by conducting following research components:

- An evaluative study of geosynthetic reinforced pavements (Chapter 2), which allowed for,
    - Identification of governing mechanism for the their improved performance over unreinforced pavements
    - Compilation of current laboratory, field, and numerical methods conducted to quantify this governing mechanism
    - Identification of limitations of current flexible pavement methodologies for incorporating geosynthetic into their design

- An analytical study of geosynthetic reinforced pavements (Chapter 3), which allowed for
    - Identifying a suitable test method to quantify the soil-geosynthetic interaction using a laboratory test
    - Compilation of current pullout test data interpretation techniques to quantify soil-geosynthetic interface properties
    - Development of a new simplified analytical model to predict soil-geosynthetic interface properties at low displacement magnitudes using pullout test results

- A laboratory study of geosynthetic reinforced pavements (Chapter 4), which allowed for,
    - Development of a new pullout test equipment capable of conducting test to obtain parameters as proposed by above model
    - Evaluation of assumptions made to derive the parameter for the analytical model using the new equipment
    - Evaluation of equipment boundary conditions and specimen dimensions on obtained value of parameters
    - Evaluation of parameter value for various type of geosynthetics (geotextile and geogrids) used for reinforcing pavements

- A field study of geosynthetic reinforced pavements (Chapter 5), which allowed for,
    - Evaluating the performance of geosynthetics used in laboratory study under actual field loading conditions
    - Comparison of field performance with laboratory predicted performance of these geosynthetics
    - Evaluation of benefit of using geosynthetics for preventing longitudinal cracking due to environmental loading along with their use as reinforcement for improving performance under traffic loading

The specific background information for each research component was presented in the individual chapters. The main conclusions for each component of this study are summarized in the subsequent sections.

6.2 CONCLUSIONS FROM EVALUATIVE STUDY

The contribution of geosynthetics to flexible pavements improved performance have been attributed to lateral restraint provided by the geosynthetics against the movement of base particles under wheel loading. This mechanism of lateral restraint has been studied using laboratory unconfined and confined geosynthetic tests.

- The unconfined tests do not take into account the soil interaction with the geosynthetic and were not recommended for use in the design of geosynthetic reinforced pavements.
- The confined geosynthetic cyclic tests reproduced the field wheel loading, thus better represent the governing mechanism. However, these tests have not been able to distinguish the performance among geosynthetics due to lack of repeatability of test results for a given geosynthetic. Also the variability in test results is high such that it has been difficult to distinguish performance of one geosynthetic from another.

Based on this review, it was decided to focus the present research effort in the area of laboratory testing involving confined setting with monotonic loading to quantify the interface mechanism between soil and geosynthetic realistically and in repeatable manner for various geosynthetics.

6.3 CONCLUSIONS FROM ANALYTICAL STUDY

In this research, a new solution to the governing differential equation for a geosynthetic confined in pullout box was proposed to capture small displacement behavior for application to pavement design. The model was called soil geosynthetic interface (SGI) model.

- The model relies on two parameters which are the yield shear stress (τ_y) and confined stiffness (J_c) of the system.
- The model predicts a unique confined force-displacement relationship for a given soil-geosynthetic system for the applied normal pressure on the interface.
- A coefficient of soil-geosynthetic interaction (K_{SGI}) was defined based on proposed model. The constant K_{SGI} combined both the model parameters in a single framework.

6.4 CONCLUSIONS FROM LABORATORY STUDY

Laboratory pullout equipment was developed to validate the SGI model. The bounds on the value of K_{SGI} value for a given soil-geosynthetic at a given normal pressure were established by conducting tests in the modified pullout box equipment.

- K_{SGI} value was dependent on the specimen length, specimen width, normal pressure and type of geosynthetic used in the pullout test.
- Based on the pullout test results, performance order for the four geosynthetics tested using new pullout equipment was established.
- Based on results it was shown that the laboratory pullout testing is a useful tool to investigate the soil-geosynthetic interaction mechanisms for the reinforced pavements.

6.5 CONCLUSIONS FROM FIELD STUDY

To quantify the actual performance of geosynthetics, a comprehensive field investigation study was done to on a low volume farm to market road, FM-2 where 32 test sections consisting of control section and three different geosynthetic reinforced sections with and without lime stabilization with four repeats for each profile were constructed. The site was monitored for both environmental and traffic loading in the post construction phase, in terms of moisture sensors, visual inspection and FWD testing.

- The addition of geosynthetic in the pavement led to reduced deflections as observed from analysis of FWD test results conducted over span of three years.
- The addition of geosynthetics led to reduction in longitudinal cracks based on visual inspection of unreinforced and reinforced sections.
- It was found that lime treatment stiffened the pavement, but localized stress zones still existed due to non-uniform mixing of the lime with the pavement soils.
- Based on the preliminary field investigations, the three geosynthetics used in the case study were observed to have different performance under the given traffic loading. The pavement sections reinforced with geosynthetic G1 were observed to perform better than those reinforced with geosynthetic G2 and G3.
- The performance observed in the field testing was similar to that predicted based on the laboratory pullout testing in terms of K_{SGI} value.

This provided evidence for validity of the laboratory pullout testing approach when accompanied with the analytical model to effectively quantify the governing mechanism of lateral restraint at low displacement magnitudes.

6.6 RECOMMENDATIONS FOR FUTURE RESEARCH

The findings from this research helped in establishing a laboratory method which can be used to quantify the governing mechanism of geosynthetic reinforced pavements based on the proposed analytical model. The quantitative laboratory performance of various geosynthetics was compared with the qualitative response obtained from the field

tests sections. The research which may be helpful to advance our understanding in these areas is as follows:

1. An analytical model which can solve the differential equation with appropriate boundary conditions incorporating bi-linear shear stress distribution and non-linear confined stiffness will be useful to represent the geosynthetic conditions under confinement realistically.
2. The laboratory pullout tests should be carried out with actual pavement soils, specifically, base-course material to compute the parameter obtained in this research. Furthermore, a design methodology incorporating this parameter for flexible pavement design should be developed.
3. New pullout test equipments which are smaller than the ASTM recommended size should be used to obtain the proposed parameter. This would help to reduce the testing time and use the test as an index for easy comparison of various geosynthetics to be in used in a project.
4. Field test sections should be constructed for controlled loading conditions so the effect of geosynthetics under traffic loads can be quantified clearly. Similarly, attempts should be made to conduct moisture migration studies on geosynthetic reinforced pavements independent of the traffic loads.
5. FEM and DEM models which can incorporate the mechanism of lateral restraint in pavements should be developed to better understand the soil-geosynthetic interaction at low strain magnitudes.

References

Abdelouhab, A., Dias, D. Freitag, N. and Bennani, Y., (2008), "Pullout Tests Analytical Modeling to deduce the Constitutive Soil-Reinforcement Interface Behavior", Paper No. 63, 4th European Conference on Geosynthetics, EuroGeo4, Edinburgh

Abramento, M. and Whittle, A.J., (1995), "Analysis of Pullout Tests for Planar Reinforcements in Soil", Journal of Geotechnical Engineering, Vol. 121, No. 6, pp. 476-485

Abusaid, A.H. (2006) "Development of a Method to Test Geogrid Reinforcement of Base Materials in Flexible Pavements" M.S. Thesis, Department of Civil Engineering, The University of Texas at Austin

Alfaro, M.C., Miura, N. and Bergado, D.T., (1995), "Soil-geogrid Reinforcement Interaction by Pullout and Direct Shear Tests", Geotechnical Testing Journal, 18, 157-167

Alobaidi, I.M, Hoare, D.J. and Ghataora, G.S., (1997), "Load Transfer Mechanism in Pullout tests", Geosynthetics International, Vol. 4, No. 5, pp. 509-521

Al-Qadi, I.L (2006), "Pavement Interlayer System Mechanisms: Separation Reinforcement and Reflective Cracking Control" Lecture, Chinese Society of Pavement Engineering, Taipei, Taiwan, June 2, 2006

Al-Qadi, I.L., Brandon, T.L., and Bhutta, A., (1997), "Geosynthetic Stabilized flexible pavements, " Proceedings of geosynthetics 97, IFAI, Vol. 2, Long Beach, California, pp.647-662

Al-Qadi, I.L., Brandon, T.L., Valentine, R.J., Lacina, B.A. and Smith, T.E., (1994), "Laboratory Evaluation of Geosynthetic Reinforced Pavement Sections", Transportation Research Record 1439, pp. 647-662

Al-Qadi, I.L., Dessouky, S.H., Kwon J. and Tutumluer, E. (2008), "Geogrids in Flexible Pavements: Validated Mechanisms", Transportation Research Record, Journal of the Transportation Research Board, No. 2045, Transportation Research Board of the National Academies, Washington, D.C., 2008. pp. 102-109

American Association of State Highway and Transportation Officials, (1993), "AASHTO Guide for Design of Pavement Structures", Washington, DC USA

Anderson, P. and Killeavy, M, (1989), "Geotextiles and Geogrids: Cost Effective Alternate Materials for Pavement Design and Construction", Proceedings of Geosynthetics '89, IFAI, Vol. 2, Sand Diego, California, USA, February 1989, pp. 353-360

ASTM D2488 (2001), "Standard Practice for Description and Identification of soils (Visual-Manual Procedure)", American Society for Testing and Materials, West Conshohocken, PA

ASTM D35 (1995), "ASTM Standards on Geosynthetics", sponsored by ASTM Committee D-35 on Geosynthetics, Fourth Edition, 178p

ASTM D422 (2007), "Standard Test Method for Particle-Size Analysis of Soils", American Society for Testing and Materials, West Conshohocken, PA

ASTM D4318 (2001), "Standard Test Methods for Liquid Limit, Plastic Limit and Plasticity Index of Soils", American Society for Testing and Materials, West Conshohocken, PA

ASTM D4595 (2001), "Standard Test Method for Tensile Properties of Geotextiles by the Wide-Width Strip Method", American Society for Testing and Materials, West Conshohocken, PA

ASTM D4632 (2008), "Standard Test Method for Grab breaking load and elongation of Geotextiles", American Society for Testing and Materials, West Conshohocken, PA

ASTM D5311 (2004), "Standard Test Method for Load Controlled Cyclic Triaxial Strength of Soil", American Society for Testing and Materials, West Conshohocken, PA

ASTM D5617 (2004), "Standard Test Method for Multi-axial Tension test for Geosynthetics", American Society for Testing and Materials, West Conshohocken, PA

ASTM D6337 (2009), "Standard Test Method for Determining Tensile Properties of Geogrids by the Single or Multi-rib Tensile Method", American Society for Testing and Materials, West Conshohocken, PA

ASTM D6706 (2003), "Standard Test Method for Measuring Geosynthetic Pullout Resistance in Soil", American Society for Testing and Materials, West Conshohocken, PA

ASTM D698 (2001), "Standard Test Methods for Laboratory Compaction Characteristics of Soil Using Standard Effort (12400 ft-lbf/ft^3 (600 kN-m/m^3))", American Society for Testing and Materials, West Conshohocken, PA

ASTM D854 (2007), "Standard Test Methods for Specific Gravity of Soil Solids by Water Pycnometer", American Society for Testing and Materials, West Conshohocken, PA

Barker, W.R., (1987), "Open-Graded based for Airfield Pavements", Technical report GL-87-16, U.S. Army Corps of Engineers, Waterways Experiment Station, Vicksburg, Mississippi, USA, 76p

Barksdale, R.D., Brown, S.F. and Chan, F. (1989), "Potential Benefits of Geosynthetics in Flexible Pavement System", National Cooperative Highway Research Program, Report No. 315, Transportation Research Board, Nation Research Council, Washington, DC

Bathurst, R.J. (2007) "Geosynthetics Classification". IGS Leaflets on Geosynthetics Applications, IGS Education Committee, *at www.geosyntheticssociety.org*.

Bay, J.A., and Stokoe, K.H. (1998), "Development of a Rolling Dynamic Deflectometer for Continuous Deflection Measurements of Pavements," Center of Transportation Research, Report 1422-3F, University of Texas, Austin, TX. 1998.

Bender, D.A. and Barnberg, E.J, (1978), "Design of soil-fabric-aggregate systems", Transportation Research Record 671, pp 64-75

Benjamin, C.V.S., Bueno, B., Zornberg, J.G., (2007), "Field Monitoring Evaluation of Geotextile-Reinforced Soil Retaining Walls", Geosynthetics International Journal, April, Vol. 14, No. 1

Berg, R.R., Christopher, B.R. and Perkins, S.W. (2000), "Geosynthetic reinforcement of the aggregate base/subbase courses of flexible pavement structures-GMA white paper II", Geosynthetic Materials Association, Roseville, MN, USA, 176p.

Bergado, D.T., Teerawattanasuk, C., (2008), "2D and 3D numerical simulations of reinforced embankments on soft ground", Geotextiles and Geomembranes 26(1), 39–55

Bonaparte, R., Holtz, R.D., and Giroud, J.P., (1987), "Soil reinforcement using Geotextiles and Geogrids", Geotextile Testing and the Design Engineer, ASTM STP 952, J.E. Fluet, Jr., Ed., American Society for Testing and Materials, Philadelphia, 1987, pp. 69-116

Bray, J.D. and Merry, S.M., (1999), "A comparison of the response of geosynthetics in the multi-axial and uniaxial test devices", Geosynthetics International, Vol.6, No. 1, pp. 19-40

Brown, S.F., Jones, C.P.D. and Brodrick, B.V., (1982), " Use of Non-Woven fabrics in permanent road pavements", Proceedings of the Institution of Civil Engineers, part 2, Vol. 73, pp. 541-563

Bueno, B.S., Benjamin, C.V., and Zornberg, J.G. (2005), "Field Performance of a Full-scale Retaining Wall Reinforced with Non-woven Geotextiles", Slopes and Retaining Structures under Seismic and Static Conditions, ASCE Geotechnical Special Publication No. 140, January 2005, Austin, Texas (CD-ROM)

Bueno, B.S., Costanzia, M.A., and Zornberg, J.G. (2005), "Conventional and Accelerated Creep Tests on Nonwoven Needle-punched Geotextiles", Geosynthetics International, December, Vol. 12, No. 6, pp. 276-287

Burd, H.J and Houlsby, G.T. (1986), "A Large Strain Finite Element Formulation for One Dimensional Membrane Elements", Computers and Geotechnics, Vol. 2, pp. 3-22

Burd, H.J. and Brocklehurst, C.J. (1990), "Finite element studies of the mechanics of reinforced unpaved roads", Proceedings of the 4th International conference on

Geotextiles, Geomembranes and Related Products, The Hague, Netherlands, pp. 217-221

Cancelli, A., Montanelli, F., Rimoldi, P. and Zhao, A., (1996), "Full scale laboratory testing on Geosynthetic reinforced paved roads", Earth Reinforcement, Ochiai, H., Yasufuku, N., and Omine, K., Editors, Balkema, , Proceeding of the International Symposium on Earth Reinforcement, Fukuoka, Kyushu, Japan, November 1996, pp. 573-578

Chang, J.C., Hannon, J.B., Forsyth, R.A., (1977), "Pullout resistance and interaction of earthwork reinforcement and soil", Transportation Research Record, 640, National Research Council, Washington D.C. pp. 1-7

Christopher, B.R., Holtz, R.D., and Bell, W.D. (1986), "New tests for determining the In-Soil Stress-Strain properties of Geotextiles", Proceedings of 3rd International Conference on Geotextiles, Vol. 3, Vienna, pp. 683-688

Collin, J.G., Kinney, T.C. and Fu, X., (1996), "Full scale highway load test of flexible pavement systems with geogrid reinforced base courses", Geosynthetics International, Vol. 3, No. 4, pp. 537-549

Cuelho, E.L. and Perkins, S.W., (2005), "Resilient interface shear modulus from short-strip cyclic pullout tests", GSP-140, Slopes and retaining structures under seismic and static conditions, Geofrontiers, Austin, TX

Decagon Devices, (2006), "ECH_20 Dielectric Probes vs. Time Domain Reflectometry (TDR)", Application Note

Dondi, G. (1994), "Three-Dimensional Finite Element Analysis of a Reinforced paved Road", Proceedings of the Fifth International Conference on Geotextiles, Geomembranes and Related Products, Singapore, pp. 95-100

Dougan, Charles (2007), "Mechanistic-Empirical Pavement Design Guide: project Level pavement management" Lecture Session 1a: PMS to support New MEPDG Norfolk, VA, May 7, 2007

Edil, T.B., Kim, W-H., Benson, C.H., Tanyu, B.F., (2007), "Contribution of geosynthetic reinforcement to granular layer stiffness", GSP 169, Soil and Material inputs for Mechanistic-Empirical Pavement Design, Geo Denver 2007, ASCE

Elias, V., Christopher, B.R. and Berg, R.R., (2001), "Mechanically stabilized earth walls and reinforced soil slopes design and construction guidelines", National Highway Institute (NHI), Course No 132042, Report No FHWA-NHI-00-043, 394p

Elias, V., Zehong, Y., Swan, R.H. and Bachus, R.C., (1998), "Development of protocols for confined extension and creep testing of geosynthetics for highway applications", FHWA-RD-97-143, Final report, 201 p.

Fanin, R.J. and Sigurdsson, O., (1996), "Field observations on the stabilization of unpaved roads with geosynthetics", ASCE Journal of Geotechnical Engineering, Vol. 122(7), 544-553

Fannin, R.J. and Raju, D.M., (1993), "Large scale pullout test results on geosynthetics", Proceedings of Geosynthetics ′93 Conference, Vol. 2, Vancouver, Canada, pp. 633-643

Farrag, K., Yalcin A.B., and Juran, I., (1993), "Pull-Out Resistance of Geogrid Reinforcements", Geotextiles and Geomembranes, Vol. 12, 133-159

Ferreira J.A.Z., Bueno, B.S. and Zornberg J.G., (2008), "Pavement reinforcement study using small dimensional pullout equipment", 1st Pan American Geosynthetics Conference, Geoamericas 2008, Cancun, Mexico 2-5 March, 2008

Finnefrock, L.T. (2008) "Bending stiffness index test for geogrid reinforcement of pavement base course material" M.S. Thesis, Department of Civil Engineering, The University of Texas at Austin

Ghionna, V. N., Moraci, N., and Rimoldi, P., (2001), "Experimental evaluation of the factors affecting pull-out test results on geogrids", Proceedings of International Symposium: Earth Reinforcement, Fukuoka, Japan

Giroud, J.P. and Noiray, L., (1981), "Geotextile-Reinforced Unpaved Roads", Journal of Geotechnical Engineering Division, American Society of Civil Engineers, Vol. 107, No GT9, pp. 1233-1254.

Giroud, J.P., Ah-Line, C., and Bonaparte, R., (1984), " Design of unpaved roads and trafficked areas with geogrids," Polymer Grid Reinforcement: A conference sponsored by SERC and Netlon, Ltd., Thomas Telford, London, England, pp. 116-127

Gupta, R., McCartney, J.S., Nogueira, C.L. and Zornberg, J.G., (2008), "Moisture migration in geogrid reinforced expansive subgrades", Geoamericas 2008, Cancun, Mexico

Halliday, A.R. and Potter, J.F., (1984), "The performance of a flexible pavement constructed on a strong fabric", Transport and Road Research Laboratory, Report 1123, Crowthorne, Berkshire, United Kingdom, 15p

Han, J., Zhang, Y., and Parsons, R.L, (2008), "Development of a performance-based laboratory test method for evaluating geosynthetic-soil confinement", Geosynthetics Committee (AFS70) TRB 2008 Annual meeting, Washington DC

Hayashi, S., Alfaro, M.C., and Watanbe, K., (1996), "Dilatancy effects of granular soil on the pullout resistance of strip reinforcement", Proceedings of the International Symposium: Earth Reinforcement, Fukuoka, Kyushu, Japan, pp. 39–44

Holtz, R.D, Christopher, B.R. and Berg, R.R, (1998), "Geosynthetic Design and Construction Guidelines", U.S. Department of Transportation, Federal Highway Administration, Washington, DC, FHWA-HI-98-038, 460 p

Hsieh, C. and Mao, L. (2005), "A bench-scale performance test for evaluation of the geosynthetic reinforcement effects on granular base courses", GRI-18 Geosynthetics Research and Development in Progress, Geofrontiers, Austin, TX

Huang, Y.H. (1993). Pavement analysis and design, Prentice-Hall, Englewood Cliff, NJ

Hugo, F., McCullough B.F., and Vander Walt B.(1991), "Full-scale accelerated pavement testing for the Texas State Department of Highways and Public Transportation",

Transportation Research Record 1293, Transportation Research Board, National Research Council, Washington, D.C., 1991, pp. 52-60

Ingold, T.S. (1983), "Laboratory pull-out testing of grid reinforcement in sand", Geotechnical Testing Journal, 6 (3), 101-111

Jewell, R.A. (1981), "Some effects of reinforcement on soils", PhD. Thesis, University of Cambridge, UK

Johnston, R.S. and Romstad, K.M., (1989), "Dilation and boundary effects in large scale pull-out tests ", 12th International Conference on soil Mechanics and Foundation Engineering, Rio de Janeiro, Brazil, Vol. 2, 1263-1266

Juran, I. and Chen, C.L., (1988), "Soil-Geotextile Pull-Out Interaction Properties: Testing and Interpretation", Transportation Research Record 1188, 37-47

Kinney, T.C. and Yuan, X. (1995), "Geogrid aperture rigidity by in-plane rotation", Proceedings of Geosynthetics 1995, pp 525-537

Koerner, R.M. (2005). Designing With Geosynthetics, 5th Edition, Prentice-Hall Inc., Englewood Cliffs, NJ, 1998, 796 p

Konietzky, H., Kamp L., Groeger, T. and Jenner, C, (2004), "Use of DEM to model the interlocking effect of geogrids under static and cyclic loading", International PFC symposium 28-29 October, 2004, Kyoto, Japan, pp. 3-12

Kupec, J. and McGown, A. (2004), "The load-strain behavior of biaxial geogrids", Proceedings of 3rd Asian Regional Conference on Geosynthetics, Seoul, South Korea, pp. 349-356

Kwon, J., Tutumluer, E. and Kim, M. (2005), "Development of a mechanistic model for geosynthetic-reinforce flexible pavements", Geosynthetics International, Vol. 12, No. 6, 310-320

Kwon, J., Tutumluer, E. and Konietzky, H. (2008), "Aggregate base residual stress affecting geogrid reinforced flexible pavement response", International Journal of Pavement Engineering, Vol. 9, No. 4, August, 2008, pp. 275-285

Li, C., (2005), "Mechanical Response of Fiber-Reinforced Soil", Ph.D. Dissertation, the University of Texas at Austin, Texas, USA

Ling H.I, Wu, J.T.H. and Tatsuoka, F., (19920, "Short-term strength and deformation characteristics of Geotextiles under typical operational conditions", Geotextiles and Geomembranes, 11 (2), 185-219

Lopes, M.L. and Ladeira, M. (1996), "Influence of the confinement, soil density and displacement ratio on soil-geogrid interaction", Geotextiles and Geomembranes, 14(10), 543-554

Madhav, M.R., Gurung, N. and Iwao, Y., (1998), "A Theoretical Model for the Pull-Out Response of Geosynthetic Reinforcement", Geosynthetics International, Vol. 5, No. 4, pp. 399-424

McDowell, G.R., Harireche, O., Konietzky H., Brown, S.F., and Thom, N.H. (2006), "Discrete element modeling of geogrid-reinforced aggregates", Proceedings of

the Institution of Civil Engineers, Geotechnical Engineering 159, January 2006, Issue GE1, pp.35-48

McGown, A., Andrawes, K.Z. and Al-Hasani, M.M., (1978), "Effect of Inclusion Properties on the Behavior of Sand", Geotechnique, Vol. 28, No. 3, pp. 327-346

McGown, A., Kupec, J. Heerten, G. and Maubeuge K. von, (2005), "Testing biaxial geogrids for specification and design purposes", GRI-18 Geosynthetics research and development in progress, ASCE, Austin, Texas

Miller, J.S. and Bellinger, W.Y., (2003), "Distress Identification Manual for the Long-Term Pavement Performance Program, Fourth Revised Edition", Report No. FHWA-RD-030031, June 2003, 164p

Miura, N., Sakai, A., Taesiri, Y., Yamanouchi, T. and Yasuhara, K., (1990), "Polymer grid reinforced pavement on soft clay grounds", Geotextiles and Geomembranes, Vol. 9, No. 1, pp. 99-123

Moghaddas-Nejad, F. and Small, J.C., (1996), "Effect of geogrid reinforcement in model track tests on pavements", Journal of Transportation Engineering, Vol. 122, No. 6, pp. 468-474

Moraci, N., Romano, G., and Montanelli, F., (2004), "Factors affecting the interface apparent coefficient of friction in pullout conditions" 3rd European Geosynthetics Conference, Vol. 1, Monaco, pp. 313-318

NCHRP (2000), NCHRP Project 1-28A, Harmonized Test Methods for Laboratory Determination of Resilient Modulus for Flexible Pavement Design, Volume 1, Unbound Granular Material, 198p

Muench, S., (2006), *http://pavementinteractive.org/index.php?title=Image:Hma.jpg*

NCHRP (2004), NCHRP Project 1-37A, Guide for Mechanistic-Empirical Design of new and rehabilitated pavement structures, Washington, D.C.

Ochiai, H., Otani, J., Hayashic, S., and Hirai, T., (1996), "The pullout resistance of geogrids in reinforced soil", Geotextiles and Geomembranes, Vol. 14, 19-42

Olidis, C. and Hein, D. (2004), "Guide for Mechanistic-Empirical Design of New and Rehabilitated Pavement Structures: Material Characterization." Annual Conference of the Transportation Association of Canada, Quebec City, Quebec

Palmeira, E.M. (1987), "The study of soil-reinforcement interaction by means of large scale laboratory tests" PhD. Thesis, University of Oxford, UK, 238p

Palmeira, E.M. (2004), "Bearing force mobilization in pullout tests on geogrids", Geotextiles and Geomembranes, 22 (6), 481-509

Palmeira, E.M. (2008), "Soil-geosynthetic interaction: Modeling and Analysis", Mercer Lecture, presented at 4th European Conference on Geosynthetics-EuroGeo4, Edinburgh 2008

Palmeira, E.M. and Milligan, G.W.E., (1989), "Large scale direct shear tests on reinforced sand", Soils and Foundations, 29(1), 18-30

Palmeira, E.M. and Milligan, G.W.E., (1989), "Scale and other factors affecting the results of pull-out tests of grid buried in sand", Geotechnique, 11 (3), 511–524

Perkins, S.W (2002), “Evaluation of Geosynthetic Reinforced Flexible Pavement systems using two Pavement Test facilities”, Final report, FHWA/MT-02-008/20040, Federal Highway Administration, Washington DC, 120p

Perkins, S.W. (1999), “Geosynthetic reinforcement of flexible pavements: laboratory based pavement test sections”, U.S. Department of Transportation, Federal Highway Administration, Washington DC, Report No. FHWA/MT-99/8106-1, 140p

Perkins, S.W. (1999), “Mechanical Response of Geosynthetic-Reinforced Flexible pavements”, Geosynthetics International, Vol. 6, No. 5, pp. 347-382

Perkins, S.W. (2001), “Numerical Modeling of Geosynthetic Reinforced Flexible Pavements”, Final report, FHWA/MT-01-003/99160-2, 97p

Perkins, S.W. and Cortez, E.R. (2005), “Evaluation of base-reinforced pavements using a heavy vehicle simulator”, Geosynthetic International, Vol. 12, No.2, pp. 86-98

Perkins, S.W. and Cuelho, E.V., (1999), “Soil-geosynthetic interface strength and stiffness relationships from pullout tests” Geosynthetics International, 6(5), 321-346

Perkins, S.W. and Edens, M.Q (2002), “Finite element and distress models for geosynthetic reinforced pavements”, International Journal of Pavement Engineering, Vol. 3, No. 4, pp. 239-250

Perkins, S.W. and Ismeik, M., (1997a), "A Synthesis and Evaluation of Geosynthetic Reinforced Base Course Layers in Flexible Pavements: Part I Experimental Work," Geosynthetics International, Vol. 4, No. 6, pp. 549-604.

Perkins, S.W. and Ismeik, M., (1997b), "A Synthesis and Evaluation of Geosynthetic Reinforced Base Course Layers in Flexible Pavements: Part II Analytical Work," Geosynthetics International, Vol. 4, No. 6, pp. 605-621

Perkins, S.W. and Svanø, G. (2004), “ Assessment of interface shear growth from measured geosynthetic strains in a reinforced pavement subject to repeated loads”, In Compendium of Papers CD-ROM, 83rd Transportation Research Board (TRB) Annual Meeting, Washington, DC, 2004

Perkins, S.W., Bowders J.J, Christopher, B.R., and Berg, R.R. (2005), “Advances in geosynthetic reinforcement in pavement systems”, Geofrontiers, Austin, TX

Perkins, S.W., Christopher, B.R., Cuelho, E.L., Eiksund, G.R., Hoff, I., Schwartz C.W., Svanø, G. and Want, A., (2004), “Development of design methods for geosynthetic reinforced flexile pavements”, FHWA-DTFH61-01-X-00068, Final report, 263p.

Raju, D.M. (1995), “Monotonic and cyclic pullout resistance of geosynthetics”, PhD. Thesis, University of British Columbia, Canada

Reck, N.C. (2009), “Mechanistic empirical design of geogrid reinforced paved flexible pavements”, Jubilee symposium on Polymer Grid Reinforcement, Institute of Civil Engineers, London, England

Rowe, R.K. and Mylleville, B.L.J. (1994), "Analysis and Design of Reinforced Embankments on Soft or Weak Foundations", Chapter 7 in Soil Structure Interaction: Numerical Analysis and Modeling, (Ed.) J. Bull, E and F.N. Spon (Chapman & Hall), pp. 231-260

Shukla, S.K. (2002), Geosynthetics and their application, 1st edition, Thomas Telford Ltd., 425 p

Sieira, A.C.C.F. Gerscovich, D.M.S., Sayao, A.S.F.J., (2009), "Displacement and load transfer mechanisms of geogrids under pullout condition", Geotextiles and Geomembranes, Vol. 27, pp. 241-253

Sobhi, S. and Wu, J.T.H., (1996), "An Interface Pullout Formula for Extensible Sheet Reinforcement", Geosynthetics International, Vol. 3, No. 5, pp. 565-582

Sprague, C.J, Lothspeich, S., Chuck, F., and Goodman, R., (2004), "Geogrid reinforcement of road base aggregate-measuring the confinement benefit", Proceedings of Geo-Trans 2004 Conference, Los Angeles, 2004, 996 -1005

Sugimoto, M., Alagiyawanna, A.N.M. and Kadoguchi, K. (2001), "Influence of rigid and flexible face on geogrid pullout tests", Geotextiles and Geomembranes, 19(5), 257-277

Sugimoto, M., and Alagiyawanna, A.N.M., (2003), "Pullout behavior of Geogrid by Test and Numerical Analysis", Journal of Geotechnical and Geoenvironmental Engineering, Vol. 129, No. 4, April 1, 2003, pp. 361-371

Teixeira, S.H.C. (1999), " Construction and calibration of a large pullout test device", M.S. Thesis, Department of Geotechnical Engineering, Engineering School of Sao Carlos, University of Sao Paulo (in Portuguese)

Teixeira, S.H.C. (2003), "Estudo da interação solo-geogrelha em testes de arrancamento e a sua aplicação na análise e dimensionamento de maciços reforçados", PhD. dissertation, Department of Geotechnical Engineering, Engineering School of Sao Carlos, University of Sao Paulo (in Portuguese)

Teixeira, S.H.C., Bueno, B.S. and Zornberg, J.G., (2007), "Pullout Resistance of Individual Longitudinal and Transverse Geogrid Ribs", Journal of Geotechnical and Geoenvironmental Engineering, Vol. 133, No. 1, January 1, 2007, pp. 37-50

Tensar (2002), "Base reinforcement-Light Aircraft pavement", Technical memorandum, available at www.tensarcorp.com*/uploadedFiles/SPECTRA_TTN_BASE_3.doc*

TRI (2001), "In-plane rotational stiffness: Is this a relevant property for base reinforcement of geosynthetics?" Internal report available at www.tri-env.com

Tutumluer, E. and Dawson, A, (2004), "Resilient characterization of compacted aggregate", PowerPoint from TRB Workshop on describing aggregate behavior for today's pavements, Washington, DC

Voottipruex, P., Bergado, D.T., Ounjaichon, P., (2000), "Pullout and direct shear resistance of hexagonal wire mesh reinforcement in weathered Bangkok clay", Geotechnical Engineering Journal, 31(1), 43-62

Wartman, J., Harmanos, D., and Ibanez, P (2005), "Development of a versatile device for measuring the tensile properties of geosynthetic", Proceeding of GRI-18 Conference, ASCE, Austin, Texas, 4097-4102

Wathugala, G.W., Huang, B. and Pal, S. (1996), "Numerical Simulation of Geosynthetic Reinforced Flexible pavement", Transportation Research Record 1534, TRB, National Research Council, Washington, DC, USA, pp. 58-65

Watts, G.R.A., and Blackman, D.I. (2009), "Pavement trafficking trials", Jubilee symposium on Polymer Grid Reinforcement, Institute of Civil Engineers, London, England

Webster, S.L., (1993), "Geogrid reinforced base courses for flexible pavements for light aircraft , test section construction, behavior under traffic, laboratory tests, and design criteria", Technical report GL-93-6, U.S. Army Corps of Engineers, Waterways Experiment Station, Vicksburg, Mississippi, USA, 86p

Williams, N.D. and Houlihan, M.F., (1987), "Evaluation of interface friction properties between geosynthetics and soils", Geosynthetics Conference, New Orleans, Vol. 2, pp. 616-627

Wilson-Fahmy, R.F., Koerner, R.M., and Sansone, L.J. (1994), "Experimental behavior of polymeric geogrids in pullout", Journal of Geotechnical Engineering, 120(4), ASCE, USA, 661-677

WSDOT (2007), "Design Parameters for flexible pavements" http://training.ce.washington,edu/wsdot/modulues/04_design_parameters

Yang, K.H, (2009), "Stress distribution within geosynthetic-reinforced soil structures", Ph.D. Dissertation, the University of Texas at Austin, Texas, USA

Yoder, E.J., and Witczak, M.W., (1975). Principles of pavement design, second edition, John Wiley and Sons, 711p

Yuan, Z. (2005), "Theoretical analysis of bending stiffness test on geosynthetic reinforced base layer", Proceedings of NAGS/GRI-19 Cooperative Conference, Dec.14-16, Las Vegas, Nevada, 2005

Yuan, Z. and Chua, K.M., (1991), "Analytical Model for Pullout of Soil Reinforcement", Transportation Research Record 1330, pp. 64-71

Zornberg, J.G, Prozzi, J.A., Gupta, R., Luo, R., McCartney, J.S., Ferreira, J.A.Z. and Nogueira, C., (2008), "Validating mechanisms in geosynthetic reinforced pavements", Report No. FHWA/TX-08/0-4829-1, submitted to Center of Transportation Research at Austin, February 2008, 247 p.

Zornberg, J.G. and Gupta, R. (2009), "Reinforced pavements over expansive clay subgrades", 17th International Conference on Soil Mechanics and Geotechnical Engineering, ICSMGE 2009, Alexandria, Egypt

Zornberg, J.G. and Kang, Y., (2005), "Pullout of Geosynthetic Reinforcement with In-plane Drainage Capability", GRI-18, Geosynthetics Research and Development in Progress, Geofrontiers 2005, Austin, USA

Zornberg, J.G., (1994), "Performance of Geotextile Reinforced Soil Structures", Ph.D. Dissertation, Department of Civil Engineering, University of California, Berkeley, California, USA

Zornberg, J.G., Abu-Hejleh, N., and Wang, T. (2001), "Geosynthetic-Reinforced Soil Bridge Abutments in Highway Applications" Geotechnical Fabrics Report, Vol. 19, No. 2, March 2001, pp. 52-55

Zornberg, J.G., and Christopher, B.R. (2006), "Chapter 27: Geosynthetics", The Handbook of Groundwater Engineering, Jacques W. Delleur (Editor-in-Chief), CRC Press Inc., Boca Raton, Florida

Zornberg, J.G., and Christopher, B.R., Editors (2000). Advances in Transportation and Geoenvironmental Systems using Geosynthetics, ASCE Geotechnical Special Publication No. 103, ASCE Press, ISBN 0-7844-0515-8, 422p

Zornberg, J.G., Gupta, R., Prozzi, J.A., and Goehl, D, (2008), "Case histories on geogrid reinforced pavements to mitigate problems associated with expansive subgrade soils", Geoamericas 2008, Cancun, Mexico

Vita

Ranjiv attended high school at D.A.V. College, Chandigarh, India and graduated in May, 1998. After graduating from high school, he enrolled at Punjab Engineering College, Chandigarh, India for undergraduate studies. He graduated with a Bachelor's degree in Civil Engineering with highest honors in year 2002. He received a University Gold Medal for Excellence in Academic Studies as he was ranked first among the graduating class of students for that year. He also received the Best Undergraduate Research Project Award from the university.

In August 2002, Ranjiv qualified for a Government of India scholarship provided by Ministry of Human Resource and Development to pursue graduate studies in engineering. He then enrolled at the Indian Institute of Technology, New Delhi, India for his graduate studies in the area of Geotechnical and Geoenvironmental Engineering. He worked with Dr. K.G. Sharma for his graduate research on stability analysis of earth and rock filled dams. After completing his Master's degree in May 2004, he decided to pursue research in the area of geotechnical engineering. In September 2004, he enrolled at the University of Texas, Austin, USA for his Ph.D. degree. For his doctoral research, he worked under the supervision of Dr. J.G. Zornberg in the area of geosynthetic engineering. Ranjiv received financial support throughout his doctoral studies from the Texas Department of Transportation.

Permanent address: 41-Brij Puri Colony, Yamuna Nagar,
Haryana -135001, India

This dissertation was typed by Ranjiv Gupta.